Dynamical correlations of $S = 1/2$ quantum spin chains

by

Rodrigo Gonçalves Pereira

B.Sc., State University of Campinas, 2002
M.Sc., State University of Campinas, 2004

A THESIS SUBMITTED IN PARTIAL FULFILMENT OF
THE REQUIREMENTS FOR THE DEGREE OF

DOCTOR OF PHILOSOPHY

in

The Faculty of Graduate Studies

(Physics)

THE UNIVERSITY OF BRITISH COLUMBIA
(Vancouver)

June 2008

Abstract

Spin-1/2 chains demonstrate some of the striking effects of interactions and quantum fluctuations in one-dimensional systems. The XXZ model has been used to study the unusual properties of anisotropic spin chains in an external magnetic field. The zero temperature phase diagram for this model exhibits a critical or quasi-long-range-ordered phase which is a realization of a Luttinger liquid. While many static properties of spin-1/2 chains have been explained by combinations of analytical techniques such as bosonization and Bethe ansatz, the standard approach fails in the calculation of some time-dependent correlation functions. I present a study of the longitudinal dynamical structure factor for the XXZ model in the critical regime. I show that an approximation for the line shape of the dynamical structure factor in the limit of small momentum transfer can be obtained by going beyond the Luttinger model and treating irrelevant operators associated with band curvature effects. This approach is able to describe the width of the on-shell peak and the high-frequency tail at finite magnetic field. Integrability is shown to affect the low-energy effective model at zero field, with consequences for the line shape. The power-law singularities at the thresholds of the particle-hole continuum are investigated using an analogy with the X-ray edge problem. Using methods of Bethe ansatz and conformal field theory, I compute the exact exponents for the edge singularities of the dynamical structure factor. The same methods are used to study the long-time asymptotic behavior of the spin self-correlation function, which is shown to be dominated by a high-energy excitation.

Table of Contents

Appendices

List of Tables

List of Figures

List of Abreviations

BA: Bethe Ansatz

CFT: Conformal Field Theory

DMRG: Density Matrix Renormalization Group

DSF: Dynamical Structure Factor

ESR: Electron Spin Resonance

FT: Field Theory

NMR: Nuclear Magnetic Resonance

RPA: Random Phase Approximation

TBA: Thermodynamic Bethe Ansatz

tDMRG: Time-dependent Density Matrix Renormalization Group

Acknowledgements

First of all, I thank my supervisor, Ian Affleck, for all the support and guidance he provided during my PhD. His example of ethics and dedication is an inspiration that I will carry in my future career.

I would also like to thank the members of my Ph.D. supervisory committee Doug Bonn, Marcel Franz and Moshe Rozali, for asking thought-provoking questions during our meetings.

I am indebted to my collaborators in this project, Jesko Sirker, Jean-Sébastien Caux and Steve White, who were always very kind in answering any questions I had.

My experience as a graduate student was complemented by the interaction with many members of the Condensed Matter Theory group at UBC. I want to express my special gratitude to the members of our coffee club: Ming-Shyang Chang, Nicolas Laflorencie, Justin Malecki, Dominic Marchand, Yoshitaka Maeda and Eran Sela. I learned a lot from our daily conversations, physics related or not.

I wish to thank my M.Sc. thesis supervisor Eduardo Miranda, for introducing me into this exciting field of research. Despite the distance, he has remained as a friend and source of advice.

I thank all my friends for making my life in Vancouver such a delightful and enriching experience. I was fortunate to spend three years as a resident of Green College, where I met many people with diverse backgrounds and academic interests. Alejandro Liu Cheng deserves a special mention for bugging me with his philosophical questions about parallel universes. The comment about the connection between spin chains and string theory on page 1 was

meant for him.

Of course I could not have accomplished any of this without the support of my parents, my brother and my sister, who always encouraged me to pursue my studies, even when that meant going so far away from them. My goal has always been to make them proud.

Finally, I must acknowledge financial support by Brazilian agency Conselho Nacional de Desenvolvimento Científico e Tecnológico (CNPq), through scholarship number 200612/2004-2.

Statement of Co-Authorship

This thesis is based on a research project which required many analytical and numerical methods and in which several people were involved. I contributed with the field theory and Bethe ansatz calculations, in which I was helped by my supervisor, Ian Affleck, and by postdoctoral fellow Jesko Sirker. I was also involved in the analysis of the numerical data and manuscript preparation. I wrote most of the long paper which became Chapter 2 of this thesis. The numerical Bethe Ansatz results were computed by Jean-Sébastien Caux and Rob Hagemans. All the graphs in Chapter 2 were produced and analyzed either by myself or by Jesko Sirker. The derivation of the width of the two-particle continuum from the Bethe ansatz equations in Chapter 2 is due to Jean-Sébastien Caux. The DMRG results for the sum rules in Chapter 2 are due to Steven R. White, who is also responsible for the tDMRG results presented in Chapter 3. The paper where the results of Chapter 3 were reported was written primarily by myself.

Chapter 1

Introduction

Quantum spin chains provide simple yet rich examples of strongly correlated systems. For a theoretical physicist, one-dimensional (1D) arrays of interacting spins that behave according to the rules of quantum mechanics are interesting because they are amenable to detailed analytical and numerical studies [1]. These studies have revealed that spin chains exhibit exotic properties which contradict our classical intuition about magnetic ordering. For instance, spin-1/2 chains with an isotropic antiferromagnetic exchange interaction do not order even at zero temperature, and their spectrum is best interpreted in terms of fractional excitations named spinons which are very different from spin waves in three-dimensional magnets. But spin chains are not confined to the theoretical realm. They also exist in the real world, in the form of chemical compounds in which, due to the lattice structure, the coupling between magnetic ions is highly anisotropic and strongest along one spatial direction [2]. Indeed, thanks to steady advances in materials science, the research field of 1D quantum magnetism has benefited from the interplay between theory and experiment that is essential in condensed matter physics. The interest in spin chain models is actually quite general, ranging from applications in quantum computation [3] to mathematical tools in string theory [4].

Given the long history of studies of spin chains, it is fair to say that most relevant *static* thermodynamic properties, such as specific heat and magnetic susceptibility, are well understood by now. However, despite various efforts, the problem of calculating *dynamical* properties, such as the dynamical structure factor probed directly in inelastic neutron scattering experiments, poses

a challenge to standard theoretical approaches and has remained unsolved. The need to clarify some of the open questions concerning the dynamics of spin chains motivated the work reported in this thesis. The results presented here are primarily useful to interpret neutron scattering data, but may also be relevant for other experiments which probe dynamic responses of one-dimensional systems, such as nuclear magnetic resonance in spin chain compounds and Coulomb drag in quantum wires.

1.1 Heisenberg model

Electrons are charged spin-1/2 particles which carry an intrinsic magnetic moment. In the early days of quantum mechanics, Werner Heisenberg [5] pointed out that the spin-independent Coulomb interaction between two electrons in a diatomic molecule, with a properly anti-symmetrized wave function, gives rises to an exchange interaction that couples the electron spins. The generalization of this idea to a large number of electrons leads to an important mechanism for magnetism in solids [2]. The Heisenberg model describes a bilinear exchange interaction between nearest neighbor spins at fixed positions on a lattice

$$H = J \sum_{\langle ij \rangle} \vec{S}_i \cdot \vec{S}_j \tag{1.1}$$

where J is the exchange integral and $\vec{S}_i$ denotes the spin operator at site i, which obeys commutation relations of angular momentum operators [6]. If these are electrons spins (total spin $S = 1/2$), there are two states for each lattice site, denoted by $\{|\uparrow\rangle_i, |\downarrow\rangle_i\}$. The Hilbert space has dimension 2^N, where N is the number of lattice sites. The components of the spin operator can be represented by Pauli matrices $\vec{\sigma} = (\sigma^x, \sigma^y, \sigma^z)$ in the form $\vec{S}_i = \hbar\vec{\sigma}_i/2$, corresponding to the generators of the SU(2) group. More generally, the $\vec{S}_i$ operators can represent atomic spins, which depend on the electronic

configuration and can be integer or half-integer.

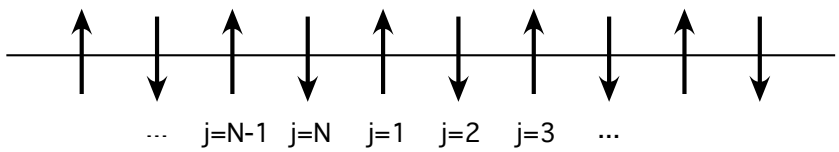

Figure 1.1: Schematic representation of a spin chain with N sites and periodic boundary conditions.

The type of magnetic order (or the lack thereof) in the ground state of the Heisenberg model depends on the sign of the exchange coupling J, dimensionality and lattice structure. For $J < 0$, the exchange interaction favors a state in which all the spins point along the same direction. The ground state picks out a particular direction in space and spontaneously breaks the rotational symmetry of the Hamiltonian. This is actually the true ground state of the *ferromagnetic* model. We speak of long-range order in the ground state since the correlation between spins stays finite at arbitrarily large distances. For $J > 0$, the spins at neighboring sites would like to point along opposite directions. In the classical picture, the ground state breaks translational invariance and the system splits up into two sublattices with opposite magnetization. This classical state is called the Néel state and is illustrated in Fig. (1.1) for a one-dimensional lattice. Unlike the ferromagnetic case, this state is not an eigenstate of the Hamiltonian (1.1) because the sublattice magnetization is not a good quantum number. This suggests that quantum fluctuations play an important role in the *antiferromagnetic* model. Although the resulting physics can be quite interesting in two and three dimensions (see, for example, the search for spin liquid states in frustrated magnets [2]), the effects of quantum fluctuations become extreme in the 1D case. While the classical Néel state is a good starting point for linear spin wave theory [7] in many three-dimensional lattices at finite temperature, it fails dramatically in 1D. In fact, the Mermin-Wagner-Hohenberg theorem

[8, 9] rules out finite temperature phase transitions in the isotropic model in one and two dimensions. Even at zero temperature, it can be shown that the quantum corrections to the sublattice magnetization diverge in 1D and destroy the long-range order of the ground state [7]. The impossibility of spontaneous breaking at $T = 0$ of a continuous symmetry in a 1D model with short-range interactions was also discovered by Coleman in the context of quantum field theory [10]. But, if the classical picture fails, how should we think about the ground state of the 1D quantum antiferromagnet?

1.2 An example of a Heisenberg spin chain

Before we say more about the theoretical analysis of the model, let us discuss a concrete realization of an antiferromagnetic spin chain. The Heisenberg model (1.1) can be obtained more realistically from the Hubbard model, which describes electrons hopping on a lattice and repelling each other when two electrons occupy the same site. At half-filling and in the limit of strong on-site repulsion, there is exactly one electron per lattice site and charge fluctuations can be neglected at energies much lower than the interaction strength. The orbital degrees of freedom are frozen and only the spin degrees of freedom at each lattice site have to be considered. Kinetic exchange that results from virtual hopping processes lifts the spin degeneracy of the ground state and the low-energy effective model is the Heisenberg model with $J > 0$ (antiferromagnetic) [2]. This means that antiferromagnetism appears naturally in Mott insulators, as is indeed observed in real compounds.

Although bulk materials are three dimensional, the value of the exchange coupling J can be different along different directions of the lattice. In the copper oxide compound Sr_2CuO_3 [11], the crystal structure is characterized by CuO_4 squares sharing oxygen corners (Fig. 1.2). The experimental interest in this compound was motivated by the discovery of high-temperature superconductivity in related doped cuprates. In Sr_2CuO_3 the copper ions are

in a $3d^9$ configuration and have spin 1/2. The overlap with the oxygen atoms in the 180 degree Cu-O-Cu bonds is responsible for a strong superexchange interaction [12]. The effective J along the copper-oxygen chain is as large as $J/k_B = (2200 \pm 200)$K [11]. On the other hand, the interchain coupling is very weak, resulting in a very low Néel temperature, $T_N \sim 5$K, below which three-dimensional magnetic ordering sets in. Therefore, over a wide temperature range, $T_N < T < J/k_B$, Sr_2CuO_3 is well described by the one-dimensional Heisenberg model (1.1). Other examples of effective spin-1/2 Heisenberg chains with smaller values of J include $KCuF_3$ ($J/k_B \approx 190$K) [13] and copper pyrazine dinitrate, $Cu(C_4H_4N_2)(NO_3)_2$ ($J/k_B \approx 10$K) [14].

1.3 The Bethe ansatz

As the semiclassical approach fails in 1D, understanding the one-dimensional antiferromagnet requires a whole new theoretical framework. Such framework actually appeared even before spin wave theory. In 1931, Hans Bethe [15] showed that the 1D Heisenberg model can be solved exactly, in the sense that one can construct the exact eigenstates and eigenvalues of the Hamiltonian (1.1). The key for Bethe's solution was the fact that in the Heisenberg model any scattering among spin excitations can be factorized into a series of two-body scattering processes. The many-body wave functions are superpositions of plane waves with relative amplitudes fixed by the two-body phase shift. The allowed values of quasi-momenta for given boundary conditions are determined by solving coupled nonlinear equations known as the Bethe equations. The reduction to two-particle scattering is not a general property of interacting Hamiltonians, but is valid for the Heisenberg model because the latter is *integrable*, meaning that it has an infinite number of local conserved quantities.[1] Remarkably, integrability is not so unusual in one

[1] Actually, the definition of integrability is clear for classical models, but ambiguous in quantum mechanics because linearly independent conserved quantities can be constructed for any quantum model (see discussion in [16]). It is more useful to think of quantum

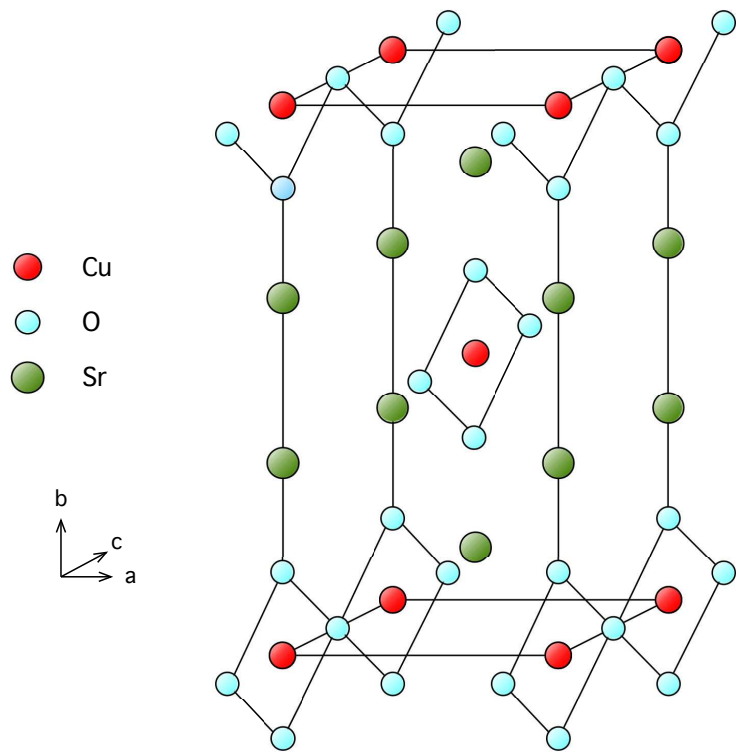

(a) Crystal structure of Sr_2CuO_3, a $S = 1/2$ Heisenberg chain compound. Adapted from Ref. [11].

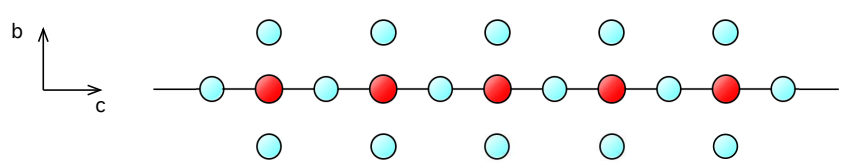

(b) A cut on the bc plane showing the Cu-O chain. The chain oxygens mediate a superexchange interaction between the magnetic copper ions.

Figure 1.2:

dimension. Other widely studied 1D models, such as the Lieb-Liniger model [17] (interacting Bose gas) and the Hubbard model [18], are also integrable. The Bethe ansatz is also applicable to these models.

The Bethe ansatz solution [19, 20] proves that the ground state of the spin-1/2 Heisenberg chain is unique and has total spin equal to zero (a singlet state) if the number of sites is even. The spectrum is gapless (or "massless") in the thermodynamic limit. The elementary excitation is called a spinon and corresponds to a hole in the set of roots of the Bethe equations. A single spinon is a fractional excitation which carries spin 1/2 and cannot be created alone without changing the boundary conditions. In order for the total S^z of the chain to change by an integer number, as required by superselection rules, the spinons have to be created in pairs. This implies, for instance, that the simplest triplet excitation lies in a two-parameter continuum (whose lower bound is known as the de Cloizeaux-Pearson dispersion [21]), in contrast with the single-magnon peak predicted by semiclassical spin wave theory. This has in fact been observed in inelastic neutron scattering experiments [22], in a clear demonstration of one-dimensional behavior.

The Bethe ansatz equations for the Heisenberg spin-1/2 chain have been extensively studied, in an attempt to extract useful properties of the model. Due to the complexity of the solution, this is not always possible. It suffices to say that, seventy seven years after the original paper, not even the completeness of the Bethe eigenstates for the XXZ model (without an assumption about the distribution of complex roots known as the string hypothesis) has been proved yet [23]. In the thermodynamic limit, the Bethe ansatz equations assume the form of integral equations for the density of quasi-momenta. Some exact results which have been obtained by manipulating these equations include the ground state energy [24], zero temperature susceptibility [25] and spin wave velocity [21]. An application of the Bethe ansatz equations

integrability as the absence of diffraction or three-particle scattering, as is the case for the Bethe ansatz solvable models.

for finite systems is the calculation of the finite size spectrum [26], which is important in conformal field theory [27]. It is also possible to compute finite temperature static properties (e.g. specific heat, finite temperature susceptibility) using a set of nonlinear integral equations known as Thermodynamic Bethe Ansatz (TBA) [28]. However, this procedure has been criticized for relying on the string hypothesis to describe the spectrum of the XXZ model.

It is worth mentioning that models describing spin chains with higher values of S are not integrable. The case $S = 1/2$ is therefore special since we have access to an exact solution with which approximate analytical and numerical results can be compared. However, according to the Lieb-Shultz-Mattis-Affleck theorem [29, 30], a gapless spectrum is generic in isotropic half-integer spin chains, unless parity symmetry is spontaneously broken and the ground state is degenerate. The theorem does not hold for integer values of S. In fact, Haldane [31] conjectured that integer spin chains should exhibit a finite gap to the lowest excited state, while the SU(2) symmetry remains unbroken. Haldane's conjecture has been confirmed by numerical calculations as well as experimentally, and the existence of a gap was proven rigorously for the related bilinear biquadratic $S = 1$ Affleck-Kennedy-Lieb-Tasaki (AKLT) model [32]. The difference between integer and half-integer spin chains can be attributed to the effects of a topological term in the nonlinear sigma model [33, 34].

1.4 Anisotropic spin chains

The generalization of the model (1.1) which introduces exchange anisotropy as well as a finite external magnetic field is the so-called XXZ model in a field

$$H = J \sum_{j=1}^{N} [S_j^x S_{j+1}^x + S_j^y S_{j+1}^y + \Delta S_j^z S_{j+1}^z - h S_j^z]. \tag{1.2}$$

In comparison with the Heisenberg (or XXX) model, the symmetry of the XXZ model has been reduced from SU(2) to U(1) (rotation around the z axis). The total magnetization $S^z = \sum_j S_j^z$ is still a good quantum number. Moreover, this model is also integrable by the Bethe ansatz [35, 36]. While some exact analytical results can be derived for the model with $h = 0$, in general the Bethe equations for the XXZ model at finite magnetic field have to be solved numerically [19].[2]

The first reason to study the XXZ model is that one should not expect perfectly isotropic exchange interactions in real materials. On a lattice the rotational symmetry of the spin interaction can be broken by spin-orbit or dipolar interactions. However, this effect is weak and bulk spin chain materials are very close to being isotropic [37]. But the second and most important reason why the XXZ model is interesting is because it appears as an effective model whenever a physical system can be described as a one-dimensional lattice with two states per site. One example is that of $S = 1/2$ two-leg ladders in the strong coupling limit $J_\perp \gg J_\parallel$, where $J_\perp$ and $J_\parallel$ are the couplings along the rungs and along the chain, respectively [38]. Two-leg ladders are similar to $S = 1$ chains in the sense that there is an energy gap to the triplet state on each rung. But an external magnetic field can lower the energy of the triplet state with total S^z parallel to the field. Near the critical field, the singlet-triplet gap closes and the two low-lying states form a doublet which acts as an effective spin-1/2 degree of freedom. The effective model for a $S = 1/2$ ladder with $J_\perp \gg J_\parallel$ is the XXZ model with $\Delta = 1/2$ [39, 40]. Artificial systems which have phases described by effective XXZ models, with arbitrary values of Δ, include Josephson junction arrays [41], linear arrays of qubits [42], coupled photonic cavities [43], and ultracold bosonic atoms (with two internal hyperfine states) trapped in optical lattices [44]. In the latter, it should be even possible to observe phenomena associated with the

[2] A simple program to solve the Bethe ansatz equations for the XXZ model numerically can be found in the appendix of Ref. [1].

integrability of the 1D model, such as the absence of relaxation mechanisms [45].

The Bethe ansatz solution allows us to map out the phase diagram of the XXZ model by looking at the energy of the low-lying excitations as a function of exchange anisotropy Δ and magnetic field h (Fig. 1.3). Along the zero field line in parameter space, the limits $\Delta \to -\infty$ and $\Delta \to +\infty$ correspond to the classical Ising ferromagnet and antiferromagnet, respectively. These are both known to have a gapped spectrum, with domain-wall-type excitations. We also know that the model is gapless at the Heisenberg point $\Delta = 1$, so we should expect quantum phase transitions by simply varying the anisotropy parameter Δ. As a matter of fact, the Bethe ansatz reveals that the XXZ chain is gapless along an entire critical line $-1 < \Delta \leq 1$ (sometimes called the easy plane anisotropy regime). There is a gapped ferromagnetic phase for $\Delta < -1$ and a gapped Néel phase for $\Delta > 1$. Including the magnetic field, one finds the ground state phase diagram represented in Fig. 1.3 [16]. There is a whole region where the spectrum of the spin chain is gapless. Starting from the gapless phase, the system enters the ferromagnetic phase if the field is increased above the saturation field. On the other hand, a finite magnetic field can close the gap for $\Delta > 1$.

The gapped, Ising-like phases of the XXZ spin chain can be understood with simple semiclassical pictures, but the gapless phase seems more exotic. Long-range order should not exist in this phase, which includes the Heisenberg model. What we would really like to know in order to characterize this phase and make connection with experiments is how spin-spin correlation functions decay at large distances. Unfortunately, this cannot be done by employing directly the Bethe ansatz solution. Even when we know the exact eigenstates and the spectrum, calculating correlation functions requires computing matrix elements (so-called *form factors*) between an unmanageable number of complicated wave functions (recall that the size of the Hilbert space grows as 2^N). This calls for an alternative, approximate yet more

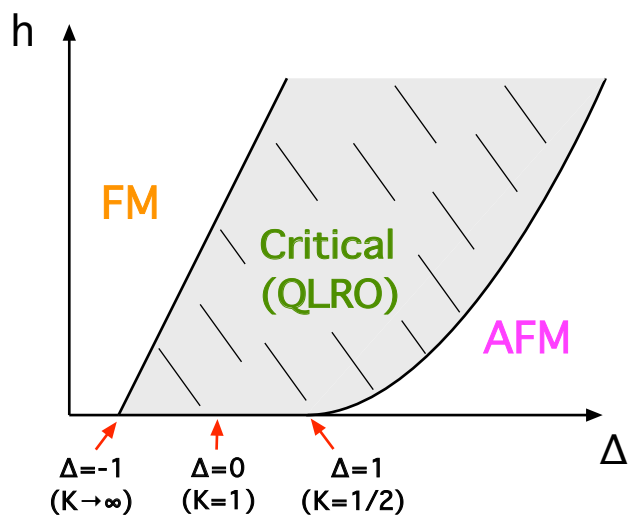

Figure 1.3: Phase diagram for the XXZ model as a function of anisotropy parameter Δ and magnetic field h. Between the gapped ferromagnetic (FM) and antiferromagnetic (AFM) phases, there is a critical regime characterized by quasi-long range order (QLRO). This is a Luttinger liquid phase which includes the Heisenberg antiferromagnet $\Delta = 1$. The exact value of the Luttinger parameter K at special points along the zero field line are indicated.

intuitive approach to the physics of one-dimensional magnets.

1.5 Field theory methods

Another reason to consider the anisotropic model is that the XXZ spin chain is equivalent to a model of interacting spinless fermions. This is made clear by the Jordan-Wigner transformation, which maps the S_j^z operator onto a local density of fermions [1]. This way, the spin-up state is equivalent to a particle and the spin-down state to a hole. Under this transformation the x and y terms of the exchange interaction in (1.2) are mapped onto a kinetic energy (hopping) term, whereas the z part translates into a density-density interaction term. As a result, the model with $\Delta = 0$, known as the XY model, is equivalent to free fermions on the lattice and can be solved very easily by performing a Fourier transform to momentum space. The ground state of the XY model is understood as a Fermi sea of the Jordan-Wigner fermions, whose density is fixed by the magnetization of the spin chain. In particular, the zero field case corresponds to a half-filled band, with one fermion per every other lattice site. Excitations with total $S^z = 0$ correspond to the creation of particle-hole pairs. This solution of the XY model makes it possible to calculate some correlation functions exactly [29, 46]. The correlation functions are found to decay very slowly (as power laws) in the large distance limit, which leads to the notion of *quasi-long range order* in 1D gapless systems.

The solution of the XY model also provides a convenient starting point for exploring the entire gapless phase once we find a way to treat the fermion-fermion interactions for $\Delta \neq 0$. In three dimensions, Landau's Fermi liquid theory [47] shows that the excitations of a system of interacting fermions[3] are quasiparticles which resemble the "bare" electron in the Fermi gas and differ

[3]Assuming the interactions are repulsive. Attractive interactions lead to a superconducting (BCS) instability.

only by the renormalization of a few parameters such as the effective mass [48]. The situation is very different in one dimension, because again quantum fluctuations have a drastic effect and lead to the breakdown of Fermi liquid theory in 1D [49]. The method of choice to describe the low-energy excitations of an interacting 1D fermionic system is called bosonization [50]. This approach starts by taking the continuum limit and linearizing the dispersion of the particle-hole excitations about the Fermi points with momentum $\pm k_F$. One then introduces an effective bosonic field associated with the collective density fluctuations of the Fermi gas. The advantage of the bosonization method is that "forward" fermionic interactions can be treated exactly. Their effect is simply to renormalize the velocity and "stiffness" of the *non-interacting* bosons. The resulting free boson model is known as the Luttinger model [51]. The unusual properties predicted by the Luttinger model for 1D interacting fermionic systems have been observed in quantum wires [52], carbon nanotubes [53], anisotropic organic conductors (Bechgaard salts) [54], and edge states of the fractional quantum Hall effect [55]. There is no clear correspondence between the bosons of the Luttinger model and the exact eigenstates found in the Bethe ansatz. However, it is possible to define a kink in the bosonic field that carries spin-1/2 and for $\Delta = 1$ obeys semionic statistics, in close analogy with the spinons of the Heisenberg model [56].

The bosonization approach is asymptotically exact in the limit of low energies and long wavelengths. Haldane [57] introduced the concept of the Luttinger liquid, pointing out that the Luttinger model should be the fixed point of any gapless 1D system with a linear dispersion in the low-energy limit. Residual boson-boson interactions which perturb the Luttinger liquid fixed point are either irrelevant or drive the system into a gapped phase under the renormalization group. This is a powerful result. In our case, it means that we can write down an effective field theory that is valid in the entire gapless phase of the XXZ chain. All we need to do is to determine the two

parameters of the Luttinger model, namely the renormalized spin velocity v and the so-called Luttinger parameter K, as a function of Δ and h in the original lattice model (1.2). These parameters can be fixed by comparing the field theory predictions for the low-energy spectrum and susceptibility with the corresponding results obtained from the Bethe ansatz [19]. However, the bosonization approach is more general than the Bethe ansatz in the sense that it can be applied to nonintegrable models as well. This enables one to compute universal properties which are independent of integrability.

Since the low energy effective theory for the XXZ model is a free boson model, it is possible to compute the asymptotic large distance behavior of correlation functions [58]. The result is that the spin correlation functions decay as power laws with non-universal exponents which depend on the Luttinger parameter K. Since K is known exactly from the Bethe ansatz solution, these results are nonperturbative in the interaction strength (i.e. anisotropy parameter) Δ. In particular, the Luttinger liquid theory applies to the (strongly interacting) Heisenberg point $\Delta = 1$, although at zero field it is important to consider the effects of a marginally irrelevant bulk operator [59].[4] A power law decay implies that the correlation length is infinite; in the language of phase transitions, the effective theory is *critical*. A great deal of information, particularly finite temperature correlation functions and finite size spectrum, can be obtained using techniques of conformal field theory [60]. A review of field theory methods for spin chains can be found in [61].

The combination of Bethe ansatz, field theory and various numerical methods (such as Quantum Monte Carlo [62] and Density Matrix Renormalization Group [63]) has a long and successful history. It has provided us with a deep understanding of several properties of spin-1/2 chains, many

[4]The field theory approach also explains the phase transitions of the XXZ model. For $\Delta > 1$, Umklapp scattering becomes relevant and the system goes through a Kosterlitz-Thouless transition. The effective field theory for the Néel phase is the quantum sine-Gordon model, which has massive excitations (solitons, anti-solitons and breathers). On the other side of the phase diagram, the system enters the ferromagnetic phase when the spin susceptibility diverges ($\chi \propto K \to \infty$).

of which have been confirmed by experiments. To mention a few examples, Eggert, Affleck and Takahashi [64] showed that the finite temperature susceptibility of the Heisenberg chain approaches the zero temperature value with an infinite slope (a logarithmic singularity that results from the effect of the marginally irrelevant bulk operator). This prediction was used to fit the susceptibility and extract the effective exchange coupling constant J for Sr_2CuO_3 [11]. Another example is the contribution of the staggered part of the correlation function to the spin-lattice relaxation rate $1/T_1$ and the spin-echo decay rate $1/T_{2G}$ probed by nuclear magnetic resonance (NMR) [65, 66]. Finally, a third example is the calculation of the temperature and magnetic field dependence of the line width of the absorption intensity in electron spin resonance (ESR) experiments on Cu benzoate [67].

1.6 The problem of dynamical correlation functions

Inelastic neutron scattering experiments yield access to dynamical spin correlation functions. This is because neutrons carry spin-1/2 and can interact (via a dipolar interaction) with individual ions in a magnetic material, transfering both energy and momentum to the lattice. It can be shown [68] that the cross section for non-spin flip scattering, measured in experiments with polarized neutron beams, is directly proportional to the longitudinal dynamical structure factor

$$S^{zz}(q,\omega) = \frac{1}{N}\sum_{j,j'=1}^{N} e^{-iq(j-j')} \int_{-\infty}^{+\infty} dt\, e^{i\omega t} \left\langle S_j^z(t) S_{j'}^z(0) \right\rangle , \tag{1.3}$$

where $\langle \ldots \rangle$ denotes the expectation value in the ground state of the Hamiltonian (1.2) (at zero temperature). The cross section for spin flip scattering

is proportional to the transverse dynamical structure factor.[5] Unlike static thermodynamic quantities, the dynamical structure factors are given by the Fourier transform of *time-dependent* correlation functions.

The first neutron scattering experiments on $S = 1/2$ Heisenberg chains in 1973 [69] pointed to an asymmetric line shape, with a peak at lower energies. This was later confirmed by further experiments [14, 70]. Moreover, the data suggested a double peak structure at finite magnetic field. As mentioned in section 1.3, these results were a direct proof that spin wave theory could not be used to describe 1D antiferromagnets. Early theoretical approaches based on the Hartree-Fock approximation [71] and Holstein-Primakoff representation (a large S expansion) [72] led to unphysical results and failed to explain the asymmetry of the line shape of $S^{zz}(q, \omega)$ for the Heisenberg chain.

The XY model can serve as a starting point for an appropriate quantum mechanical treatment of the dynamical structure factor in the gapless phase. The expression for $S^{zz}(q, \omega)$ in (1.3) is equivalent to the Fourier transform of the density-density correlation function of the fermions defined in the Jordan-Wigner transformation [29]. Since for the XY model these fermions are noninteracting, $S^{zz}(q, \omega)$ turns out to be given by the density of states for excitations with a single particle-hole pair. The exact line shape derived for the XY model at zero magnetic field (half-filling) is illustrated in Fig. 1.4. It shows a step discontinuity at the lower threshold of the two-particle continuum and a square-root divergence at the upper threshold. There is no spectral weight outside the two-particle continuum.

Luther and Peschel [58] applied bosonization to treat the effects of fermionic interactions and calculate time-dependent correlation functions for the XXZ

[5] The longitudinal and transverse functions are equivalent for the Heisenberg model at zero field due to SU(2) symmetry, but not for the general anisotropic case. The transverse correlation function is more difficult to calculate because, while S_j^z maps onto a local density of fermions under the Jordan-Wigner transformation, the mapping of the operators $S_j^{\pm} = S_j^x \pm iS_j^y$ involves a nonlocal string operator. For this reason, there are no analytic expressions for the transverse dynamical structure factor even for the XY model. I will not discuss the transverse structure factor in this thesis.

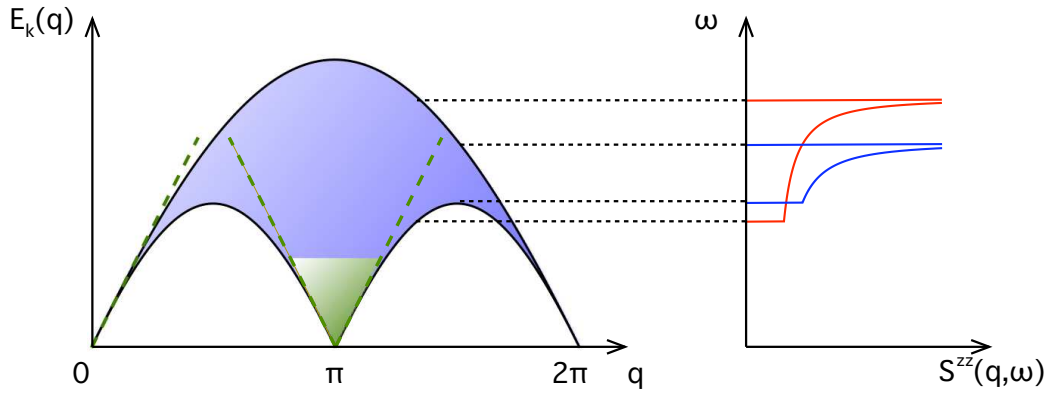

Figure 1.4: Particle-hole excitation spectrum and exact line shape of $S^{zz}(q,\omega)$ for the XY model at zero magnetic field. The two curves on the right-hand side represent two different q values. Note the square root divergence at the upper threshold and the step discontinuity at the lower threshold of the continuum. The dashed lines represent the single boson dispersion at $q \sim 0$ and the approximate lower bounds for the continuum at $q \sim \pi$ obtained by linearizing the dispersion about the Fermi points $k_F = \pm\pi/2$.

model in the low energy limit. However, the result for the dynamical structure factor is somewhat disappointing. As discussed above, one of the very first steps in the bosonization procedure is the approximation of linear dispersion of the low lying excitations. Without this assumption, the model is not solvable. In the fermionic approach, the effect of a nonlinear dispersion is understood as the violation of the Ward identities which guarantee the cancelation of bubble diagrams with more than two interaction lines [73]. In the bosonic language, band curvature terms introduce interactions between the bosons of the Luttinger model [57]. These interactions are irrelevant in the renormalization group sense, which means that they give subleading corrections to the large distance asymptotics of correlation functions. Yet, due to the linear dispersion approximation the Luttinger model does not capture

the correct continuum of particle-hole excitations. The low-energy spectrum predicted by the Luttinger model is represented by the dashed green lines in Fig. 1.4. There is a linear mode near $q \sim 0$, corresponding to a single boson with infinite lifetime, and a continuum near $q \approx \pi$ for $h = 0$,[6] bounded from below by two straight lines. The result of Luther and Peschel is consistent with this approximate spectrum. They found that $S^{zz}(q, \omega)$ has two contributions at low energies: (*i*) for $q \approx 0$, the line shape is given by a delta function peak at the energy carried by the single boson, $S^{zz}(q, \omega) \sim \delta(\omega - vq)$; (*ii*) for $q \approx \pi$, there is a power law singularity at the (approximate) lower edge of the continuum, $S^{zz}(q, \omega) \sim [\omega^2 - v^2(q - \pi)^2]^{K-1}$.

There are several reasons why the Luttinger liquid result for $S^{zz}(q, \omega)$ is not satisfactory. First, the delta function peak in contribution (*i*) does not say anything about the line shape probed by experiments. It contains even less information than the exact solution for the XY model, where we know that $S^{zz}(q, \omega)$ has well defined lower and upper thresholds. All this Luttinger liquid result predicts is that the line shape should become infinitely narrow in the limit $q \to 0$. This is indeed the case for the XY model, where it can be verified that the width of the particle-hole continuum vanishes as q^3 for $h = 0$ and q^2 for $h \neq 0$ [29]. Second, based on general arguments for interacting field theories, we expect that for $\Delta \neq 0$ a continuous spectrum should appear at energies above the "mass shell" of the bosonic excitations, $\omega = vq$, corresponding to an incoherent contribution from multiple-particle states. There is no such contribution in the Luttinger liquid result (*i*). Third, result (*ii*) does tell us that there is a power law singularity at some lower threshold, which becomes a square root divergence for $\Delta = 1$ ($K = 1/2$ at the isotropic point). This is in qualitative agreement with the asymmetry of the line shape observed in experiments.[7] However, the straight lines in Fig.

[6] For $h \neq 0$, the low energy continuum appears at $q \approx 2k_F = \pi + 2\pi\langle S_j^z \rangle$, where k_F is the effective Fermi momentum and $\langle S_j^z \rangle$ is the average magnetization per site.

[7] The theory predicts a power law singularity only at $T = 0$. At finite temperatures, the singularity is replaced by a rounded maximum near the lower edge of the continuum.

1.4 are not the real edges of the two-particle continuum, except at $q = \pi$. There is no guarantee that the Luttinger liquid exponent for the power law singularity is the correct one away from $q = \pi$. Furthermore, result (*ii*) does not predict the behavior of $S^{zz}(q, \omega)$ at higher energies, particularly at the upper threshold of the two-particle continuum, which is beyond the reach of this approximation.

Given the lack of a useful field theory result, in 1979 Müller *et al.* [74] put forward an approximate analytic expression for $S^{zz}(q, \omega)$ for the Heisenberg chain. Their proposal (detailed in [75]) was inspired by the exact solution for the XY model, selection rules for classes of Bethe ansatz eigenstates, numerical results for short chains ($N \leq 10$) as well as known sum rules [76]. The formula which became known as the Müller ansatz assumes that almost all the spectral weight is confined within the thresholds of the (later named) two-spinon continuum. The line shape predicted by the Müller ansatz is plotted in Fig. 1.5. Note that, contrary to the result for the XY model, there is a power law divergence at the lower threshold and a step function at the upper threshold. The square root singularity at the lower threshold was chosen to agree with the field theory result of Luther and Peschel at $q \approx \pi$. As Müller *et al.* noted themselves, their formula could not be exact, not only because it cannot satisfy all the sum rules simultaneously, but also because it does not account for the spectral weight above the upper boundary of the two-spinon continuum, which was clearly seen in the numerical results. Nonetheless, the Müller ansatz proved quite useful in analyzing experimental data [77]. A generalization of the Müller ansatz for the XXZ chain in the gapless regime was presented in [78].

Later it was shown that the dynamical structure factor for the related Haldane-Shastry model (isotropic spin-1/2 chain with long range $1/r^2$ interaction) can be calculated exactly [79]. This model is equivalent to a gas of noninteracting spinons, therefore only two-spinon excitations contribute to

This is what is seen in experiments.

$S^{zz}(q,\omega)$. Interestingly, the exact result for $S^{zz}(q,\omega)$ of the Haldane-Shastry model coincides with the Müller ansatz, although the expressions for the thresholds of the two-spinon continuum are different.

Substantial progress was made in 1996 when Bougourzi *et al.* [80] applied quantum group methods developed by Jimbo and Miwa [81] and calculated the exact two-spinon contribution to $S^{zz}(q,\omega)$ for the Heisenberg model at zero field. Their solution exploits the infinite symmetry of the XXZ chain in the massive Néel phase directly in the thermodynamic limit. The expression for the form factors for the two-spinon states are obtained by taking the limit $\Delta \to 1$ from above. The two-spinon dynamical structure factor [82] is illustrated in Fig. 1.5. Although more complicated than the Müller ansatz, this result confirms a square root divergence, accompanied by a logarithmic correction, at the lower edge of the two-spinon continuum. At the upper edge, however, the two-spinon contribution vanishes in a square-root cusp. Note that this is still not the full solution for the Heisenberg chain, since higher multi-spinon states also contribute to $S^{zz}(q,\omega)$, but there are no general analytic formulas for the corresponding form factors.[8] However, the exact two spinon result by itself is a good approximation because it accounts for 72.89% of the total spectral weight in the integrated intensity [82]. In fact, the two-spinon solution was shown to be in better agreement with experiments than the Müller ansatz [14], since the latter overestimates the spectral weight at the upper boundary of the two-spinon band.

The solution of Bougourzi *et al.* is not applicable in the gapless regime of the XXZ chain. Moreover, there are no such analytical results for the Heisenberg chain at nonzero magnetic field. However, more recently a method based on the Algebraic Bethe Ansatz (or Quantum Inverse Scattering Method [19]) was developed which allows one to derive determinant expressions for form factors between Bethe ansatz eigenstates for finite chains [84]. These expressions can be evaluated numerically for fairly large chains (of the order

[8] Recently the exact four-spinon contribution has also been computed [83].

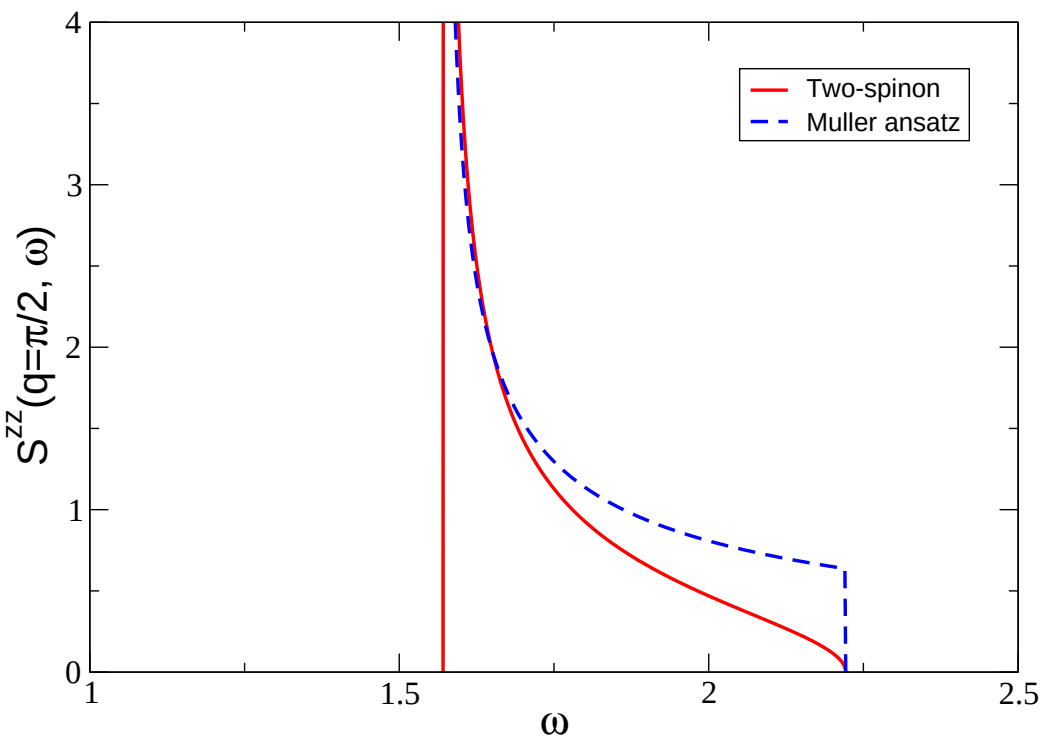

Figure 1.5: Two approximations for the dynamical structure factor $S^{zz}(q, \omega)$ for the Heisenberg chain at zero magnetic field. Dashed line: Müller ansatz (analytic expression given in [75]). Solid line: exact two-spinon contribution (calculated numerically using equations in [82]).

of a few hundred sites in most cases). By focusing on the dominant classes of eigenstates, the dynamical structure factors can be computed numerically for arbitrary values of anisotropy and field [85]. The main drawback of this approach is strong finite size effects.

Remarkably, the study of dynamical correlation functions had advanced more on the Bethe ansatz front than on the field theoretical one, which had been so fruitful in the calculation of thermodynamic properties and equal-time correlations. At the time the research reported here was started, a field theory interpretation of the emergence of a two-particle continuum with edge singularities having the Luttinger model as the starting point was still missing.

1.7 Beyond the Luttinger liquid paradigm

The calculation of the dynamical structure factor exposes a limitation of the Luttinger model as the effective field theory for the XXZ spin chain. The peak in the line shape of $S^{zz}(q,\omega)$ for small q is infinitely sharp because the Luttinger model is Lorentz invariant, implying that the bosonic excitations propagate ballistically with velocity v. Lorentz invariance is not a symmetry of the original lattice model; it only emerges in the low-energy limit. In order to obtain a peak with finite width, it is necessary to go beyond the free boson picture and treat irrelevant interactions properly. This turns out to be a nontrivial task, because simple perturbation theory in the irrelevant operators can lead to infrared divergences [86].

The problem of the finite width of the dynamical structure factor also appears in the context of electron transport in quasi-1D wires. The related quantity there is the imaginary part of the density-density correlation function. It was pointed out in [87] that, as a consequence of the linear dispersion approximation, the Luttinger model does not account for the leading contribution to the Coulomb drag response between quantum wires with different

electronic densities. Following an alternative route to bosonization, Pustilnik *et al.* [88] studied the dynamical structure factor for spinless fermions with parabolic dispersion using perturbation theory in the interaction. This problem is analogous to the spin chain at finite magnetic field in the limit $\Delta \ll 1$. The fermionic approach to calculate $S^{zz}(q, \omega)$ treats band curvature exactly, but faces logarithmic divergences which appear in all orders of perturbation theory. The divergences can be dealt with by using a formalism developed in the study of X-ray edge singularities in metals [89]. Pustilnik *et al.* found that the most striking effect of interactions on the dynamical structure factor is to induce power-law singularities at the thresholds of the particle-hole continuum. The q-dependent exponents are not clearly related to any previously known exponents calculated in Luttinger liquid theory. Interestingly, an extrapolation of the results of Pustilnik *et al.* to strong interactions seemed very promising since the asymmetric line shape that results from their approach is reminiscent of the one expected for spin chains. However, the two-spinon result for the Heisenberg point suggests that the exponents should be independent of momentum in the zero field (particle-hole symmetric) case.

The limitations of the Luttinger model are even more critical when it comes to correlation functions at finite temperature. In general, one expects that at finite temperature inelastic scattering will generate a finite decay rate for the quasiparticles of an interacting system. In the Luttinger model, however, the dynamical structure factor for small q remains a delta function peak for $T > 0$. This means that the bosonic modes still propagate ballistically in the scaling limit [65]. The question then is whether this remains true once we include irrelevant interactions between the bosons. Surprisingly, the answer seems to depend on *high-energy* properties such as the integrability of the lattice model. One way to probe the propagation of excitations is by means of transport properties. It is now well accepted that the dc heat conductivity calculated using the Kubo formula [90] should be infinite for

the XXZ model because the heat current operator is a nontrivial conserved quantity [91]. Indeed, experiments show that the mean free path for thermal transport in spin chain compounds is limited by spin defects, rather than intrinsic scattering between spinons [92].

The problem of spin transport (equivalent to charge transport in the fermionic version) is less clear. The spin current operator does not commute with the Hamiltonian, except in the trivial noninteracting case (the XY model). Nonetheless, Zotos *et al.* [91] have conjectured that the spin Drude weight, defined as the coefficient of the delta function peak in the conductivity at zero frequency, should be finite for integrable models. A finite Drude weight implies an infinite dc spin conductivity at finite temperatures. This means that the existence of nontrivial conserved quantities should protect the ballistic propagation of the excitations. So far it has not been possible to address this question using field theory methods because not much is known about the role of integrability in low-energy effective models. It has been suggested that, contrary to the conjecture, a finite Drude weight could be generic to 1D models which have the Luttinger model as fixed point [93]. However, this conclusion cannot be correct because, as pointed out in [94], the presence of certain irrelevant interactions neglected in [93] can make the Drude weight vanish, rendering the conductivity finite.

Evidence for a diffusive behavior in Heisenberg spin chains has been claimed in [95]. By doing oxygen NMR in Sr_2CuO_3, Thurber *et al.* were able to separate the contribution from the low-energy modes with $q \approx 0$ to the spin-lattice relaxation rate $1/T_1$. The Luttinger model predicts that $1/(T_1T)$ is given by a magnetic-field-independent constant at low temperatures. However, the experiment suggested that $1/(T_1T)$ diverges with decreasing field as $1/\sqrt{\omega_n} \propto h^{-1/2}$, where ω_n is the nuclear magnetic resonance frequency. This is a signature of diffusive behavior, which is well established in higher dimensions [96]. The frequency dependence of the NMR response is related to the long-time decay of short distance spin correlations, in particular the

self-correlation function $\langle S_j^z(t)S_j^z(0)\rangle$. In one dimension, diffusive behavior is equivalent to a $1/\sqrt{t}$ decay of the self-correlation function. This is not the result expected within the Luttinger model, but the long-time behavior is not necessarily determined by low-energy modes. Apparently, spin diffusion conflicts with the picture of ballistically propagating bosons which is the basis of the Luttinger liquid paradigm. It also seems to contradict the conjecture about ideal transport in integrable spin chains. If correct, this experimental result could change the way we think about excitations of 1D models. Understanding the behavior of time-dependent correlation functions at zero temperature constitutes an important step towards answering these questions.

1.8 Overview

This thesis is a theoretical study of various aspects of the longitudinal dynamical structure factor for the XXZ model at zero temperature. Our goal was to derive analytic formulas for the width, tail and edge singularities of $S^{zz}(q,\omega)$ which are nonperturbative in the anisotropy parameter Δ and therefore hold in the entire critical region of the phase diagram. This could only be accomplished by combining field theory methods with the exact Bethe ansatz solution in ways that had not been explored before.

The next chapters are organized as follows. Chapter 2 focuses mainly on the broadening of the on-shell peak and high-frequency tail of $S^{zz}(q,\omega)$ at finite magnetic field and in the limit of small q. By treating the leading irrelevant operators which account for band curvature effects, I show that the width of the on-shell peak scales as q^2 in the interacting case, similar to the exact result for the XY model. I relate the coefficient of the q^2 dependence to a coupling constant of the low-energy effective model which can be calculated using the Bethe ansatz solution. This provides a formula for the width of $S^{zz}(q,\omega)$ at finite field which is asymptotically exact in the limit

of small q. Another important result in this chapter is that the line shape which arises from adding boson decay processes to the Luttinger model is not a Lorentzian. Within the approximation which neglects dimension-four and higher irrelevant operators, the peak has a rectangular shape with well-defined lower and upper thresholds. These are identified with the energy thresholds for the creation of particle-hole pair excitations in the Bethe ansatz solution. Still in chapter 2, I show that the low-energy effective theory with irrelevant operators can also account for the spectral weight above the upper threshold of the particle-hole continuum. Besides deriving formulas for the high-frequency tail of $S^{zz}(q,\omega)$ at both zero and finite magnetic field, I show that integrability affects the line shape of $S^{zz}(q,\omega)$ at zero field in a noticeable way. This is because the conservation of the energy current operator rules out a boson decay process which, if present in the effective Hamiltonian, would modify the high-frequency tail near the upper threshold of the two-particle continuum. Throughout this chapter, the field theory results are compared with exact form factors for finite chains computed numerically by Jean-Sébastien Caux and Rob Hagemans using the Algebraic Bethe Ansatz. The question of what happens at the thresholds of the two-particle continuum is addressed in chapter 3. I apply the aforementioned analogy with the X-ray edge problem and derive an effective Hamiltonian to study the edge singularities of $S^{zz}(q,\omega)$. The analysis in this chapter is not restricted to low energies or small q. The results are presented first as they appeared in the published version. Details of the calculations can be found in section 3.6. The main result in this chapter is the derivation of exact formulas for the singularity exponents in terms of phase shifts which can be extracted from the Bethe ansatz equations. This approach reproduces the singularities of the two-spinon dynamical structure factor for the Heisenberg chain as a special case. In addition, I show that the edge singularities govern the long-time behavior of the self-correlation function. I prove that the leading term in the long-time asymptotics is not the one given by the Luttinger liquid result,

but involves high-energy particle-hole excitations near the top and bottom of the band. The field theory result is used to interpret numerical results from the time-dependent Density Matrix Renormalization Group computed by Steven R. White. Finally, in chapter 4 I make some concluding remarks and suggestions for future research.

Bibliography

[1] T. Giamarchi, *Quantum Physics in One Dimension* (Clarendon Press, Oxford, 2004).

[2] P. Fazekas, *Lecture Notes on Electron Correlation and Magnetism* (World Scientific, Singapore, 1999).

[3] S. C. Benjamin and S. Bose, Phys. Rev. Lett. **90**, 247901 (2003).

[4] S. Schäffer-Nameki, J. Stat. Mech.: Theory Exp. p. N12001 (2006).

[5] W. Heisenberg, Z. Phys. **49**, 619 (1928).

[6] P. A. M. Dirac, *The Principles of Quantum Mechanics* (Oxford University Press, London, 1947).

[7] P. W. Anderson, Phys. Rev. **86**, 694 (1952).

[8] N. D. Mermin and H. Wagner, Phys. Rev. Lett. **17**, 1133 (1966).

[9] P. C. Hohenberg, Phys. Rev. **158**, 383 (1967).

[10] S. Coleman, Comm. Math. Phys. **31**, 259 (1973).

[11] N. Motoyama, H. Eisaki, and S. Uchida, Phys. Rev. Lett. **76**, 3212 (1996).

[12] P. W. Anderson, Phys. Rev. **115**, 2 (1959).

[13] I. Yamada and H. Onda, Phys. Rev. B **49**, 1048 (1994).

[14] M. B. Stone, D. H. Reich, C. Broholm, K. Lefmann, C. Rischel, C. P. Landee, and M. M. Turnbull, Phys. Rev. Lett. **91**, 037205 (2003).

[15] H. Bethe, Z. Phys. **71**, 205 (1931).

[16] B. Sutherland, *Beautiful Models* (World Scientific, 2004).

[17] E. H. Lieb and W. Liniger, Phys. Rev. **130**, 1605 (1963).

[18] E. H. Lieb and F. Y. Wu, Phys. Rev. Lett. **20**, 1445 (1968).

[19] V. E. Korepin, N. M. Bogoliubov, and A. G. Izergin, *Quantum inverse scattering method and correlation functions* (Cambridge University Press, 1993).

[20] M. Takahashi, *Thermodynamics of one-dimensional solvable problems* (Cambridge University Press, 1999).

[21] J. des Cloizeaux and J. J. Pearson, Phys. Rev. **128**, 2131 (1962).

[22] B. Lake, D. A. Tennant, C. D. Frost, and S. E. Nagler, Nature Materials **4**, 329 (2005).

[23] R. Hagemans and J.-S. Caux, J. Phys. A: Math. Theor. **40**, 14605 (2007).

[24] L. Hulthén, Arkiv Mat. Astron. Fysik **26A**, 1 (1938).

[25] R. B. Griffiths, Phys. Rev. **133**, A768 (1964).

[26] F. Woynarovich and H.-P. Eckle, J. Phys. A: Math. Gen. **20**, L97 (1987).

[27] J. L. Cardy, J. Phys. A: Math. Gen. **17**, L385 (1984).

[28] M. Takahashi, Prog. Theor. Phys. **46**, 401 (1971).

[29] E. Lieb, T. Schultz, and D. Mattis, Ann. Phys. (N.Y) **16**, 407 (1961).

[30] I. Affleck and E. H. Lieb, Lett. Math. Phys. **12**, 57 (1986).

[31] F. D. M. Haldane, Phys. Lett. **93A**, 464 (1983).

[32] I. Affleck, T. Kennedy, E. H. Lieb, and H. Tasaki, Phys. Rev. Lett. **59**, 799 (1987).

[33] F. D. M. Haldane, Phys. Rev. Lett. **61**, 1029 (1988).

[34] I. Affleck, J. Phys.: Condens. Matter **1**, 3047 (1989).

[35] R. Orbach, Phys. Rev. **112**, 309 (1958).

[36] C. N. Yang and C. P. Yang, Phys. Rev. **150**, 321 (1966).

[37] I. Affleck and M. Oshikawa, Phys. Rev. B **60**, 1038 (1999).

[38] B. C. Watson, V. N. Kotov, M. W. Meisel, D. W. Hall, G. E. Granroth, W. T. Montfrooij, S. E. Nagler, D. A. Jensen, R. Backov, M. A. Petruska, et al., Phys. Rev. Lett. **86**, 5168 (2001).

[39] F. Mila, Eur. Phys. J. B **6**, 201 (1998).

[40] K. Totsuka, Phys. Rev. B **57**, 3454 (1998).

[41] L. I. Glazman and A. I. Larkin, Phys. Rev. Lett. **79**, 3736 (1997).

[42] F. Meier, J. Levy, and D. Loss, Phys. Rev. Lett. **90**, 047901 (2003).

[43] D. G. Angelakis, M. F. Santos, and S. Bose, Phys. Rev. A **76**, 031805(R) (2007).

[44] L.-M. Duan, E. Demler, and M. D. Lukin, Phys. Rev. Lett. **91**, 090402 (2003).

[45] T. Kinoshita, T. Wenger, and D. S. Weiss, Nature **440**, 900 (2006).

[46] B. M. McCoy, Phys. Rev. **173**, 531 (1968).

[47] L. D. Landau, Sov. Phys. JETP **8**, 70 (1959).

[48] A. A. Abrikosov, L. P. Gorkov, and I. E. Dzyaloshinski, *Methods of Quantum Field Theory in Statistical Physics* (Dover Publications, New York, 1975).

[49] J. Voit, Rep. Prog. Phys. **57**, 977 (1994).

[50] A. O. Gogolin, A. A. Nersesyan, and A. M. Tsvelik, *Bosonization Approach to Strongly Correlated Systems* (Cambridge University Press, 1999).

[51] J. M. Luttinger, J. Math. Phys. **4**, 1154 (1963).

[52] O. M. Auslaender, A. Yacoby, R. de Picciotto, K. W. Baldwin, L. N. Pfeiffer, and K. W. West, Phys. Rev. Lett. **84**, 1764 (2000).

[53] M. Bockrath, D. H. Cobden, J. Lu, A. G. Rinzler, R. E. Smalley, L. Balents, and P. L. McEuen, Nature **397**, 598 (1999).

[54] A. Schwartz, M. Dressel, G. Grüner, V. Vescoli, L. Degiorgi, and T. Giamarchi, Phys. Rev. B **58**, 1261 (1998).

[55] X. G. Wen, Phys. Rev. B **41**, 12838 (1990).

[56] M. G. K.-V. Pham and P. Lederer, Phys. Rev. B **61**, 16397 (2000).

[57] F. D. M. Haldane, J. Phys. C **14**, 2585 (1981).

[58] A. Luther and I. Peschel, Phys. Rev. B **12**, 3908 (1975).

[59] I. Affleck, J. Phys. A: Math. Gen. **31**, 4573 (1998).

[60] P. Di Francesco, P. Mathieu, and D. Sénéchal, *Conformal Field Theory* (Springer-Verlag, New York, 1997).

[61] I. Affleck, *Fields, Strings and Critical Phenomena* (Les Houches, Session XLIX, Amsterdam: North-Holland, 1988), p. 563, edited by E. Brézin and J. Zinn-Justin.

[62] W. M. C. Foulkes, L. Mitas, R. J. Needs, and G. Rajagopal, Rev. Mod. Phys. **73**, 33 (2001).

[63] U. Schollwöck, Rev. Mod. Phys. **77**, 259 (2005).

[64] S. Eggert, I. Affleck, and M. Takahashi, Phys. Rev. Lett. **73**, 332 (1994).

[65] S. Sachdev, Phys. Rev. B **50**, 13006 (1994).

[66] M. Takigawa, N. Motoyama, H. Eisaki, and S. Uchida, Phys. Rev. Lett. **76**, 4612 (1996).

[67] M. Oshikawa and I. Affleck, Phys. Rev. Lett. **82**, 5136 (1999).

[68] S. M. Lovesey, *Theory of Thermal Neutron Scattering from Condensed Matter* (Clarendon Press, Oxford, 1984).

[69] Y. Endoh, G. Shirane, R. J. Birgeneau, P. M. Richards, and S. L. Holt, Phys. Rev. Lett. **32**, 170 (1973).

[70] I. U. Heilmann, G. Shirane, Y. Endoh, R. J. Birgeneau, and S. L. Holt, Phys. Rev. B **18**, 3530 (1978).

[71] T. Todani and K. Kawasaki, Prog. Theor. Phys. Jpn. **50**, 1216 (1973).

[72] H. J. Mikeska, Phys. Rev. B **12**, 2794 (1975).

[73] J. Sólyom, Adv. Phys. **28**, 201 (1979).

[74] G. Müller, H. Beck, and J. C. Bonner, Phys. Rev. Lett. **43**, 75 (1979).

[75] G. Müller, H. Thomas, H. Beck, and J. C. Bonner, Phys. Rev. B **24**, 1429 (1981).

[76] P. C. Hohenberg and W. F. Brinkman, Phys. Rev. B **10**, 128 (1952).

[77] S. E. Nagler, D. A. Tennant, R. A. Coweley, T. G. Perring, and S. K. Satija, Phys. Rev. B **44**, 12361 (1991).

[78] G. Müller, H. Thomas, M. Puggat, and H. Beck, J. Phys. C: Solid State Phys. **14**, 3399 (1981).

[79] F. D. M. Haldane and M. R. Zirnbauer, Phys. Rev. Lett. **71**, 4055 (1993).

[80] A. H. Bougourzi, M. Couture, and M. Kacir, Phys. Rev. B **54**, R12669 (1996).

[81] M. Jimbo and T. Miwa, *Algebraic analysis of Solvable Lattice Models* (Providence, RI: AMS, 1995).

[82] M. Karbach, G. Müller, A. H. Bougourzi, A. Fledderjohann, and K.-H. Mütter, Phys. Rev. B **55**, 12510 (1997).

[83] J.-S. Caux and R. Hagemans, J. Stat. Mech.: Theory Exp. p. P12013 (2006).

[84] N. Kitanine, J. M. Maillet, and V. Terras, Nucl. Phys. B **554**, 647 (1999).

[85] J.-S. Caux and J. M. Maillet, Phys. Rev. Lett. **95**, 077201 (2005).

[86] K. Samokhin, J. Phys.: Cond. Mat. **10**, L533 (1998).

[87] M. Pustilnik, E. G. Mishchenko, L. I. Glazman, and A. V. Andreev, Phys. Rev. Lett. **91**, 126805 (2003).

[88] M. Pustilnik, M. Khodas, A. Kamenev, and L. I. Glazman, Phys. Rev. Lett. **96**, 196405 (2006).

[89] K. D. Schotte and U. Schotte, Phys. Rev. **182**, 479 (1969).

[90] G. D. Mahan, *Many-Particle Physics* (Kluwer/Plenum, New York, 2000), 3rd ed.

[91] X. Zotos, F. Naef, and P. Prelovšek, Phys. Rev. B **55**, 11029 (1997).

[92] T. Kawamata, N. Takahashi, T. Adachi, T. Noji, K. Kudo, N. Kobayashi, and Y. Koike, J. Phys. Soc. Jpn. **77**, 034607 (2008).

[93] S. Fujimoto and N. Kawakami, Phys. Rev. Lett. **90**, 197202 (2003).

[94] A. Rosch and N. Andrei, Phys. Rev. Lett. **85**, 1092 (2000).

[95] K. R. Thurber, A. W. Hunt, T. Imai, and F. C. Chou, Phys. Rev. Lett. **87**, 247202 (2001).

[96] P. G. de Gennes, J. Phys. Chem. Solids **4**, 223 (1958).

Chapter 2

Dynamical structure factor for small q

The problem of a spin-1/2 chain with anisotropic antiferromagnetic exchange interaction has been extensively studied [97] and constitutes one of the best known examples of strongly correlated one-dimensional systems [98].[1] The XXZ model is integrable and exactly solvable by Bethe Ansatz [99, 100], which makes it possible to calculate exact ground state properties as well as thermodynamic quantities. At the same time, it exhibits a critical regime as a function of the anisotropy parameter, in which the system falls into the universality class of the Luttinger liquids. The long distance asymptotics of correlation functions can then be calculated by applying field theory methods. The combination of field theory and Bethe Ansatz has proven quite successful in explaining low energy properties of spin chain compounds such as Sr_2CuO_3 and $KCuF_3$ [101].

Recently, most of the interest in the XXZ model has turned to the study of dynamical correlation functions. The relevant quantities for spin chains are the dynamical structure factors $S^{\mu\mu}(q,\omega)$, $\mu = x, y, z$, defined as the Fourier transform of the spin-spin correlation functions [102]. These are directly probed by inelastic neutron scattering experiments [103, 104]. They are also probed indirectly by nuclear magnetic resonance [105], since the spin lattice relaxation rate is proportional to the integral of the transverse structure

[1] A version of this chapter has been published. R. G. Pereira, J. Sirker, J.-S. Caux, R. Hagemans, J. M. Maillet, S. R. White and I. Affleck. Dynamical structure factor at small q for the XXZ spin-1/2 chain. J. Stat. Mech.: Theory Exp. (2007) P08022. Copyright (2007) by the Institute of Physics.

factor over momentum [106, 107].

Even though one can use the Bethe Ansatz to construct the exact eigenstates, the evaluation of matrix elements, which still need to be summed up in order to obtain the correlation functions, turns out to be very complicated in general. In the last ten years significant progress has been made with the help of quantum group methods [108]. It is now possible to write down analytical expressions for the form factors for the class of two-spinon excitations for the Heisenberg chain (the isotropic point) at zero field [109, 110, 111], as well as for four-spinon ones [112, 113, 114]. No such expressions are available for general anisotropy in the gapless regime or for finite magnetic field, but in those cases the form factors can be expressed in terms of determinant formulas [115, 116, 117] which can then be evaluated numerically for finite chains for two-particle states [118, 119, 120] or for the general multiparticle contributions throughout the Brillouin zone [117, 121].

From a field theory standpoint, dynamical correlations can be calculated fairly easily using bosonization [122]. However, this approach is only asymptotically exact in the limit of very low energies and relies on the approximation of linear dispersion for the elementary excitations. In some cases, the main features of a dynamical response depend on more detailed information about the excitation spectrum of the system at finite energies – namely the breaking of Lorenz invariance by band curvature effects. That poses a problem to the standard bosonization approach, in which nonlinear dispersion and interaction effects cannot be accommodated simultaneously. For that reason, a lot of effort has been put into understanding 1D physics beyond the Luttinger model [123, 124, 125, 126, 127, 128, 129, 130, 131, 132].

In particular, using the bosonization prescription one can relate the longitudinal dynamical structure factor $S^{zz}(q,\omega)$ at small momentum q to the spectral function of the bosonic modes of the Luttinger model. In the linear dispersion approximation, the conventional answer is that $S^{zz}(q,\omega)$ is a delta function peak at the energy carried by the noninteracting bosons [98]. As in

the higher-dimensional counterparts, the broadening of the peak is a signature of a finite lifetime. The problem of calculating the actual line shape of $S^{zz}(q,\omega)$ at small q is thus related to the fundamental question of the decay of elementary excitations in 1D.

In the bosonization approach, interactions are included exactly, but band curvature effects must be treated perturbatively. All the difficulties stem from the fact that band curvature operators introduce interactions between the bosons and ruin the exact solvability of the Luttinger model. To make things worse, perturbation theory in those operators breaks down near the mass shell of the bosonic excitations [133] and no proper resummation scheme is known to date. The best alternative seems to be guided by the fermionic approach, which treats band curvature exactly but applies perturbation theory in the interaction [124].

In this chapter we address this question using both bosonization and Bethe Ansatz. Our goal is to make predictions about $S^{zz}(q,\omega)$ that are non-perturbative in the interaction (*i.e.*, anisotropy) parameter and are therefore valid in the entire gapless regime of the XXZ model (including the Heisenberg point). We focus on the finite field case, which in the bosonization approach is described by a simpler class of irrelevant operators. To go beyond the weakly interacting regime we can resort to the Bethe Ansatz equations in the thermodynamic limit to calculate the exact coupling constants of the low energy effective model. Our analysis is supported by another type of Bethe Ansatz based method, which calculates the exact form factors for finite chains. This provides a nontrivial consistency check of our results.

The outline is as follows. In section 2.1, we introduce the longitudinal dynamical structure factor for the XXZ model in a finite magnetic field and review the exact solution for the XY model. In section 2.2 we describe the effective bosonic model and explain how to fix the coupling constants of the irrelevant operators. Section 2.3 provides a short description of the Bethe Ansatz framework which is relevant for our analysis. In section 2.4, we show

how to obtain the broadening of $S^{zz}(q,\omega)$ in a finite magnetic field both from field theory and Bethe Ansatz and compare our formula with the exact form factors for finite chains. In section 2.5 we present a more detailed derivation of the high-frequency tail of $S^{zz}(q,\omega)$ reported in [128]. The zero field case is briefly addressed in section 2.6. Finally, we check the sum rules for the numerical results in section 2.7.

2.1 XXZ model

We consider the XXZ spin-1/2 chain in a magnetic field

$$H = J\sum_{j=1}^{N}\left[S_j^x S_{j+1}^x + S_j^y S_{j+1}^y + \Delta S_j^z S_{j+1}^z - hS_j^z\right]. \tag{2.1}$$

Here, J is the exchange coupling, Δ is the anisotropy parameter, h is the magnetic field in units of J and N is the number of sites in the chain with periodic boundary conditions. We focus on the critical regime (given by $-1 < \Delta \leq 1$ for $h = 0$). We are interested in the longitudinal dynamical structure factor at zero temperature

$$S^{zz}(q,\omega) = \frac{1}{N}\sum_{j,j'=1}^{N} e^{-iq(j-j')}\int_{-\infty}^{+\infty} dt\, e^{i\omega t}\left\langle S_j^z(t)\, S_{j'}^z(0)\right\rangle, \tag{2.2}$$

where q takes the discrete values $q = 2\pi n/N$, $n \in \mathbb{Z}$. It is instructive to write down the Lehmann representation for $S^{zz}(q,\omega)$

$$S^{zz}(q,\omega) = \frac{2\pi}{N}\sum_{\alpha}\left|\left\langle 0\left|S_q^z\right|\alpha\right\rangle\right|^2 \delta\left(\omega - E_\alpha + E_{GS}\right), \tag{2.3}$$

where $S_q^z = \sum_j S_j^z e^{-iqj}$, $|\alpha\rangle$ is an eigenstate with energy E_α and E_{GS} is the ground state energy. The matrix elements $\left\langle 0\left|S_q^z\right|\alpha\right\rangle$ are called form factors. We denote by $F^2 \equiv \left|\left\langle 0\left|S_q^z\right|\alpha\right\rangle\right|^2$ the transition probabilities that appear

in (2.3). For a finite system, $S^{zz}(q,\omega)$ is a sum of delta function peaks at the energies of the eigenstates with fixed momentum q. In this sense, $S^{zz}(q,\omega)$ provides direct information about the excitation spectrum of the spin chain. In the thermodynamic limit $N \to \infty$, the spectrum is continuous and $S^{zz}(q,\omega)$ becomes a smooth function of q and ω. Eq. (2.3) also implies that $S^{zz}(q,\omega)$ is real and positive and can be expressed as a spectral function

$$S^{zz}(q,\omega) = -2\theta(\omega)\,\mathrm{Im}\chi^{ret}(q,\omega)\,, \tag{2.4}$$

$\chi^{ret}(q,\omega)$ is the retarded spin-spin correlation function and can be obtained from the Matsubara correlation function

$$\chi(q,i\omega_n) = -\frac{1}{N}\sum_{j,j'=1}^{N} e^{-iq(j-j')}\int_0^\beta d\tau\, e^{i\omega_n\tau}\left\langle S_j^z(\tau)\,S_{j'}^z(0)\right\rangle, \tag{2.5}$$

where β is the inverse temperature, by the analytical continuation $i\omega_n \to \omega + i\varepsilon$.

It is well known that the one-dimensional XXZ model is equivalent to interacting spinless fermions on the lattice. The mapping is realized by the Jordan-Wigner transformation

$$\begin{aligned} S_j^z &\to n_j - \frac{1}{2}, \\ S_j^+ &\to (-1)^j\, c_j^\dagger e^{i\pi\phi_j}, \\ S_j^- &\to (-1)^j\, c_j e^{-i\pi\phi_j}, \end{aligned} \tag{2.6}$$

where c_j is the annihilation operator for fermions at site j, $n_j = c_j^\dagger c_j$ and $\phi_j = \sum_{\ell=1}^{j-1} n_\ell$. In terms of fermionic operators, the Hamiltonian (2.1) is written as

$$H = J\sum_{j=1}^{N}\left[-\frac{1}{2}\left(c_j^\dagger c_{j+1} + h.c.\right) - h\left(c_j^\dagger c_j - \frac{1}{2}\right)\right.$$

$$+\Delta\left(n_j-\frac{1}{2}\right)\left(n_{j+1}-\frac{1}{2}\right)\Bigg]. \tag{2.7}$$

2.1.1 Exact solution for the XY model

One case of special interest is the XX point $\Delta = 0$, at which (2.7) reduces to a free fermion model [134]. As the free fermion point will serve as a guide for the resummation of the bosonic theory, we reproduce the solution in detail here. For $\Delta = 0$ the Hamiltonian (2.7) can be easily diagonalized by introducing the operators in momentum space

$$c_p = \frac{1}{\sqrt{N}}\sum_{j=1}^{N} e^{-ipj} c_j. \tag{2.8}$$

with $p = 2\pi n/N$, $n \in \mathbb{Z}$, for periodic boundary conditions. The free fermion Hamiltonian is then

$$H_0 = \sum_p \epsilon_p c_p^\dagger c_p, \tag{2.9}$$

where $\epsilon_p = -J\left(\cos p + h\right)$ is the fermion dispersion. In the fermionic language, the dynamical structure factor reads

$$\begin{aligned} S^{zz}\left(q,\omega\right) &= \frac{1}{N}\int_{-\infty}^{+\infty} dt\, e^{i\omega t}\left\langle n_q\left(t\right) n_{-q}\left(0\right)\right\rangle \\ &= \frac{2\pi}{N}\sum_\alpha \left|\left\langle 0\left|n_q\right|\alpha\right\rangle\right|^2 \delta\left(\omega - E_\alpha + E_{GS}\right), \end{aligned} \tag{2.10}$$

where $n_q = \sum_j e^{-iqj} n_j = \sum_p c_p^\dagger c_{p+q}$.

We construct the ground state $|0\rangle$ by filling all the single-particle states up to the Fermi momentum k_F. The latter is determined by the condition $\epsilon_{k_F} = 0$, which gives

$$k_F = \arccos\left(-h\right) = \pi\left(\frac{1}{2}+\sigma\right), \tag{2.11}$$

where $\sigma \equiv \left\langle S_j^z \right\rangle = \langle n_j \rangle - \frac{1}{2}$ is the magnetization per site. We can also describe the excited states in terms of particle-hole excitations created on the Fermi sea. The only nonvanishing form factors appearing in $S^{zz}(q,\omega)$ are those for excited states with only one particle-hole pair carrying total momentum q: $|\alpha\rangle = c_{p+q}^\dagger c_p |0\rangle$. The form factors are simply

$$\left\langle 0 \left| S_q^z \right| \alpha \right\rangle = \theta\left(k_F - |p|\right) \theta\left(|p+q| - k_F\right). \tag{2.12}$$

For a finite system there are $qN/2\pi$ states with form factor 1, corresponding to different choices for the hole momentum p below the Fermi surface. In the limit $N \to \infty$, (2.10) reduces to the integral

$$\begin{aligned} S^{zz}(q,\omega) &= \int_{-\pi}^{\pi} dp\, \theta\left(k_F - |p|\right) \theta\left(|p+q| - k_F\right) \delta\left(\omega - \epsilon_{p+q} + \epsilon_p\right) \\ &= \frac{\theta\left(\omega - \omega_L(q)\right) \theta\left(\omega_U(q) - \omega\right)}{\left(d\omega_{pq}/dp\right)\big|_{\omega_{pq}=\omega}}, \end{aligned} \tag{2.13}$$

where $\omega_{pq} = \epsilon_{p+q} - \epsilon_p$ is the energy of the particle-hole pair and $\omega_L(q)$ and $\omega_U(q)$ are the lower and upper thresholds of the two-particle spectrum, respectively. For the cosine dispersion, we have

$$\omega_{pq} = 2J \sin\left(p + \frac{q}{2}\right) \sin\frac{q}{2}. \tag{2.14}$$

The expressions for the lower and upper thresholds depend on the proximity to half-filling (zero magnetic field). Here we shall restrict ourselves to finite field and small momentum $|q| \ll k_F$. More precisely, we impose the condition

$$|q| < |2k_F - \pi| = 2\pi|\sigma|. \tag{2.15}$$

For $k_F < \pi/2$ ($\sigma < 0$), we have

$$\omega_L(q) = 2J \sin\frac{|q|}{2} \sin\left(k_F - \frac{|q|}{2}\right), \tag{2.16}$$

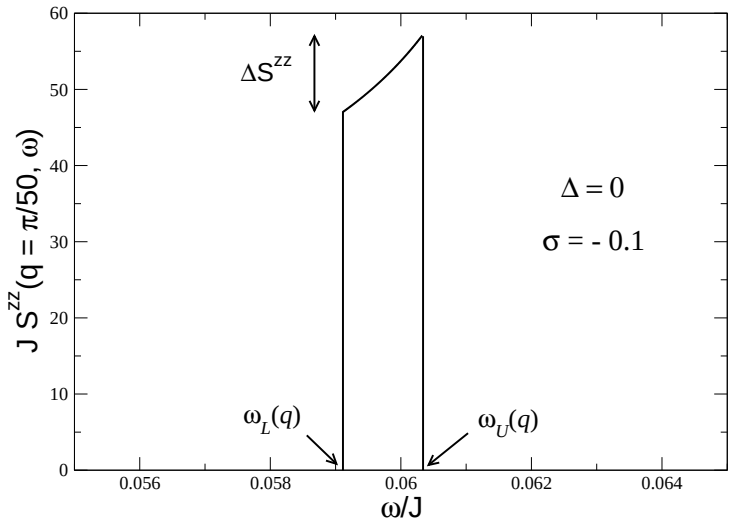

Figure 2.1: Exact dynamical structure factor $S^{zz}(q,\omega)$ for the free fermion point $\Delta = 0$. For this graph we set $\sigma = -0.1$ ($k_F = 2\pi/5$) and $q = \pi/50$.

$$\omega_U(q) \quad = \quad 2J \sin\frac{|q|}{2} \sin\left(k_F + \frac{|q|}{2}\right). \tag{2.17}$$

If $k_F > \pi/2$, the above expressions for $\omega_L(q)$ and $\omega_U(q)$ are exchanged. Hereafter we take $k_F < \pi/2$ and $q > 0$. It follows from (2.16) and (2.17) that $S^{zz}(q,\omega)$ for fixed q is nonzero within an energy interval of width

$$\delta\omega_q = \omega_U(q) - \omega_L(q) = 4J \cos k_F \sin^2\left(\frac{q}{2}\right) \approx (J \cos k_F)\, q^2 \tag{2.18}$$

for small q. In fact, we can calculate $S^{zz}(q,\omega)$ explicitly using (2.13). The result is

$$S^{zz}(q,\omega) = \frac{\theta(\omega - \omega_L(q))\,\theta(\omega_U(q) - \omega)}{\sqrt{\left(2J \sin\frac{q}{2}\right)^2 - \omega^2}}, \tag{2.19}$$

which is illustrated in figure 2.1. Note that, although the form factors are constant, $S^{zz}(q,\omega)$ is peaked at the upper threshold because of the larger density of states. The values of $S^{zz}(q,\omega)$ at the lower and upper thresholds

are both finite

$$S^{zz}\left(q,\omega\to\omega_{L,U}\left(q\right)\right)=\left[2J\sin\frac{q}{2}\cos\left(k_F\mp\frac{q}{2}\right)\right]^{-1}. \tag{2.20}$$

In the small-q limit, only excitations created around the Fermi surface contribute to $S^{zz}\left(q,\omega\right)$. For this reason, a simplifying approach would be to expand the fermion dispersion around the Fermi points

$$\epsilon_k^{R,L}\approx\pm v_F k+\frac{k^2}{2m}\mp\frac{\gamma k^3}{6}+\ldots, \tag{2.21}$$

where $k\equiv p\mp k_F$ for right (R) or left (L) movers, $v_F=J\sin k_F$ is the Fermi velocity, $m=\left(J\cos k_F\right)^{-1}$ is the effective mass at the Fermi level and $\gamma=J\sin k_F$. The free fermion Hamiltonian is then approximated by

$$H_0=\sum_{k=-\infty}^{\infty}\left[\epsilon_k^R:c_{kR}^\dagger c_{kR}:+\epsilon_k^L:c_{kL}^\dagger c_{kL}:\right], \tag{2.22}$$

where $c_{kR,L}$ are the annhilation operators for fermions with momentum around $\pm k_F$, respectively, and $::$ denotes normal ordering with respect to the ground state. If we retain only the linear term in the expansion of Eq. (2.21), ω_{kq} turns out to be independent of k. This means that all particle-hole excitations are degenerate, and $S^{zz}\left(q,\omega\right)$ is given by a single delta function peak at the corresponding energy $\omega=v_F q$

$$S^{zz}\left(q,\omega\right)=q\,\delta\left(\omega-v_F q\right). \tag{2.23}$$

This is a direct consequence of the Lorentz invariance of the model with linear dispersion. In order to get the broadening of $S^{zz}\left(q,\omega\right)$, we must account for the nonlinearity of the dispersion, *i.e.*, band curvature at the Fermi level. If

we keep the next (quadratic) term in $\epsilon_k^{R,L}$, we find

$$S^{zz}(q,\omega) = \frac{m}{q}\,\theta\left(\frac{q^2}{2m} - |\omega - v_F q|\right). \tag{2.24}$$

We note that this flat distribution of spectral weight is a good approximation to the result in (2.18) and (2.19) in the limit $q \ll \cot k_F$, in the sense that the difference between the values of $S^{zz}(q,\omega)$ at the lower and upper thresholds is small compared to the average height of the peak (see figure 2.1). This difference stems from the energy dependence of the density of states factor $1/(d\omega_{pq}/dp)|_{\omega_{pq}=\omega}$, which is recovered if we keep the k^3 term in the dispersion. It is easy to verify that for $q \ll \cot k_F$ ($\gamma m q \ll 1$)

$$\Delta S^{zz} \equiv S^{zz}(q,\omega_U(q)) - S^{zz}(q,\omega_L(q)) \approx \gamma m^2. \tag{2.25}$$

ΔS^{zz} is independent of q, therefore $\Delta S^{zz}/(m/q) \sim q$ vanishes as $q \to 0$. This means that if we compare $S^{zz}(q,\omega)$ for different values of q – taking into account that $\delta\omega_q \sim q^2$ and $S^{zz}(q,\omega) \sim 1/q$ inside the peak and rescaling the functions accordingly – the *rescaled* function becomes flatter as $q \to 0$. On the other hand, the slope $\partial S^{zz}/\partial\omega$ near the center of the peak diverges as $q \to 0$.

The thresholds for the two-particle continuum,

$$\omega_{U,L}(q) \approx v_F q \pm \frac{q^2}{2m}, \tag{2.26}$$

are easy to interpret. For $k_F < \pi/2$, the lower threshold corresponds to creating a hole at the state with momentum q below k_F (a "deep hole") and placing the particle right above the Fermi surface, whereas the upper one corresponds to the excitation composed of a "high-energy particle" at $k_F + q$ and a hole right at the Fermi surface [124].

Alternatively, we could have calculated the density-density correlation

function, which for $\Delta = 0$ is given by the fermionic bubble

$$\chi(q, i\omega) = \int \frac{dk}{2\pi} \frac{\theta(-k)\,\theta(k+q)}{i\omega - \epsilon_{k+q} + \epsilon_k} - (\omega \to -\omega)\,. \tag{2.27}$$

Using the quadratic dispersion $\epsilon_k \approx v_F k + k^2/2m$, we find

$$\chi(q, i\omega) = \frac{m}{2\pi q} \log\left(\frac{i\omega - v_F q + q^2/2m}{i\omega - v_F q - q^2/2m}\right) - (\omega \to -\omega)\,. \tag{2.28}$$

The result (2.24) is then obtained by taking the imaginary part of $\chi^{ret}(q, \omega)$ according to (2.4).

2.2 Low energy effective Hamiltonian

2.2.1 The free boson Hamiltonian

For a general anisotropy $\Delta \neq 0$, the Hamiltonian (2.7) describes interacting spinless fermions. The standard approach to study the low-energy (long-wavelength) limit of correlation functions of interacting one-dimensional systems is to use bosonization to map the problem to a free boson model – the Luttinger model [97]. This approach has the advantage of treating interactions exactly. As a first step, one introduces the fermionic field operators $\psi_{R,L}(x)$

$$c_j \to \psi(x = j) = e^{ik_F x}\psi_R(x) + e^{-ik_F x}\psi_L(x)\,, \tag{2.29}$$

$$\psi_{R,L}(x) \;=\; \frac{1}{\sqrt{L}} \sum_{k=-\Lambda}^{+\Lambda} c_{kR,L} e^{\pm ikx}, \tag{2.30}$$

where $L = N$ is the system size (we set the lattice spacing to 1) and $\Lambda \ll k_F$ is a momentum cutoff. In the continuum limit, the kinetic energy part of the

Hamiltonian in (2.22) can be written as

$$\begin{aligned} H_0 &= \int_0^L dx \left\{ : \psi_R^\dagger \left[v_F \left(-i\partial_x\right) + \frac{\left(-i\partial_x\right)^2}{2m} + \ldots \right] \psi_R : \right. \\ &\quad \left. + : \psi_L^\dagger \left[v_F \left(-i\partial_x\right) + \frac{\left(-i\partial_x\right)^2}{2m} + \ldots \right] \psi_L : \right\}. \end{aligned} \tag{2.31}$$

The $1/m$ term is usually dropped using the argument that it has a higher dimension and is irrelevant in the sense of the renormalization group. However, it introduces corrections to the Luttinger liquid fixed point which are associated with band curvature effects. Similarly, if we write the interaction term in (2.7) in the continuum limit, we get (following [98])

$$\begin{aligned} H_{int} &= \Delta J \int_0^L dx \; : \psi^\dagger \left(x\right) \psi \;\; \left(x\right) : : \psi^\dagger \left(x+1\right) \psi \;\; \left(x+1\right) : \\ &= \Delta J \int_0^L dx \; \{ \rho_R \left(x\right) \rho_R \left(x+1\right) + \rho_L \left(x\right) \rho_L \left(x+1\right) \\ &\quad + \rho_R \left(x\right) \rho_L \left(x+1\right) + \rho_L \left(x\right) \rho_R \left(x+1\right) \\ &\quad + \left[e^{i2k_F} \psi_R^\dagger \left(x\right) \psi_L \left(x\right) \psi_L^\dagger \left(x+1\right) \psi_R \left(x+1\right) + h.c. \right] \\ &\quad + \left[e^{-i2k_F(2x+1)} \psi_R^\dagger \left(x\right) \psi_L \left(x\right) \psi_R^\dagger \left(x+1\right) \psi_L \left(x+1\right) + h.c. \right] \Big\}, \end{aligned} \tag{2.32}$$

where $\rho_{R,L} \equiv : \psi_{R,L}^\dagger \psi_{R,L} :$. The last term corresponds to Umklapp scattering and is oscillating except at half-filling (where $4k_F = 2\pi$). We will neglect that term for the finite field case, but will restore it in section 2.6 when we discuss the zero field case.

We now use Abelian bosonization and write the fermion fields as

$$\psi_{R,L} \left(x\right) \sim \frac{1}{\sqrt{2\pi\alpha}} \, e^{-i\sqrt{2\pi}\phi_{R,L}(x)}, \tag{2.33}$$

where $\alpha \sim k_F^{-1}$ is a short-distance cutoff and $\phi_{R,L}$ are the right and left

components of a bosonic field $\tilde{\phi}$ and its dual field $\tilde{\theta}$

$$\tilde{\phi} = \frac{\phi_L - \phi_R}{\sqrt{2}}, \tag{2.34}$$

$$\tilde{\theta} = \frac{\phi_L + \phi_R}{\sqrt{2}}, \tag{2.35}$$

which satisfy $[\tilde{\phi}(x), \partial_{x'}\tilde{\theta}(x')] = i\delta(x - x')$. The density of right- and left-moving fermions can be shown to be related to the derivative of the bosonic fields

$$\rho_{R,L} \sim \mp \frac{1}{\sqrt{2\pi}} \partial_x \phi_{R,L}, \tag{2.36}$$

so that

$$n(x) \sim \frac{1}{2} + \sigma + \frac{1}{\sqrt{\pi}} \partial_x \tilde{\phi} + \frac{1}{2\pi\alpha} \cos\left(\sqrt{4\pi}\tilde{\phi} - 2k_F x\right). \tag{2.37}$$

Here we are interested in the uniform (small q) part of the fluctuation of $S_j^z \sim n(x)$, which is proportional to the derivative of the bosonic field $\tilde{\phi}$. Bosonizing the linear term in the kinetic energy (2.31), we find

$$\begin{aligned} H_0^{lin} &= \int_0^L dx\, i v_F \left(: \psi_R^\dagger \partial_x \psi_R : - : \psi_L^\dagger \partial_x \psi_L : \right) \\ &= \frac{v_F}{2} \int_0^L dx \left[(\partial_x \phi_R)^2 + (\partial_x \phi_L)^2 \right]. \end{aligned} \tag{2.38}$$

The terms that appear in the interaction part are

$$\begin{aligned} \rho_{R,L}(x)\, \rho_{R,L}(x+1) &= \frac{1}{2\pi} (\partial_x \phi_{R,L})^2, \\ \rho_R(x)\, \rho_L(x+1) &= -\frac{1}{2\pi} \partial_x \phi_R \partial_x \phi_L, \end{aligned}$$

$$\begin{gathered} \psi_R^\dagger(x)\, \psi_L(x)\, \psi_L^\dagger(x+1)\, \psi_R(x+1) = \\ -\tfrac{\cos(2k_F)}{2\pi} (\partial_x \phi_R - \partial_x \phi_L)^2 + \tfrac{\sin(2k_F)}{3\sqrt{2\pi}} (\partial_x \phi_R - \partial_x \phi_L)^3 + \ldots, \end{gathered} \tag{2.39}$$

where we have set $\alpha = 1$ (equal to the level spacing; see [98]). If we keep only the marginal operators (quadratic in $\partial_x \phi_{R,L}$), we get an exactly solvable model

$$H_{LL} = \frac{v_F}{2} \int dx \left\{ \left(1 + \frac{g_4}{2\pi v_F}\right) \left[(\partial_x \phi_R)^2 + (\partial_x \phi_L)^2\right] - \frac{g_2}{\pi v_F} \partial_x \phi_L \partial_x \phi_R \right\}, \tag{2.40}$$

where $g_2 = g_4 = 2J\Delta[1 - \cos(2k_F)] = 4J\Delta \sin^2 k_F$. The Hamiltonian (2.40) can be rewritten in the form

$$H_{LL} = \frac{1}{2} \int dx \left[vK \left(\partial_x \tilde{\theta}\right)^2 + \frac{v}{K} \left(\partial_x \tilde{\phi}\right)^2 \right], \tag{2.41}$$

where v (the renormalized velocity) and K (the Luttinger parameter) are given by

$$v = v_F \sqrt{\left(1 + \frac{g_4}{2\pi v_F}\right)^2 - \left(\frac{g_2}{2\pi v_F}\right)^2} \approx v_F \left(1 + \frac{2\Delta}{\pi} \sin k_F\right), \tag{2.42}$$

$$K = \sqrt{\frac{1 + \frac{g_4}{2\pi v_F} - \frac{g_2}{2\pi v_F}}{1 + \frac{g_4}{2\pi v_F} + \frac{g_2}{2\pi v_F}}} \approx 1 - \frac{2\Delta}{\pi} \sin k_F. \tag{2.43}$$

Expressions (2.42) and (2.43) are approximations valid in the limit $\Delta \ll 1$. The Luttinger model describes free bosons that propagate with velocity v and is the correct low energy fixed point for the XXZ chain for any value of Δ and h in the gapless regime. However, the correct values of v and K for finite Δ must be obtained by comparison with the exact Bethe Ansatz (BA) solution. In the case $h = 0$, the BA equations can be solved analytically and yield

$$v(\Delta, h = 0) = \frac{J\pi}{2} \frac{\sqrt{1 - \Delta^2}}{\arccos \Delta}, \tag{2.44}$$

$$K(\Delta, h = 0) = \frac{\pi}{2(\pi - \arccos \Delta)}. \tag{2.45}$$

There are also analytical expressions for $h \approx 0$ and h close to the critical field [135]. For arbitrary fields, one has to solve the BA equations numerically in order to get the exact v and K.

The Luttinger parameter in the Hamiltonian (2.41) can be absorbed by performing a canonical transformation that rescales the fields in the form $\tilde{\phi} \to \sqrt{K}\phi$ and $\tilde{\theta} \to \theta/\sqrt{K}$. H_{LL} then reads

$$H_{LL} = \frac{v}{2} \int dx \left[(\partial_x \theta)^2 + (\partial_x \phi)^2 \right]. \tag{2.46}$$

We can also define the right and left components of these rescaled bosonic fields by

$$\varphi_{R,L} = \frac{\theta \mp \phi}{\sqrt{2}}. \tag{2.47}$$

These are related to $\phi_{R,L}$ by a Bogoliubov transformation. An explicit mode expansion (neglecting zero mode operators) is

$$\varphi_{R,L}(x,\tau) = \sum_{q>0} \frac{1}{\sqrt{qL}} \left[a_q^{R,L} e^{-q(v\tau \mp ix)} + a_q^{R,L\dagger} e^{q(v\tau \mp ix)} \right], \tag{2.48}$$

where $a_q^{R,L}$ are bosonic operators obeying $[a_q^{R,L}, a_{q'}^{R,L\dagger}] = \delta_{qq'}$ and $q = 2\pi n/L$, $n \in \mathbb{Z}$, for periodic boundary conditions. The Hamiltonian (2.46) is then diagonal in the boson operators

$$H_{LL} = \sum_{q>0} vq \left[a_q^{R\dagger} a_q^R + a_q^{L\dagger} a_q^L \right]. \tag{2.49}$$

We can calculate the propagators for the free fields $\partial_x \varphi_{R,L}$ from the mode expansion in (2.48). In real space, for $L \to \infty$ and zero temperature ($\beta \to \infty$), the propagators read

$$D_{R,L}^{(0)}(x,\tau) = \langle \partial_x \varphi_{R,L}(x,\tau)\, \partial_x \varphi_{R,L}(0,0) \rangle_0 = \frac{1}{2\pi} \frac{1}{(v\tau \mp ix)^2}. \tag{2.50}$$

In momentum space,

$$\begin{aligned} D_{R,L}^{(0)}(q, i\omega_n) &\equiv -\int_0^L dx\, e^{-iqx} \int_0^\beta d\tau\, e^{i\omega_n \tau} D_{R,L}^{(0)}(x, \tau) \\ &= \frac{\pm q}{i\omega_n \mp vq}. \end{aligned} \tag{2.51}$$

In order to calculate the dynamical structure factor defined in (2.2), we express the fluctuation of the spin operator in terms of the bosonic field ϕ. From (2.6) and (2.37), we have

$$S_j^z \sim \sqrt{\frac{K}{\pi}} \partial_x \phi. \tag{2.52}$$

In the continuum limit,

$$\begin{aligned} \chi(q, i\omega_n) &= -\frac{K}{\pi} \int_0^L dx\, e^{-iqx} \int_0^\beta d\tau\, e^{i\omega_n \tau} \langle \partial_x \phi(x, \tau)\, \partial_x \phi(0, 0) \rangle_0 \\ &= \frac{K}{2\pi} D^{(0)}(q, i\omega_n), \end{aligned} \tag{2.53}$$

where $D^{(0)}(q, i\omega_n)$ is the free boson propagator (for the $\partial_x \phi$ field)

$$D^{(0)}(q, i\omega) \equiv D_R^{(0)}(q, i\omega) + D_L^{(0)}(q, i\omega) = \frac{2vq^2}{(i\omega)^2 - (vq)^2}. \tag{2.54}$$

It follows that the retarded correlation function is

$$\chi^{ret}(q, \omega) = \frac{Kq}{2\pi} \left[\frac{1}{\omega - vq + i\eta} - \frac{1}{\omega + vq + i\eta} \right]. \tag{2.55}$$

Finally, using (2.4), the dynamical structure factor for the free boson model is ($q > 0$)

$$S^{zz}(q, \omega) = Kq\, \delta(\omega - vq). \tag{2.56}$$

The result in (2.56) is analogous to (2.23). Since the Luttinger model exhibits Lorentz invariance, $S^{zz}(q, \omega)$ is a delta function peak at the energy carried

by the single boson with momentum q. This solution should be asymptotically exact in the limit $q \to 0$, which means that any corrections to it must be suppressed by higher powers of momentum. However, the free boson result misses many of the features that the complete solution must have. For example, the exact solution for the XX point suggests a broadening of the delta peak with a width $\delta\omega_q \sim q^2$. Like in that case, it is necessary to incorporate information about band curvature at the Fermi level by keeping the quadratic term in the fermion dispersion in order to get a finite width for $S^{zz}(q,\omega)$. As we shall discuss in the next section, the problem is that such a term is mapped via bosonization onto a boson-boson interaction term. Even though the interaction term is irrelevant, finite-order perturbation theory in these operators leads to a singular frequency dependence close to $\omega = vq$. It turns out that broadening the delta function peak within a field theory approach is a not an easy task. A complete solution that recovers the scaling $\delta\omega_q \sim q^2$ requires summing an infinite series of diagrams, as we will point out in section 2.4. Another feature expected for $S^{zz}(q,\omega)$ when $\Delta \neq 0$ is a high-frequency tail associated with multiple particle-hole excitations. This tail can be calculated in the region $\delta\omega_q \ll \omega - vq \ll J$ by lowest-order perturbation theory in the fermionic interaction ($\propto \Delta$) starting from a model of free fermions with quadratic dispersion [123]. In section 2.5 we obtain this result by including fermionic interactions exactly (finite Δ) and doing perturbation theory in the band curvature terms.

2.2.2 Irrelevant operators

In order to go beyond the Luttinger model, we need to treat the irrelevant operators that break Lorenz invariance. There are two sources of such terms: band curvature terms, which are quadratic in fermions but involve higher derivatives, and irrelevant interaction terms [129]. The first type appeared in (2.31) and corresponds to the k^2 term in the expansion of the fermion

dispersion

$$\delta\mathcal{H}_{bc} = -\frac{1}{2m}\left(:\psi_R^\dagger\partial_x^2\psi_R: + :\psi_L^\dagger\partial_x^2\psi_L:\right). \tag{2.57}$$

We derive the bosonized version of a general band curvature term in the following way (see [136]). We define the operator

$$\begin{aligned} F(x,\epsilon) &= \psi_R^\dagger\left(x+\frac{\epsilon}{2}\right)\psi_R\left(x-\frac{\epsilon}{2}\right) \\ &= \sum_{k=0}^{\infty}\frac{1}{k!}\left(\frac{\epsilon}{2}\right)^k\partial_x^k\psi_R^\dagger\sum_{l=0}^{\infty}\frac{1}{l!}\left(-\frac{\epsilon}{2}\right)^l\partial_x^l\psi_R \\ &= \sum_{n=0}^{\infty}\left(-\frac{\epsilon}{2}\right)^n\psi_R^\dagger\partial_x^n\psi_R\sum_{k=0}^{n}\frac{1}{k!(n-k)!}+\ldots, \end{aligned} \tag{2.58}$$

where $\ldots$ is a total derivative. Organizing by powers of ϵ, we can write

$$F(x,\epsilon)=\sum_{n=0}^{\infty}\frac{(-1)^n}{n!}\epsilon^n F^{(n)}(x), \tag{2.59}$$

where

$$F^{(n)}(x)=\psi_R^\dagger\partial_x^n\psi_R. \tag{2.60}$$

According to (2.33), we have

$$\psi_R\sim\frac{1}{\sqrt{2\pi\alpha}}e^{-i\sqrt{2\pi}\phi_R}\sim\frac{1}{\sqrt{L}}e^{-i\sqrt{2\pi}\phi_R^+}e^{-i\sqrt{2\pi}\phi_R^-}, \tag{2.61}$$

where $\phi_R^\pm$ are the creation and annihilation parts of $\phi_R(x) = \phi_R^+(x) + \phi_R^-(x)$ and we have used the identity $e^{A+B}=e^Ae^Be^{-[A,B]/2}$ for $[[A,B],A] = [[A,B],B]=0$, with

$$\left[\phi_R^-(x),\phi_R^+(y)\right]\approx-\frac{1}{2\pi}\log\left[-\frac{2\pi i}{L}(x-y+i\alpha)\right], \tag{2.62}$$

for large L. Then we express $F(x,\epsilon)$ in terms of the bosonic fields

$$F(x,\epsilon) = \frac{1}{L} e^{i\sqrt{2\pi}\phi_R^+(x+\epsilon/2)} e^{i\sqrt{2\pi}\phi_R^-(x+\epsilon/2)} e^{-i\sqrt{2\pi}\phi_R^+(x-\epsilon/2)} e^{-i\sqrt{2\pi}\phi_R^-(x-\epsilon/2)}. \quad (2.63)$$

After normal ordering the operators, we can do the expansion in ϵ (dropping the normal ordering sign)

$$\begin{aligned} & \psi_R^\dagger\left(x+\frac{\epsilon}{2}\right)\psi_R\left(x-\frac{\epsilon}{2}\right) \\ = & -\frac{1}{2\pi i\epsilon}\exp\left\{i\sqrt{2\pi}\left[\phi_R\left(x+\frac{\epsilon}{2}\right)-\phi_R\left(x-\frac{\epsilon}{2}\right)\right]\right\} \\ = & -\sum_{\ell=0}^{\infty}\frac{\left(2\sqrt{2\pi}i\right)^\ell}{2\pi i\epsilon\,\ell!}\sum_{\{m_j\}}\frac{\ell!}{\prod_j m_j!}\left(\frac{\epsilon}{2}\right)^{\sum_j' jm_j}\prod_{j=1,3,\cdots}\left(\frac{\partial_x^j\phi_R}{j!}\right)^{m_j}. \quad (2.64) \end{aligned}$$

From (2.59) and the coefficient of the ϵ^n term in (2.64), we have

$$F^{(n)}(x) = \frac{(-1)^{n+1}n!}{2^{n+1}2\pi i}\sum_{\{m_j\}}\frac{\left(2\sqrt{2\pi}i\right)^{\sum_j m_j}}{\prod_j(m_j!)}\prod_{j=1,3,\cdots}\left(\frac{\partial_x^j\phi_R}{j!}\right)^{m_j}, \quad (2.65)$$

where the m_j's obey the constraint $\sum_j jm_j = n+1$. In particular, for $n=2$ the sum in (2.65) contains only two terms (either $m_1=3$, $m_3=0$ or $m_1=0$, $m_3=1$). We get

$$F^{(2)}(x) = \psi_R^\dagger\partial_x^2\psi_R = \frac{\sqrt{2\pi}}{3}\left(\partial_x\phi_R\right)^3 - \frac{1}{12\sqrt{2\pi}}\partial_x^3\phi_R. \quad (2.66)$$

The last term is a total derivative and can be omitted from the Hamiltonian. Similar expressions for the left-moving field ϕ_L are obtained straightforwardly by using the symmetry under the parity transformation $x\to -x$, $R\to L$. The bosonized version of the band curvature terms in (2.57) is then

$$\delta\mathcal{H}_{bc} = \frac{\sqrt{2\pi}}{6m}\left[\left(\partial_x\phi_L\right)^3 - \left(\partial_x\phi_R\right)^3\right]. \quad (2.67)$$

We now rewrite $\delta\mathcal{H}_{bc}$ in terms of the right and left components of the rescaled field ϕ. Using (2.34) and (2.35),

$$\begin{aligned}\delta\mathcal{H}_{bc} &= \frac{\sqrt{2\pi}}{6m}\left[\left(\frac{\partial_x\tilde{\theta}+\partial_x\tilde{\phi}}{\sqrt{2}}\right)^3-\left(\frac{\partial_x\tilde{\theta}-\partial_x\tilde{\phi}}{\sqrt{2}}\right)^3\right] \\ &= \frac{\sqrt{\pi/K}}{6m}\int_0^L dx\,\left[3\left(\partial_x\theta\right)^2\partial_x\phi+K^2\left(\partial_x\phi\right)^3\right]. \qquad (2.68)\end{aligned}$$

Finally, using (2.47), we get (in accordance with [131])

$$\begin{aligned}\delta\mathcal{H}_{bc} &= \frac{\sqrt{2\pi/K}}{6}\frac{3+K^2}{4m}\left[\left(\partial_x\varphi_L\right)^3-\left(\partial_x\varphi_R\right)^3\right] \\ &\quad+\frac{\sqrt{2\pi/K}}{6}\frac{3(1-K^2)}{4m}\left[\left(\partial_x\varphi_L\right)^2\partial_x\varphi_R-\left(\partial_x\varphi_R\right)^2\partial_x\varphi_L\right]. \qquad (2.69)\end{aligned}$$

Besides $\delta\mathcal{H}_{bc}$, we need to include the irrelevant operators which arise from the expansion of the fermionic interaction in the lattice spacing, as we encountered in (2.39). In terms of $\varphi_{R,L}$, this contribution reads

$$\begin{aligned}\delta\mathcal{H}_{int} &= \frac{J\Delta K^{3/2}}{3\sqrt{2\pi}}\sin(2k_F)\left\{\left[\left(\partial_x\varphi_L\right)^3-\left(\partial_x\varphi_R\right)^3\right]\right. \\ &\quad\left.-3\left[\left(\partial_x\varphi_L\right)^2\partial_x\varphi_R-\left(\partial_x\varphi_R\right)^2\partial_x\varphi_L\right]\right\}. \qquad (2.70)\end{aligned}$$

Combining (2.69) and (2.70), we can write the irrelevant operators in the most general form

$$\begin{aligned}\delta H &= \frac{\sqrt{2\pi}}{6}\int dx\,\left\{\eta_-\left[\left(\partial_x\varphi_L\right)^3-\left(\partial_x\varphi_R\right)^3\right]\right. \\ &\quad\left.+\eta_+\left[\left(\partial_x\varphi_L\right)^2\partial_x\varphi_R-\left(\partial_x\varphi_R\right)^2\partial_x\varphi_L\right]\right\}. \qquad (2.71)\end{aligned}$$

To first order in Δ, the coupling constants $\eta_\pm$ are given by

$$\eta_- \approx \frac{1}{m}\left(1+\frac{2\Delta}{\pi}\sin k_F\right), \qquad (2.72)$$

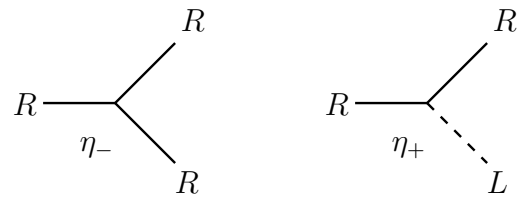

Figure 2.2: Interaction vertices in the low energy effective Hamiltonian. The solid (dashed) lines represent propagators for right- (left-) moving bosons $D_R^{(0)}(D_L^{(0)})$.

$$\eta_+ \approx -\frac{3\Delta}{\pi m}\sin k_F. \tag{2.73}$$

The perturbation δH in (2.71) might as well have been introduced phenomenologically in the effective Hamiltonian. In fact, the dimension-three operators $(\partial_x\varphi_{R,L})^3$ are the leading irrelevant operators that are allowed by symmetry. They obey the parity symmetry $\varphi_L \to \varphi_R$, $x \to -x$, but not spin reversal (or particle-hole) symmetry $\varphi_{R,L} \to -\varphi_{R,L}$, which is absent for $h \neq 0$. Such terms give rise to three-legged interaction vertices which scale with powers of the momenta of the scattered bosons (figure 2.2). They are responsible, for example, for corrections to the long distance asymptotics of the correlation functions [136]. Note that as $\Delta \to 0$ ($K \to 1$), $\eta_- \to 1/m$ while η_+ vanishes because there is no mixing between right and left movers at the free fermion point. Moreover, the weak coupling expressions predict that both η_- and η_+ vanish in the limit $h \to 0$ ($m \to \infty$), in which particle-hole symmetry is recovered. (See, however, figure 2.14 below.) For $h = 0$ the leading irrelevant operators are the dimension-four operators $(\partial_x\varphi_{R,L})^4$, $(\partial_x\varphi_R)^2(\partial_x\varphi_L)^2$ and the umklapp interaction $\cos(4\sqrt{\pi K}\phi)$, which becomes nonoscillating [128].

The condition that a general model of the form $H_{LL} + \delta H$ be unitarily equivalent to free fermions up to dimension-four operators [129] amounts to imposing that the Bogoliubov transformation that diagonalizes H_{LL} in the

R/L basis also diagonalizes the cubic operators in δH. In our notation, this condition is expressed as $\eta_+ = 0$. That condition is not satisfied by the XXZ model except for the trivial case $\Delta = 0$. However, the contributions from this extra (*i.e.*, not present for free fermions) dimension-three operator to $S^{zz}(q,\omega)$ are of $O(\eta_+^2)$, as we will discuss in section 2.5.

Similarly to what happens for v and K, (2.72) and (2.73) should be regarded as weak-coupling expressions. Again we can use the fact that the XXZ model is integrable and obtain the exact (renormalized) values of $\eta_\pm$ by comparison with Bethe Ansatz. In section 2.2.3 we will discuss how to fix these coupling constants in order to obtain a parameter-free theory.

2.2.3 Determination of the renormalized coupling constants

As mentioned in section 2.2.2, the renormalized parameters $\eta_\pm$ can be determined by comparison with exact Bethe Ansatz results for infinite length. We will proceed by analogy with the calculation for the zero-field case in [137]. One difficulty is that there are no analytical solutions of the Bethe Ansatz equations for finite fields, so we must be satisfied with a numerical evaluation of the parameters. In the following, we will relate $\eta_\pm$ to the coefficients of the expansion of v and K as functions of the magnetic field, by comparing the corrections to the free boson result for the free energy calculated in two different ways.

Let us consider the response to a small variation in the magnetic field around a finite value h_0. In the limit $\delta h = h - h_0 \ll 1$, such a response is well described by the Luttinger model

$$H = \int dx \left\{ \frac{v}{2} \left[(\partial_x \theta)^2 + (\partial_x \phi)^2 \right] - J\delta h \sqrt{\frac{K}{\pi}} \partial_x \phi \right\}, \tag{2.74}$$

where $v\,(h)$ and $K\,(h)$ are known exactly from the Bethe Ansatz equations.

For $h_0 = 0$, the cutoff-independent terms of the free energy density according to field theory read

$$f\left(h_0 = 0\right) \sim -\frac{\pi T^2}{6v} - \frac{K}{2\pi v}\left(J\delta h\right)^2, \tag{2.75}$$

where v and K are given by (2.44) and (2.45), respectively. The magnetic susceptibility at zero temperature is $\chi = -J^{-2}\left(\partial^2 f/\partial h^2\right)|_{T=0} = K/\pi v$, which is the familiar free boson result. For finite field $h_0 \neq 0$, the free energy assumes some general form

$$f\left(h_0 \neq 0\right) \sim -\frac{\pi T^2}{6v(h)} - C\left(h\right), \tag{2.76}$$

and the $T = 0$ susceptibility is obtained by

$$\chi = -\frac{1}{J^2}\left(\frac{\partial^2 f}{\partial h^2}\right)\bigg|_{h,T=0} = -\frac{1}{J^2}\left(\frac{\partial^2 C}{\partial\left(\delta h\right)^2}\right)\bigg|_{h,T=0} = \frac{K(h)}{\pi v(h)}, \tag{2.77}$$

where the last identity holds for any Luttinger liquid.

We would like to calculate the corrections to f and χ that involve higher powers of the perturbation δh. Our first approach is to assume that the field dependence is already completely contained in the definitions of $v(h)$ and $K(h)$, so that we can employ the expansion

$$v(h) = v(h_0)\left[1 + a\,\delta h + O\left(\delta h^2\right)\right], \tag{2.78}$$

$$K(h) = K(h_0)\left[1 + b\,\delta h + O\left(\delta h^2\right)\right], \tag{2.79}$$

where the coefficients a and b can be extracted from the exact v and K by linearizing the field dependence around $h = h_0$. Consequently, the lowest-order correction to the free boson susceptibility around $h = h_0$ is

$$\chi = \frac{K(h_0)}{\pi v(h_0)}\left[1 - (a - b)\,\delta h + O\left(\delta h^2\right)\right]. \tag{2.80}$$

Likewise, the free energy at finite temperature must contain a term of the form

$$\delta f \sim a \frac{\pi\, \delta h\, T^2}{6v(h_0)}, \tag{2.81}$$

due to the field dependence of the velocity. Both a and b depend on h_0 and the anisotropy Δ. As an example, at the XX point, $K = 1$ for any value of the field, therefore $b(\Delta = 0, h_0) = 0$. From (2.11), we have

$$v_F = J \sin k_F = J\sqrt{1-h^2} \approx v_F(h_0) - \frac{J^2 h_0}{v_F(h_0)}\, \delta h + O\left(\delta h^2\right), \tag{2.82}$$

so that we get

$$a\left(\Delta = 0, h_0\right) = -\frac{J^2 h_0}{v_F^2(h_0)} = \frac{\cos k_F}{\sin^2 k_F}. \tag{2.83}$$

In our second approach, we take $v = v(h_0)$ and $K = K(h_0)$ to be fixed and assume that the corrections to the free boson result are generated by the irrelevant operators. We consider the effective Hamiltonian $H = H_{LL} + \delta H$, with δH defined in (2.71). An equivalent Lagrangian formulation in imaginary time is

$$\mathcal{L} = \mathcal{L}_0 + \delta\mathcal{L}, \tag{2.84}$$

$$\mathcal{L}_0 = \frac{\left(\partial_\tau \phi\right)^2}{2v} + \frac{v}{2}\left(\partial_x \phi\right)^2 - J\delta h \sqrt{\frac{K}{\pi}} \partial_x \phi, \tag{2.85}$$

$$\delta\mathcal{L} = -\frac{A\sqrt{\pi}}{6v^2}\left(\partial_\tau \phi\right)^2 \partial_x \phi + \frac{B\sqrt{\pi}}{6}\left(\partial_x \phi\right)^3 + O\left(\eta_\pm^2\right), \tag{2.86}$$

where $A = 3\eta_- + \eta_+$ and $B = \eta_- - \eta_+$. We shift the field by $\phi \to \phi + \frac{J\delta h}{v}\sqrt{\frac{K}{\pi}} x$ to absorb the term linear in $\partial_x \phi$ and get

$$\mathcal{L}_0 = \frac{\left(\partial_\tau \phi\right)^2}{2v} + \frac{v}{2}\left(\partial_x \phi\right)^2 + \frac{K\left(J\delta h\right)^2}{2\pi v}, \tag{2.87}$$

$$\delta\mathcal{L} = -\frac{A\sqrt{K} J\delta h}{6v^3}\left(\partial_\tau \phi\right)^2 + \frac{B\sqrt{K} J\delta h}{2v}\left(\partial_x \phi\right)^2$$

$$+\frac{BK^{3/2}\left(J\delta h\right)^{3}}{6\pi v^{3}}+\text{ odd powers of }\phi. \tag{2.88}$$

We then calculate the free energy density from the partition function

$$Z=\int\mathcal{D}\phi\,\exp\left\{-\int_{0}^{\beta}d\tau\int_{0}^{L}dx\,\left(\mathcal{L}_{0}+\delta\mathcal{L}\right)\right\}, \tag{2.89}$$

$$f=-\frac{T}{L}\ln Z\approx f_{0}+\frac{T}{L}\int_{0}^{\beta}d\tau\int_{0}^{L}dx\,\left\langle\delta\mathcal{L}\right\rangle, \tag{2.90}$$

where f_0 reproduces the free boson result

$$f_{0}\sim-\frac{\pi T^{2}}{6v}-\frac{K}{2\pi v}\left(J\delta h\right)^{2}, \tag{2.91}$$

and $\langle\delta\mathcal{L}\rangle$ is the expectation value of $\delta\mathcal{L}$ calculated with the unperturbed Hamiltonian. In order to compute $\langle\delta\mathcal{L}\rangle$, we need the finite temperature propagators

$$\begin{aligned}\left\langle\partial_{x}\phi\left(x+\epsilon\right)\partial_{x}\phi\left(x\right)\right\rangle &= -\frac{1}{v^{2}}\left\langle\partial_{\tau}\phi\left(x+\epsilon\right)\partial_{\tau}\phi\left(x\right)\right\rangle\\ &= -\frac{1}{2\pi}\frac{\left(\pi T/v\right)^{2}}{\sinh^{2}\left(\pi T\epsilon/v\right)}.\end{aligned} \tag{2.92}$$

Now we use the expansion $\sinh^{-2}\left(\pi T\epsilon/v\right)\approx\left(v/\pi T\epsilon\right)^{2}-1/3$ for $\epsilon\to0$ and drop the cutoff-dependent terms in δf. The reason is that the latter simply renormalize the corresponding terms in f_0 and have already been accounted for in the renormalization of v and K. The correction to the free energy to first order in A and B becomes

$$\begin{aligned}\delta f &= \frac{T}{L}\int_{0}^{\beta}d\tau\int_{0}^{L}dx\,\left\langle\delta\mathcal{L}\right\rangle\\ &\sim (A+3B)\,\frac{\pi\sqrt{K}J\delta h\,T^{2}}{36v}+B\,\frac{K^{3/2}\left(J\delta h\right)^{3}}{6\pi v^{3}}.\end{aligned} \tag{2.93}$$

The susceptibility obtained from $f_0 + \delta f$ is

$$\chi = -\frac{1}{J^2}\left.\frac{\partial^2 (f_0 + \delta f)}{\partial (\delta h)^2}\right|_{T=0} = \frac{K}{\pi v} - B\,\frac{K^{3/2} J \delta h}{\pi v^3} + O\left(\delta h^2\right). \tag{2.94}$$

Comparing with the expression (2.80), we can identify

$$a - b = \frac{\sqrt{K} J}{v^2}\, B = \frac{\sqrt{K} J}{v^2}\left(\eta_- - \eta_+\right). \tag{2.95}$$

Besides, from the $\delta h\, T^2$ term in (2.81) and (2.93), we have

$$a = \frac{\sqrt{K} J}{6 v^2}\left(A + 3B\right) = \frac{\sqrt{K} J}{3 v^2}\left(3\eta_- - \eta_+\right). \tag{2.96}$$

Finally, combining (2.95) and (2.96) and writing $a = v^{-1}\partial v/\partial h$ and $b = K^{-1}\partial K/\partial h$, we find the formulas first presented in [128]

$$J\eta_- = \frac{v}{K^{1/2}}\frac{\partial v}{\partial h} + \frac{v^2}{2K^{3/2}}\frac{\partial K}{\partial h}, \tag{2.97}$$

$$J\eta_+ = \frac{3v^2}{2K^{3/2}}\frac{\partial K}{\partial h}. \tag{2.98}$$

The above relations allow us to calculate the renormalized values of $\eta_\pm$ once we have the field dependence of v and K. Notice that $\eta_+ \propto \partial K/\partial h$ and as expected vanishes at the XX point. On the other hand, η_- remains finite at $\Delta = 0$ because $\partial v/\partial h \neq 0$ and we recover $\eta_- = (v_F/J)\partial v_F/\partial h = J\cos k_F = m^{-1}$. It is also possible to check the validity of (2.97) and (2.98) explicitly in the weak coupling limit, using the expressions for $v\,(\Delta \ll 1, h)$ and $K\,(\Delta \ll 1, h)$ in (2.42) and (2.43) as well as the weak coupling expressions for $\eta_\pm$ in (2.72) and (2.73).

2.3 Bethe Ansatz solution

Although the Bethe Ansatz is first and foremost a method for calculating the energy levels of an exactly solvable model (readers who are unfamiliar with the subject are invited to consult standard textbooks, for example [135, 138, 139]), recent progress stemming from the Algebraic Bethe Ansatz means that we can now use it to make many nontrivial statements about dynamical quantities. Assuming that certain specific families of excited states carry the dominant part of the structure factor, we can delimit the energy and momentum continua where we expect most of the correlation weight to be found, and provide the specific line shape of the structure factor both within this interval, and further up within the higher-energy tail. We start here by introducing the important aspects of the Bethe Ansatz which we will make use of later on when studying the correspondence with field theory results.

2.3.1 Bethe Ansatz setup and fundamental equations

As is well-known, an eigenbasis for the XXZ chain (2.1) on N sites is obtained from the Bethe Ansatz [99, 100],

$$\Psi_M(j_1, ..., j_M) = \sum_P (-1)^{[P]} e^{i\sum_{a=1}^{M} k_{P_a} j_a - \frac{i}{2}\sum_{1\leq a<b\leq M}\phi(k_{P_a}, k_{P_b})}. \tag{2.99}$$

Here, $M \leq N/2$ represents the number of overturned spins, starting from the reference state $|0\rangle = \otimes_{i=1}^{N} |\uparrow\rangle_i$ (*i.e.* the state with all spins pointing upwards in the $\hat{z}$ direction). The total magnetization of the system along the $\hat{z}$ axis, $S^z_{tot} = N\sigma = \frac{N}{2} - M$ is conserved by the Hamiltonian. P represents a permutation of the integers $\{1, ..., M\}$ and j_i are the lattice coordinates. The quasi-momenta k are parametrized in terms of rapidities λ,

$$e^{ik} = \frac{\sinh(\lambda + i\zeta/2)}{\sinh(\lambda - i\zeta/2)}, \qquad \Delta = \cos\zeta, \tag{2.100}$$

such that the two-particle scattering phase shift becomes a function of the rapidity difference only, $\phi(k_a, k_b) = \phi_1(\lambda_a - \lambda_b)$ with ϕ_1 defined below. An individual eigenstate is thus fully characterized by a set of rapidities $\{\lambda\}$, satisfying the quantization conditions (Bethe equations) obtained by requiring periodicity of the Bethe wavefunction (2.99):

$$\phi_1(\lambda_j) - \frac{1}{N}\sum_{k=1}^{M}\phi_2(\lambda_j - \lambda_k) = 2\pi\frac{I_j}{N}, \qquad j = 1, ..., M, \tag{2.101}$$

in which I_j are half-odd integers for $N - M$ even and integers for $N - M$ odd, and where we have defined the functions

$$\phi_n(\lambda) = 2\arctan\left(\frac{\tanh(\lambda)}{\tan(n\zeta/2)}\right). \tag{2.102}$$

The energy and momentum of an eigenstate are simple functions of its rapidities,

$$\begin{aligned} E &= -\pi J \sin\zeta \sum_j a_1(\lambda_j) - hS^z_{tot}, \\ P &= \pi M - \sum_j \phi_1(\lambda_j) = \pi M - \frac{2\pi}{N}\sum_j I_j \end{aligned} \tag{2.103}$$

in which

$$a_n(\lambda) = \frac{1}{2\pi}\frac{d}{d\lambda}\phi_n(\lambda) = \frac{1}{\pi}\frac{\sin(n\zeta)}{\cosh(2\lambda) - \cos(n\zeta)}. \tag{2.104}$$

Each solution of the set of coupled nonlinear equations (2.101) for sets of non-coincident rapidities represents an eigenstate (if two rapidities coincide, the Bethe wavefunction (2.99) formally vanishes). The space of solutions is not restricted to real rapidities: it has been known since Bethe's original paper that there exist solutions having complex rapidities ('string' states), representing bound states of magnons. In fact, obtaining *all* wavefunctions from solutions to the Bethe equations (or degenerations thereof) remains to

this day an open problem in the theory of integrable models. It is however possible to construct the vast majority of eigenstates using this procedure, allowing one to obtain reliable results for thermodynamic quantities and correlation functions. In all our considerations in the present work, we can and will restrict ourselves to real solutions to the Bethe equations.

2.3.2 Ground state and excitations

The simplest state to construct is the ground state, which is obtained by setting the quantum numbers I_j to (we consider N even from now on for simplicity)

$$I_j^{GS} = -\frac{M+1}{2} + j, \qquad j = 1, ..., M. \tag{2.105}$$

The simplest excited states which can be constructed at finite magnetic field are obtained by introducing particle-hole excitations on the ground-state quantum number distributions, see figure (2.3). Since we limit ourselves to real solutions to the Bethe equations, we require $|\lambda_j| < \infty$ and thus $|I| < I_\infty$, where, from (2.101),

$$I_\infty = \frac{N-M}{2} - (\frac{N}{2} - M)\frac{\zeta}{\pi}. \tag{2.106}$$

The momentum of an excited state is simply given by the left-displacement of the quantum numbers with respect to those in the ground state, $q = \frac{2\pi}{N}\delta_l I$, where $\delta_l I = \sum_j (I_j^{GS} - I_j)$. At a given fixed (small) momentum, we can thus construct $qN/2\pi$ two-particle states by shifting the particle and hole quantum numbers, leaving their difference fixed. Since the energies of these two-particle states at fixed momentum are non-degenerate, this defines a two-particle continuum whose characteristics will be studied later. Higher-particle states can be similarly constructed and counted.

The restriction to real rapidities and a single particle-hole pair therefore means that our subsequent arguments will apply only to the region $q <$

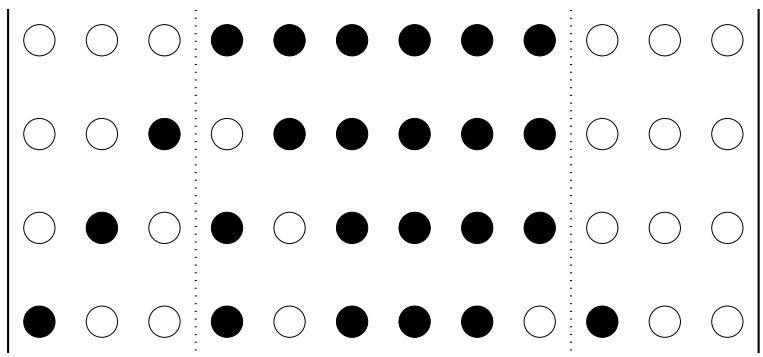

Figure 2.3: Representation of various quantum number configurations: a black (empty) circle represents an occupied (unoccupied) allowable quantum number (which here are taken to be half-odd integers; the figure is centered on zero). The top set represents the ground state configuration, whereas the second and third from top represent two-particle excitations at different momenta, obtained by creating a particle-hole pair on the ground-state configuration. The bottom set is for a four-particle state obtained from two particle-hole pairs. The dotted line delimits the ground state interval, whereas the solid lines delimit the quantum numbers for which real solutions to the Bethe equations can be obtained in this illustrative case (see main text).

$\mathrm{Min}(2k_F, k_\infty)$ where $k_F = \pi\frac{M}{N}$ and k_∞ is given by the maximal displacement of the outermost quantum number, $k_\infty = 2\pi\frac{I_\infty - M/2}{N}$. We can thus write our restriction as

$$q < \mathrm{Min}\{\pi(1-2\sigma), 2\sigma(\pi-\zeta)\} \tag{2.107}$$

in terms of the magnetization, noting in particular that the window of validity of our arguments vanishes in the case of zero magnetic field.

For a finite chain with N sites and M overturned spins, the Hilbert space is finite, and therefore so is the sum over intermediate states in the Lehmann representation for the structure factor (2.3). Each intermediate state is obtained by solving the Bethe equations, the space of states being reconstructed by spanning through the sets of allowable quantum numbers. The form factor of a local spin operator between the ground state and a particular excited state is obtained from the Algebraic Bethe Ansatz as a determinant of a matrix depending only on the rapidities of the eigenstates involved [115, 116] even in the case of string states with complex rapidities [117]. This enables one to obtain extremely accurate results on the full dynamical spin-spin correlation functions in integrable Heisenberg chains [117, 121]. We will make use of this method in what follows to compare results from the Bethe Ansatz to field theory predictions for the structure factor at small momentum.

2.4 Width of the on-shell peak

Linearizing the dispersion around the Fermi points is a key step for the bosonization technique. By doing so all the particle-hole excitations with the same momentum $q \ll k_F$ become exactly degenerate and one can associate a particular linear combination with a single-boson state [136]. In this approximation, the single boson state $|b\rangle \equiv a_q^{R\dagger}|0\rangle$ is the only state that couples to the ground state via S_q^z. The associated weight in $S^{zz}(q,\omega)$ is given by

$$\left|\left\langle 0\left|S_{q>0}^z\right|b\right\rangle\right|^2 = \frac{KqN}{2\pi}\left|\left\langle 0\left|a_q^R\right|b\right\rangle\right|^2 = \frac{KqN}{2\pi}. \tag{2.108}$$

However, as we will see in section 2.4.3, the exact eigenstates in the Bethe Ansatz solution, whose energies are given by (2.103), are nondegenerate. In fact, most of the above spectral weight is shared by $qN/2\pi$ two-particle states whose energies are spread around $\omega = vq$. This is reminiscent of the exact solution for the free fermion point in section 2.1.1. In the bosonic picture, on the other hand, the broadening $\delta\omega_q$ is related to a finite lifetime for the bosons of the Luttinger model. Once band curvature is introduced via the irrelevant operators in (2.71), the single boson is allowed to decay and the coupling to the multiboson states lifts the previous degeneracy. The fact that the irrelevant operators have the same scaling dimension as in the noninteracting case suggests that for $\Delta \neq 0$ the width should also vanish as q^2 in the limit $q \to 0$. In this section we argue in favor of a q^2 scaling for $\delta\omega_q$ for all values of Δ in the gapless regime, *as long as* $\eta_- \neq 0$, based on two different approaches. First, we explain how the expansion of the bosonic diagrams in the interaction vertex η_-, neglecting η_+, coincides with the expansion of the free fermion result (2.28) in powers of $1/m$. η_- is then interpreted as a renormalized inverse mass, in the sense that the width of the peak for $\Delta \neq 0$ is given by $\delta\omega_q = |\eta_-|q^2$. Second, we derive from the Bethe Ansatz equations an analytical expression for the width of the two-particle continuum at finite fields and show that it coincides with the field theory prediction for the width of $S^{zz}(q,\omega)$. Finally, we confirm these results directly by analyzing the numerical form factors calculated for finite chains of lengths up to 7000 sites.

2.4.1 Width from field theory

We saw that the width $\delta\omega_q$ is well defined for the free fermion point, in which case $S^{zz}(q,\omega)$ has sharp lower and upper thresholds $\omega_{L,U}(q)$. For the interacting case, $S^{zz}(q,\omega)$ still vanishes below some finite lower threshold $\omega_L(q)$ at zero temperature due to simple kinematic constraints. However, the on-shell peak has to match a high-frequency tail somewhere around $\omega_U(q)$,

hence the meaning of an upper threshold is no longer clear.

In their solution for weakly interacting spinless fermions, Pustilnik *et al.* [124] found that ω_U has to be interpreted as the energy at which the peak joins the high frequency tail by approaching a finite value with an infinite slope. Although it is actually possible that the singularity at $\omega_U(q)$ gets smoothed out if one treats the decay of the "high-energy electron" for a general model [132], the singularity may be protected in integrable models such as the XXZ model.

Of course the situation is a lot simpler for models with no high-frequency tail, where the dynamical structure factor is finite only within the interval $\omega_L(q) < \omega < \omega_U(q)$. Such is the case for the Calogero-Sutherland model [140]. The absence of a tail for $S(q,\omega)$ in the Calogero-Sutherland model can be attributed to the remarkable property that the quasiparticles are all right movers [125]. As we will discuss in section 2.5, the η_+ term that mixes R and L in our low energy effective Hamiltonian (figure 2.2) is responsible for the high-frequency tail for $h \neq 0$ because it allows for intermediate states with two bosons moving in opposite directions, thus carrying small momentum and high energy $\omega \gg vq$.

In contrast, the η_- interaction has matrix elements between multiboson states which contain only right movers. All these states have $\omega \approx vq$. Therefore η_- must be related to the broadening of the on-shell peak. It has already been pointed out in [129] that the model with $\eta_+ = 0$ is equivalent to free fermions up to irrelevant operators with dimension four and higher. For this case one can write down an approximate expression for the dynamical structure factor which misses more subtle features in the line shape (*e.g.*, the power law singularities at the thresholds) but accounts for the renormalization of the width due to interactions. Even for models with nonzero η_+, such as the XXZ model in the entire gapless regime, it is reasonable to expect that $\delta\omega_q$, if well defined, will depend primarily on the interaction between excitations created around the same Fermi point. For that reason, we

will neglect the η_+ interaction in an attempt to derive an expression for the width of $S^{zz}(q,\omega)$ from the bosonic Hamiltonian. In the following we apply perturbation theory in η_- up to *fourth order* and show that it recovers the expansion of the logarithm for the density-density correlation function. This fact has already been noticed in [130, 131] up to $O(\eta_-^2)$. However, irrelevant interaction terms such as (2.70) were neglected in [130, 131]. Such terms are crucial to obtain the correct effective inverse mass, since the correction of first order in the fermionic interaction Δ stems from (2.70).

For $\eta_+ = 0$, the Hamiltoninan $H_{LL} + \delta H$ decouples into right and left movers. For excitations with $q > 0$, we can consider only right movers and work with

$$\mathcal{H}_R = \frac{v}{2}\left(\partial_x \varphi_R\right)^2 - \frac{\sqrt{2\pi}}{6}\eta_-\left(\partial_x \varphi_R\right)^3 . \tag{2.109}$$

The first attempt to broaden the delta function peak in $S^{zz}(q,\omega)$ would be to calculate the corrections to the propagator

$$\chi(q,i\omega) = -\frac{K}{2\pi}\int_{-\infty}^{+\infty} dx\, e^{-iqx}\int_0^\beta d\tau\, e^{i\omega\tau}\left\langle T_\tau \partial_x\varphi_R(x,\tau)\,\partial_x\varphi_R(0,0)\right\rangle , \tag{2.110}$$

by using perturbation theory in the cubic term. Unfortunately, any finite order perturbation theory in η_- breaks down near $\omega \approx vq$. Even using the Born approximation, which sums an infinite series but not all the diagrams, one finds that the self-energy to $O(\eta_-^2)$ is divergent: $\mathrm{Im}\,\Sigma(q,\omega) \sim \delta(\omega - vq)$ [133]. This is actually not surprising if we look at the exact solution for the free fermion point. Expanding the positive-frequency part of (2.28) in powers of $1/m$, we get

$$\chi(q,i\omega) = \frac{q}{2\pi w}\left[1 + \frac{1}{3}\left(\frac{q^2/m}{2w}\right)^2 + \frac{1}{5}\left(\frac{q^2/m}{2w}\right)^4 + \dots\right], \tag{2.111}$$

where $w \equiv i\omega - v_F q$. Stricly speaking, such an expansion is valid only for $\omega - v_F q \gg q^2/2m$. For $\omega \approx v_F q$, the expansion in band curvature produces

increasingly singular terms that need to be summed up to produce the finite result in (2.28).

In any case, it is legitimate to examine the expansion of bosonic diagrams and ask whether it can at least reproduce the free fermion result. We use the bare propagator $D_R^{(0)}(x,\tau) = \langle T_\tau \partial_x \varphi_R(x,\tau)\, \partial_x \varphi_R(0,0)\rangle_0$ in (2.50), with Fourier transform

$$D_R^{(0)}(q, i\omega) = \frac{q}{w}, \tag{2.112}$$

to calculate the expansion of $\chi_R(q, i\omega)$ up to $O\left(\eta_-^4\right)$, as represented in figure 2.4. The zeroth-order result is simply the same as in (2.55)

$$\chi^{(0)}(q,\omega) = \frac{Kq}{2\pi w}. \tag{2.113}$$

The $O(\eta_-^2)$ correction is

$$\begin{aligned}
\chi^{(2)}(q, i\omega) &= -\frac{K}{2\pi}\int d^2x\, e^{-iqx+i\omega\tau}\int d^2x_1 \int d^2x_2 \frac{1}{2}\left(\frac{\sqrt{2\pi}}{6}\eta_-\right)^2 \times \\
&\quad \times \left\langle T_\tau \partial_x\varphi_R(x)\left[\partial_x\varphi_R(1)\right]^3\left[\partial_x\varphi_R(2)\right]^3 \partial_x\varphi_R(0)\right\rangle \\
&= \frac{K}{2\pi}\left[D_R^{(0)}(q, i\omega)\right]^2 \Pi_{RR}(q, i\omega),
\end{aligned} \tag{2.114}$$

where $\Pi_{RR}(q, i\omega)$ is the bubble with two right-moving bosons

$$\begin{aligned}
\Pi_{RR}(q, i\omega) &\equiv -\pi\eta_-^2 \int_0^q \frac{dk}{2\pi}\int_{-\infty}^{+\infty}\frac{d\nu}{2\pi} D_R^{(0)}(k, i\nu)\, D_R^{(0)}(q-k, i\omega - i\nu) \\
&= \frac{\eta_-^2 q^3}{12w}.
\end{aligned} \tag{2.115}$$

Note that Π_{RR} is singular at $\omega = vq$, which prevents us from treating it as a self-energy. The origin of the singularity is that the two right-moving bosons in the intermediate state always carry energy $\omega = vq$, no matter how the momentum is distributed between the pair. Substituting (2.115) back into

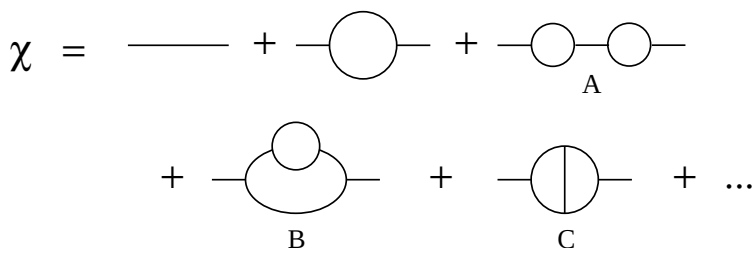

Figure 2.4: Perturbative diagrams up to fourth order in η_-.

(2.114), we get

$$\chi^{(2)}(q, i\omega) = \frac{Kq}{2\pi w}\frac{1}{12}\left(\frac{\eta_- q^2}{w}\right)^2. \tag{2.116}$$

To $O\left(\eta_-^4\right)$, there are three topologically distinct diagrams (figure 2.4), which give the following contributions

$$\begin{aligned}
\chi_A^{(4)}(q, i\omega) &= \frac{Kq}{2\pi w}\frac{1}{144}\left(\frac{\eta_- q^2}{w}\right)^4, \\
\chi_B^{(4)}(q, i\omega) &= \frac{Kq}{2\pi w}\frac{1}{504}\left(\frac{\eta_- q^2}{w}\right)^4, \\
\chi_C^{(4)}(q, i\omega) &= \frac{Kq}{2\pi w}\frac{1}{280}\left(\frac{\eta_- q^2}{w}\right)^4.
\end{aligned} \tag{2.117}$$

The coefficients for each diagram are nontrivial and result from both combinatorial factors and integration over internal momenta (recall that the interaction vertex is momentum-dependent because of the derivatives in (2.71)). Remarkably, all the fourth-order diagrams have the same q and ω dependence with comparable amplitudes. We are not allowed to drop any of them and there is no justification for the use of a self-consistent Born approximation, for example [133]. Putting all the terms together, we end up with the expansion

$$\chi\left(q,i\omega\right)=\frac{Kq}{2\pi w}\left[1+\frac{1}{3}\left(\frac{\eta_{-}q^{2}}{2w}\right)^{2}+\frac{1}{5}\left(\frac{\eta_{-}q^{2}}{2w}\right)^{4}+\ldots\right], \tag{2.118}$$

which is analogous to (2.111) with the replacements $1/m \to \eta_-$, $v_F \to v$ and an extra factor of K. This proves that the expansion of bosonic diagrams reproduces the expansion of the free fermion result up to fourth order in $1/m$. Since there is no simple way to predict the prefactors of each diagram, all we can do is to check this correspondence order by order in perturbation theory. However, *if we believe that the bosonic theory reproduces the free fermion result to all orders in* η_-, we must conclude that in the interacting case the series in (2.118) sums up to give the result

$$\chi\left(q,i\omega\right)=\frac{K}{2\pi\eta_{-}q}\log\left[\frac{i\omega-vq+\eta_{-}q^{2}/2}{i\omega-vq-\eta_{-}q^{2}/2}\right], \tag{2.119}$$

from which we obtain

$$S^{zz}\left(q,\omega\right)=\frac{K}{|\eta_{-}|q}\theta\left(\frac{|\eta_{-}|q^{2}}{2}-|\omega-vq|\right). \tag{2.120}$$

This result predicts that $S^{zz}\left(q,\omega\right)$ is finite and flat within an interval of width

$$\delta\omega_{q}=|\eta_{-}|q^{2}. \tag{2.121}$$

This line shape (illustrated in figure 2.5) is the exact one for the case of free fermions with quadratic dispersion. The reason is simple: because the bosonization of the operator $\sim k^2 c_k^\dagger c_k$ only generates the η_- term, one could invert the problem and refermionize the Hamiltonian (2.109) to an effective free fermion model with inverse mass η_-. In a more general model, more irrelevant operator have to be added to the effective Hamiltonian to reproduce details of the line shape that are higher order in q. For example, we expect the power-law singularities present at $\omega_{L,U}$ for $\Delta \neq 0$ [124] to be associated with dimension-four operators such as $\left(\partial_x^2\varphi_R\right)^2$ and $\left(\partial_x\varphi_R\right)^4$ (with corrections

of $O(\eta_+^2)$, see section 2.6). This means that if we write

$$S^{zz}(q,\omega) \equiv \frac{q}{\delta\omega_q} f\left(q, \frac{\omega - vq}{\delta\omega_q}\right), \tag{2.122}$$

the *rescaled* function $f(q,x)$ approaches the flat distribution of figure 2.5 in the limit $q \to 0$. Finally, we note that this approximate solution yields the same sum rules as the free boson result

$$\int_0^\infty d\omega\, S^{zz}(q,\omega) = Kq, \tag{2.123}$$

$$\int_0^\infty d\omega\, \omega S^{zz}(q,\omega) = vKq^2, \tag{2.124}$$

and also the magnetic susceptibility

$$\chi = \chi(q=0) = \lim_{q\to 0} \frac{1}{\pi} \int_0^\infty \frac{d\omega}{\omega} S^{zz}(q,\omega) = \frac{K}{\pi v}, \tag{2.125}$$

independent of the value of η_-.

2.4.2 Width from Bethe Ansatz

The purpose of this section is to provide an analytical derivation of the quadratic width formula (2.121), making use of standard methods associated with the thermodynamic Bethe Ansatz, and assuming that single particle-hole type excitations in the Bethe eigenstates basis carry the most important part of the structure factor. We first set our notations and underline certain characteristics of the ground state of the infinite chain in a field which will prove to be useful for our purposes. We then discuss particle-hole excitations in the thermodynamic limit, and obtain a relationship giving the width in terms of solutions of integral equations, simplifying to the conjectured field theory result in the small momentum limit.

Let us begin by taking the thermodynamic limit $N \to \infty$ of the equations

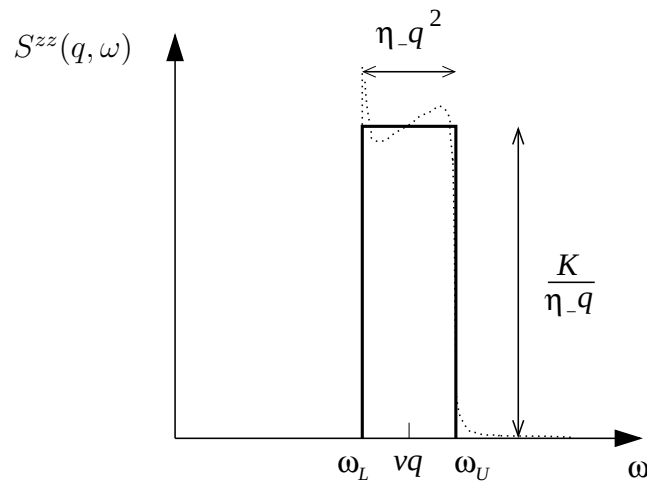

Figure 2.5: Line shape in the approximation with the η_- interaction only (solid line). The dotted line illustrates the expected true line shape for small Δ (see section 2.4.3).

of section 4. To do this, we first define particle and hole densities as functions of the continuous variable $x = \frac{I}{N}$,

$$\rho(x) = \frac{1}{N}\sum_{l\in\{I\}} \delta\left(x - \frac{l}{N}\right), \qquad \rho^h(x) = \frac{1}{N}\sum_{m\notin\{I\}} \delta\left(x - \frac{m}{N}\right) \tag{2.126}$$

in such a way that $\rho(x) + \rho^h(x) \to 1$ as $N \to \infty$. We can also write these in rapidity space by using the transformation rule for δ functions, so that the Bethe equations become

$$\phi_1(\lambda) - \int_{-\infty}^{\infty} d\lambda' \phi_2(\lambda - \lambda')\rho(\lambda') = 2\pi x(\lambda) \tag{2.127}$$

where we view x as an implicit function of λ. Taking the derivative of this with respect to λ and using $\frac{dx(\lambda)}{d\lambda} = \rho(\lambda) + \rho^h(\lambda)$ yields

$$a_1(\lambda) - \int_{-\infty}^{\infty} d\lambda' a_2(\lambda - \lambda')\rho(\lambda') = \rho(\lambda) + \rho^h(\lambda), \quad \lambda \in \mathbf{R}. \tag{2.128}$$

For the particular case of the ground state, the occupation density $\rho_{GS}(\lambda)$ is non-vanishing in a symmetric interval $[-B, B]$, with $\rho^h_{GS}(\lambda)$ vanishing. Outside of this interval, ρ_{GS} vanishes but not ρ^h_{GS}. $\lambda = \pm B$ therefore represent the two Fermi points in the rapidity distribution of the ground state, which is obtained by solving

$$\rho_{GS}(\lambda) + \int_{-B}^{B} d\lambda' a_2(\lambda - \lambda')\rho_{GS}(\lambda') = a_1(\lambda), \quad \lambda \in [-B, B]. \tag{2.129}$$

The magnetic field dependence is encoded in the constraint

$$\int_{-B}^{B} d\lambda \rho_{GS}(\lambda) = \frac{M}{N} = \frac{1}{2} - \sigma \tag{2.130}$$

where σ is the field-dependent average magnetization per site along the z axis. These two equations determine B and ρ_{GS}, and therefore also ρ^h_{GS}. We can write a formal solution as follows. Let us define the inverse operator $L(\lambda, \lambda')$, $\lambda, \lambda' \in [-B, B]$, inverse of the kernel in (2.129) in the sense that

$$\int_{-B}^{B} d\lambda' [\delta(\lambda - \lambda') + L(\lambda, \lambda')][\delta(\lambda' - \bar{\lambda}) + a_2(\lambda' - \bar{\lambda})] = \delta(\lambda - \bar{\lambda}). \tag{2.131}$$

This operator is symmetric, $L(\lambda, \lambda') = L(\lambda', \lambda)$, unique and analytic in its domain of definition [141]. In particular, the definition implies the identity

$$a_2(\lambda - \bar{\lambda}) + L(\lambda, \bar{\lambda}) + \int_{-B}^{B} d\lambda' L(\lambda, \lambda') a_2(\lambda' - \bar{\lambda}) = 0, \quad \lambda, \bar{\lambda} \in [-B, B]. \tag{2.132}$$

In terms of this operator, we have the explicit solution of Eq. (2.129) for the ground state distribution,

$$\rho_{GS}(\lambda) = \begin{cases} \int_{-B}^{B} d\lambda' [\delta(\lambda - \lambda') + L(\lambda, \lambda')] a_1(\lambda') & |\lambda| \leq B, \\ 0 & |\lambda| > B. \end{cases} \tag{2.133}$$

Knowing ρ_{GS} then yields ρ^h_{GS} from (2.128), namely

$$\rho^h_{GS}(\lambda) = \begin{cases} 0 & |\lambda| \leq B, \\ a_1(\lambda) - \int_{-B}^{B} d\lambda' a_2(\lambda - \lambda')\rho_{GS}(\lambda') & |\lambda| > B. \end{cases} \tag{2.134}$$

The ground state can also be obtained from the thermodynamic Bethe Ansatz formalism [141] in the following way. Given distributions $\rho(\lambda)$ and $\rho^h(\lambda)$, the free energy $f = (E - TS)/N$ is written to leading order in N as

$$f = -\frac{h}{2} + \int_{-\infty}^{\infty} d\lambda \left[\varepsilon_0\rho - T(\rho + \rho^h)\ln(\rho + \rho^h) + T\rho\ln\rho + T\rho^h\ln\rho^h\right] \tag{2.135}$$

in which we have suppressed the λ functional arguments and defined the bare energy

$$\varepsilon_0(\lambda) = h - \pi J \sin\zeta a_1(\lambda). \tag{2.136}$$

Introducing the quasi-energy $\varepsilon(\lambda) = T\ln\frac{\rho^h(\lambda)}{\rho(\lambda)}$, the condition of thermodynamic equilibrium $\delta F = 0$ under the constraint of the Bethe equations (2.128) then gives after standard manipulations [141] (taking the limit $T \to 0$, so here and in what follows, $\varepsilon(\lambda)$ is for the ground state configuration)

$$\varepsilon(\lambda) + \int_{-B}^{B} d\lambda' a_2(\lambda - \lambda')\varepsilon(\lambda') = \varepsilon_0(\lambda), \quad \lambda \in]-\infty, \infty[. \tag{2.137}$$

In particular, we have that

$$\varepsilon(\pm B) = 0, \quad \varepsilon(\lambda) \leq 0 (> 0) \text{for} \lambda \in (\notin)[-B, B]. \tag{2.138}$$

Similarly to (2.133), we can also solve for $\varepsilon(\lambda) = \varepsilon^-(\lambda) + \varepsilon^+(\lambda)$ with $\varepsilon^\pm(\lambda) \geq (\leq) 0$ using the inverse integral kernel:

$$\varepsilon^-(\lambda) = \begin{cases} \int_{-B}^{B} d\lambda'[\delta(\lambda - \lambda') + L(\lambda, \lambda')]\varepsilon_0(\lambda') & |\lambda| \leq B, \\ 0 & |\lambda| > B, \end{cases} \tag{2.139}$$

$$\varepsilon^+(\lambda) = \begin{cases} 0 & |\lambda| \leq B, \\ \varepsilon_0(\lambda) - \int_{-B}^{B} d\lambda' a_2(\lambda - \lambda')\varepsilon^-(\lambda') & |\lambda| > B. \end{cases} \tag{2.140}$$

The free energy simplifies to

$$f = -\frac{h}{2} + \int_{-B}^{B} d\lambda a_1(\lambda)\varepsilon(\lambda). \tag{2.141}$$

The magnetic equilibrium condition $\frac{\partial F}{\partial h} = 0$ then is

$$\int_{-B}^{B} d\lambda a_1(\lambda)\frac{\partial \varepsilon(\lambda)}{\partial h} = \frac{1}{2}. \tag{2.142}$$

By defining the dressed charge $Z(\lambda)$ as solution to

$$Z(\lambda) + \int_{-B}^{B} d\lambda' a_2(\lambda - \lambda')Z(\lambda') = 1, \tag{2.143}$$

which we can solve as

$$Z(\lambda) = 1 + \int_{-B}^{B} d\lambda' L(\lambda, \lambda'), \tag{2.144}$$

we have the identity $Z(\lambda) = \frac{\partial \varepsilon(\lambda)}{\partial h}$ by making use of (2.136) and (2.137). The Luttinger parameter K is given by the square of the dressed charge at the Fermi boundary (see *e.g.* [135]),

$$K = Z^2(-B). \tag{2.145}$$

The magnetic field dependence of the Fermi boundary B can be obtained by taking the h derivative of (2.137):

$$\int_{-B}^{B} d\lambda'[\delta(\lambda - \lambda') + a_2(\lambda - \lambda')]\frac{\partial \varepsilon(\lambda')}{\partial B} = \frac{\partial h}{\partial B}. \tag{2.146}$$

Since $\varepsilon(-B) = 0$, we have

$$\frac{\partial \varepsilon(\lambda)}{\partial \lambda}|_{\lambda=-B} = \frac{\partial \varepsilon(\lambda)}{\partial B}|_{\lambda=-B} \tag{2.147}$$

and therefore

$$\frac{\partial h}{\partial B} = \frac{\varepsilon'(-B)}{Z(-B)}. \tag{2.148}$$

The magnetization is

$$\sigma = -\frac{\partial f}{\partial h} = \frac{1}{2} - \int_{-B}^{B} d\lambda a_1(\lambda) \frac{\partial \varepsilon(\lambda)}{\partial h} = \frac{1}{2} - \int_{-B}^{B} d\lambda a_1(\lambda) Z(\lambda). \tag{2.149}$$

To get the susceptibility, we start from

$$\frac{\partial \sigma}{\partial B} = -\int_{-B}^{B} d\lambda a_1(\lambda) \frac{\partial Z(\lambda)}{\partial B} - a_1(B)Z(B) - a_1(-B)Z(-B). \tag{2.150}$$

The integral equation for the dressed charge (2.143) gives

$$\begin{aligned} \frac{\partial Z(\lambda)}{\partial B} &= -\int_{-B}^{B} d\lambda' [\delta(\lambda - \lambda') + L(\lambda, \lambda')] \\ &\quad \times [Z(B)a_2(\lambda' - B) + Z(-B)a_2(\lambda' + B)] \end{aligned} \tag{2.151}$$

which yields after simple manipulations and use of symmetry

$$\frac{\partial \sigma}{\partial B} = -2\rho_{GS}(-B)Z(-B). \tag{2.152}$$

The susceptibility is therefore given by

$$\chi = \frac{\partial \sigma}{\partial h} = \frac{\partial B}{\partial h}\frac{\partial \sigma}{\partial B} = -2\frac{\rho_{GS}(-B)Z^2(-B)}{\varepsilon'(-B)}. \tag{2.153}$$

This expression will be related to the Fermi velocity after discussing elementary excitations (see Eq.(2.175)).

Finally, we will need the slope of the ground state rapidity distribution

at the Fermi boundary, $\frac{\partial \rho_{GS}(\lambda)}{\partial B}|_{-B}$. From the integral equation for ρ_{GS}, we can write

$$\frac{\partial \rho_{GS}(\lambda)}{\partial B} = \rho_{GS}(-B)[L(\lambda, B) + L(\lambda, -B)]. \tag{2.154}$$

This can be related to the derivative of the dressed charge by using the representation

$$\frac{\partial Z(\lambda)}{\partial B} = L(\lambda, B) + L(\lambda, -B) + \int_{-B}^{B} d\lambda' \frac{\partial L(\lambda, \lambda')}{\partial B}. \tag{2.155}$$

From the definition of $L(\lambda, \lambda')$, we can show that

$$\frac{\partial L(\lambda, \lambda')}{\partial B} = L(\lambda, B)L(\lambda', B) + L(\lambda, -B)L(\lambda', -B) \tag{2.156}$$

and therefore

$$\frac{\partial Z(\lambda)}{\partial B} = [L(\lambda, B) + L(\lambda, -B)]Z(-B), \tag{2.157}$$

finally yielding

$$\frac{\partial \rho_{GS}(\lambda)}{\partial B}|_{-B} = \frac{\rho_{GS}(-B)}{Z(-B)} \frac{\partial Z(\lambda)}{\partial B}|_{-B}. \tag{2.158}$$

We will make use of these identities later, while relating the width of the two-particle continuum to field-dependent physical quantities.

Let's now construct an excited state over the finite-field ground state by generating a single particle-hole pair. That is, we select a quantum number $I_p \notin \{I^{GS}\}$ associated to a particle and $I_h \in \{I^{GS}\}$ associated to a hole, and write the excited state densities in x space as

$$\begin{aligned} \rho(x) &= \rho_{GS}(x) + \frac{1}{N}\delta\left(x - \frac{I_p}{N}\right) - \frac{1}{N}\delta\left(x - \frac{I_h}{N}\right), \\ \rho^h(x) &= \rho^h_{GS}(x) - \frac{1}{N}\delta\left(x - \frac{I_p}{N}\right) + \frac{1}{N}\delta\left(x - \frac{I_h}{N}\right), \end{aligned} \tag{2.159}$$

with once again $\rho(x) + \rho^h(x) \to 1$ as $N \to \infty$. We can again map to rapidity space, with $\lambda_p \leq -B$ and $|\lambda_h| \leq B$. Upon creating such a particle-hole pair,

the induced distribution $\rho(\lambda)$ will be only very slightly shifted (order $1/N$) as compared to the ground state one (for $\lambda \neq \lambda_p, \lambda_h$). We therefore define a backflow function $K(\lambda; \lambda_p, \lambda_h) \sim \mathrm{O}(N^0)$ as

$$\rho(\lambda) = \rho_{GS}(\lambda) + \frac{1}{N}\left[K(\lambda; \lambda_p, \lambda_h) + \delta(\lambda - \lambda_p) - \delta(\lambda - \lambda_h)\right]. \tag{2.160}$$

By subtracting the equations for the ground state from those of the excited state, the backflow function is shown to obey the constraint

$$K(\lambda; \lambda_p, \lambda_h) + \int_{-B}^{B} d\lambda'\, a_2(\lambda - \lambda') K(\lambda'; \lambda_p, \lambda_h) = -a_2(\lambda - \lambda_p) + a_2(\lambda - \lambda_h) \tag{2.161}$$

for $\lambda \in [-B, B]$, with $K = 0$ outside of this domain. We can again formally solve for K by applying the inverse integral operator $1 + L$,

$$K(\lambda; \lambda_p; \lambda_h) = -a_2(\lambda - \lambda_p) - \int_{-B}^{B} d\lambda'\, L(\lambda, \lambda') a_2(\lambda' - \lambda_p) - L(\lambda, \lambda_h). \tag{2.162}$$

In terms of this kernel, the energy of the excited state is

$$\begin{aligned} E - E_{GS} &= N \int_{-\infty}^{\infty} d\lambda\, \varepsilon_0 \left[\rho - \rho_{GS}\right] \\ &= \varepsilon_0(\lambda_p) - \varepsilon_0(\lambda_h) + \int_{-B}^{B} d\lambda\, \varepsilon_0(\lambda) K(\lambda; \lambda_p, \lambda_h), \end{aligned} \tag{2.163}$$

which can be rewritten after basic manipulations as ($|\lambda_p| > B$ and $|\lambda_h| < B$)

$$E - E_{GS} = \varepsilon(\lambda_p) - \varepsilon(\lambda_h). \tag{2.164}$$

Similarly, the momentum of the excited state is

$$P - P_{GS} = -\phi_1(\lambda_p) + \phi_1(\lambda_h) - \int_{-B}^{B} d\lambda\, \phi_1(\lambda) K(\lambda; \lambda_p, \lambda_h). \tag{2.165}$$

Single particle-hole pairs as described above constitute a set of two-

particle excitations labeled by the particle and hole rapidities λ_p and λ_h. This continuum is well-defined and spanned by the intervals $\lambda_p \in \ ]-\infty, -B]$, $\lambda_h \in [-B, B]$. Assuming that the mapping from (λ_p, λ_h) to (ω, q) is one-to-one and onto and that the particle dispersion curvature is greater than the hole one (this monotonicity assumption will be discussed further in section 2.4.3), the highest energy state at a given fixed momentum q will be given by the choice $\lambda_p = \lambda_p(q)$, $\lambda_h = -B$, where $\lambda_p(q)$ is solution to

$$q = -\phi_1(\lambda_p(q)) + \phi_1(-B) + \int_{-B}^{B} d\lambda\, \phi_1(\lambda) K(\lambda; \lambda_p(q); -B). \tag{2.166}$$

Similarly, the lowest energy state will correspond to the choice $\lambda_p = -B$, $\lambda_h = \lambda_h(q)$, where $\lambda_h(q)$ is solution to

$$q = \phi_1(\lambda_h(q)) - \phi_1(-B) - \int_{-B}^{B} d\lambda\, \phi_1(\lambda) K(\lambda; -B; \lambda_h(q)). \tag{2.167}$$

As discussed in section 4, this continuum is well-defined (*i.e.* finite real solutions to both (2.166) and (2.167) can be found) as long as $q \leq \mathrm{Min}(2k_F, k_\infty)$, with $2k_F = \pi(1 - 2\sigma)$ and $k_\infty = 2\sigma(\pi - \zeta)$. This is illustrated in Figure (2.6). The width of the two-particle continuum defined by these excitations will thus be given by the energy difference between these two limiting configurations, namely

$$W(q) = \varepsilon(\lambda_p(q)) + \varepsilon(\lambda_h(q)) - 2\varepsilon(-B) = \varepsilon(\lambda_p(q)) + \varepsilon(\lambda_h(q)) \tag{2.168}$$

where we have used $\varepsilon(\pm B) = 0$. These functions are exact in the thermodynamic limit, in the sense that they allow one at least in principle to obtain the exact function $W(q)$ for the momentum region where these excitations are defined. These coupled equations unfortunately cannot be solved explicitly at nonzero magnetic field (where B is finite). We can however obtain analytical results in the small momentum limit, where these excitations always

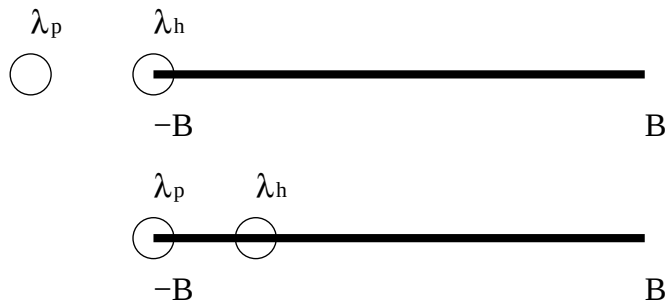

Figure 2.6: Highest and lowest energy two-particle excited states at fixed momentum. The straight line represents the interval $\lambda \in [-B, B]$ within which the ground-state rapidity $\rho_{GS}(\lambda)$ is nonvanishing. λ_p and λ_h respectively represent the positions of the particle and hole rapidities for the highest (top) and lowest (bottom) two-particle excited states at a fixed value of momentum.

exist in a finite region at finite field.

At small momentum, we can expand the width at fixed magnetic field as

$$W = qW^{(1)} + q^2 W^{(2)} + O(q^3) \tag{2.169}$$

with coefficients given explicitly by

$$W^{(1)} = \frac{\partial}{\partial q}(\varepsilon(\lambda_p(q)) + \varepsilon(\lambda_h(q)))|_{q=0}, \tag{2.170}$$

$$W^{(2)} = \frac{1}{2}\frac{\partial^2}{\partial q^2}(\varepsilon(\lambda_p(q)) + \varepsilon(\lambda_h(q)))|_{q=0}. \tag{2.171}$$

Let us treat the linear term first. Considering that (2.167) also defines a function $q(\lambda_h)$, we can rewrite the hole contribution to the coefficient as

$$\frac{\partial}{\partial q}\varepsilon(\lambda_h(q))|_{q=0} = \frac{\frac{\partial \varepsilon(\lambda_h)}{\partial \lambda_h}|_{\lambda_h=-B}}{\frac{\partial q(\lambda_h)}{\partial \lambda_h}|_{\lambda_h=-B}}. \tag{2.172}$$

The denominator is obtained from (2.167) as

$$\frac{\partial q}{\partial \lambda_h} = 2\pi a_1(\lambda_h) - \int_{-B}^{B} d\lambda \phi_1(\lambda) \frac{\partial K(\lambda; -B; \lambda_h)}{\partial \lambda_h} = 2\pi \rho_{GS}(\lambda_h) \tag{2.173}$$

where we have used (2.162), the symmetry of L and partial integration. This contribution is by definition related to the field-dependent Fermi velocity, namely

$$\frac{\partial}{\partial q}\varepsilon(\lambda_h)|_{q=0} = \frac{1}{2\pi} \lim_{\lambda \to -B^+} \frac{\varepsilon^{-\prime}(\lambda)}{\rho_{GS}(\lambda)} \equiv -v. \tag{2.174}$$

In particular, this allows us to relate the susceptibility to the Fermi velocity and the dressed charge using relation (2.153),

$$Z^2(-B) = \pi v \chi. \tag{2.175}$$

For the particle contribution to the linear term, we find similarly that $\frac{\partial q}{\partial \lambda_p} = -2\pi \rho^h_{GS}(\lambda_p)$. Since $\lim_{\lambda \to -B^-} \rho^h_{GS}(\lambda) = \lim_{\lambda \to -B^+} \rho_{GS}(\lambda)$, we also have

$$\frac{\partial}{\partial q}\varepsilon(\lambda_p)|_{q=0} = \frac{-1}{2\pi} \lim_{\lambda \to -B^-} \frac{\varepsilon^{+\prime}(\lambda)}{\rho^h_{GS}(\lambda)} = v \tag{2.176}$$

since ε is smooth around this point. Therefore, in the momentum expansion (2.169) for the width, the linear term vanishes:

$$W^{(1)} = \frac{\partial}{\partial q}(\varepsilon(\lambda_p(q)) + \varepsilon(\lambda_h(q)))|_{q=0} = 0. \tag{2.177}$$

The width therefore depends at least quadratically on momentum. To compute the coefficient of the quadratic term, we first note that given a function $\lambda(q)$ and its inverse $q(\lambda)$, the chain rule allows us to write

$$\frac{\partial^2}{\partial q^2}\varepsilon(\lambda(q))\bigg|_{q=0} = \left[\frac{\partial q}{\partial \lambda}\bigg|_{-B}\right]^{-2} \left(\frac{\partial^2 \varepsilon(\lambda)}{\partial \lambda^2}\bigg|_{-B} - \frac{\partial^2 q}{\partial \lambda^2}\bigg|_{-B} \frac{\partial \varepsilon(\lambda)}{\partial \lambda}\bigg|_{-B}\right). \tag{2.178}$$

From (2.166) and (2.167), we have that the particle and hole parts are related through

$$\left.\frac{\partial q(\lambda_p)}{\partial \lambda_p}\right|_{\lambda_p=-B} = -\left.\frac{\partial q(\lambda_h)}{\partial \lambda_h}\right|_{\lambda_h=-B}, \tag{2.179}$$

$$\left.\frac{\partial^2 q(\lambda_p)}{\partial \lambda_p^2}\right|_{\lambda_p=-B} = -\left.\frac{\partial^2 q(\lambda_h)}{\partial \lambda_h^2}\right|_{\lambda_h=-B}, \tag{2.180}$$

so using (2.178) for $\lambda_p(q)$ and $\lambda_h(q)$, we obtain that the quadratic coefficient of the width can be simplified to

$$W^{(2)} = \frac{1}{2}\frac{\partial^2}{\partial q^2}(\varepsilon(\lambda_p(q)) + \varepsilon(\lambda_h(q)))\Big|_{q=0} = \left[\left.\frac{\partial q}{\partial \lambda}\right|_{-B}\right]^{-2} \left.\frac{\partial^2 \varepsilon(\lambda)}{\partial \lambda^2}\right|_{-B}. \tag{2.181}$$

While this expression for the width is an end in itself, it is much more enlightening to relate it to more physical quantities by making use of the identities derived earlier. Starting from $\frac{\partial^2 \varepsilon(\lambda)}{\partial \lambda^2}|_{-B} = \frac{\partial^2 \varepsilon(\lambda)}{\partial B^2}|_{-B}$ and using (2.174) together with (2.158) and (2.175), we get

$$\left.\frac{\partial^2 \varepsilon(\lambda)}{\partial \lambda^2}\right|_{-B} = -2\pi\rho_{GS}(-B)\left(\frac{3}{2}\frac{\partial v}{\partial B} + \frac{1}{2}\frac{v}{\chi}\frac{\partial \chi}{\partial B}\right). \tag{2.182}$$

Putting this in (2.181) and making use of (2.148), (2.174) and (2.175) again, this finally gives

$$W^{(2)} = \sqrt{\frac{v}{\pi\chi}}\left[\frac{3}{2}\frac{\partial v}{\partial h} + \frac{1}{2}\frac{v}{\chi}\frac{\partial \chi}{\partial h}\right]. \tag{2.183}$$

Since we have the identity $K = Z^2(-B) = \pi v \chi$, this coincides with (2.97). It also reduces to the formula derived in [128] for $\Delta \ll 1$ by linearizing the Bethe Ansatz equations. While our derivation was done for the anisotropic chain in the gapless regime, the same calculation can be performed for the isotropic antiferromagnet by simply using the appropriate scattering kernels in the Bethe equations. This result is however limited to chains with finite magnetization, in view of the fact that the region of validity of the excitations

we have used to compute the width collapses to zero when the field vanishes.

2.4.3 Comparison with numerical form factors

In order to compare the field theory results with the dynamical structure factor for finite chains, we first fix the parameters of the bosonic model introduced in section 2.2.1. We do that by calculating $v(\Delta, h)$ and $K(\Delta, h) = \pi v(\Delta, h)\chi(\Delta, h)$ numerically using the Bethe Ansatz integral equations in the thermodynamic limit. η_- and η_+ are obtained by linearizing the field dependence of v and K around some fixed h_0 and using (2.97) and (2.98). As examples, we consider three values of the anisotropy, $\Delta = 0.25$, $\Delta = 0.75$ and the Heisenberg point $\Delta = 1$, at a fixed magnetization per site $\sigma = -0.1$. Table 2.1 lists the values of the important parameters (we set $J = 1$). Note that b is negative for $\sigma < 0$ ($m > 0$) because K decreases as we approach half-filling [98].

Table 2.1: Parameters for the low-energy effective model for $\Delta = 0.25$, $\Delta = 0.75$ and $\Delta = 1$ and finite magnetic field h_0 (in all cases the magnetization per site is $\sigma = -0.1$).

Δ	h_0	v	K	a	b	η_-	η_+
0.25	-0.414	1.087	0.871	0.306	-0.050	0.356	-0.095
0.75	-0.652	1.313	0.699	0.271	-0.145	0.409	-0.449
1	-0.791	1.399	0.639	0.256	-0.188	0.397	-0.690

As mentioned in section 2.3.2, we are able to calculate the exact transition probabilities $F^2(q, \omega) \equiv \left|\langle 0 \left| S_q^z \right| \alpha\rangle\right|^2$ for finite chains by means of the Algebraic Bethe Ansatz [115, 116, 117]. Figure 2.7 illustrates a typical result obtained for finite anisotropy and finite magnetic field. In contrast with the free fermion case, we observe two main differences when we turn on the fermion interaction Δ: First, the form factors for the two-particle (on-shell) states become ω-dependent; second, the form factors for multiparticle states are now finite and account for a finite spectral weight extending up to high

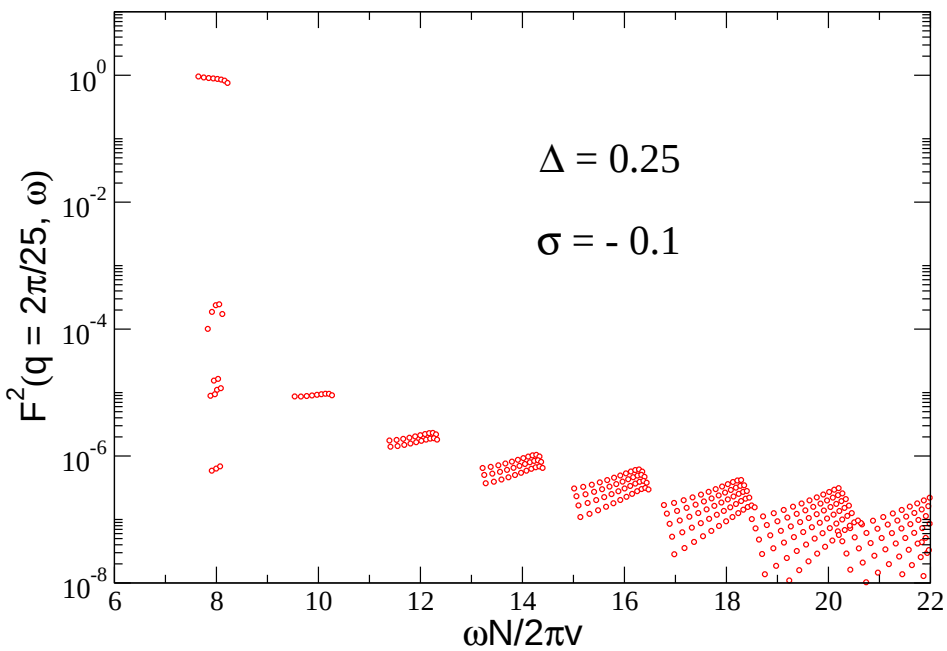

Figure 2.7: Numerical form factors squared (transition probabilities) for states with momentum $q = 2\pi/25$, for a chain with $N = 200$ sites, anisotropy $\Delta = 0.25$, magnetization per site $\sigma = -0.1$. The energies of the eigenstates are rescaled by the level spacing of the bosonic states predicted by field theory. The on-shell states are the ones at $\omega N/2\pi v = qN/2\pi = 8$.

energies. For the four-particle states (two particle-hole pairs), we expect $\langle 0 \left| S_q^z \right| \alpha \rangle \sim O(\Delta)$, but this is not true near $\omega \approx vq$ where perturbation theory in the interaction diverges [124]. Figure 2.7 suggests that most of the exact form factors evolve smoothly from the XX point, except close to the lower and upper thresholds. If that is the case, the two-particle states still carry most of the spectral weight. In the thermodynamic limit, $F^2(q,\omega)$ has to be combined with the density of states factor

$$D(q,\omega) = \frac{2\pi}{N} \sum_{\alpha} \delta(\omega - E_\alpha + E_{GS}), \tag{2.184}$$

to define the line shape of $S^{zz}(q,\omega)$ (see (2.3)).

We can count the states at each energy level of the finite system in the Bethe Ansatz the same way we count states for weakly interacting fermions. For example, in figure 2.7 we see $n \equiv qN/2\pi = 8$ two-particle states with $F^2 \sim O(1)$. One can also verify that for $n = 8$ there are 14 states with two right-moving particle-hole pairs (of the form $c^\dagger_{p_1+q_1,R} c_{p_1,R} c^\dagger_{p_2+q_2,R} c_{p_2,R} |0\rangle$) and no states with three or more pairs. The 14 on-shell states with $F^2(q,\omega) < 10^{-3}$ in figure 2.7 are all four-particle states. Furthermore, for small Δ the main contribution to the high-frequency tail ($\ell \equiv \omega N/2\pi v > n$) is due to states containing two particle-hole excitations created around the two different Fermi points [123]. If the momenta of the pairs at the right and left branches are $q_1 = 2\pi n_1/N > 0$ and $q_2 = 2\pi n_2/N < 0$, such that $n_1 = (\ell + n)/2$ and $n_2 = -(\ell - n)/2$, then the number of such states is given by $|n_1 \times n_2| = (\ell^2 - n^2)/4$. This is in agreement with the counting of states in figure 2.7. We also find much smaller form factors for states with three particle-hole pairs (not shown in the figure).

We now focus on the two-particle states inside the peak, with $\omega \approx vq$. If we seek only these states with dominant form factors it is possible to reach much larger system sizes (we go up to 7000 sites). The number of two-particle states is always $n = qN/2\pi$. Figure 2.8 shows $F^2(q,\omega)$ for a fixed value of

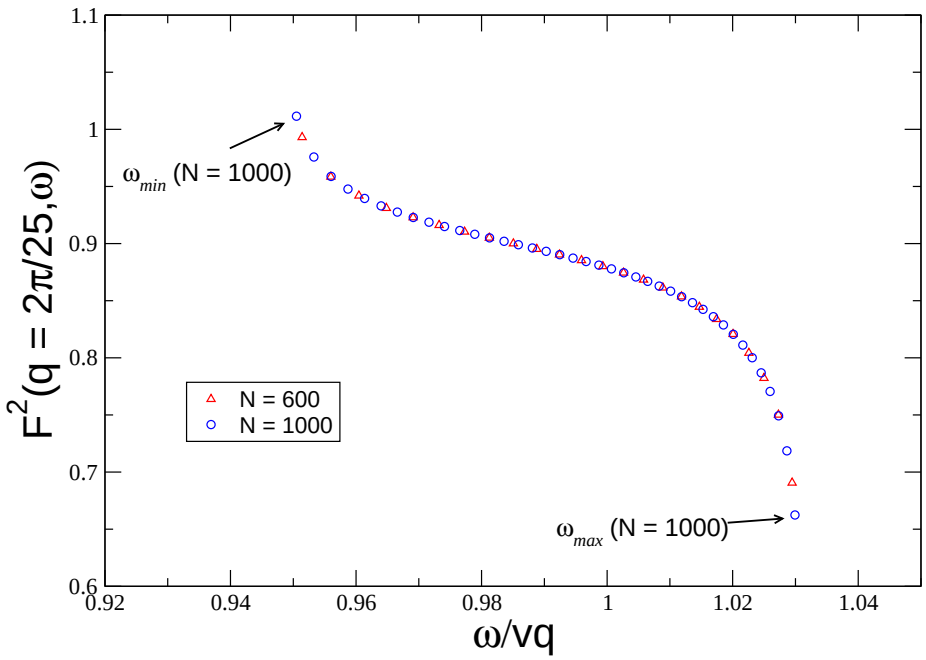

Figure 2.8: Form factors squared for the two-particle states for two values of system size N (we set $q = 2\pi/25$, $\Delta = 0.25$ and $\sigma = -0.1$). The points seem to collapse on a single curve, showing very little size dependence. The minimum and maximum energies converge to the thresholds of the two-particle continuum when $N \to \infty$.

$q = 2\pi/25$ and two different system sizes.

We extract $\delta\omega_q$ from the numerical form factors as follows. We see from figure 2.8 that the separation between energy levels inside the peak is of order $\delta\omega_q/N$ and decreases from $\omega_L(q)$ to $\omega_U(q)$. As N increases, the maximum and minimum energies $\omega_{max,min}(N)$ converge to fixed values which we identify as the thresholds of the two-particle continuum. Both the minimum and maximum energies are found to scale linearly with $1/N$. We use the finite size scaling to determine the lower and upper thresholds $\omega_{L,U}(q)$ in the thermodynamic limit for several values of q.

We then calculate the width $\delta\omega_q = \omega_U(q) - \omega_L(q)$. As expected, we find

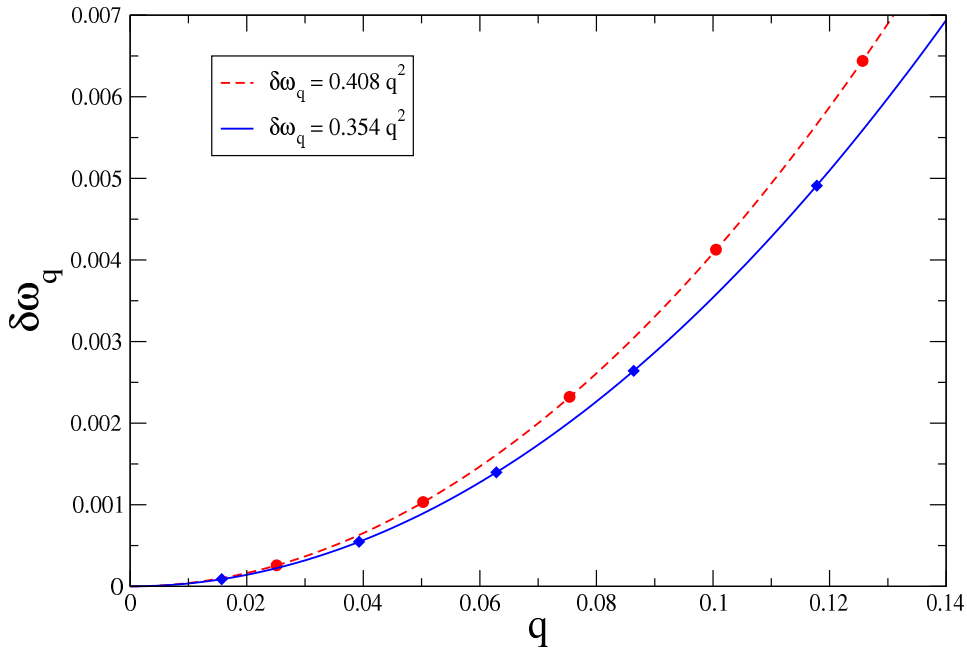

Figure 2.9: Width of the on-shell peak (based on the two-particle contribution) as a function of momentum q for $\sigma = -0.1$ and two values of anisotropy: $\Delta = 0.25$ (blue diamonds) and $\Delta = 0.75$ (red circles). The lines are the best fit to the data.

that $\delta\omega_q = q^2/m^*$ for small q (figure 2.9). Table 2.2 compares the coefficients $1/m^*_{FIT}$ obtained by fitting the data with the predicted values of η_- taken from Table 2.1. The perturbative result in (2.72) is also shown for comparison. The agreement supports our formula for the width in the strongly interacting (finite Δ) regime. Note that η_- is a nonmonotonic function of Δ.

In figure 2.10 we confirm that, despite the enhancement (suppression) near the lower (upper) threshold, $F^2(q,\omega)$ converges to the constant value $F^2(q,\omega) = K$ in the limit $q \to 0$, as expected from the box-like shape shown in figure 2.5 (see however the subtleties about the thermodynamic limit discussed in [142]). This is in agreement with the fact that the exponents of the

Table 2.2: Effective inverse mass, defined as the coefficient of the q^2 scaling of the width $\delta\omega_q$. The data are for $\sigma = -0.1$ and anisotropy parameters $\Delta = 0.25, 0.75, 1$.

Δ	$1/m^*_{FIT}$	η_-	$\frac{1}{m}\left(1+\frac{2\Delta}{\pi}\sin k_F\right)$
0.25	0.354	0.356	0.356
0.75	0.408	0.409	0.449
1	0.396	0.397	0.496

singularities at the edges are linear in q for $h \neq 0$ [124]. Notice that $F^2(q,\omega)$ (and therefore $S^{zz}(q,\omega)$) is *not* a scaling function of $(\omega - vq)/\delta\omega_q$.

If the density of states $D(q,\omega)$ for the two-particle states were constant, the extrapolation of figure 2.8 to the thermodynamic limit would be representative of the line shape of $S^{zz}(q,\omega)$. This would be exactly the case if the exact energies $E_\alpha - E_{GS}$ could be written as the sum of the energies of particles and holes with parabolic dispersion (as in a Galilean-invariant system, *e.g.* the Calogero-Sutherland model [125]). This is also the case considered in [124]. In our case $D(q,\omega)$ does vary inside the peak because of the cubic terms in the dispersion of the particles in the Bethe Ansatz. For large enough N we can include the density of states factor (2.184) if we rescale $F^2(q,\omega)$ by the separation between energy levels inside the peak

$$S^{zz}(q,\omega) = D(q,\omega)F^2(q,\omega) \approx \frac{2\pi}{N}\frac{F^2(q,\omega)}{E_{j+1}-E_j}, \tag{2.185}$$

where E_j and E_{j+1} are the energies of the two-particles states, ordered in energy, with $E_j - E_{GS} = \omega$. The approximate density of states calculated this way is illustrated in figure 2.11. The resulting line shape is shown in figure 2.12. This line shape should be contrasted with the free fermion result in figure 2.1. The exact boundaries of the two-particle continuum (dotted line in figure 2.12) are actually shifted to lower energies relatively to the prediction $\omega_{U,L}(q) = vq \pm \eta_- q^2/2$ (dashed lines) because of the cubic term

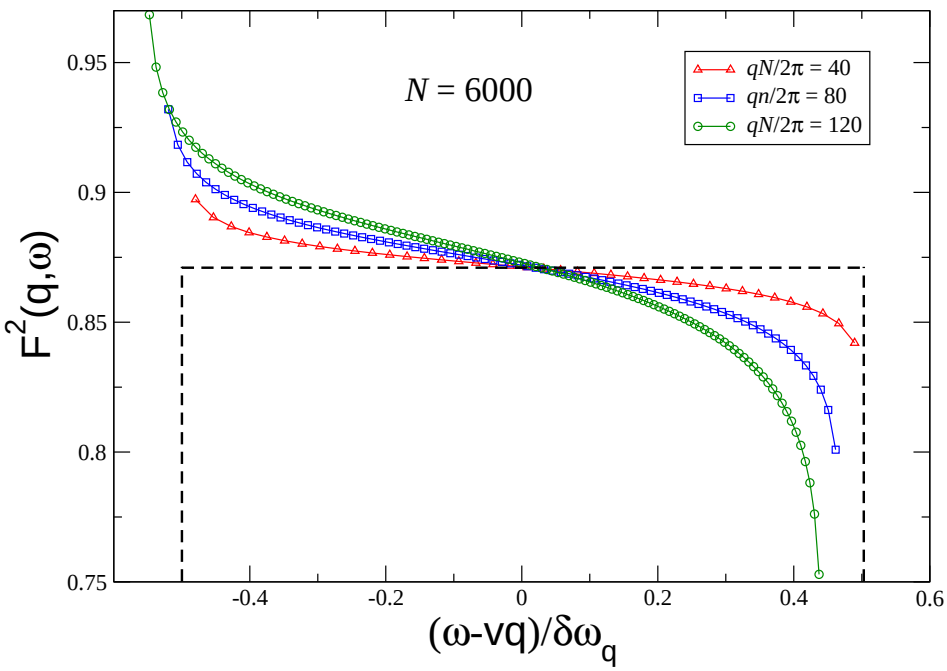

Figure 2.10: Frequency dependence of the form factors squared for $N = 6000$, $\Delta = 0.25$, $\sigma = -0.1$, and three values of momentum. The dashed line represents the field theory prediction $F^2(q,\omega) = K \approx 0.871$, as in figure 2.5.

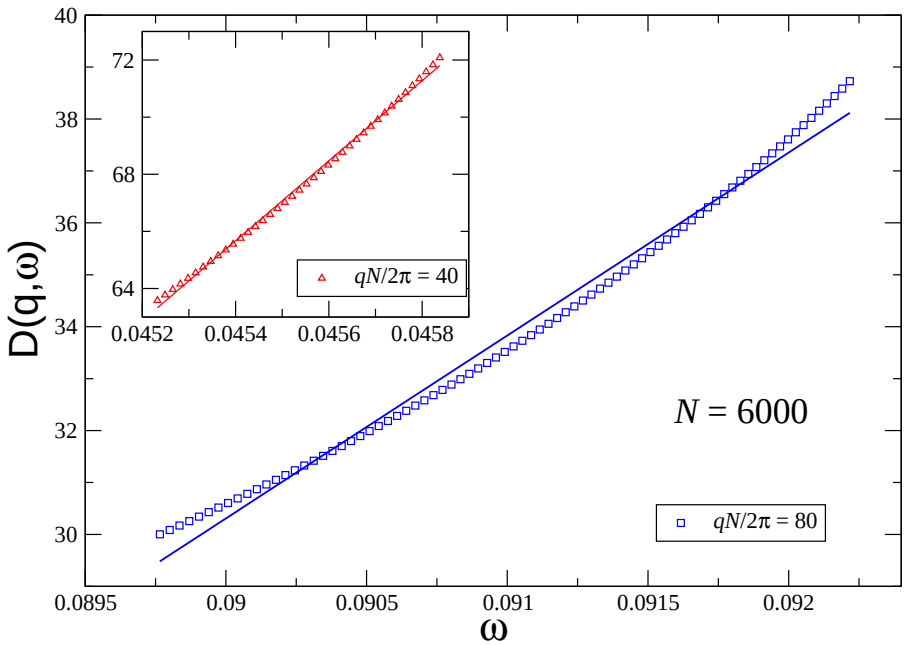

Figure 2.11: Density of states $D(q,\omega)$ for the two-particle states obtained using (2.185). As in figure 2.10, we use $N = 6000$, $\Delta = 0.25$ and $\sigma = -0.1$. The main graph is for $qN/2\pi = 80$. The inset shows the density of states for a smaller value of momentum, $qN/2\pi = 40$. The solid lines are meant to illustrate the deviation of $D(q,\omega)$ from the linear dependence in ω.

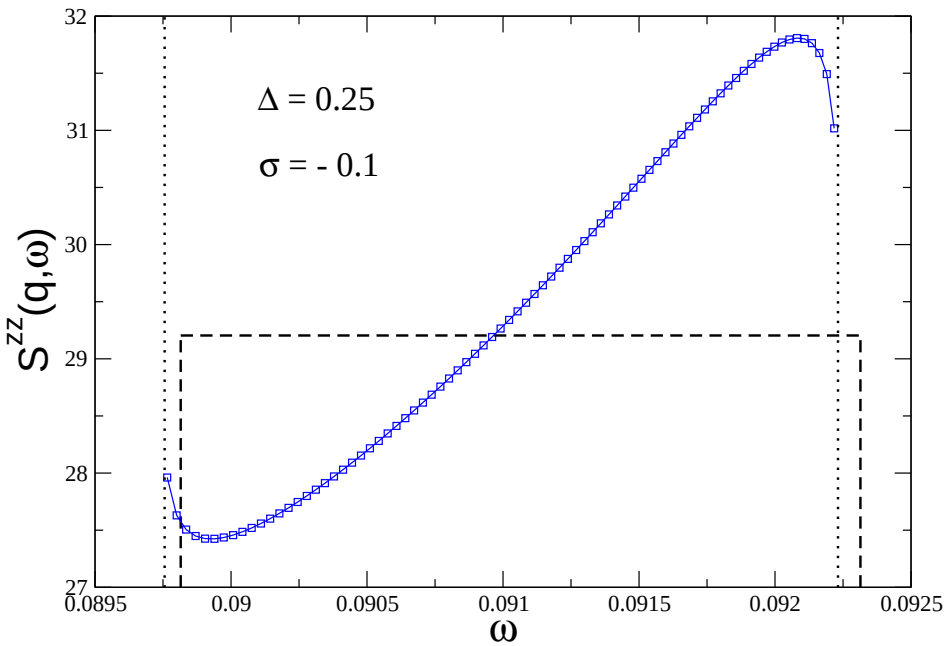

Figure 2.12: Line shape of $S^{zz}(q,\omega)$ estimated from the two-particle states. For this graph $\Delta = 0.25$, $\sigma = -0.1$, $N = 6000$ and $qN/2\pi = 80$. The dashed line is the flat distribution of figure 2.5 (zoom on the top of the peak). The dotted lines are the exact boundaries of the two-particle continuum in the thermodynamic limit.

in the exact dispersion, which was neglected in the field theory approach. Notice that there appears to be a peak at the exact lower threshold of the two-particle continuum. The result of Pustilnik *et al.* predicts that there is actually a power-law singularity at $\omega_L(q)$, which is related to the physics of the X-ray edge problem [124]. We do not attempt to study the singularity in the form factors here. Finite size effects in the contribution from each family of Bethe ansatz eigenstates prevent us from extracting the exponents directly from the numerical form factors. (A more detailed discussion about finite size scaling can be found in [142]). Interestingly, however, the density of states competes with the energy dependence of the form factors, leading to a minimum in $S^{zz}(q,\omega)$ above $\omega_L(q)$ and a rounded peak below $\omega_U(q)$. In the limit $q \ll \cot k_F$ we can linearize the density of states for the two-particle states

$$D(q,\omega) \approx \frac{2\pi/N}{E_{j+1}-E_j} \approx \frac{1}{\eta_- q}\left[1+\frac{\tilde{\gamma}q}{\eta_-}\frac{\omega - vq}{\delta\omega_q}\right], \tag{2.186}$$

where $\tilde{\gamma}$ is a fitting parameter analogous to γ in (2.21) for the free fermion model. The inset of figure 2.11 shows the density of states for a smaller value of $q = 2\pi(40/6000)$. We have checked that $D(q,\omega)$ becomes more linear and $\tilde{\gamma}$ converges to a finite value as q decreases. For $\Delta = 0.25$ and $\sigma = -0.1$ we estimate $\tilde{\gamma} \approx 1.11$, which is larger than the value for free fermions $\gamma = \sin(2\pi/5) \approx 0.951$. Combining this density of states with the power-law singularity proposed in [124], the behavior near the lower threshold is described by the function

$$S^{zz}(q,\omega) \approx \frac{K}{\eta_- q}\left[1-\frac{\tilde{\gamma}q}{2\eta_-}+\frac{\tilde{\gamma}q}{\eta_-}\frac{\omega-\omega_L(q)}{\delta\omega_q}\right]\left[\frac{\omega-\omega_L(q)}{\delta\omega_q}\right]^{-\mu_q}, \tag{2.187}$$

where μ_q is the exponent of the X-ray edge singularity. The position of the minimum is then

$$\frac{\omega^* - \omega_L(q)}{\delta\omega_q} \approx \frac{\eta_-\mu_q}{\tilde{\gamma}q}, \tag{2.188}$$

for $\tilde{\gamma}q/\eta_- \ll 1$ and $\mu_q \ll 1$. Since $\mu_q \propto q$ for small q, the right-hand side of

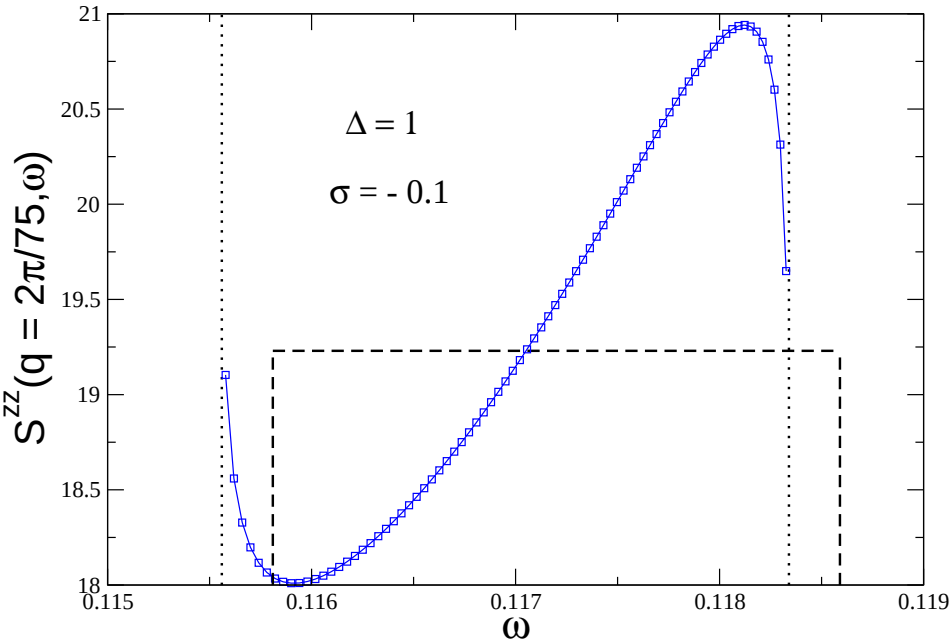

Figure 2.13: Line shape for the Heisenberg chain at finite field ($\Delta = 1$, $\sigma = -0.1$, $N = 6000$ and $qN/2\pi = 80$). Lines and symbols are represented as in figure 2.12.

(2.188) becomes constant in the limit $q \to 0$. In this sense, the X-ray edge singularity and the energy dependence of the density of states are effects of the same order in q. We notice that the difference ΔS^{zz}, defined between the maximum and the minimum of $S^{zz}(q,\omega)$, converges to a finite value as $q \to 0$ (as it did for free fermions). The precise value depends on both the density of states $D(q,\omega)$ and the frequency dependence of $F^2(q,\omega)$ (which is approximately linear with a negative slope for $|\omega - vq| \ll \delta\omega_q$). As a result, the slope of $S^{zz}(q,\omega)$ near the center of the peak diverges as $1/q^2$ as $q \to 0$. This is a rather singular dependence of the line shape on $\tilde{\gamma}$ and is potentially important for systems in which the dispersion is not exactly parabolic (*e.g.* due to band mixing in semiconductor quantum wires).

Figure 2.13 shows the line shape for the isotropic point $\Delta = 1$ and the

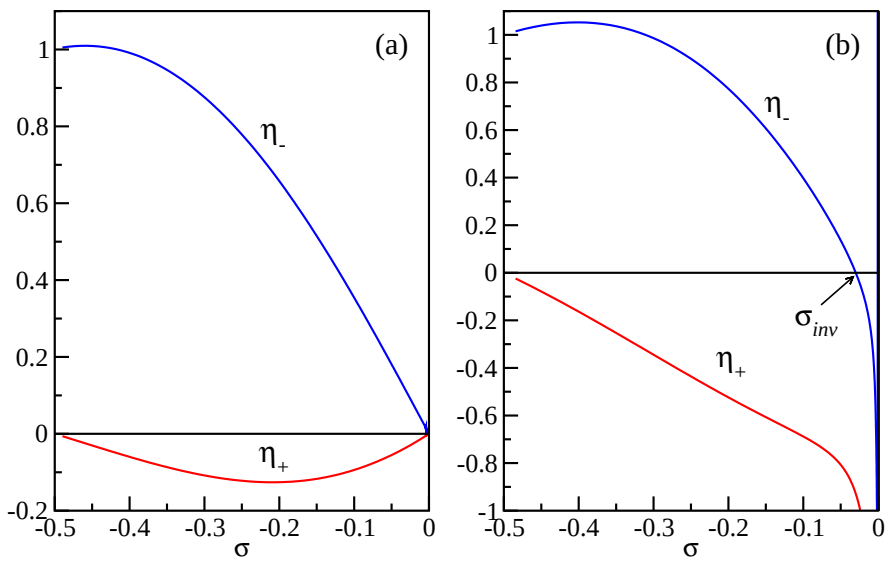

Figure 2.14: Parameters $\eta_\pm$ for the low energy effective Hamiltonian as a function of the magnetization $\sigma < 0$ for two values of anisotropy: (a) $\Delta = 0.25$; (b) $\Delta = 1$. For $\sigma > 0$, we have $\eta_\pm(-\sigma) = -\eta_\pm(\sigma)$.

same values of σ and q used in figure 2.12. In comparison with the weak coupling value $\Delta = 0.25$, there is an enhancement of the singularities near the lower and upper thresholds. The shift of the peak to lower energies (another "q^3 effect") is also more pronounced, but the width is very well described by the field theory formula (prefactor given in table 2.2).

Finally, let us comment on the validity of the q^2 scaling for the width as a function of magnetic field. Figure 2.14 shows the dependence of the coupling constants of the irrelevant operators on the magnetization σ for $\Delta = 0.25$ and $\Delta = 1$. From the field theory standpoint, we expect that the q^2 scaling is valid as long as $\eta_- q^2 \ll vq$ (the peak is narrow) and $\eta_\pm q^2 \gg \tilde{\gamma} q^3$ (the cubic terms yield the leading correction to the free boson result and we can drop operators with dimension four and higher in the effective Hamiltonian). For $\Delta = 0.25$, we see that $\eta_\pm$ follow the behavior predicted by the weak coupling expressions (2.72) and (2.73), vanishing at $\sigma = 0$. In this case, $\eta_\pm$ are always of $O(1)$.

The restrictions are similar to the ones for the approximation (2.24) for the dynamical structure factor of the XY model, namely $q \ll k_F$ and $q \ll \cot k_F$ (which becomes $q \ll \pi\sigma$ for small σ). On the other hand, for $\Delta = 1$ we find that $|\eta_\pm| \to \infty$ as $\sigma \to 0$. This is a direct consequence of formulas (2.97) and (2.98) in the strong coupling regime. It is known that the magnetic susceptibility at small fields is given by $\chi(h) \sim \text{const} + C_1 h^2 + C_2 h^{8K-4}$, where $C_{1,2}$ are constants [139, 143]. The exponent $8K - 4$ is a manifestation of the Umklapp scattering term at zero magnetic field. As a result, $\partial\chi/\partial h$ diverges as $h \to 0$ for $K < 5/8$ or $\Delta > \cos(\pi/5) \approx 0.81$. In other words, the Luttinger parameter has an infinite slope at $h = 0$ (see [144] for the isotropic case). Since $\partial K/\partial h$ and $\partial v/\partial h$ have opposite signs, η_- goes through zero for a finite value of σ. Therefore, we predict that $\delta\omega_q$ is a nonmonotonic function of σ for $\Delta > \cos(\pi/5)$ and $|\sigma| \ll 1$. The sign change in η_- is reflected in the Bethe Ansatz data as the inversion of the ordering of the energies of the two-particle states as a function of hole momentum. For $\Delta = 1$, the "inversion point" where $\eta_- = 0$ occurs at $|\sigma_{inv}| \approx 0.030$. At this point we observe that $\delta\omega_q \propto q^3$ for $q \ll \pi\sigma$. However, $\eta_+ \sim O(1)$, so the line shape defined by the two-particle states must be different from the one at zero field, where there is also a q^3 scaling (see section 2.6). We have also confirmed that the q^2 scaling holds in the region where $\eta_- < 0$ and $q \ll \pi|\sigma|$ (figure 2.15). In this regime we find that the sign change of η_- is accompanied by the inversion of the line shape of $S^{zz}(q, \omega)$: The form factors appear to vanish at the lower threshold and are peaked near the upper threshold (with a possible divergence at ω_U) (figure 2.16). There is no maximum or minimum near the edges in this case. In order to understand this result, we recall that a *converging X-ray edge* is possible in strongly interacting systems. An important point is that the exponents of the X-ray edge singularities calculated in [124], which predict a diverging X-ray edge, are valid only to first order in the interactions. Second order corrections, which usually have the opposite sign because of the orthogonality catastrophe, tend to kill the divergence at the lower edge [145].

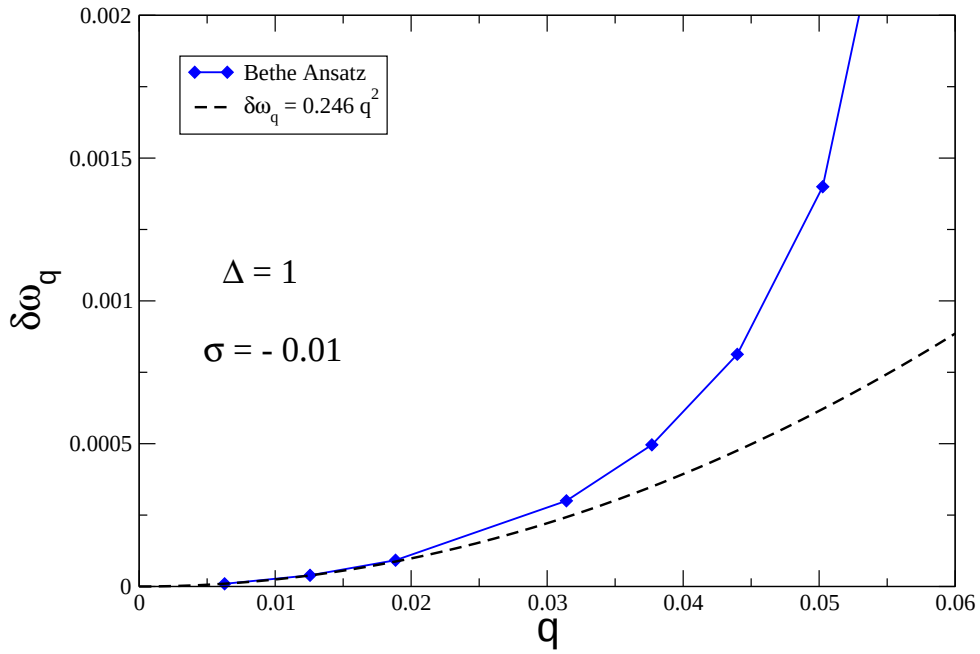

Figure 2.15: Width $\delta\omega_q$ for $\Delta = 1$ and $\sigma = -0.01$ (in the region where $\eta_- < 0$). The blue diamonds represent the width defined as the difference between the maximum and minimum energies of the two-particle states calculated in the Bethe Ansatz, extrapolated to the thermodynamic limit. For $q \ll \pi|\sigma|$, we recover the behavior $\delta\omega_q = |\eta_-|q^2$, with $|\eta_-| \approx 0.246$ (dashed line).

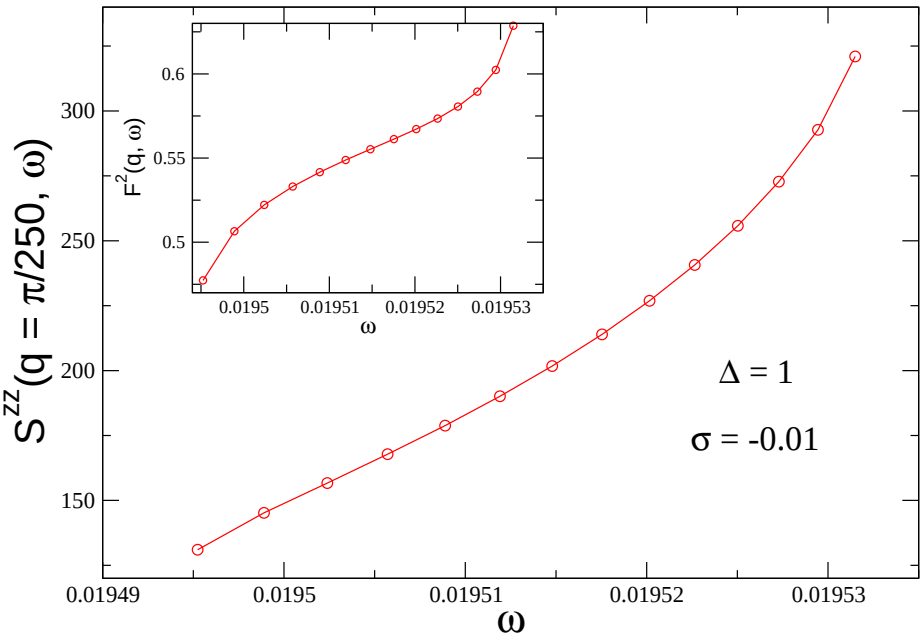

Figure 2.16: Line shape of $S^{zz}(q, \omega)$ for magnetization below the inversion point, *i.e.* $|\sigma| < \sigma_{inv}$ ($\Delta = 1$, $\sigma = -0.01$, $N = 7000$ and $qN/2\pi = 14$). This value of q is in the domain where $\delta\omega_q \sim q^2$ (see figure 2.15), but the line shape is inverted. In contrast with figure 2.8, the form factors (shown in the inset) are peaked at the upper threshold of the two-particle continuum.

For even smaller values of σ, the divergence of η_- seems to be consistent with the Bethe Ansatz results. For $|\sigma| < \sigma_{inv}$, the width increases as $|\sigma|$ decreases at least down to $\sigma = -0.001$, the lowest magnetization we were able to analyze. In the limit $\sigma \to 0$ and $|\eta_\pm| \gg 1$, we expect for the isotropic point (using the results of [144, 146])

$$\frac{\eta_+}{3} \to \eta_- \to \frac{J}{8\sqrt{2}\sigma \ln |\sigma_0/\sigma|}, \tag{2.189}$$

where $\sigma_0 = \sqrt{32/\pi e}$. According to the conditions $\tilde{\gamma} q^2 \ll \eta_- q \ll v$, the field theory result which predicts the q^2 scaling for a small fixed q breaks down

both near the inversion point σ_{inv} and for $\sigma \to 0$. In the limit $\sigma \to 0$, as mentioned in section 4.2, the set of allowable quantum numbers for the single particle-hole excitations becomes empty, as the I_∞ quantum number tends to $N/2$ (meaning that the particle part becomes trapped at the Fermi surface), and this family of excitations disappears. The vanishing field two-particle continuum at nonvanishing momentum is then obtained by considering the next simplest excitations, which are states having two holes (spinons) within the ground state configuration together with a single negative parity one-string (or, for the XXX chain, an infinite rapidity). At finite but small field, the contributions from these states dominate $S^{zz}(q,\omega)$ for $q \gg \pi\sigma$ and allow to smoothly recover the zero field behavior. A full discussion of all the possible line shapes as a function of Δ and σ together with the characterization of the dominant families of excitations is accessible from the results of [117], but is beyond the scope of the present work.

2.5 High-frequency tail

We now turn to the calculation of $S^{zz}(q,\omega)$ in the frequency range $\gamma_q \ll \omega - vq \ll J$, where finite order perturbation theory is expected to be valid. This off-shell spectral weight is possible because the η_+ interaction allows for two-boson intermediate states with total momentum $q = q_1 + q_2$ but energy $\omega = v\,|q_1| + v\,|q_2| > v\,|q|$ if $\mathrm{sign}(q_1) = -\mathrm{sign}(q_2)$. In other words, the incoming boson can decay into one right-moving and one left-moving boson, which together can carry small momentum but high energy $\omega \gg v\,|q|$. In the limit $\Delta \ll 1$, this is equivalent to a state with two particle-hole pairs created around the two different Fermi points [123]. In this sense, our η_+ is analogous to the U_q interaction in [124]. We should stress that, although the tail carries a small fraction of the spectral weight of $S^{zz}(q,\omega)$, it is important for response functions that depend on the overlap of two spectral functions, *e.g.* the drag resistivity in the fermionic version of the problem [123]. In

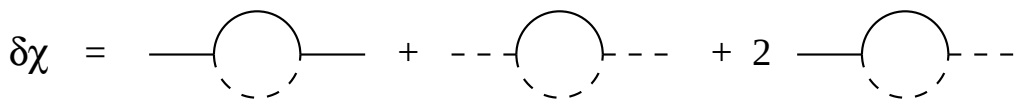

Figure 2.17: Diagrams at $O(\eta_+^2)$ for the calculation of the tail.

our formalism the calculation of the tail provides a direct quantitative check of the accuracy of the low energy effective model against the form factors calculated by Bethe Ansatz.

2.5.1 Field theory prediction

The lowest-order correction to $\chi(q, i\omega_n)$ due to the η_+ interaction is

$$\delta\chi(q, i\omega_n) = -\int_0^L dx\, e^{-iqx} \int_0^\beta d\tau\, e^{i\omega\tau} \delta\chi(x, \tau), \tag{2.190}$$

where $\delta\chi(x, \tau)$ is the correlation function in real space given by

$$\begin{aligned} \delta\chi(x, \tau) &= \frac{K}{\pi}\frac{1}{2}\left(\frac{\sqrt{2\pi}}{6}\eta_+\right)^2 \int d^2x_1 \int d^2x_2 \\ &\quad \times \left\langle \partial_x\phi(x)\left[(\partial_x\varphi_L(1))^2 \partial_x\varphi_R(1) - (R \leftrightarrow L)\right]\right. \\ &\quad \times \left.\left[(\partial_x\varphi_R(2))^2 \partial_x\varphi_L(2) - (R \leftrightarrow L)\right]\partial_x\phi(0).\right\rangle \end{aligned} \tag{2.191}$$

This corresponds to the diagrams in figure 2.17. $\delta\chi$ can be factored in the form

$$\delta\chi(q, i\omega) = \frac{K}{2\pi}\left[D_R^{(0)}(q, i\omega) + D_L^{(0)}(q, i\omega)\right]^2 \Pi_{RL}(q, i\omega), \tag{2.192}$$

where $\Pi_{RL}(q, i\omega)$ is the bubble with right- and left-moving bosons

$$\Pi_{RL}(q, i\omega) = -\frac{2\pi\eta_+^2}{9}\int_{-\infty}^{+\infty} dx\, e^{-iqx} \int_0^\beta d\tau\, e^{i\omega\tau} D_R^{(0)}(x, \tau)\, D_L^{(0)}(x, \tau)$$

$$= -\frac{2\pi\eta_+^2}{9}\int_{-\Lambda}^{+\Lambda}\frac{dk}{2\pi}\int_{-\infty}^{+\infty}\frac{d\nu}{2\pi}D_R^{(0)}(k,i\nu) \times D_L^{(0)}(q-k,i\omega-i\nu), \tag{2.193}$$

where $\Lambda \sim k_F$ is a momentum cutoff. After integrating over frequency, we get

$$\Pi_{RL}^{ret}(q,\omega) = -\frac{\eta_+^2}{9}\left[\int_0^{\Lambda} dk\,\frac{k(q+k)}{\omega+vq+2vk+i\eta} + \int_q^{\Lambda} dk\,\frac{k(q-k)}{\omega+vq-2vk+i\eta}\right]. \tag{2.194}$$

Note that the real part of Π_{RL}^{ret} is ultraviolet-divergent, but the imaginary part is not. The integration over the internal momentum yields

$$\Pi_{RL}^{ret}(q,\omega) = -\frac{\eta_+^2}{9}\left\{\frac{\Lambda^2}{2v} - \frac{\omega^2-v^2q^2}{8v^3}\log\left[\frac{(vq)^2-(\omega+i\eta)^2}{4v^2\Lambda^2}\right]\right\}. \tag{2.195}$$

Finally, using Eqs. (2.192) and (2.4), we find that the high-frequency tail of $S^{zz}(q,\omega)$ is given by

$$\delta S^{zz}(q,\omega) = \frac{K\eta_+^2 q^4}{18v}\,\frac{\theta(\omega-vq)}{\omega^2-v^2q^2}. \tag{2.196}$$

This is the same ω^{-2} dependence obtained for weakly interacting fermions with parabolic dispersion [123]. Since the small parameter is $\eta_+ \sim \Delta/m$, we approach the perturbative regime either by $\Delta \to 0$ or $m \to \infty$ (more precisely, $q/mv \to 0$). In this limit, our result (2.196) agrees with Eq.(19) of [123] if we use (2.73) and $U(q) = (\Delta/2)\cos q$.

Since our model predicts that $\delta S^{zz}(q,\omega \gg vq) \sim O(\eta_+^2)$, one interesting consequence is that there will be no tail in $S(q,\omega)$ for models where the Luttinger parameter K is independent of particle density, since then $\eta_+ = 0$ according to (2.98). This is the case for the Calogero-Sutherland model,

where K is a function of the amplitude of the long-range interaction only [147].

The divergence of the high-frequency tail of $\delta S^{zz}(q,\omega)$ as $\omega \to vq$ confirms that the on-shell region is not accessible by our standard perturbation theory in the band curvature terms. The matching of the tail to the on-shell peak at $\omega_U(q)$ is a complicated problem that has only been addressed in the regime $\Delta \ll 1$ (see [124]). The $(\omega - vq)^{-1}$ divergence in (2.196) comes from the frequency dependence of the external legs in the diagrams of figure 2.17. It is easy to see that if the bosonic propagators are replaced by the "dressed" propagator (all orders in η_-) given by (2.119), the singularity at the upper threshold $\omega_U(q)$ becomes only logarithmic. This supports the picture that the η_+ interaction only modifies the shape of the on-shell peak very close to the edges. We expect that η_+ will contribute to the exponent of the singularity at the edges, since the exponent μ_q derived in [124] picks up corrections of second order in the interaction between right and left movers, *i.e.* $O(\eta_+^2)$. As discussed in section 2.4.1, we believe that η_+ does not affect the width to $O(q^2)$. Evidence for that is that the perturbation theory in η_+ (second order given by (2.195)) does not generate terms with the same q and ω dependence as in (2.116) and (2.117). If the frequency dependence is regularized in the peak region by summing the perturbation theory in η_-, the diagrams involving η_+ are always suppressed by higher powers of q because of simple kinematics. Inside the peak the energy of the left moving boson that is put on shell when taking the imaginary part of $\chi(q,\omega)$ (as in the "unitarity condition" method used in [131]) has to be of order $\delta\omega_q = \eta_- q^2$ or smaller, which constrains the phase space for the internal momenta.

2.5.2 Comparison with numerical form factors

For a finite system with size N, the result for $\delta S^{zz}(q,\omega)$ must be expressed in terms of the transition probabilities $F^2(q,\omega)$. If the intermediate bosons carry momenta $q_{1,2} = 2\pi n_{1,2}/N$, such that $q_1 + q_2 = q \equiv 2\pi n/N$, the energy

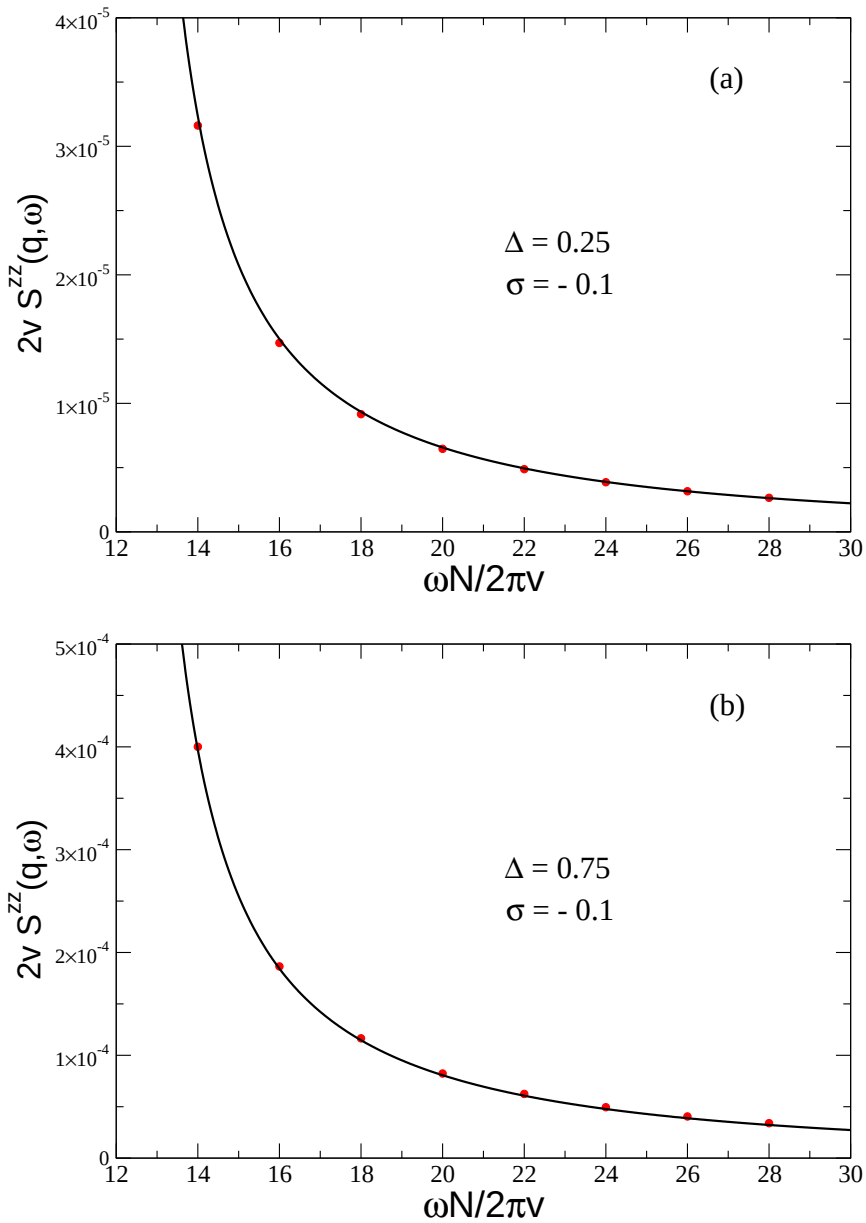

Figure 2.18: Tail of $S^{zz}(q,\omega)$ for $q = 2\pi/50$ and $\delta\omega_q \ll \omega - vq \ll J$. The red dots represent the sum of the numerical $F^2(q,\omega)$ identified with each energy level predicted by field theory (*c.f.* figure 2.7). The solid line is the field theory result (2.199). The chain length is $N = 600$. (a) $\sigma = -0.1$, $\Delta = 0.25$; (b) $\sigma = -0.1$, $\Delta = 0.75$.

levels are given by the sum of their individual energies $\omega = v\,|q_1| + v\,|q_2|$, *i.e.*,

$$\omega_\ell = \frac{2\pi v \ell}{N} \qquad , \qquad \ell = n+2, n+4, \ldots . \tag{2.197}$$

Thus field theory predicts a uniform level spacing $4\pi v/N$ above the mass shell. It is easy to verify (by simply replacing the integrals by sums in momentum space) that $\delta S^{zz}(q,\omega)$ for the finite system can be written as

$$\delta S^{zz}\left(q = \frac{2\pi n}{N}, \omega\right) = \frac{2\pi}{N} \sum_\ell F^2(q,\omega)\,\delta(\omega - \omega_\ell)\,, \tag{2.198}$$

where $F^2(q,\omega) = \left|\left\langle 0 \left| S_q^z \right| \alpha \right\rangle\right|^2$, with $|\alpha\rangle$ a two-boson intermediate state, is the transition probability for the state with energy ω_ℓ and is given by

$$F^2(q,\omega) = 2v\,\delta S^{zz}(q,\omega) = \frac{4\pi^2 K \eta_+^2}{9v^2 N^2}\,\frac{n^4}{\ell^2 - n^2}. \tag{2.199}$$

We compare our field theory prediction with the form factors calculated numerically for a chain with $N = 600$ sites. We take $q = 2\pi/50$ ($n = 12$) and the previous values $\sigma = -0.1$ and $\Delta = 0.25$ or $\Delta = 0.75$ (for which the parameters are shown in table 2.1). As we saw in figure 2.7, the energies of the eigenstates calculated by BA are actually scattered around the values of ω_ℓ predicted in (2.197). For $N = 600$, the broadening becomes comparable with the level spacing $4\pi v/N$ when $\ell \approx 30$ ($\omega \approx 0.4J$). Again the number of states agrees with a picture of multiple particle-hole excitations based on perturbation theory in the interaction. These features are not predicted by the bosonization approach. In order to make the comparison with (2.199), we group the form factors that can be identified with a given energy level ω_ℓ and plot the total $F^2(q,\omega)$ as a function of the integers $\ell = \omega N/2\pi v$. We emphasize that for very large ℓ we expect deviations from the lowest-order field theory result due to the effect of more irrelevant operators we have neglected. The results are shown in figure 2.18.

2.6 The zero field case

So far we have focused on the dynamical structure factor at finite magnetic field, which is somewhat analogous to interacting fermions with parabolic dispersion. One may then ask whether the field theory calculations can be applied to the case $h = 0$ ($k_F = \pi/2$). Let us first review what is known for the free fermion point $\Delta = 0$. In this case $S^{zz}(q,\omega)$ is still given by (2.19) (with an extra factor of 2 [102]), but the thresholds of the two-particle (two-spinon in the Bethe Ansatz solution) continuum are given by

$$\omega_L(q) = J \sin q, \tag{2.200}$$

$$\omega_U(q) = 2J \sin \frac{q}{2}. \tag{2.201}$$

As a result, $S^{zz}(q,\omega)$ develops a square root divergence at the upper threshold $\omega_U(q)$. The width now scales like q^3 for small q

$$\delta\omega_q = \omega_U(q) - \omega_L(q) \approx \frac{Jq^3}{8}. \tag{2.202}$$

A crossover from q^2 to q^3 is observed as we decrease the magnetic field (or, equivalently, increase $q \ll k_F$) so as to violate (2.15) or (2.107). The result (2.202) is also obtained by keeping the leading correction to the linear dispersion around k_F

$$\epsilon_k^{R,L} \approx \pm\left(v_F k - \frac{\gamma k^3}{6} + \ldots\right), \tag{2.203}$$

where $\gamma = v_F = J$. Bosonizing the band curvature term according to (2.65), we find

$$\delta\mathcal{H}_{bc} = -\frac{\pi\gamma}{12} : (\partial_x\phi_R)^4 : -\frac{\gamma}{24} : \left(\partial_x^2\phi_R\right)^2 : +(R \to L), \tag{2.204}$$

which can be rewritten as

$$\delta\mathcal{H}_{bc} = -\frac{\pi\gamma}{12} : (\partial_x\phi_R)^2 :: (\partial_x\phi_R)^2 : +(R \to L), \tag{2.205}$$

as follows from the operator product expansion of (2.205).

In the interacting case we also have to keep track of the irrelevant interaction terms, including the Umklapp interaction in (2.32). The general form for the leading irrelevant operators for zero field is [128, 137]

$$\begin{aligned}\delta\mathcal{H} &= \frac{\pi\zeta_-}{12}\left[: (\partial_x\varphi_R)^2 :: (\partial_x\varphi_R)^2 : + : (\partial_x\varphi_L)^2 :: (\partial_x\varphi_L)^2 :\right] \\ &\quad + \frac{\pi\zeta_+}{2} : (\partial_x\varphi_R)^2 :: (\partial_x\varphi_L)^2 : + \frac{\lambda_1}{2\pi}\cos(4\sqrt{\pi K}\phi) + \ldots, \end{aligned} \tag{2.206}$$

where the dots stand for higher dimensional local counterterms. The coupling constants to first order in Δ can be obtained from the bosonization of the band curvature term and the irrelevant interaction terms. We find

$$\zeta_- \approx -J\left(1 + \frac{\Delta}{\pi}\right), \quad \zeta_+ \approx -\frac{\Delta J}{\pi}, \quad \lambda_1 \approx \frac{\Delta J}{\pi}. \tag{2.207}$$

The exact coupling constants for finite Δ can be taken from [137]

$$\zeta_- = -\frac{v}{4\pi K}\frac{\Gamma\left(\frac{6K}{4K-2}\right)\Gamma^3\left(\frac{1}{4K-2}\right)}{\Gamma\left(\frac{3}{4K-2}\right)\Gamma^3\left(\frac{2K}{4K-2}\right)}, \tag{2.208}$$

$$\zeta_+ = -\frac{v}{2\pi}\tan\left(\frac{\pi K}{2K-1}\right), \tag{2.209}$$

$$\lambda_1 = -\frac{4v\,\Gamma(2K)}{\Gamma(1-2K)}\left[\frac{\Gamma\left(1+\frac{1}{4K-2}\right)}{2\sqrt{\pi}\Gamma\left(1+\frac{K}{2K-1}\right)}\right]^{4K-2}, \tag{2.210}$$

where v and K are given by (2.44) and (2.45), respectively.

One important point is that the other possible type of dimension-four operator $(\partial_x\varphi_R)^3\,\partial_x\varphi_L + R \leftrightarrow L$ is absent from the effective Hamiltonian for the XXZ model. We see this directly when calculating the coupling constants

to first order in Δ, but we can also show that it remains true for finite Δ by imposing the constraint that the XXZ model is integrable [128]. Integrability implies the existence of nontrivial conserved quantities, the simplest one of which is the energy current operator $J^E = \sum_j j_j^E$ given by [148, 149]

$$\begin{aligned} J^E &= J^2 \sum_j \left[S_{j-1}^y S_j^z S_{j+1}^x - S_{j-1}^x S_j^z S_{j+1}^y + \Delta(S_{j-1}^x S_j^y S_{j+1}^z - S_{j-1}^z S_j^y S_{j+1}^x) \right. \\ &\quad \left. + \Delta(S_{j-1}^z S_j^x S_{j+1}^y - S_{j-1}^y S_j^x S_{j+1}^z) \right] . \end{aligned} \tag{2.211}$$

The latter is defined by the continuity equation of the energy density at zero field

$$j_{j+1}^E - j_j^E = -\partial_t \mathcal{H}_j = i[\mathcal{H}_j, H], \tag{2.212}$$

where $H = \sum_j \mathcal{H}_j$ is the Hamiltonian (2.1) with $h = 0$. One can then verify that J^E is conserved in the sense that $[J^E, H] = 0$.

Let us now look at the corresponding quantity in the low energy effective model. In the general case, we consider the Hamiltonian density $\mathcal{H} = \mathcal{H}_{LL} + \delta\mathcal{H} + \delta\mathcal{H}_3$, where δH is given by (2.206) and we also add the interaction

$$\delta\mathcal{H}_3 = \pi\zeta_3 \left[(\partial_x \varphi_R)^3 \partial_x \varphi_L + (\partial_x \varphi_L)^3 \partial_x \varphi_R \right] . \tag{2.213}$$

We obtain the energy current operator from the continuity equation in the continuum limit

$$\partial_x j^E(x) = -\partial_t \mathcal{H}(x) = i \int dy \, [\mathcal{H}(x), \mathcal{H}(y)] . \tag{2.214}$$

The energy current operator for the Luttinger model (with $\zeta_{\pm,3} = \lambda_1 = 0$) takes the form

$$\begin{aligned} J_0^E &= \int dx \, j_0^E(x) = \frac{v^2}{2} \int dx \left[(\partial_x \varphi_R)^2 - (\partial_x \varphi_L)^2 \right] \\ &= -v^2 \int dx \, \partial_x \phi \partial_x \theta . \end{aligned} \tag{2.215}$$

This coincides with the spatial translation operator of the Gaussian model [150]. A nontrivial consequence of the conservation law arises when we consider the corrections to J^E due to the irrelevant operators. We keep corrections up to operators of dimension four. Using (2.214), we find $J^E = J_0^E + \delta J^E$ with [128]

$$\begin{aligned} \delta J^E &= \pi v \int dx \left\{ \frac{\zeta_-}{3} \left[(\partial_x \varphi_R)^4 - (\partial_x \varphi_L)^4 \right] \right. \\ &\quad \left. + 2\zeta_3 \left[(\partial_x \varphi_R)^3 \partial_x \varphi_L - (\partial_x \varphi_L)^3 \partial_x \varphi_R \right] \right\} . \end{aligned} \tag{2.216}$$

Note that there are no first-order corrections to J^E associated with the ζ_+ interaction or the Umklapp scattering λ_1. (The case of the Umklapp perturbation was discussed in [151]). The conservation of J^E up to dimension-four operators implies

$$[J^E, H] = [J_0^E, H_{LL}] + [J_0^E, \delta H] + [J_0^E, \delta H_3] + [\delta J^E, H_{LL}] = 0. \tag{2.217}$$

Since J_0^E is conserved in the Luttinger model, we have $[J_0^E, H_{LL}] = 0$. In fact, J_0^E commutes with any local operator of the form $\int dx\, O(x)$ under periodic boundary conditions [150]. As a result, $[J_0^E, \delta H] = [J_0^E, \delta H_3] = 0$ as well. We are left with the condition that the commutator $[\delta J^E, H_{LL}]$ vanishes. This is automatically satisfied by the contribution from the ζ_- term because it does not mix R and L and $\left[(\partial_x \varphi_R)^4 - (\partial_x \varphi_L)^4 , H_{LL} \right]$ is a total derivative. We then have

$$\begin{aligned} [\delta J^E, H_{LL}] &= \pi v^2 \zeta_3 \int dx \int dx' \times \\ &\quad \left[(\partial_x \varphi_R)^3 \partial_x \varphi_L - (\partial_x \varphi_L)^3 \partial_x \varphi_R , (\partial_{x'} \varphi_R)^2 + (\partial_{x'} \varphi_L)^2 \right] \\ &= 4\pi i v^2 \zeta_3 \int dx \left[(\partial_x \varphi_R)^3 \partial_x^2 \varphi_L + (\partial_x \varphi_L)^3 \partial_x^2 \varphi_R \right] . \end{aligned} \tag{2.218}$$

Therefore, $[J^E, H] = 0 \Leftrightarrow \zeta_3 = 0$.

This argument also applies to the finite field case. The model is still

integrable for $h \neq 0$. Although the relevant quantity for thermal transport is now a linear combination of the energy current and the spin current operator (which is not conserved for the XXZ model), the energy current operator given by (2.211) commutes with the Hamiltonian (2.1) for all values of h [149, 152]. The corresponding conserved quantity in the low energy theory is the current operator J^E obtained from the effective Hamiltonian at zero field, which has no dependence on the coupling constants $\eta_\pm$. Clearly, $[J_0^E, \delta H(h \neq 0)] = 0$ for $\delta H(h \neq 0)$ given by (2.71), so integrability poses no constraints on the coupling constants $\eta_\pm$.

We have checked that $\zeta_3 \neq 0$ for a nonintegrable model obtained by adding to the XXZ model the following next-nearest neighbour interaction

$$\delta H_{nnn} = J\Delta' \sum_j S_j^z S_{j+2}^z, \tag{2.219}$$

which is mapped by bosonization onto

$$\delta H_{nnn} = J\Delta' \int dx \left[-\frac{3}{\pi} \left(\partial_x \tilde{\phi} \right)^2 + \frac{16}{3} \left(\partial_x \tilde{\phi} \right)^4 + \ldots \right]. \tag{2.220}$$

The first term in (2.220) is quadratic in the bosons and modifies the velocity and the Luttinger parameter of the Luttinger model. The second term is the irrelevant operator. To first order in Δ and Δ', we find that it gives rise to a ζ_3 term in the Hamiltonian, which is given by

$$\delta H_{nnn} \sim -\frac{29}{6} J\Delta' \left[(\partial_x \varphi_R)^3 \partial_x \varphi_L + (\partial_x \varphi_L)^3 \partial_x \varphi_R \right]. \tag{2.221}$$

This shows that, unlike the XXZ model, a low energy effective model describing a nonintegrable model must in general contain the ζ_3 interaction.

This result establishes a connection between integrability and the field theory approach, by means of a restriction on the coupling constant of a band curvature type operator in the low energy effective model. More generally, if

we keep more irrelevant operators in the effective Hamiltonian, integrability should manifest itself as a fine tuning of the coupling constants and the absence of certain perturbations. This connection may be important for understanding the role of integrability in the transport properties of one-dimensional systems [148].

With $\zeta_3 = 0$, only ζ_+ and λ_1 mix right and left movers. We can apply second order perturbation theory in these interactions to calculate two contributions to the high-frequency tail in the frequency range $\delta\omega_q \ll \omega - vq \ll J$ [128]. For a finite chain with N sites and fixed momentum $q = 2\pi n/N$, the ζ_+ operator gives rise to intermediate states with discrete energies $\omega_\ell = 2\pi v\ell/N$, $\ell = n+2, n+4, \ldots$. In the thermodynamic limit, the contribution to the tail is

$$\delta S^{zz}_{\zeta_+}(q,\omega) = \frac{K(\zeta_+/v)^2}{192v} q^2 \left(\frac{\omega^2 - v^2q^2}{v^2}\right) \theta(\omega - vq). \tag{2.222}$$

The states generated by the Umklapp operator have energies $\omega_\ell = 2\pi v(\ell + 4K)/N$, $\ell = n, n+2, \ldots$. For $4\pi v/N \gg \delta\omega_q$ it is easy to separate this contribution from the ζ_+ one because of the shift in the energy levels by the noninteger factor $4K$. The corresponding contribution to the tail is

$$\delta S^{zz}_{\lambda_1}(q,\omega) = \frac{2\lambda_1^2 K^2}{\Gamma^2(4K)} (2v)^{3-8K} q^2 \left(\omega^2 - v^2q^2\right)^{4K-3} \theta(\omega - vq). \tag{2.223}$$

The derivation of equations (2.222) and (2.223), as well as the result for the finite system, is presented in the appendix.

Computing the broadening $\delta\omega_q$ for $h = 0$ from bosonization is much more challenging. Since ζ_- is the only vertex present at the free fermion point, the naive expectation is that we could derive the renormalization of the width at zero field by summing all orders of ζ_-, as we did for η_- in section 2.4.1. Although we now have to deal with a four-legged vertex, which introduces three-boson intermediate states, the calculation of the lowest order diagrams is not much harder than the finite field case. However, the fundamental difference is that for $h = 0$ the broadening has to be produced by dimension-

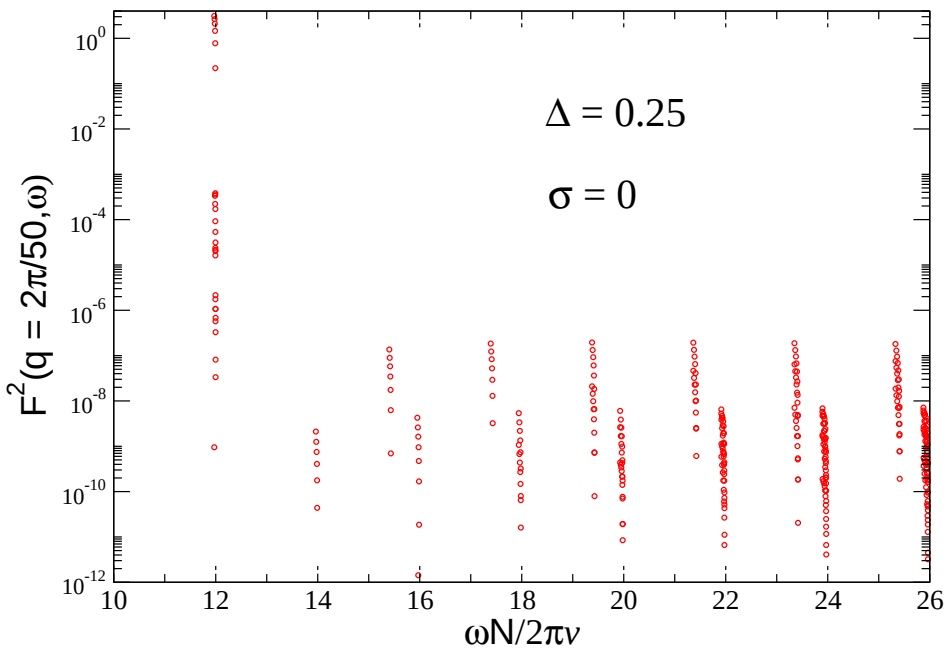

Figure 2.19: Numerical form factors squared for $\Delta = 0.25$ and zero field. The chain length is $N = 600$ and the momentum is set to $q = 2\pi/50$.

four operators and is therefore of the same order of q as the changes in the line shape (*i.e.*, the density of states factor and the singularities near the thresholds). That implies that the line shape of $S^{zz}(q,\omega)$ for $\Delta \neq 0$ cannot be approximated by the free fermion result in the limit $q \to 0$. Therefore it is not clear what the expansion of bosonic diagrams should sum up to.

Figure 2.19 shows the form factors for $\Delta = 0.25$ and $h = 0$ calculated numerically by Bethe Ansatz for a chain of $N = 600$ sites. In agreement with the field theory prediction, the states in the high-frequency tail cluster around the energy levels $\omega N/2\pi v = \ell$ (corresponding to the ζ_+ contribution) and $\omega N/2\pi v = \ell + 4K \approx \ell + 3.45$ (the λ_1 contribution). The comparison between the Bethe Ansatz data and the field theory results for the tail at zero field is shown in Fig. (2.20) [128]. It confirms the validity of (2.222) and (2.223) for $\delta\omega_q \ll \omega - vq \ll J$. An important consequence of integrability for

the line shape at zero field is that for $\Delta < 1/2$ ($K > 3/4$) the tail decreases as $\omega \to vq$. A finite ζ_3 interaction would produce a contribution to the tail that diverges as $\omega \to vq$, similarly to the finite field case (see appendix). There is no such contribution in the Bethe Ansatz data for small Δ.

To study the peak region we can focus on the two-spinon states only (with $\omega \approx vq$ and form factors of $O(1)$) and reach lengths up to $N = 4000$. We see that $F^2(q,\omega)$ is dominated by the two-spinon contribution, except very close to the upper threshold, where that contribution vanishes (inset of figure 2.21). Unlike the finite field case, the rescaled $F^2(q,\omega)$ does not become flat in the limit $q \to 0$. The density of states for the two-spinon states is known exactly

$$D(q,\omega) = \frac{1}{\sqrt{\omega_U^2(q) - \omega^2}}, \tag{2.224}$$

where $\omega_U(q) = 2v\sin(q/2)$. The two-spinon contribution to $S^{zz}(q,\omega)$ for zero field and $\Delta = 0.25$ obtained by multiplying $F^2(q,\omega)$ by the above density of states is shown in figure 2.21.

We know from the exact solution for the two-spinon dynamical structure factor at the Heisenberg point $\Delta = 1$ that there is a square-root divergence (with a logarithmic correction) at $\omega_L(q)$ and that the same contribution vanishes at $\omega_U(q)$ [153]. Such behavior is completely opposite to what happens at the free fermion point (see [102]). Numerical results suggest that the exponents change smoothly from $\Delta = 0$ to $\Delta = 1$, with spectral weight being transferred from the upper threshold to the lower threshold as Δ increases [117, 120, 121].[2]

In addition, the renormalization of $\delta\omega_q$ defined as the width of the two-particle continuum in the Bethe Ansatz solution is known exactly. The thresholds of the two-spinon continuum for $0 < \Delta < 1$ are a simple generalization of (2.200) and (2.201), with J replaced by the renormalized velocity

[2]It turns out the upper edge exponent is discontinuous at $\Delta = 0$, as we discuss in chapter 3.

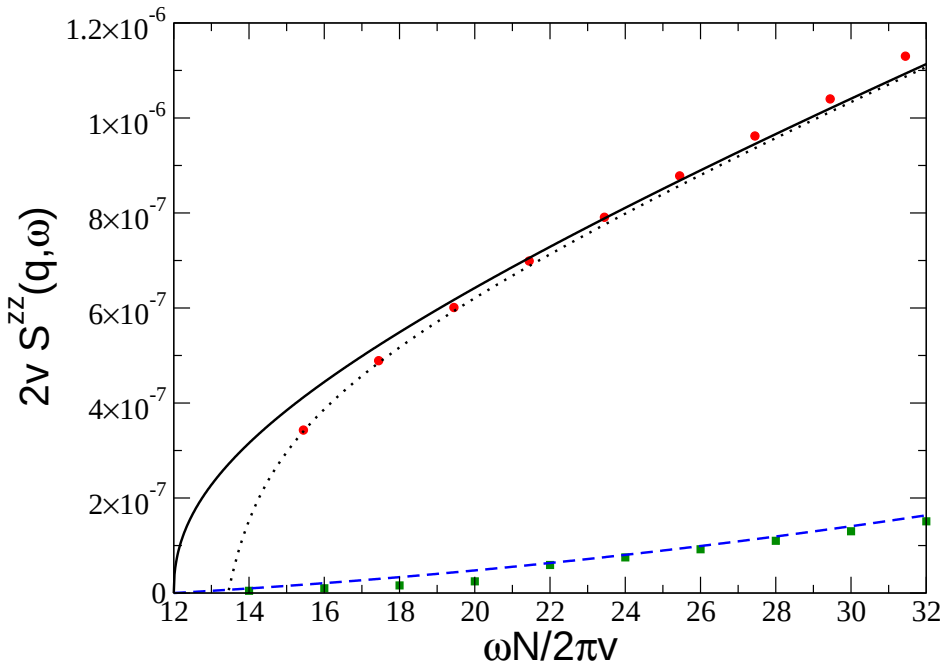

Figure 2.20: High-frequency tail for zero magnetic field. The Bethe ansatz data is for $N = 600$, $\Delta = 0.25$ and $q = 2\pi/50$, as in Fig. 2.19. The squares represent the sum of form factors squared for the states with energies $\omega \approx 2\pi v\ell/N$. The circles represent the sum of form factors for states with energies $\omega \approx 2\pi v(\ell + 4K)/N$. The dashed and solid lines correspond to Eq. (2.222) and Eq. (2.223), respectively. The dotted line is the result for the Umklapp tail taking into account finite size effects, as explained in Appendix A.2.

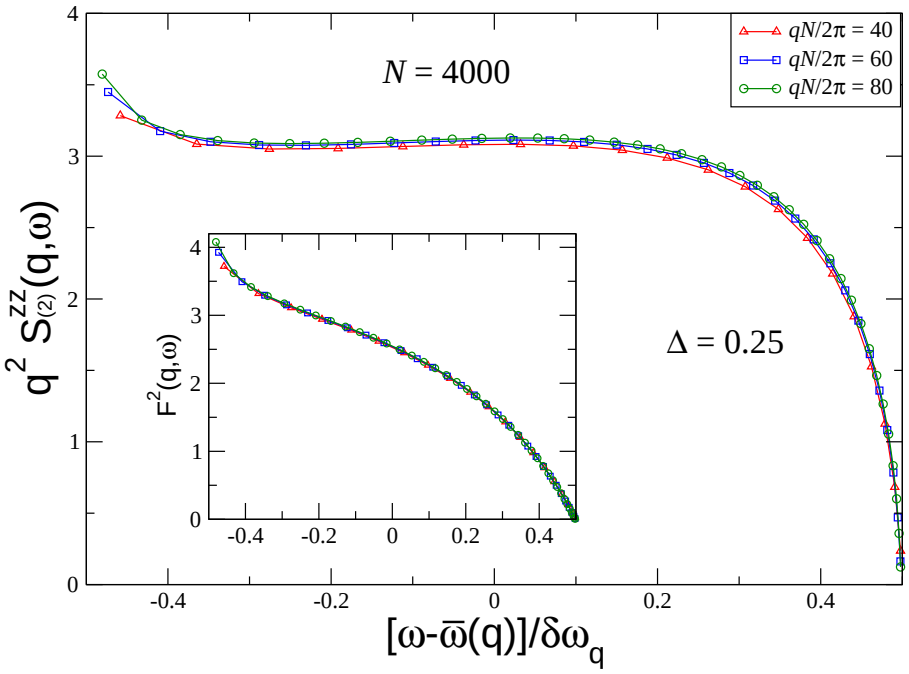

Figure 2.21: Two-spinon contribution to $S^{zz}(q,\omega)$ at zero field for $N = 4000$, $\Delta = 0.25$ and three values of q. The number of two-spinon states is given by $qN/4\pi$. Inset: transition probabilities $F^2(q,\omega)$ used to calculate $S^{zz}(q,\omega)$. We denote $\delta\omega_q = \omega_U(q) - \omega_L(q)$ and $\bar{\omega}(q) = [\omega_U(q) + \omega_L(q)]/2$.

v given by (2.44) [119, 135]. As a result, the width for finite Δ is

$$\delta\omega_q \approx \frac{vq^3}{8}. \tag{2.225}$$

Since $v \approx J(1+2\Delta/\pi)$ for $\Delta \ll 1$, the above expression is different from the renormalization of ζ_-. Therefore, the renormalization of $\delta\omega_q$ by interactions is *not* given by ζ_-.

A proper treatment of the dimension-four operators which allows one to predict the line shape of $S^{zz}(q,\omega)$ at zero field remains an open question.

2.7 Sum rules

We checked the accuracy of the Bethe Ansatz data by calculating the following sum rules

$$I\,(q) \equiv \int_0^\infty \frac{d\omega}{2\pi}\, S^{zz}(q,\omega) = \frac{1}{N}\langle S_q^z S_{-q}^z\rangle \tag{2.226}$$

and

$$L\,(q) \equiv \int_0^\infty \frac{d\omega}{2\pi}\, \omega S^{zz}(q,\omega) = -2\frac{\langle H_{xy}\rangle}{N}\sin^2\frac{q}{2}\ . \tag{2.227}$$

These sum rules can be expressed in terms of sums over the form factors calculated by Bethe Ansatz for finite chains as

$$I_{BA}(q) = \frac{1}{N}\sum_\alpha \left|\left\langle 0\left|S_q^z\right|\alpha\right\rangle\right|^2, \tag{2.228}$$

$$L_{BA}(q) = \frac{1}{N}\sum_\alpha \left(E_\alpha - E_{GS}\right)\left|\left\langle 0\left|S_q^z\right|\alpha\right\rangle\right|^2. \tag{2.229}$$

The identity in (2.227) is a consequence of the f-sum rule. The first moment sum rule $L(q)$ can then be calculated exactly by using the BA result for $\langle H_{xy}\rangle$. (For $h=0$, $\langle H_{xy}\rangle/N = 2\langle S_j^x S_{j+1}^x\rangle = e_0 - \Delta\partial e_0/\partial\Delta$, where e_0 is the ground state energy per site [154]). Since there are no exact results for

N	$I(2\pi/50)$	$I(2\pi/25)$	ε	m
50	0.017237038	0.034518387	7.5×10^{-13}	1200
100	0.017237380	0.034518764	9.4×10^{-11}	1200
100	0.017237138	0.034518522	2.1×10^{-11}	1600
100	0.017237109	0.034518505	1.5×10^{-12}	2400
200	0.017237364	0.034518657	1.2×10^{-10}	2400

Table 2.3: DMRG results for $I(q)$, for $\Delta = 0.25$ and zero field ($\sigma = 0$). The truncation error is ε and m is the number of states kept per block. Between 10 ($m = 1200$) and 14 ($m = 2400$) sweeps were performed.

$I(q)$, we first compare I_{BA} with the lowest-order field theory result in (2.123)

$$I(q) \approx I_{FT}(q) = \frac{K}{2\pi} q. \tag{2.230}$$

This should be a reasonably good approximation for small q.

The other possibility is to calculate the static correlation function by DMRG. In Table 2.3 we show DMRG results for periodic XXZ chains. The results used the standard DMRG finite system method [155, 156, 157], but with extra noise terms added to the density matrix to speed convergence in the number of sweeps for the more difficult periodic boundaries case [158]. We see that for these measurements the finite size effects are very small for $N = 100$, and that the truncation error depends significantly on N. We can obtain results for $I(q)$ to an accuracy of 10^{-6} or 10^{-7} by using the $m = 2400$ results for $N = 100$. Finite size corrections for larger N appear to be roughly the same size.

A comparison between the sum rules obtained for the BA data and the values expected from the equations above is shown in tables 2.4 and 2.5. In all the cases shown here the Bethe Ansatz agrees with the DMRG and the exact results to better than 0.1%.

	I_{BA}	I_{FT}	I_{DMRG}	L_{BA}	L_{exact}
$q = \frac{2\pi}{50}$	0.017236	0.017228	0.017237	0.002498	0.002498
$q = \frac{2\pi}{25}$	0.034513	0.034457	0.034518	0.009952	0.009953

Table 2.4: Sum rules for $\Delta = 0.25$ and zero field ($\sigma = 0$). First sum rule: Results for the BA data, I_{BA}, with a chain length of $N = 400$ compared with the field theory approximation (2.230), I_{FT}, and results from DMRG, I_{DMRG}, for a chain with $N = 100$ sites. Second sum rule: Results for the same BA data, L_{BA}, compared to the exact result (2.227), L_{exact}.

	I_{BA}	I_{FT}	I_{DMRG}	L_{BA}	L_{exact}
$q = \frac{2\pi}{50}$	0.017418	0.0174	0.017419	0.002376	0.002378
$q = \frac{2\pi}{25}$	0.034880	0.0348	0.034883	0.009468	0.009474

Table 2.5: Same sum rules as in table 2.4, but for finite field ($\sigma = -0.1$).

2.8 Summary

Based on a low-energy effective theory which includes the leading (band curvature type) irrelevant operators we have studied the longitudinal dynamical structure factor $S^{zz}(q,\omega)$ for the XXZ spin-1/2 chain in a magnetic field. By comparing with results for free fermions we have conjectured a method to sum up the entire perturbation series in one of these irrelevant operators allowing us to obtain an approximation for the shape of the peak of $S^{zz}(q,\omega)$ which is valid for small q and is non-perturbative in the interaction strength (anisotropy Δ). Besides the velocity v and Luttinger parameter K, the important parameters to determine the line shape are the coupling constants $\eta_\pm$ of the leading (dimension-three) irrelevant operators, which we relate to derivatives of v and K with respect to the magnetic field. A summation of the entire series is necessary because perturbation theory in the band curvature terms is divergent on shell, $\omega \sim vq$, although these operators are formally irrelevant. Our field theory approach is valid in the regime $\tilde{\gamma}q^2 \ll \eta_- q \ll v$, where $\tilde{\gamma}$ is of order of the coupling constants of the next-leading (dimension-

four) irrelevant operators which we neglected for the case of a finite magnetic field. The result is a rectangular peak with width $\delta\omega_q = |\eta_-|q^2$ and height $K/|\eta_-|q$, similar to the exact $S^{zz}(q,\omega)$ for the XY model (free fermion point).

The field-theoretical results for the width of the peak are supported by Bethe Ansatz calculations. Since the XXZ model is integrable, we used the Bethe Ansatz equations in the thermodynamic limit to determine the parameters $\eta_\pm(\Delta,\sigma)$ numerically, so that the low-energy effective theory and the results obtained for $S^{zz}(q,\omega)$ are *parameter free*. We have shown that the width of the peak obtained in field theory agrees with the analytically calculated width of the two-particle continuum in the Bethe Ansatz. Furthermore, we have demonstrated that the form factors obtained numerically by Bethe Ansatz approach the flat distribution predicted by field theory for $q \to 0$. Applying our results to the strongly interacting case (large Δ), we found that for $\Delta > \cos(\pi/5) \approx 0.81$ the parameter η_- goes through zero for a finite value of the magnetic field. At the "inversion point" where $\eta_-(\Delta,\sigma_{inv}) = 0$, the q^2 scaling breaks down and the width of the two-particle continuum scales like $\delta\omega_q \sim q^3$. The q^2 scaling is recovered for $0 < |\sigma| < \sigma_{inv}$. As a result, the width $\delta\omega_q$ is a non-monotonic function of σ, with a minimum at the inversion point.

The power-law singularities found in [124] for $\Delta \ll 1$ near the lower and upper thresholds $\omega_L(q)$, $\omega_U(q)$ are not captured by our calculations. Within the effective low-energy theory these singularities seem to be related to higher dimension operators. Within the Bethe Ansatz, on the other hand, it is not clear if these singularities can be obtained by considering only the form factors for two-particle states. It seems possible that the finite size effects near these boundaries are complicated and form factors for multi-particle excitations at very large system sizes have to be studied. Nevertheless, for finite chains and small Δ the behavior of the dominant form factors for the two-particles states agrees qualitatively with the result of [124]. However, taking into account the energy dependence of the density of states leads to

a maximum and a minimum of $S^{zz}(q,\omega)$ inside the two-particle continuum. In the strongly interacting regime $\Delta > \cos(\pi/5)$, we have found that for $|\sigma| < \sigma_{inv}$ the dynamical structure factor exhibits a rather distinct line shape, reminiscent of a converging X-ray singularity at the lower threshold.

We also showed that in the interacting case $S^{zz}(q,\omega)$ has a high-frequency tail $\delta S^{zz}(q,\omega)$. Within the effective theory this tail is related to an irrelevant operator (with coupling constant η_+) mixing excitations at the right and left Fermi points. Contrary to the calculation for the on-shell region, this term can be treated in finite-order perturbation theory for $\delta\omega_q \ll \omega - vq \ll J$ and we find that the tail for finite field decays as $\delta S^{zz}(q,\omega) \sim q^4/(\omega^2 - v^2q^2)$. This result is again supported by numerical calculations based on the Bethe ansatz.

We have proposed that the integrability of the XXZ model is manifested in the low-energy effective Hamiltonian at the order of the dimension-four, band curvature type operators. The conservation of the energy current operator imposes that the interaction denoted as ζ_3 is absent. This has consequences for the line shape of $S^{zz}(q,\omega)$ at zero magnetic field, since a nonzero ζ_3 would change the behavior of the tail near the upper threshold of the two-particle continuum.

One promising test of our theory would be to measure, by means of inelastic neutron scattering experiments, the width of the peak as a function of q and h (equations (2.121) and (2.97)). In some spin-1/2 compounds it is experimentally possible to go all the way up to the saturation field. The main limitation is the low intensity of the signal for small-q scattering. However, one important point that may facilitate the experiment is that in the transverse channel the low energy spectral weight is shifted to a finite wave vector, $\pm\sigma$ (the magnetization). The gap at $q = 0$ is of order h for transverse excitations. So there is a "protected region" of zero transverse spectral weight at small q and ω inside of which the longitudinal structure function could perhaps be observed.

Finally, we would like to emphasize that the formulas (2.97) and (2.98) for the coupling constants of the irrelevant operators are also valid for non-integrable models. This allows us to predict the width of the dynamical structure factor $S^{zz}(q,\omega)$ at small q once the field dependence of v and K is determined from thermodynamic quantities. For example, the value of σ_{inv}, below which we expect to see nontrivial effects due to strong interactions, can be increased by adding a ferromagnetic next-nearest neighbour interaction. The isotropic $J_1 - J_2$ model also contains a marginally irrelevant operator, whose amplitude can be tuned by the J_2 interaction. A ferromagnetic J_2 ($J_2 < 0$) would increase the constant σ_0 inside the logarithm in Eq.(2.189). On more general grounds, the nonmonotonic behavior of the width $\delta\omega_q$ and the inversion of the line shape should occur whenever the derivatives of the velocity and the Luttinger parameter with respect to magnetic field/chemical potential have opposite signs and the latter one is singular. In principle, this could also be observed in the dynamical structure factor of quantum wires, since $\partial K/\partial n$, where n is the electron density, changes sign and diverges in the low-density limit (Wigner crystal regime) [159]. This suggests that the evolution of the line shape as a function of density could be richer than what was proposed in [124].

Bibliography

[97] I. Affleck, *Fields, Strings and Critical Phenomena* (Les Houches, Session XLIX, Amsterdam: North-Holland, 1988), p. 563, edited by E. Brézin and J. Zinn-Justin.

[98] T. Giamarchi, *Quantum Physics in One Dimension* (Clarendon Press, Oxford, 2004).

[99] H. Bethe, Z. Phys. **71**, 205 (1931).

[100] R. Orbach, Phys. Rev. **112**, 309 (1958).

[101] N. Motoyama, H. Eisaki, and S. Uchida, Phys. Rev. Lett. **76**, 3212 (1996).

[102] G. Müller, H. Thomas, H. Beck, and J. C. Bonner, Phys. Rev. B **24**, 1429 (1981).

[103] S. E. Nagler, D. A. Tennant, R. A. Coweley, T. G. Perring, and S. K. Satija, Phys. Rev. B **44**, 12361 (1991).

[104] M. B. Stone, D. H. Reich, C. Broholm, K. Lefmann, C. Rischel, C. P. Landee, and M. M. Turnbull, Phys. Rev. Lett. **91**, 037205 (2003).

[105] K. R. Thurber, A. W. Hunt, T. Imai, and F. C. Chou, Phys. Rev. Lett. **87**, 247202 (2001).

[106] T. Moriya, Prog. Theor. Phys. **16**, 23 (1956).

[107] J. Sirker, Phys. Rev. B **73**, 224424 (2006).

[108] M. Jimbo and T. Miwa, *Algebraic analysis of Solvable Lattice Models* (Providence, RI: AMS, 1995).

[109] A. H. Bougourzi, M. Couture, and M. Kacir, Phys. Rev. B **54**, R12669 (1996).

[110] M. Karbach, G. Müller, A. H. Bougourzi, A. Fledderjohann, and K.-H. Mütter, Phys. Rev. B **55**, 12510 (1997).

[111] A. H. Bougourzi, M. Karbach, and G. Müller, Phys. Rev. B **57**, 11429 (1998).

[112] A. H. Bougourzi, Mod. Phys. Lett. B **10**, 1237 (1996).

[113] A. Abada, A. H. Bougourzi, and B. Si-Lakhal, Nucl. Phys. B **497**, 733 (1997).

[114] J.-S. Caux and R. Hagemans, J. Stat. Mech.: Theory Exp. p. P12013 (2006).

[115] N. Kitanine, J. M. Maillet, and V. Terras, Nucl. Phys. B **554**, 647 (1999).

[116] N. Kitanine, J. M. Maillet, and V. Terras, Nucl. Phys. B **567**, 554 (2000).

[117] J.-S. Caux, R. Hagemans, and J. M. Maillet, J. Stat. Mech.: Theory Exp. p. P09003 (2005).

[118] D. Biegel, M. Karbach, and G. Müller, Europhys. Lett. **59**, 882 (2002).

[119] D. Biegel, M. Karbach, and G. Müller, J. Phys. A **36**, 5361 (2003).

[120] J. Sato, M. Shiroishi, and M. Takahashi, J. Phys. Soc. Jpn. **73**, 3008 (2004).

[121] J.-S. Caux and J. M. Maillet, Phys. Rev. Lett. **95**, 077201 (2005).

[122] H. J. Schulz, Phys. Rev. B **34**, 6372 (1986).

[123] M. Pustilnik, E. G. Mishchenko, L. I. Glazman, and A. V. Andreev, Phys. Rev. Lett. **91**, 126805 (2003).

[124] M. Pustilnik, M. Khodas, A. Kamenev, and L. I. Glazman, Phys. Rev. Lett. **96**, 196405 (2006).

[125] M. Pustilnik, Phys. Rev. Lett. **97**, 036404 (2006).

[126] A. Abanov and P. B. Wiegmann, Phys. Rev. Lett. **95**, 076402 (2005).

[127] P. Pirooznia and P. Kopietz, Eur. Phys. J. B **58**, 291 (2007).

[128] R. G. Pereira, J. Sirker, J.-S. Caux, R. Hagemans, J. M. Maillet, S. R. White, and I. Affleck, Phys. Rev. Lett **96**, 257202 (2006).

[129] A. V. Rozhkov, Phys. Rev. B **74**, 245123 (2006).

[130] S. Teber, Phys. Rev. B **76**, 045309 (2007).

[131] D. N. Aristov, Phys. Rev. B **76**, 085327 (2007).

[132] M. Khodas, M. Pustilnik, A. Kamenev, and L. I. Glazman, Phys. Rev. B **76**, 155402 (2007).

[133] K. Samokhin, J. Phys.: Cond. Mat. **10**, L533 (1998).

[134] E. Lieb, T. Schultz, and D. Mattis, Ann. Phys. (N.Y) **16**, 407 (1961).

[135] V. E. Korepin, N. M. Bogoliubov, and A. G. Izergin, *Quantum inverse scattering method and correlation functions* (Cambridge University Press, 1993).

[136] F. D. M. Haldane, J. Phys. C **14**, 2585 (1981).

[137] S. Lukyanov, Nucl. Phys. B **522**, 533 (1998).

[138] M. Gaudin, *La fonction d'onde de Bethe* (Masson, Paris, 1983).

[139] M. Takahashi, *Thermodynamics of one-dimensional solvable problems* (Cambridge University Press, 1999).

[140] B. Sutherland, *Beautiful Models* (World Scientific, 2004).

[141] C. N. Yang and C. P. Yang, Phys. Rev. **150**, 321 (1966).

[142] R. G. Pereira, J. Sirker, J.-S. Caux, R. Hagemans, J. M. Maillet, S. R. White, and I. Affleck, J. Stat. Mech.: Theory Exp. p. P08022 (2007).

[143] J. Sirker and M. Bortz, J. Stat. Mech.: Theory Exp. p. P01007 (2006).

[144] I. Affleck and M. Oshikawa, Phys. Rev. B **60**, 1038 (1999).

[145] G. D. Mahan, *Many-Particle Physics* (Kluwer/Plenum, New York, 2000), 3rd ed.

[146] N. M. Bogoliubov, A. G. Izergin, and V. E. Korepin, Nucl. Phys. B **275**, 687 (1986).

[147] N. Kawakami and S.-K. Yang, Phys. Rev. Lett. **67**, 2493 (1991).

[148] X. Zotos, F. Naef, and P. Prelovšek, Phys. Rev. B **55**, 11029 (1997).

[149] F. Heidrich-Meisner, A. Honecker, and W. Brenig, Phys. Rev. B **71**, 184415 (2005).

[150] S. Fujimoto and N. Kawakami, Phys. Rev. Lett. **90**, 197202 (2003).

[151] K. Saito, Phys. Rev. B **67**, 064410 (2003).

[152] K. Sakai and A. Klümper, J. Phys. Soc. Jpn. **74**, 196 (2005).

[153] D. Biegel, M. Karbach, G. Müller, and K. Wiele, Phys. Rev. B **69**, 174404 (2004).

[154] M. Jimbo and T. Miwa, J. Phys. A **29**, 2923 (1996).

[155] S. R. White, Phys. Rev. Lett. **69**, 2863 (1992).

[156] S. R. White, Phys. Rev. B **48**, 10345 (1993).

[157] U. Schollwöck, Rev. Mod. Phys. **77**, 259 (2005).

[158] S. R. White, Phys. Rev. Lett. **72**, 180403 (2005).

[159] W. Häusler, L. Kecke, and A. H. MacDonald, Phys. Rev. B **65**, 085104 (2002).

Chapter 3

Edge singularities and long-time behavior

The XXZ $S = 1/2$ spin chain, with Hamiltonian

$$H = J \sum_{j=1}^{L} [S_j^x S_{j+1}^x + S_j^y S_{j+1}^y + \Delta S_j^z S_{j+1}^z - h S_j^z], \tag{3.1}$$

is one of the most studied models of strongly correlated systems.[1] It is equivalent by a Jordan-Wigner transformation to a model of interacting spinless fermions, with the corresponding Fermi momentum $k_F = \pi(1/2 + \langle 0|S_j^z|0\rangle)$ [160]. The model with $\Delta = 1$ describes Heisenberg antiferromagnets. The regime $0 < \Delta < 1$ is also of experimental interest; for example, the model with $\Delta = 1/2$ can be realized in $S = 1/2$ spin ladders near the critical field [161, 162]. In optical lattices, it should be even possible to tune the anisotropy Δ and explore the entire critical regime [163].

While some aspects of the model have been solved for exactly by Bethe ansatz [164], it has been very difficult to obtain correlation functions that way. Field theory (FT) methods give the low energy behavior at wave-vectors near 0 and $2k_F$ [160]. From the experimental viewpoint [165], a relevant quantity

[1] A version of this chapter has been published. R. G. Pereira, S. R. White, and I. Affleck. Exact edge singularities and dynamical correlations in spin-1/2 chains. Phys. Rev. Lett. **100**, 027206 (2008). Copyright (2008) by the American Physical Society.

is the dynamical structure factor (DSF)

$$S^{zz}(q,\omega) = \sum_{j=1}^{L} e^{-iqj} \int_{-\infty}^{+\infty} dt\, e^{i\omega t} \langle 0|S_j^z(t) S_0^z(0)|0\rangle. \tag{3.2}$$

This is the Fourier transform of the density correlation function in the fermionic model. For $\Delta = 1$ and $h = 0$, the exact two-spinon contribution to $S^{zz}(q,\omega)$ was obtained from the Bethe ansatz [166], partially agreeing with the Müller conjecture [167]. More recently a number of new methods have emerged which now make this problem much more accessible. These include time-dependent DMRG [168, 169, 170, 171, 172, 173], calculation of form factors from Bethe ansatz [174, 175] and new field theory approaches which go beyond the Luttinger model [176, 177]. The results point to a very nontrivial line shape at zero temperature for $S^{zz}(q,\omega)$ of the XXZ model [177] and of one-dimensional models in general [176]. In the weak coupling limit $\Delta \ll 1$ and for small q, the singularities at the thresholds of the two-particle continuum have been explained by analogy with the X-ray edge singularity in metals [176].

In this chapter we combine the methods of Ref. [176] with the Bethe ansatz to investigate the singularity exponents of $S^{zz}(q,\omega)$ for the XXZ model for finite interaction strength Δ and general momentum q. In addition, we determine the exponents of the long-time asymptotic behavior of the spin self-correlation function, which is *not* dominated by low energy excitations. We check our predictions against high accuracy numerical results calculated by DMRG.

3.1 Effective Hamiltonian for edge singularities

In the non-interacting, $\Delta = 0$ case, only excited states with a single particle-hole pair contribute to $S^{zz}(q,\omega)$. All the spectral weight is confined between the lower and upper thresholds $\omega_{L,U}(q)$ of the two-particle continuum. The choices of momenta corresponding to the thresholds depend on both k_F and q. For zero field, $k_F = \pi/2$, $\omega_L(q)$ for any $q > 0$ is defined by the excitation with a hole at $k_1 = \pi/2 - q$ and a particle right at the Fermi surface (or a hole at the Fermi surface and a particle at $k_2 = \pi/2 + q$), while ω_U is defined by the symmetric excitation with a hole at $k_1 = \pi/2 - q/2$ and a particle at $k_2 = \pi/2 + q/2$. For finite field and $q < |2k_F - \pi|$, $\omega_{L,U}(q)$ are defined by excitations with either a hole at k_F and a particle at $k_F + q$ or a hole at $k_F - q$ and a particle at k_F. For $h \neq 0$ and $q > |2k_F - \pi|$, there is even a third "threshold" between ω_L and ω_U where $S^{zz}(q,\omega)$ has a step discontinuity (see [167]).

For $\Delta \neq 0$, $S^{zz}(q,\omega)$ exhibits a tail associated with multiple particle-hole excitations [177]. However, the thresholds of the two-particle continuum are expected to remain as special points at which power-law singularities develop [176]. In order to describe the interaction of the high energy particle and/or hole with the Fermi surface modes, we integrate out all Fourier modes of the fermion field $\psi(x)$ except those near $\pm k_F$ and near the momentum of the hole, k_1, or particle, k_2, writing

$$\psi(x) \sim e^{ik_F x}\psi_R + e^{-ik_F x}\psi_L + e^{ik_1 x}d_1 + e^{ik_2 x}d_2. \tag{3.3}$$

Linearizing the dispersion relation about $\pm k_F$ we obtain relativistic fermion fields which we bosonize in the usual way [160]. We also expand the dispersion of the $d_{1,2}$ particles around $k = k_{1,2}$ up to quadratic terms. This yields the

effective Hamiltonian density

$$\begin{aligned}\mathcal{H} &= \sum_{\alpha=1,2} d_\alpha^\dagger \left(\varepsilon_\alpha - iu_\alpha \partial_x - \frac{\partial_x^2}{2m_\alpha}\right) d_\alpha \\ &\quad + \frac{v}{2}\left[(\partial_x\varphi_L)^2 + (\partial_x\varphi_R)^2\right] + V_{12} d_1^\dagger d_1 d_2^\dagger d_2 \\ &\quad + \frac{1}{\sqrt{2\pi K}} \sum_{\alpha=1,2} \left(\kappa_L^{(\alpha)} \partial_x\varphi_L - \kappa_R^{(\alpha)} \partial_x\varphi_R\right) d_\alpha^\dagger d_\alpha. \end{aligned} \tag{3.4}$$

This Hamiltonian describes a Luttinger liquid coupled to one or two mobile impurities [178, 179, 180]. In the derivation of Eq. (3.4) from Eq. (3.1), we drop terms of the form $(d_\alpha^\dagger d_\alpha)^2$ because we only consider processes involving a single d_1 and/or a single d_2 particle. Here $\varphi_{R,L}$ are the right and left components of the rescaled bosonic field. The long wavelength fluctuation part of S_j^z is given by $S_j^z \sim \sqrt{K/2\pi}\,(\partial_x\varphi_L - \partial_x\varphi_R)$. The spin velocity v and Luttinger parameter K are known exactly from the Bethe ansatz [164]. For zero field, $v = (\pi/2)\sqrt{1-\Delta^2}/\arccos\Delta$ and $K = [2 - 2\arccos(\Delta)/\pi)]^{-1}$ (we set $J = 1$). To first order in Δ, the coupling constants describing the scattering between the d particles and the bosons are $\kappa_{R,L}^{(\alpha)} = 2\Delta[1-\cos(k_F \mp k_\alpha)]$. The direct d_1-d_2 interaction V_{12} is also of order Δ. The exact values of $\kappa_{R,L}^{(\alpha)}$ play a crucial role in the singularities and will be determined below.

We may eliminate the interaction between the d particles and the bosonic modes by a unitary transformation

$$U = \exp\left\{ i \sum_\alpha \int \frac{dx}{\sqrt{2\pi K}} \left(\gamma_R^{(\alpha)}\varphi_R - \gamma_L^{(\alpha)}\varphi_L\right) d_\alpha^\dagger d_\alpha \right\}, \tag{3.5}$$

with parameters $\gamma_{R,L}^{(\alpha)} = \kappa_{R,L}^{(\alpha)}/(v \mp u_\alpha)$. In the resulting Hamiltonian $\bar{H} = U^\dagger H U$, $\varphi_{R,L}$ are free up to irrelevant interaction terms [179]. As in the X-ray edge problem, $\gamma_{R,L}^\alpha$ may be related to the phase shifts at the Fermi points due to the creation of the high energy d_α particle.

3.2 Determination of the renormalized coupling constants

Fortunately, we have access to the high energy spectrum of the XXZ model by means of the Bethe Ansatz. Following the formalism of Ref. [180], we calculate the finite size spectrum from the Bethe ansatz equations with an impurity term corresponding to removing (adding) a particle with dressed momentum $k_1 = k(\lambda_1)$ ($k_2 = k(\lambda_2)$), where $\lambda_{1,2}$ are the corresponding rapidities. The term of $O(1)$ yields $\varepsilon_\alpha = \epsilon(k_\alpha)$, the dressed energy of the particle. For zero field, we have the explicit formula $\epsilon(k) = -v\cos k$. The excitation spectrum for a single impurity to $O(1/L)$ reads

$$\Delta E = \frac{2\pi v}{L}\left[\frac{1}{4K}\left(\Delta N - n^\alpha_{imp}\right)^2 + K\left(D - d^\alpha_{imp}\right)^2 + n_+ + n_-\right], \tag{3.6}$$

with a conventional notation for ΔN, D and $n_\pm$ [164]. The phase shifts n^α_{imp} and d^α_{imp} are given by

$$n^\alpha_{imp} = \int_{-B}^{+B} d\lambda\, \rho^\alpha_{imp}(\lambda), \tag{3.7}$$

$$d^\alpha_{imp} = \int_{-\infty}^{-B} d\lambda\, \frac{\rho^\alpha_{imp}(\lambda)}{2} - \int_{B}^{+\infty} d\lambda\, \frac{\rho^\alpha_{imp}(\lambda)}{2}, \tag{3.8}$$

where B is the Fermi boundary and $\rho^\alpha_{imp}(\lambda)$ is the solution to the integral equation

$$\rho^\alpha_{imp}(\lambda) - \int_{-B}^{+B} \frac{d\lambda'}{2\pi}\, \rho^\alpha_{imp}(\lambda') \frac{d\Theta(\lambda-\lambda')}{d\lambda} = \frac{\Phi^\alpha(\lambda)}{2\pi}, \tag{3.9}$$

where $\Theta(\lambda) = i\log[\sinh(i\zeta+\lambda)/\sinh(i\zeta-\lambda)]$, with $\Delta = -\cos\zeta$, is the two-particle scattering phase [164], and $\Phi^{1,2}(\lambda) = \mp d\Theta(\lambda-\lambda_{1,2})/d\lambda$. The spectrum of Eq. (3.6) describes a shifted $c = 1$ conformal field theory (CFT). The scaling dimensions of the various operators can then be expressed in terms of K, n^α_{imp} and d^α_{imp}. In the effective model (3.4), the shift is introduced

by the unitary transformation of Eq. (3.5), which changes the boundary conditions of the bosonic fields. The equivalence of the two approaches allows us to identify

$$\gamma^{\alpha}_{R,L}/\pi = n^{\alpha}_{imp} \pm 2K d^{\alpha}_{imp}. \tag{3.10}$$

The phase shifts can be determined analytically for zero magnetic field. In this case, $B \to \infty$ and we have $d^{\alpha}_{imp} = 0$. Moreover, by integrating Eq. (3.9) over λ we find

$$n^{1,2}_{imp} = \mp \frac{\Theta(\lambda \to \infty)}{\pi - \Theta(\lambda \to \infty)} = \pm(1-K). \tag{3.11}$$

3.3 Singularity Exponents

Once the exact phase shifts are known, the exponent for the (lower or upper) threshold determined by a single high energy particle can be calculated straightforwardly. For example, for a lower threshold defined by a deep hole, $\omega_L(q) = -\epsilon(k_F - q)$, the correlation function $\langle d_1^\dagger \psi_R(t,x) \psi_R^\dagger d_1(0,0)\rangle$ can be factorized into a free d_1 propagator and correlations of exponentials of $\varphi_{R,L}$. After Fourier transforming, we find that near the lower edge $S^{zz}(q,\omega) \sim [\omega - \omega_L(q)]^{-\mu}$ with exponent[2]

$$\mu = 1 - \frac{(1-n^1_{imp})^2}{2K} - 2K\left(\frac{1}{2} - d^1_{imp}\right)^2. \tag{3.12}$$

For $h \to 0$, we use Eq. (3.11) and obtain

$$\mu = 1 - K, \qquad (h \to 0) \tag{3.13}$$

independent of the momentum of the hole. This form for the lower edge exponent had been conjectured long ago by Müller et al. [182]. It agrees (up

[2]After this work was accepted for publication we learned of the results of Cheianov and Pustilnik (private communication and arXiv:0710.3589 [181]). We have checked that their exponent is exactly the same as ours for all q, Δ and $h \neq 0$.

to logarithmic corrections) with the exponent of the two-spinon contribution to $S^{zz}(q,\omega)$ for the Heisenberg point ($K = 1/2$) [166].

The general result of Eq. (3.12) is consistent with the weak coupling expression for μ [176]. To first order in Δ, Eq. (3.12) reduces to

$$\mu \approx \frac{\kappa_R^{(1)}}{\pi(v-u_1)} \approx \frac{2\Delta\,(1-\cos q)}{\pi\,[\sin k_F - \sin\,(k_F - q)]}. \tag{3.14}$$

For $k_F \neq \pi/2$, we expand for $q \ll k_F$ and get $\mu \approx m\Delta q/\pi$, where $m = (\cos k_F)^{-1}$ (*c.f.* [176]). For $k_F = \pi/2$, we obtain $\mu \approx 2\Delta/\pi$, which is $1-K$ to $O(\Delta)$. Note the cancellation of the q dependence of $\kappa_R^{(1)}$ and $v - u_1$ in the latter case. Momentum-independent exponents have also been derived for the Calogero-Sutherland model [183].

We now consider a threshold defined by high-energy particle and hole at $k_{1,2} = \pi/2 \mp q/2$. The relevant correlation function is the propagator of the transformed $d_2^\dagger d_1$. For simplicity, here we focus on the zero field case, in which $\varepsilon_2 = -\varepsilon_1 = v\sin(q/2)$, $u_2 = u_1$ and $-m_2 = m_1 = [v\sin(q/2)]^{-1}$. Particle-hole symmetry then implies that $\gamma^1_{R,L} = \gamma^2_{R,L}$ and $d_2^\dagger d_1$ is invariant under the unitary transformation of Eq. (3.5). In the noninteracting case, there is a square root singularity at the upper threshold due to the divergence of the joint density of states: $S^{zz}(q,\omega) \propto \sqrt{m_1/[\omega_U(q)-\omega]}$ for $\omega \approx \omega_U(q) = 2v\sin(q/2)$ [167]. For $\Delta \neq 0$, we need to treat the direct interaction V_{12} between the particle and the hole, which is not modified by U. This problem is analogous to the effect of Wannier excitons on the optical absorption rate of semiconductors [184, 185]. This simple two-body problem can be solved exactly for a delta function interaction. The result is that the upper edge exponent changes discontinuously for $\Delta \neq 0$: the square root divergence turns into a universal (for any q and Δ) square root cusp, $S^{zz}(q,\omega) \propto \sqrt{\omega_U(q)-\omega}$. This behavior contradicts the Müller ansatz [182], but is consistent with the analytic two-spinon result for $\Delta = 1$ [166]. Unlike the original exciton problem, a bound state only appears for $V_{12} < 0$

($\Delta < 0$) [186], because the particle and hole have a negative effective mass. For $\Delta \neq 0$, the upper edge cusp should intersect a high-frequency tail dominated by four-spinon excitations as proposed in [187]. This picture must be modified for $h \neq 0$, since then $\gamma^1_{R,L} \neq \gamma^2_{R,L}$ and one needs to include the bosonic exponentials. The upper edge singularity then becomes Δ- and q-dependent. The general finite field case, including the middle singularity [167] for $q > |2k_F - \pi|$, will be discussed elsewhere.

3.4 Self-correlation function

We can apply the Hamiltonian of Eq. (3.4) to study the self-correlation function $G(t) \equiv \langle 0|S^z_j(t)S^z_j(0)|0\rangle$. Even in the noninteracting case, the long-time behavior is a *high energy* property, since it is dominated by a saddle point contribution with a hole at the bottom and a particle at the top of the band [188]. In this case, $k_1 = 0$ and $k_2 = \pi$ and $d^{1,2}_{imp}$ vanish by symmetry ($\gamma^\alpha_R = \gamma^\alpha_L$). Here we restrict to zero field, but the method can be easily generalized. For $h = 0$ and $\Delta \geq 0$, $G(t)$ takes the form

$$G(t) \sim B_1 \frac{e^{-iWt}}{t^\eta} + B_2 \frac{e^{-i2Wt}}{t^{\eta_2}} + \frac{B_3}{t^\sigma} + \frac{B_4}{t^2}, \tag{3.15}$$

where $W = -\epsilon(0) = v$. The last two terms are the standard low-energy contributions, with $\sigma = 2K$. The amplitudes B_3 and B_4 are known [189]. The first term is the contribution from the hole at the bottom of the band and the particle at $k_F = \pi/2$, with exponent

$$\eta = (1+K)/2 + (1 - n^1_{imp})^2/2K = K + 1/2. \tag{3.16}$$

The term oscillating at $2W$ comes from a hole at $k = 0$ and a particle at $k = \pi$. For $\Delta = 0$, we have $\eta_2 = 1$. The exponent η_2 is connected with the singularity at the upper threshold of $S^{zz}(q,\omega)$ by $G(t) \sim \int d\omega e^{i\omega t} \int dq\, S^{zz}(q,\omega)$ for $q \approx \pi$ and $\omega \approx \omega_U(\pi) = 2v$. Due to the discontinuity of the exponent

at ω_U, η_2 jumps from $\eta_2 = 1$ to $\eta_2 = 2$ for any nonzero Δ. This behavior should be observed for $t \gg 1/(m_1 V_{12}^2) \sim 1/\Delta^2$. As a result, the asymptotic behavior of $G(t)$ is governed by the exponent $\eta < 3/2$ for $0 < \Delta < 1$. For $\Delta < 0$, we must add to Eq. (3.15) the contribution from the bound state.

3.5 Comparison with t-DMRG

We can also study $S^{zz}(q, \omega)$ with time-dependent DMRG (tDMRG) [168, 172]. The tDMRG methods directly produce $S^{zz}(x, t)$ and its spatial Fourier transform $S^{zz}(q, t)$ for short to moderate times. This information nicely complements the asymptotic information available analytically. The DMRG calculation begins with the standard finite system calculation of the ground state $\phi(t = 0)$ on a finite lattice of typical length $L =$ 200-400, where a few hundred states are kept for a truncation error less than 10^{-10}. One of the sites at the center of the lattice is selected as the origin, and the operator S_0^z is applied to the ground state to obtain a state $\psi(t = 0)$. Subsequently, the time evolution operator for a time step τ, $\exp(i(H - E_0)\tau)$ where E_0 is the ground state energy, is applied via a fourth order Trotter decomposition [173] to evolve both $\phi(t)$ and $\psi(t)$. At each DMRG step centered on site j we obtain a data point for the Green's function $G(t, j)$ by evaluating $\langle \phi(t) | S_j^z | \psi(t) \rangle$. As the time evolution progresses, the truncation error accumulates. The integrated truncation error provides a useful estimate of the error, and so longer times require smaller truncation errors at each step, attained by increasing the number m of states kept. The truncation error grows with time for fixed m, and is largest near the center where the spin operator was applied. We specify the desired truncation error at each step and choose m to achieve it, within a specified range. Typically for later times we have $m \approx 1000$. Finite size effects are small for times less than $(L/2)/v$. We are able to obtain very accurate results for $G(t, j)$, with errors between 10^{-4} and 10^{-5}, for times up to $Jt \sim$ 30-60.

Table 3.1: Exponents for the spin self-correlation function $G(t)$ for $h = 0$. The parameters W, η, η_2 and σ were obtained numerically by fitting the DMRG data according to Eq. (3.15). These are compared with the corresponding FT predictions (with v and K taken from the Bethe ansatz).

Δ	W	v	η	$\frac{1}{2}+K$	σ	$2K$	η_2	
0	1	1	1.5	1.5	2	2	1	1
0.125	1.078	1.078	1.451	1.426	1.954	1.852	1.761	2
0.25	1.153	1.154	1.366	1.361	1.811	1.723	2.034	2
0.375	1.226	1.227	1.313	1.303	1.694	1.607	2.000	2
0.5	1.299	1.299	1.287	1.25	1.491	1.5	2.120	2
0.75	1.439	1.438	1.102	1.149	1.324	1.299	2.226	2

For $Jt > 10 - 20$, we find the behavior of $S^{zz}(q,t)$ and $G(t)$ is well approximated by asymptotic expressions, determined by the singular features of $S^{zz}(q,\omega)$ and $G(\omega)$. By utilizing the leading and subleading terms for each singularity, we have been able to fit with a typical error in $S^{zz}(q,t)$ or $G(t)$ for $Jt \sim$ 20-30 between 10^{-4} and 10^{-5}. We can fit with the decay exponents determined analytically or as free parameters to check the analytic expressions. Table 3.1 shows the comparison between the exponents for $G(t)$ extracted independently from the DMRG data and the FT predictions. In all cases the agreement is very good. By smoothly transitioning from the tDMRG data to the fit as t increases, we obtain accurate results for all times. A straightforward time Fourier transform with a very long time window yields very accurate high resolution spectra. Examples of line shapes obtained this way are shown in Fig. 3.1. We also did DMRG for the hole Green's function for the fermionic model corresponding to Eq. (3.1), obtaining good agreement with the predicted singularities from the X-ray edge picture.

We have not seen any exponential damping of the η_2 term in $G(t)$ for $\Delta > 0$. This suggests that the singularity at the upper edge is not smoothed out in the integrable XXZ model, even when the stability of the excitation is not guaranteed by kinematic constraints [190]. Integrability also protects the

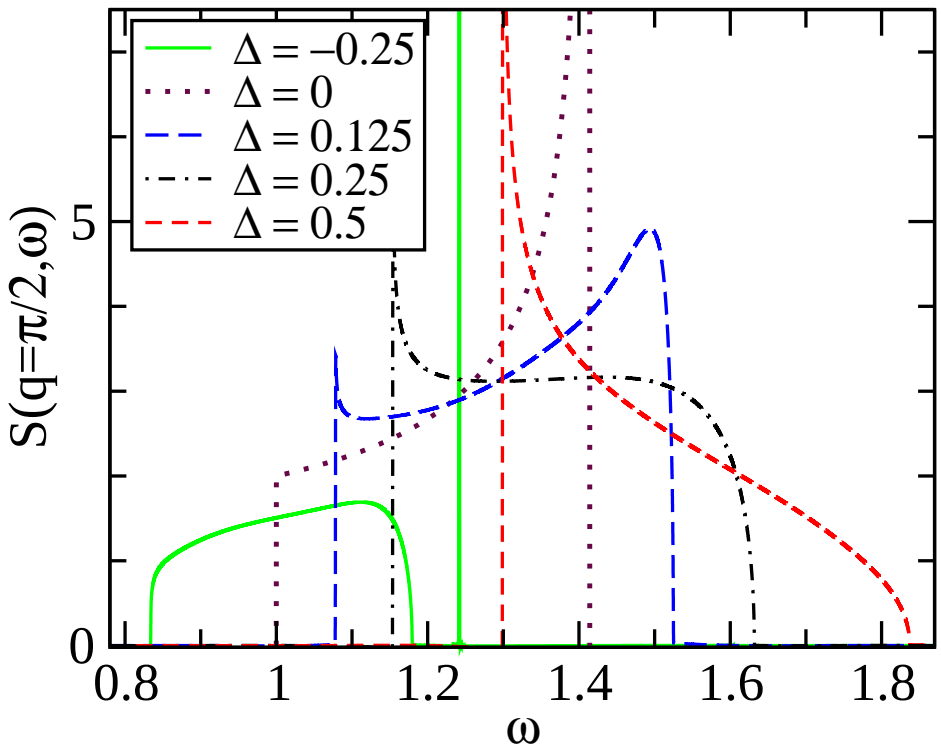

Figure 3.1: DMRG results for $S^{zz}(q,\omega)$ versus ω for $q = \pi/2$, $h = 0$ and several values of anisotropy Δ. The line shapes for $\Delta > 0$ show a divergent X-ray type lower edge and a universal square-root cusp at the upper edge. The curve for $\Delta < 0$ shows a bound state above the upper edge. The width of the peak is very small for small $|\Delta|$.

singularity at ω_U for finite field, as implied by the CFT form of the spectrum in Eq. (3.6).

3.6 Details of calculations

In this section we present detailed derivations of the results discussed in the previous sections, as well as other results that were not included in the published version [191]. These will appear in a separate publication to be submitted to Physical Review B.

3.6.1 Derivation of the X-ray edge Hamiltonian

We start by deriving the low-energy effective Hamiltonian in Eq. (3.4) from the XXZ model in Eq. (3.1). As mentioned in section 3.1, we start from the noninteracting case and identify the choices of momenta for hole and particle that define the thresholds of the two-particle continuum. The simplest case is the one for small q and finite field ($q \ll \pi |\sigma|$), which we discussed in chapter 2. Recall that in this case the lower threshold is defined by a deep hole excitation, while the upper threshold is defined by a high-energy particle excitation (see Fig. 2.6). In chapter 2, "deep" and "high-energy" meant as far from the Fermi surface as possible, but still at relatively low energies compared to the exchange coupling J because we were restricted to small values of q. Here we are allowed to take these expressions literally, meaning that we derive the exponents for arbitrary values of q, including excitations at the top and bottom of the band.

Our goal is to describe what happens near the thresholds of $S^{zz}(q,\omega)$ when we turn on the interaction between the high-energy particles or holes and the Fermi surface modes. For $\Delta \ll 1$, first order perturbation theory in the interaction shows that the correction to $S^{zz}(q,\omega)$ is small everywhere except near the thresholds, where it diverges logarithmically [176]. This means that finite order perturbation theory breaks down and one has to find

a way to sum up the logarithmic divergences. This is reminiscent of the X-ray edge problem in metals [184]. In the original version of the X-ray edge problem, a high-energy photon excites an electron from a core level in the valence band to an empty state in the conduction band, above the Fermi level. In the noninteracting case, there is a step function at the absorption edge corresponding to the energy difference between the flat valence band and the Fermi level. If the electrons interact via a screened Coulomb interaction, the core hole in the intermediate state causes a phase shift in all the states near the Fermi level. In the thermodynamic limit, the intermediate state is orthogonal to the initial state. This is Anderson's orthogonality catastrophe [192]. The solution of the X-ray edge problem by Mahan, Nozieres and DeDominicis [193, 194] shows that the logarithmic singularities that appear in the absorption rate in all orders of perturbation theory sum up to produce a power-law singularity at the absorption edge. The exponent of the power-law singularity can be written in terms of the exact phase shift due to the creation of the core hole. An elegant way to obtain the power law singularities using bosonization of the conduction electrons is due to Schotte and Schotte [195].

Pustilnik *et al.* [176] adapted Schotte and Schotte's approach to study the singularities of the DSF for interacting spinless fermions. The main idea is to define narrow subbands around the values of momentum which determine the thresholds of the two-particle continuum. This way, the modes away from the Fermi surface act like mobile impurities which shift the momentum of the states near the Fermi surface, similar to the core hole in the X-ray edge problem. Note that in this approach one writes a different effective Hamiltonian for each choice of q and $\omega \approx \omega_L(q)$ or $\omega \approx \omega_U(q)$.

We start from the XXZ Hamiltonian

$$H = H_0 + H_{int}, \tag{3.17}$$

$$H_0 = -\frac{J}{2}\sum_{j=1}^{L} c_j^\dagger c_{j+1} + h.c., \tag{3.18}$$

$$H_{int} = J\Delta\sum_{j=1}^{L} n_j n_{j+1}, \tag{3.19}$$

where we have omitted the chemical potential terms, which are incorporated in the choice of the Fermi momentum $k_F = \pi/2 + \pi\sigma$. Consider first the lower threshold with a deep hole with momentum $k_1 = k_F - q$ and a particle at the Fermi surface. We expand the fermionic field defining right and left movers as well as the extra d_1 mode with $k \approx k_1$

$$\Psi(x) \sim e^{ik_F x}\psi_R(x) + e^{-ik_F x}\psi_L(x) + e^{ik_1 x}d_1(x). \tag{3.20}$$

We bosonize right and left movers in the hopping term H_0 as done in section 2.2, expressing the density operators in terms of derivatives of bosonic fields.

$$\rho_{R,L}(x) =: \psi_{R,L}^\dagger \psi_{R,L} := \mp\frac{\partial_x \phi_{R,L}}{\sqrt{2\pi}} \tag{3.21}$$

We also expand the dispersion $\epsilon(k) = -J\cos k$ for $k \approx k_1$. This procedure yields the kinetic energy density

$$\mathcal{H}_0 \approx \frac{v_F}{2}\left[(\partial_x\phi_R)^2 + (\partial_x\phi_L)^2\right] + d_1^\dagger\left(-\varepsilon_1 - iu_1\partial_x - \frac{\partial_x^2}{2m_1}\right)d_1, \tag{3.22}$$

where $v_F = J\sin k_F$ is the bare Fermi velocity, $\varepsilon_1 = J\cos(k_F - q)$, is the energy of the deep hole below the Fermi level, $u = J\sin(k_F - q)$ is the bare velocity of the deep hole and $m = [J\cos(k_F - q)]^{-1}$ is the effective mass of the deep hole. We assume $0 < q < k_F < \pi/2$ (i.e. $\sigma < 0$), so the above parameters are all positive. Using Eq. (3.20), we obtain the density operator

$$\Psi^\dagger(x)\Psi(x) \sim \rho_R + \rho_L + \left(e^{i2k_F x}\psi_L^\dagger\psi_R + h.c.\right) + d_1^\dagger d_1$$

$$+\left[e^{i(k_F-k_1)x}d_1^\dagger\psi_R+e^{-i(k_F+k_1)x}d_1^\dagger\psi_L+h.c.\right]. \quad (3.23)$$

As a result, the interaction term becomes

$$\begin{aligned}\mathcal{H}_{int} &= \frac{g_4}{4\pi}\left[(\partial_x\phi_R)^2+(\partial_x\phi_L)^2\right]-\frac{g_2}{2\pi}\partial_x\phi_R\partial_x\phi_L \\ &+\frac{2\Delta}{\sqrt{2\pi}}d_1^\dagger d_1\left[1-\cos\left(k_F-k_1\right)\right]\partial_x\phi_R \\ &+\frac{2\Delta}{\sqrt{2\pi}}d_1^\dagger d_1\left[1-\cos\left(k_F+k_1\right)\right]\partial_x\phi_L \end{aligned} \quad (3.24)$$

where $g_2=g_4=2\Delta[1-\cos(2k_F)]=4\Delta\sin^2 k_F$. In general, for $k_1\neq 0$, the d_1 particle couples differently to right and left movers. This means that there is a coupling both to the total density and to the current of low energy modes, as assumed in [180]. In terms of the dual fields,

$$\phi_{R,L}=\frac{\tilde\theta\mp\tilde\phi}{\sqrt{2}}, \quad (3.25)$$

we have

$$\mathcal{H}_0\approx\frac{v_F}{2}\left[\left(\partial_x\tilde\theta\right)^2+\left(\partial_x\tilde\phi\right)^2\right]+d_1^\dagger\left(-\varepsilon_1-iu_1\partial_x-\frac{\partial_x^2}{2m_1}\right)d_1, \quad (3.26)$$

$$\mathcal{H}_{int}=\frac{g_2}{2\pi}\left(\partial_x\tilde\phi\right)^2+\frac{1}{\sqrt{\pi}}\left(\frac{\tilde\kappa_L^{(1)}-\tilde\kappa_R^{(1)}}{2}\partial_x\tilde\theta+\frac{\tilde\kappa_L^{(1)}+\tilde\kappa_R^{(1)}}{2}\partial_x\tilde\phi\right)d_1^\dagger d_1, \quad (3.27)$$

where, to first order in Δ, $\tilde\kappa_{R,L}^{(1)}=2\Delta\left[1-\cos\left(k_F\mp k_s\right)\right]$. We can combine Eqs. (3.26) and (3.27) and write

$$\begin{aligned}\mathcal{H} &= \frac{1}{2}\left[vK\left(\partial_x\tilde\theta\right)^2+\frac{v}{K}\left(\partial_x\tilde\phi\right)^2\right]+d_1^\dagger\left(-\varepsilon_1-iu_1\partial_x-\frac{\partial_x^2}{2m_1}\right)d_1 \\ &+\frac{1}{\sqrt{\pi}}\left(\frac{\tilde\kappa_L^{(1)}-\tilde\kappa_R^{(1)}}{2}\partial_x\tilde\theta+\frac{\tilde\kappa_L^{(1)}+\tilde\kappa_R^{(1)}}{2}\partial_x\tilde\phi\right)d_1^\dagger d_1, \end{aligned} \quad (3.28)$$

where v and K are the renormalized velocity and Luttinger parameter to lowest order in Δ; see Eqs. (2.42) and (2.43). In terms of the chiral components of the rescaled fields defined in Eq. (2.47), we find

$$\begin{aligned}\mathcal{H} \approx & \frac{v}{2}\left[(\partial_x\varphi_L)^2+(\partial_x\varphi_R)^2\right]+d_1^\dagger\left(-\varepsilon_1-iu_1\partial_x-\frac{\partial_x^2}{2m_1}\right)d_1 \\ & +\frac{1}{\sqrt{2\pi K}}\left(\kappa_L^{(1)}\partial_x\varphi_L-\kappa_R^{(1)}\partial_x\varphi_R\right)d_1^\dagger d_1, \end{aligned} \tag{3.29}$$

where

$$\kappa_{L,R}^{(1)}=\left(\frac{1+K}{2}\right)\tilde{\kappa}_{L,R}^{(1)}-\left(\frac{1-K}{2}\right)\tilde{\kappa}_{R,L}^{(1)}. \tag{3.30}$$

Eq. (3.29) is the effective Hamiltonian for a single high-energy hole. It is asymptotically exact in the limit $\omega\to\omega_L(q)$ if all the parameters are taken to be the renormalized ones. We already know how to obtain the low-energy parameters v and K from the Bethe ansatz equations. In section 3.6.2 we will describe how to fix ε_1, u_1 and m_1 by means of the exact dispersion of the deep hole in the corresponding Bethe ansatz eigenstate. We will also determine the coupling constants $\kappa_{R,L}^{(1)}$ by relating them to renormalized phase shifts. For now, we assume that these parameters are known and calculate the edge singularities that follow from this effective field theory. In order to compute correlation functions, we want to find the unitary transformation of the type

$$U=\exp\left\{-\frac{i}{\sqrt{2\pi K}}\int_{-\infty}^{+\infty}dx\,\left[\gamma_R^{(1)}\varphi_R+\gamma_L^{(1)}\varphi_L\right]d_1^\dagger d_1\right\}, \tag{3.31}$$

that decouples the d_1 particle from the bosonic fields. Defining $\bar{\varphi}_{R,L}=U\varphi_{R,L}U^\dagger$ and $\bar{d}_1=Ud_1U^\dagger$, we have

$$\partial_x\varphi_{R,L} = \partial_x\bar{\varphi}_{R,L}\pm\frac{\gamma_{R,L}^{(1)}}{\sqrt{2\pi K}}\bar{d}_1^\dagger\bar{d}_1, \tag{3.32}$$

$$d_1 = \bar{d}_1\,\exp\left[-\frac{i}{\sqrt{2\pi K}}\left(\gamma_R^{(1)}\bar{\varphi}_R+\gamma_L^{(1)}\bar{\varphi}_L\right)\right], \tag{3.33}$$

where we used that $\bar{d}_1^\dagger \bar{d}_1 = d_1^\dagger d_1$ and

$$\begin{aligned} e^{i\gamma_R^{(1)}\varphi_R/\sqrt{2\pi K}} d_1 &= e^{i\gamma_R^{(1)}\bar{\varphi}_R/\sqrt{2\pi K}} e^{i\gamma_R^{(1)}/(8\pi K)\int_{-\infty}^{+\infty} dy\, \mathrm{sgn}(x-y)\bar{d}_1^\dagger \bar{d}_1} \bar{d}_1 \\ &= e^{i\gamma_R^{(1)}\bar{\varphi}_R/\sqrt{2\pi K}} d_1. \end{aligned} \tag{3.34}$$

For given $\gamma_{R,L}^{(1)}$, the Hamiltonian in terms of the transformed fields reads

$$\begin{aligned} \mathcal{H} &= \frac{v}{2}\left(\partial_x\bar{\varphi}_L\right)^2 + \frac{v}{2}\left(\partial_x\bar{\varphi}_R\right)^2 + \bar{d}_1^\dagger\left(-\epsilon_1 - iu_1\partial_x - \frac{\partial_x^2}{2m_1}\right)\bar{d}_1 \\ &\quad -\frac{(v+u_1)\,\gamma_L^{(1)}}{\sqrt{2\pi K}}\,\partial_x\bar{\varphi}_L\bar{d}_1^\dagger\bar{d}_1 + \frac{(v-u_1)\,\gamma_R^{(1)}}{\sqrt{2\pi K}}\,\partial_x\bar{\varphi}_R\bar{d}_1^\dagger\bar{d}_1 \\ &\quad +\frac{1}{\sqrt{2\pi K}}\left(\kappa_L^{(1)}\partial_x\bar{\varphi}_L - \kappa_R^{(1)}\partial_x\bar{\varphi}_R\right)\bar{d}_1^\dagger\bar{d}_1 + \ldots, \end{aligned} \tag{3.35}$$

where $\ldots$ stands for the irrelevant operators $\partial_x\bar{\varphi}_{R,L}\bar{d}_1^\dagger\partial_x\bar{d}_1$, $(\partial_x\bar{\varphi}_{R,L})^2\bar{d}_1^\dagger\bar{d}_1$, which we neglect because they do not affect the exponent of the singularity at $\omega_L(q)$. Therefore, in order to get free fields, we must choose the parameters of the unitary transformation to be

$$\gamma_{L,R}^{(1)} = \frac{\kappa_{L,R}^{(1)}}{v \pm u_1}. \tag{3.36}$$

The shift of the bosonic fields due to the coupling to the d_1 particle gives rise to the X-ray-edge-type singularity of $S^{zz}(q,\omega)$ at the lower threshold. The term in the density that creates the excitation with the deep hole and a particle at the right Fermi point is, from Eq. (3.23),

$$\Psi^\dagger(x)\,\Psi(x) \sim e^{iqx}\psi_R^\dagger(x)\,d_1(x). \tag{3.37}$$

Therefore, the term in the spin correlation function which oscillates in x with momentum q is given by

$$\left\langle S_{j+x}^z(t)\,S_j^z(0)\right\rangle \sim \left\langle \Psi^\dagger\Psi(x,t)\,\Psi^\dagger\Psi(0,0)\right\rangle$$

$$
\begin{aligned}
&\sim \quad e^{iqx}\left\langle d_1^\dagger \psi_R\left(x,t\right)\psi_R^\dagger d_1\left(0,0\right)\right\rangle \\
&\sim \quad e^{iqx}\left\langle \bar{d}_1^\dagger\left(x,t\right)\bar{d}_1\left(0,0\right)\right\rangle \\
&\qquad \times\left\langle e^{-i\sqrt{2\pi\nu_+^{(1)}}\bar{\varphi}_R(x,t)}e^{i\sqrt{2\pi\nu_+^{(1)}}\bar{\varphi}_R(0,0)}\right\rangle \\
&\qquad \times\left\langle e^{-i\sqrt{2\pi\nu_-^{(1)}}\bar{\varphi}_L(x,t)}e^{i\sqrt{2\pi\nu_-^{(1)}}\bar{\varphi}_L(0,0)}\right\rangle, \qquad (3.38)
\end{aligned}
$$

where

$$
\nu_\pm^{(1)} = \frac{1}{4}\left[\sqrt{K} \pm \frac{1}{\sqrt{K}}\left(1 - \frac{\gamma_{R,L}^{(1)}}{\pi}\right)\right]^2. \qquad (3.39)
$$

Note that, for $\Delta \ll 1$, $\nu_+^{(1)} \sim O(1)$ whereas $\nu_-^{(1)} \sim O(\Delta^2)$. The correlation functions in Eq. (3.38) can be calculated straightforwardly since the transformed fields are noninteracting. For $k_1 \neq 0$ ($q \neq k_F$), the free d_1 propagator is well approximated by keeping only the linear term in the dispersion. We find

$$
\left\langle \bar{d}_1^\dagger\left(x,t\right)\bar{d}_1\left(0,0\right)\right\rangle \sim e^{-i\varepsilon_1 t}\int_{-\Lambda}^{+\Lambda}\frac{dk}{2\pi}\,e^{ik(x-u_1 t)} \approx e^{-i\varepsilon_1 t}\delta\left(x-u_1 t\right), \qquad (3.40)
$$

where $\Lambda \ll q$ is the momentum cutoff for the deep hole subband. Eq. (3.20) essentially means that the decoupled hole propagates ballistically with velocity $u_1 < v$. The correlation functions for the exponentials of free bosonic fields (vertex operators in conformal field theory) are given by the standard result [160]

$$
\left\langle e^{-i\sqrt{2\pi\nu_+^{(1)}}\bar{\varphi}_R(x,t)}e^{i\sqrt{2\pi\nu_+^{(1)}}\bar{\varphi}_R(0,0)}\right\rangle = \left(\frac{\eta}{\eta + ivt - ix}\right)^{\nu_+^{(1)}}, \qquad (3.41)
$$

$$
\left\langle e^{-i\sqrt{2\pi\nu_-^{(1)}}\bar{\varphi}_L(x,t)}e^{i\sqrt{2\pi\nu_-^{(1)}}\bar{\varphi}_L(0,0)}\right\rangle = \left(\frac{\eta}{\eta + ivt + ix}\right)^{\nu_-^{(1)}}, \qquad (3.42)
$$

where $\eta \sim \Lambda^{-1}$ is the short distance cutoff. This is the same cutoff prescrip-

tion as used in [196]. Eqs. (3.40), (3.41) and (3.42) imply

$$\begin{aligned} S^{zz}\left(q,\omega\approx\omega_L\right) &\sim \int_{-\infty}^{+\infty} dt\,\frac{e^{i(\omega-\omega_L)t}}{\left[(u_1-v)t+i\eta\right]^{\nu_+^{(1)}}\left[(u_1+v)t-i\eta\right]^{\nu_-^{(1)}}} \\ &\sim \int_{-\infty}^{+\infty} dt\,\frac{e^{i(\omega-\omega_L)t}}{(t-i\eta)^{1-\mu}}, \end{aligned} \tag{3.43}$$

where we substituted $\varepsilon_1=\omega_L(q)$ and defined $\mu=1-\nu_+^{(1)}-\nu_-^{(1)}$. The function $(t-i\eta)^{-1+\mu}$ in the integrand has a branch point in the upper half of the complex plane for $\mu<1$. The integral can be evaluated by contour integral methods. Forgetting about the amplitude (which is not determined in this approach anyway because it is cutoff dependent), we find that $S^{zz}\left(q,\omega\right)$ diverges at the lower threshold

$$S^{zz}\left(q,\omega\approx\omega_L\left(q\right)\right)\sim\theta\left(\omega-\omega_L(q)\right)\left[\omega-\omega_L(q)\right]^{-\mu}. \tag{3.44}$$

with exponent

$$\mu=1-\frac{1}{4}\left[\sqrt{K}+\frac{1}{\sqrt{K}}\left(1-\frac{\gamma_R^{(1)}}{\pi}\right)\right]^2-\frac{1}{4}\left[\sqrt{K}-\frac{1}{\sqrt{K}}\left(1-\frac{\gamma_L^{(1)}}{\pi}\right)\right]^2. \tag{3.45}$$

For $\Delta\ll 1$, we can obtain the exponent to first order in Δ neglecting the coupling of the deep hole to left movers. The reason is that the last term in Eq. (3.45) is of order Δ^2. Using the weak coupling expressions for K and $\kappa_R^{(1)}$, we obtain

$$\gamma_R^{(1)}=\frac{\kappa_R^{(1)}}{v-u_1}\approx\frac{2\Delta\left(1-\cos q\right)}{\sin k_F-\sin\left(k_F-q\right)}, \tag{3.46}$$

$$\mu\approx 1-\frac{1}{4}\left[K+\frac{1}{K}\left(1-\frac{\gamma_R^{(1)}}{\pi}\right)^2+2\left(1-\frac{\gamma_R^{(1)}}{\pi}\right)\right]\approx\frac{\gamma_R^{(1)}}{\pi}. \tag{3.47}$$

Therefore, we find

$$\mu = \frac{2\Delta\left(1-\cos q\right)}{\pi\left[\sin k_F - \sin\left(k_F - q\right)\right]} + O(\Delta^2), \tag{3.48}$$

which is the result in Eq. (3.14).

In the limit of vanishing magnetic field, we have explicit formulas for the renormalized coupling constants $\kappa^{(1)}_{R,L}$. In section 3.2 we stated that, as $h \to 0$, $\gamma^{(1)}_R/\pi \to \gamma^{(1)}_L/\pi \to 1-K$. (The formulas we used there are derived in section 3.6.2.) In this case, it is easy to verify that

$$\kappa^{(1)}_{R,L} = \frac{\pi(1-K)}{K}\left(v \mp u_1 K\right). \tag{3.49}$$

This is consistent with the weak coupling expansion for $\kappa^{(1)}_{R,L}$. Note that, although $\gamma^{(1)}_{R,L}$ are independent of the momentum of the hole, $\kappa^{(1)}_{R,L}$ still depend on q through the renormalized velocity $u_1 = v\cos q$.

Likewise, we can derive the exponent for the singularity at the upper threshold defined by the high-energy particle excitation. In this case, we introduce $\kappa^{(2)}_{R,L}$ as the couplings between the high-energy d_2 particle and the Fermi surface modes. However, an important difference is that $S^{zz}\left(q,\omega\right)$ does not vanish above the upper threshold of the two-particle continuum. Instead, the power-law singularity has to join the high frequency tail at $\omega = \omega_U(q)$. Repeating the calculation for the effective Hamiltonian with a single high-energy particle, we arrive at the integral

$$\begin{aligned} S^{zz}\left(q,\omega\approx\omega_U\right) &\sim \int_{-\infty}^{+\infty} dx \int_{-\infty}^{+\infty} dt e^{i\omega t}\left\langle \psi^\dagger_R d_2\left(x,t\right) d^\dagger_2 \psi_R\left(0,0\right)\right\rangle \\ &\sim \int_{-\infty}^{+\infty} dt \frac{e^{i(\omega-\omega_U)t}}{\left[(u_2-v)t+i\eta\right]^{\nu^{(2)}_+}\left[(u_2+v)t-i\eta\right]^{\nu^{(2)}_-}}, \end{aligned} \tag{3.50}$$

where $\nu^{(2)}_\pm$ are defined in analogy with Eq. (3.39). In the case $q \ll \pi\left|\sigma\right|$, we have $u_2 > v$, i.e., the high-energy particle moves faster than the hole at the

Fermi surface. As a result, the integrand in Eq. (3.50) has branch points above and below the real axis and $S^{zz}(q,\omega)$ is finite for both $\omega < \omega_U(q)$ and $\omega > \omega_U(q)$. For ω approaching $\omega_U(q)$ from below, we find

$$S^{zz}\left(q, \omega \to \omega_U(q)^-\right) \sim A + B \times \left[\omega_U(q) - \omega\right]^{\mu_2}, \tag{3.51}$$

where $\mu_2 > 0$ is given by an expression analogous to Eq. (3.45) with the corresponding $\gamma^{(2)}_{R,L}$. It follows from this result that $S^{zz}(q,\omega)$ approaches a finite value A with infinite slope as $\omega \to \omega_U(q)$. In the interacting case, the "upper" threshold must be interpreted not as the energy above which $S^{zz}(q,\omega)$ vanishes, but as the energy where the power-law singularity develops and the slope diverges. This only makes sense for integrable models, since in general we expect that higher-order decay processes will smooth out the singularity [190]. We do not attempt to calculate the constants A and B because these appear to depend on the choice of cutoff η. For ω approaching $\omega_U(q)$ from above, we find

$$S^{zz}\left(q, \omega \to \omega_U(q)^+\right) \sim A - B' \times \left[\omega - \omega_U(q)\right]^{\mu_2}. \tag{3.52}$$

The result in the weak coupling limit is discussed in [176]. The main point here is that Eq. (3.45) can be used to calculate the exact singularity exponent, once $\gamma^{(2)}_{R,L}$ are extracted from the Bethe ansatz solution.

To study the upper threshold at zero field, we need an effective Hamiltonian with two high-energy modes. The reason is that, at zero field ($k_F = \pi/2$), the high-energy particle and the deep hole are degenerate due to particle-hole symmetry. Both of them correspond to the minimum energy for a given q and therefore define the lower threshold. The upper threshold, on the other hand, is given by the excitation which minimizes the effects of band curvature, namely the symmetric particle-hole pair with both a deep hole at $\pi/2 - q/2$ and a high-energy particle at $\pi/2 + q/2$. We use the mode

expansion

$$\Psi(x) \sim e^{i\pi x/2}\psi_R(x) + e^{-i\pi x/2}\psi_L(x) + e^{i(\pi-q)x/2}d_1(x) + e^{i(\pi+q)x/2}d_2(x). \quad (3.53)$$

The kinetic energy part of the Hamiltonian now contains the dispersion for both d_1 and d_2. In the interaction part, besides the density-density coupling between d particles and bosonic fields, we must include the direct low-energy scattering between d_1 and d_2, which will be important when both high-energy particle and hole are present in the intermediate state (see section 3.6.3). In the XXZ model this interaction term stems from

$$\Psi^\dagger(x)\Psi(x) \sim d_1^\dagger(x)d_1(x) + d_2^\dagger(x)d_2(x) + \left[e^{iqx}d_1^\dagger(x)d_2(x) + h.c.\right]. \quad (3.54)$$

$$\begin{aligned} \mathcal{H}_{12} &\sim \Delta\Psi^\dagger(x)\Psi(x)\Psi^\dagger(x+1)\Psi(x+1) \\ &\sim \Delta(1-\cos q)\, d_1^\dagger(x)d_1(x)d_2^\dagger(x)d_2(x), \end{aligned} \quad (3.55)$$

where we neglected irrelevant operators. In general, the effective Hamiltonian density with both d_1 and d_2 can be written as

$$\begin{aligned} \mathcal{H} \approx\ & \frac{v}{2}\left[(\partial_x\varphi_L)^2 + (\partial_x\varphi_R)^2\right] + \sum_{\alpha=1,2} d_\alpha^\dagger\left(\varepsilon_\alpha - iu_\alpha\partial_x - \frac{\partial_x^2}{2m_\alpha}\right)d_\alpha \\ & + V_{12}d_1^\dagger d_1 d_2^\dagger d_2 + \frac{1}{\sqrt{2\pi K}}\sum_{\alpha=1,2}\left(\kappa_L^{(\alpha)}\partial_x\varphi_L - \kappa_R^{(\alpha)}\partial_x\varphi_R\right)d_\alpha^\dagger d_\alpha, \end{aligned} \quad (3.56)$$

where $V_{12} \approx 2\Delta\sin^2(q/2)$ to first order in Δ. Note that V_{12} vanishes as q^2 in the limit $q \to 0$.

The general case of finite field and large q ($q > 2\pi|\sigma|$) is more complicated because it involves a third threshold between $\omega_L(q)$ and $\omega_U(q)$. We will discuss this case, as well as the crossover to the zero field line shape, in section 3.6.5.

3.6.2 Finite size spectrum and exact coupling constants from Bethe ansatz

Here we derive the result for the finite size spectrum for the deep hole state given in Eq. (3.6). The phase shifts n_{imp} and d_{imp} that appear in the finite size spectrum fix the parameters $\gamma_{R,L}$ of the unitary transformation. Consequently, they determine the exponents of the edge singularities discussed in section 3.6.1.

First, we calculate the finite size spectrum predicted by the effective model in Eq. (3.29). This can be easily done by utilizing the results of Ref. [197]. The finite size spectrum for the spin chain with periodic boundary conditions and without the impurity is[3]

$$\Delta E = \frac{2\pi v}{L}\left[\frac{\Delta N^2}{4K} + KD^2 + n_+ + n_-\right], \tag{3.57}$$

with ΔN and D integers and $n_\pm = \sum_n n m_n^{R,L}$ also integers. ΔN corresponds to the total spin of the excited state. We can write

$$\Delta N = N_R + N_L \sim \int_0^L dx \sqrt{\frac{K}{2\pi}}\left(\partial_x\varphi_L - \partial_x\varphi_R\right). \tag{3.58}$$

Likewise, D is the number of current excitations and can be expressed in the form

$$D = \frac{N_R - N_L}{2} \sim -\frac{1}{2}\int_0^L dx \sqrt{\frac{1}{2\pi K}}\left(\partial_x\varphi_L + \partial_x\varphi_R\right). \tag{3.59}$$

In Eqs. (3.58) and (3.59) we used the expressions for the bosonized density and current operators in terms of the rescaled fields. The unitary transformation (3.31) for a single impurity, $\langle d^\dagger d\rangle = 1/L$, takes

$$\Delta N \;\rightarrow\; \Delta N - \frac{\gamma_R + \gamma_L}{2\pi}, \tag{3.60}$$

[3]For comparison with [197], our notation is $K = 1/4\pi R^2$, where R is the compactification radius of the bosonic field.

$$D \;\rightarrow\; D - \frac{\gamma_R - \gamma_L}{4\pi K}. \tag{3.61}$$

Therefore, the shifted spectrum in the presence of the d_1 hole should be

$$\Delta E = \frac{2\pi v}{L}\left[\frac{1}{4K}\left(\Delta N - \frac{\gamma_R + \gamma_L}{2\pi}\right)^2 + K\left(D - \frac{\gamma_R - \gamma_L}{4\pi K}\right)^2 + n_+ + n_-\right]. \tag{3.62}$$

Now we need to calculate the exact finite size spectrum in the Bethe ansatz approach. The following derivation applies the methods used in [198] and [180]. We start from the Bethe equations for M spin flips in a chain with N sites [164]

$$N p_0\left(\lambda_j\right) + \sum_{k=1}^{M} \theta\left(\lambda_j - \lambda_k\right) = 2\pi I_j, \tag{3.63}$$

where the I_j's are half-odd integers for M even and integers for M odd. The functions $p_0(\lambda)$ and $\theta(\lambda)$ are, respectively, the bare momentum and two-particle scattering phase shift as a function of rapidity λ

$$p_0\left(\lambda\right) = i \log\left[\frac{\cosh\left(\lambda - i\zeta/2\right)}{\cosh\left(\lambda + i\zeta/2\right)}\right], \tag{3.64}$$

$$\theta\left(\lambda\right) = i \log\left[\frac{\sinh\left(\lambda + i\zeta\right)}{\sinh\left(\lambda - i\zeta\right)}\right], \tag{3.65}$$

where $\Delta = -\cos\zeta$. A given eigenstate of the XXZ Hamiltonian with real rapidities is specified by the choice of $\{I_j\}$. Consider a state defined by taking $\{I_j\}$ to be the set of all integers (or half-odd integers) between I_+ and I_-, which are defined by

$$I_+ = \max\left\{I_j\right\} + \frac{1}{2}, \tag{3.66}$$

$$I_- = \min\left\{I_j\right\} - \frac{1}{2}. \tag{3.67}$$

This way, the total number of particles is

$$M = I_M - I_1 + 1 = I_+ - I_-. \tag{3.68}$$

The current carried by an eigenstate is given by the difference between the number of right movers and left movers. It can be written as

$$2D = I_1 + I_M = I_+ + I_-. \tag{3.69}$$

The ground state for M particles would correspond to the choice $I_- = -I_+$. We want to consider the situation in which a single deep hole is created by removing one of the integers from this "Fermi sea". Moreover, we want the corresponding low energy finite size spectrum, in which we allow adding ΔN particles on the Fermi surface as well as transfering D particles between the Fermi points *in the presence of the deep hole*.

As a first step to take the limit of large N (with M/N fixed), we define the function

$$x\left(\lambda_j\right) = x\left(\lambda(I_j)\right) = I_j/N, \tag{3.70}$$

which obeys the set of equations

$$x\left(\lambda_j\right) = \frac{1}{2\pi}\left[p_0\left(\lambda_j\right) + \frac{1}{N}\sum_k \theta\left(\lambda_j - \lambda_k\right)\right], \qquad j = 1, \ldots, M. \tag{3.71}$$

The density of rapidities is given by the derivative of $x\left(\lambda_j\right)$ (see section 2.4.2)

$$\rho\left(\lambda\right) = \frac{dx(\lambda)}{d\lambda}. \tag{3.72}$$

Therefore, the equation for $\rho(\lambda)$ in the finite system reads

$$\rho\left(\lambda_j\right) = \frac{1}{2\pi}\left[p_0'\left(\lambda_j\right) + \frac{1}{N}\sum_k K\left(\lambda_j - \lambda_k\right)\right], \;\; j = 1, \ldots, M, \tag{3.73}$$

where

$$K(\lambda) = \frac{d\theta(\lambda)}{d\lambda}. \tag{3.74}$$

If we remove one integer, denoted as I_h, from the sum in Eq. (3.73), the corresponding rapidity $\lambda_h = \lambda(I_h)$ will be determined self-consistently by the $M-1$ Bethe equations

$$Np_0(\lambda_j) + \sum_{k\neq j} \theta(\lambda_j - \lambda_k) = 2\pi I_j \;\; (I_j \neq I_h). \tag{3.75}$$

Note that removing a single root is a topological excitation, because if we want to fix the remaining I_j's to remain integers (or half-odd integers) we have to change the boundary conditions [164]. The equation for the density of rapidities after creating a hole becomes

$$\rho(\lambda_j) = \frac{1}{2\pi}\left[p_0'(\lambda_j) + \frac{1}{N}\sum_k K(\lambda_j - \lambda_k) - \frac{1}{N}K(\lambda_j - \lambda_h)\right]. \tag{3.76}$$

where the sum is over all the I_j's between I_- and I_+, including I_h. This form makes it explicit that, in comparison with Eq. (3.73), the correction due to the single hole is $\sim O(1/N)$.

To expand Eq. (3.76) for large N, we use the Euler-Maclaurin formula

$$\frac{1}{N}\sum_{n=n_1}^{n_2} f\left(\frac{n}{N}\right) \approx \int_{\frac{n_1-\frac{1}{2}}{N}}^{\frac{n_2+\frac{1}{2}}{N}} dx\, f(x) + \frac{1}{24N^2}\left[f'\left(\frac{n_1-\frac{1}{2}}{N}\right) - f'\left(\frac{n_2+\frac{1}{2}}{N}\right)\right]. \tag{3.77}$$

We obtain

$$\begin{aligned}\rho(\lambda) \;\; &\approx \;\; \frac{p_0'(\lambda)}{2\pi} + \frac{1}{2\pi}\int_{B_-}^{B_+} d\mu\, K(\lambda-\mu)\rho(\mu) - \frac{K(\lambda-\lambda_h)}{2\pi N} \\ &\quad + \frac{1}{24N^2}\left[\frac{K'(\lambda-B_+)}{\rho(B_+)} - \frac{K'(\lambda-B_-)}{\rho(B_-)}\right],\end{aligned} \tag{3.78}$$

where we introduced the Fermi boundaries $B_\pm = \lambda(I_\pm)$. We organize the

solution to this equation by orders of $1/N$. We keep terms up to order $1/N^2$ in $\rho(\lambda)$ because we are interested in the energy to order $1/N$. We expand $\rho(\lambda)$ in the form

$$\begin{aligned}\rho(\lambda) &= \rho_\infty(\lambda|B_+,B_-)+\frac{1}{N}\rho_{imp}(\lambda|B_+,B_-)\\ &\quad+\frac{1}{24N^2}\left[\frac{\rho_1(\lambda|B_+,B_-)}{\rho(B_+)}-\frac{\rho_1(-\lambda|-B_-,-B_+)}{\rho(B_-)}\right].\end{aligned} \tag{3.79}$$

Substituting Eq. (3.79) into Eq. (3.78), we find the integral equations for each term in the expansion of $\rho(\lambda)$

$$\rho_\infty(\lambda|B_+,B_-) = \frac{p_0'(\lambda)}{2\pi}+\frac{1}{2\pi}\int_{B_-}^{B_+}d\mu\, K(\lambda-\mu)\rho_\infty(\mu|B_+,B_-), \tag{3.80}$$

$$\begin{aligned}\rho_{imp}(\lambda|B_+,B_-) &= -\frac{K(\lambda-\lambda_h)}{2\pi}\\ &\quad+\frac{1}{2\pi}\int_{B_-}^{B_+}d\mu\, K(\lambda-\mu)\rho_{imp}(\mu|B_+,B_-),\end{aligned} \tag{3.81}$$

$$\begin{aligned}\rho_1(\lambda|B_+,B_-) &= \frac{K'(\lambda-B_+)}{2\pi}\\ &\quad+\frac{1}{2\pi}\int_{B_-}^{B_+}d\mu\, K(\lambda-\mu)\rho_1(\mu|B_+,B_-).\end{aligned} \tag{3.82}$$

The energy of a Bethe ansatz eigenstate is given by

$$E=\sum_{j=1}^{M}\epsilon_0\left(\lambda_j\right), \tag{3.83}$$

where

$$\epsilon_0\left(\lambda\right)=-\frac{J\sin^2\zeta}{\cosh\left(2\lambda\right)-\cos\zeta}-h \tag{3.84}$$

is the bare energy of a particle with rapidity λ. The nontrivial effects of interactions on the energy are encoded in the nonuniform density of rapidities $\rho\left(\lambda\right)$. The ground state energy (without the impurity) in the thermodynamic

limit is

$$E_{GS} = N \int_{-B}^{+B} d\mu\, \epsilon_0\left(\mu\right) \rho_{GS}\left(\mu\right), \tag{3.85}$$

where the ground state Fermi boundary B is obtained by solving

$$\int_{-B}^{B} d\lambda\, \rho_{GS}(\lambda) = \frac{1}{2} + \sigma, \tag{3.86}$$

as well as the Lieb equation

$$\rho_{GS}(\lambda) = \frac{p_0'\left(\lambda\right)}{2\pi} + \frac{1}{2\pi} \int_{-B}^{+B} d\mu\, K(\lambda - \mu)\rho_{GS}(\mu), \tag{3.87}$$

self-consistently. Ultimately, we want to express the finite size spectrum in terms of functions which are calculated with reference to the ground state. It is convenient to introduce the shorthand notation for the integral operator $\hat{K}$

$$\hat{K} \cdot f\left(\lambda\right) \equiv \int_{-B}^{B} d\mu\, K\left(\lambda - \mu\right) f\left(\mu\right). \tag{3.88}$$

This way, a general "dressing" equation such as Eq. (3.87) takes the form

$$\left(1 - \frac{\hat{K}}{2\pi}\right) \cdot f\left(\lambda\right) = f_0(\lambda), \tag{3.89}$$

where $f_0(\lambda)$ is a known function and $f(\lambda)$ has to be determined by solving the integral equation with kernel $K(\lambda)$.

The energy of the state with a deep hole is

$$E = \sum_{j \neq h} \epsilon_0\left(\lambda_j\right) = -\epsilon_0\left(\lambda_h\right) + \sum_{j} \epsilon_0\left(\lambda_j\right), \tag{3.90}$$

where the sum in the last equality runs over all I_j's between I_- and I_+. Using

the Euler-Maclaurin formula, we obtain

$$E \approx -\epsilon_0(\lambda_h) + N\int_{B_-}^{B_+} d\mu\, \epsilon_0(\mu)\,\rho(\mu) - \frac{1}{24N}\left[\frac{\epsilon_0'(B_+)}{\rho(B_+)} - \frac{\epsilon_0'(B_-)}{\rho(B_-)}\right]. \quad (3.91)$$

Using the expansion in Eq. (3.79), we obtain

$$E = N\epsilon_\infty(B_+, B_-) + \epsilon_{imp}(B_+, B_-) + \frac{1}{24N}\left[\epsilon_1(B_+, B_-) + \epsilon_1(-B_-, -B_+)\right], \quad (3.92)$$

where

$$\begin{aligned}
\epsilon_\infty(B_+, B_-) &= \int_{B_-}^{B_+} d\mu\, \epsilon_0(\mu)\,\rho_\infty(\mu|B_+, B_-), \\
\epsilon_{imp}(B_+, B_-) &= -\epsilon_0(\lambda_h) + \int_{B_-}^{B_+} d\mu\, \epsilon_0(\mu)\,\rho_{imp}(\mu|B_+, B_-), \quad (3.93)\\
\epsilon_1(B_+, B_-) &= \frac{1}{\rho(B_+)}\left[-\epsilon_0'(B_+) + \int_{B_-}^{B_+} d\mu\, \epsilon_0(\mu)\,\rho_1(\mu|B_+, B_-)\right] \quad (3.94)
\end{aligned}$$

If we set $B_+ = -B_- \equiv B$, Eq. (3.80) would reduce to the Lieb equation, Eq. (3.87), and the term of order N in Eq. (3.92) would give us the ground state energy in the thermodynamic limit. We want to compute $\Delta E = E - E_{GS}$ up to $O(1/N)$. Note that we must be careful about doing the expansion because all the integral equations, e.g. Eq. (3.80), contain terms of order $1/N$. The reason is that the creation of the deep hole shifts the position of the Fermi boundaries by

$$\begin{aligned}
\delta B_+ &= B_+ - B \sim O(1/N), \quad (3.95)\\
\delta B_- &= B_- + B \sim O(1/N). \quad (3.96)
\end{aligned}$$

The low energy excitations with $\Delta N \neq 0, D \neq 0$ have a similar effect. We will calculate these shifts of the Fermi boundaries later. First, let us expand the several terms about the Fermi boundaries for the ground state. We find

[164]

$$\begin{aligned}
\epsilon_\infty(B_+,B_-) &= \epsilon_\infty(B,-B)+\frac{\rho_{GS}(B)\epsilon'(B)}{2}\left[(\delta B_+)^2+(\delta B_-)^2\right] \\
&\quad +O(1/N^3), \qquad (3.97)\\
\epsilon_{imp}(B_+,B_-) &= \epsilon_{imp}(B,-B)+O(1/N^2), \qquad (3.98)\\
\epsilon_1(B_+,B_-) &= \epsilon_1(B,-B)+O(1/N), \qquad (3.99)
\end{aligned}$$

where we used that $\rho_\infty(\lambda|B,-B)=\rho_{GS}(\lambda)$ and defined the dressed energy $\epsilon(\lambda)$ by the integral equation

$$\left(1-\frac{\hat{K}}{2\pi}\right)\cdot\epsilon(\lambda)=\epsilon_0(\lambda). \qquad (3.100)$$

The dressed energy has the property that $\epsilon(\pm B)=0$. Collecting all the terms, we obtain

$$\begin{aligned}
E &= E_{GS}+\epsilon_{imp}(B,-B)+\frac{\epsilon_1(B,-B)}{12N} \\
&\quad +\frac{N\epsilon'(B)}{2\rho_{GS}(B)}\left\{[\rho_{GS}(B)\delta B_+]^2+[\rho_{GS}(B)\delta B_-]^2\right\}+O\left(\frac{1}{N^2}\right) \qquad (3.101)
\end{aligned}$$

Consider the second term on the rhs of Eq. (3.101), which is of order 1. We denote

$$\rho_{imp}(\lambda)\equiv\rho_{imp}(\lambda|B,-B). \qquad (3.102)$$

It follows from Eq. (3.81) that

$$\left(1-\frac{\hat{K}}{2\pi}\right)\cdot\rho_{imp}(\lambda)=-\frac{K(\lambda-\lambda_h)}{2\pi}. \qquad (3.103)$$

Defining the resolvent operator $\hat{L}$ (the inverse of the kernel of the dressing

equations) formally by

$$\left(1+\hat{L}\right)\cdot\left(1-\frac{\hat{K}}{2\pi}\right)(\lambda,\mu)=1, \tag{3.104}$$

$$L(\lambda|\mu)-\frac{K(\lambda-\mu)}{2\pi}-\frac{1}{2\pi}\int_{-B}^{+B}d\nu\,L\left(\lambda|\nu\right)K(\nu-\mu)=0, \tag{3.105}$$

it is easy to verify that

$$\rho_{imp}\left(\lambda\right)=-L(\lambda|\lambda_h). \tag{3.106}$$

Substituting this result into Eq. (3.93), we obtain

$$\epsilon_{imp}(B,-B)=-\epsilon\left(\lambda_h\right). \tag{3.107}$$

This shows that the term of $O(1)$ in the energy (*c.f.* Eq.(3.29)) is the dressed energy of the deep hole.

Now we turn to the terms of order $1/N$ in the energy in Eq. (3.101). Using Eqs. (3.100), (3.94) and (3.82), we can show that

$$\begin{aligned}\epsilon_1(B,-B) &= \frac{1}{\rho_{GS}(B)}\left\{-\epsilon_0'(B)-\frac{1}{2\pi}\int_{-B}^{+B}d\mu\,\epsilon'\left(\mu\right)K(\mu-B)\right\}\\ &= -\frac{\epsilon'(B)}{\rho_{GS}(B)}.\end{aligned} \tag{3.108}$$

But it can also be shown that the renormalized velocity is given by [164]

$$v=\frac{\epsilon'(B)}{2\pi\rho_{GS}(B)}. \tag{3.109}$$

Therefore, we conclude from Eq. (3.101) that

$$E=E_{GS}-\epsilon\left(\lambda_h\right)-\frac{\pi v}{6N}+\frac{\pi v}{N}\left\{\left[N\rho_{GS}(B)\delta B_+\right]^2+\left[N\rho_{GS}(B)\delta B_-\right]^2\right\}. \tag{3.110}$$

The third term on the rhs of Eq. (3.110) is the familiar finite size correction to the ground state energy of a conformal field theory with central charge $c = 1$ [199]. The difference between the energy of an excited state with a deep hole and the ground state energy without the hole (in a finite system) is

$$\Delta E = -\epsilon\left(\lambda_h\right) + \frac{\pi v}{N}\left\{\left[N\rho_{GS}(B)\delta B_+\right]^2 + \left[N\rho_{GS}(B)\delta B_-\right]^2\right\}. \tag{3.111}$$

Now all we have to do is to evaluate the Fermi boundary shifts $\delta B_\pm \sim O(1/N)$ due to the creation of a deep hole, as well as additional low-energy charge and current excitations. First, we note that the difference $\delta B_+ - \delta B_-$ is related to an expansion of the Fermi sea and must be related to a change in the total density. Using Eq. (3.68), we can write the particle density in the excited state as

$$\nu(B_+, B_-) \equiv \frac{M}{N} = \frac{I_+ - I_-}{N} = \int_{B_-}^{B_+} d\lambda\, \rho\left(\lambda\right). \tag{3.112}$$

We then expand $\nu(B_+, B_-)$ to $O(1/N)$

$$\begin{aligned}
\nu(B_+, B_-) &= \int_{B_-}^{B_+} d\lambda \left[\rho_\infty(\lambda|B_+, B_-) + \frac{1}{N}\rho_{imp}(\lambda|B_+, B_-)\right] \\
&= \nu_0 + \frac{n_{imp}}{N} + \delta B_+ \left.\frac{\partial \nu(B_+, B_-)}{\partial B_+}\right|_0 \\
&\quad + \delta B_- \left.\frac{\partial \nu(B_+, B_-)}{\partial B_-}\right|_0 + O\left(\frac{1}{N^2}\right),
\end{aligned} \tag{3.113}$$

where $\nu_0 = 1/2 + \sigma$ is the particle density in the ground state for fixed magnetization, n_{imp} is defined by

$$n_{imp} \equiv \int_{-B}^{+B} d\lambda\, \rho_{imp}(\lambda), \tag{3.114}$$

and the lower index 0 in Eq. (3.113) stands for setting $B_+ = -B_- = B$ and

$\rho(\lambda) = \rho_{GS}(\lambda)$. We have

$$\left.\frac{\partial \nu(B_+, B_-)}{\partial B_+}\right|_0 = -\left.\frac{\partial \nu(B_+, B_-)}{\partial B_-}\right|_0 = \rho_{GS}(B) + \int_{-B}^{+B} d\lambda \frac{\partial \rho_{GS}(\lambda)}{\partial B}. \quad (3.115)$$

Using Eq. (3.87), we can show that

$$\frac{\partial \rho_{GS}(\lambda)}{\partial B} = \rho_{GS}(B) L(\lambda|B). \quad (3.116)$$

Therefore, we find

$$\nu(B_+, B_-) = \nu_0 + \frac{n_{imp}}{N} + (\delta B_+ - \delta B_-)\, \rho_{GS}(B) Z(B) + O\left(\frac{1}{N^2}\right), \quad (3.117)$$

where $Z(\lambda)$ is the dressed charge, defined by the integral equation

$$\left(1 - \frac{\hat{K}}{2\pi}\right) \cdot Z(\lambda) = 1. \quad (3.118)$$

The value of $Z(\lambda)$ at the Fermi boundary is related to the Luttinger parameter by $K = Z^2(B)$. Therefore, the number of particles added to the state with a deep hole is related to the phase shifts by

$$\Delta N = N\left[\nu(B_+, B_-) - \nu_0\right] = n_{imp} + N\left(\delta B_+ - \delta B_-\right) \rho_{GS}(B) Z(B), \quad (3.119)$$

which implies

$$\delta B_+ - \delta B_- = \frac{\Delta N - n_{imp}}{N \rho_{GS}(B) Z(B)}. \quad (3.120)$$

We also need an equation for the sum $\delta B_+ + \delta B_-$. We note that this is only finite if the Fermi boundaries are not symmetric about zero, which means that the state carries a finite current. Eq. (3.69) can be written in

the form

$$\begin{aligned} 2D &= I_+ + I_- = N\sum_{i<I_-} -N\sum_{i>I_+} \\ &= N\int_{-\infty}^{B_-} d\lambda\,\rho\,(\lambda) - N\int_{B_+}^{+\infty} d\lambda\,\rho\,(\lambda)\,. \end{aligned} \tag{3.121}$$

We define

$$\delta(B_+, B_-) = \frac{D}{N} = \frac{1}{2}\int_{-\infty}^{B_-} d\lambda\,\rho\,(\lambda) - \frac{1}{2}\int_{B_+}^{+\infty} d\lambda\,\rho\,(\lambda)\,. \tag{3.122}$$

Using Eq. (3.79), we get

$$\delta(B_+, B_-) = \frac{d_{imp}}{N} + \delta B_+ \left.\frac{\partial\delta(B_+, B_-)}{\partial B_+}\right|_0 + \delta B_- \left.\frac{\partial\delta(B_+, B_-)}{\partial B_-}\right|_0 + O\left(\frac{1}{N^2}\right), \tag{3.123}$$

where we used that $\delta_0(B, -B) = 0$ and defined

$$d_{imp} = \frac{1}{2}\int_{-\infty}^{-B} d\lambda\,\rho_{imp}\,(\lambda) - \frac{1}{2}\int_{B}^{+\infty} d\lambda\,\rho_{imp}\,(\lambda)\,. \tag{3.124}$$

It is possible to show that

$$\left.\frac{\partial\delta(B_+, B_-)}{\partial B_+}\right|_0 = \left.\frac{\partial\delta(B_+, B_-)}{\partial B_-}\right|_0 = \rho_{GS}\,(B)\,\xi\,(B)\,, \tag{3.125}$$

where the function $\xi\,(\lambda)$ is defined by

$$\xi\,(\lambda) = \frac{1}{2}\left[1 - \int_{B}^{\infty} d\mu\,L\,(\lambda|\mu) + \int_{-\infty}^{-B} d\mu\,L\,(\lambda|\mu)\right]. \tag{3.126}$$

One can also verify that the value of $\xi(\lambda)$ at the Fermi boundary satisfies

$$2Z(B)\xi(B) = 1. \tag{3.127}$$

Then, from Eq. (3.123), we obtain

$$\frac{D}{N} = \frac{d_{imp}}{N} + \left(\delta B_+ + \delta B_-\right) \rho_{GS}\left(B\right) \xi\left(B\right), \tag{3.128}$$

which implies

$$\delta B_+ + \delta B_- = \frac{2Z(B)\left(D - d_{imp}\right)}{N\rho_{GS}(B)}. \tag{3.129}$$

Finally, substituting Eqs. (3.120) and (3.129) into Eq. (3.111), we arrive at the finite size spectrum

$$\Delta E = -\epsilon\left(\lambda_h\right) + \frac{2\pi v}{N}\left[\left(\frac{\Delta N - n_{imp}}{2Z(B)}\right)^2 + Z^2(B)\left(D - d_{imp}\right)^2\right]. \tag{3.130}$$

Comparing with Eq. (3.62), we find

$$n_{imp} = \frac{\gamma_R + \gamma_L}{2\pi}, \tag{3.131}$$

$$d_{imp} = \frac{\gamma_R - \gamma_L}{4\pi K}. \tag{3.132}$$

These are the same relations as given in Eq. (3.10).

Finally, we note that the above results can also be written in terms of the shift function $F\left(\lambda|\mu\right)$ [181]. The latter is the solution to the integral equation

$$\left(1 - \frac{\hat{K}}{2\pi}\right) \cdot F\left(\lambda|\mu\right) = \frac{\theta\left(\lambda - \mu\right)}{2\pi}. \tag{3.133}$$

$F\left(\lambda|\mu\right)$ can be interpreted as a renormalized phase shift between states with rapidities λ and μ. It can be shown by comparing dressing equations that

$$\rho_{imp}\left(\lambda\right) = \dot{F}(\lambda|\lambda_h), \tag{3.134}$$

where

$$\dot{F}(\lambda|\mu) \equiv \frac{\partial F\left(\lambda|\mu\right)}{\partial \mu}. \tag{3.135}$$

Moreover, we have the relations

$$\xi(\lambda) = \frac{Z(\lambda)}{2} + F(\lambda| - B), \tag{3.136}$$

$$\xi(-\lambda) = \frac{Z(\lambda)}{2} - F(\lambda|B). \tag{3.137}$$

Using Eqs. (3.136) and (3.137), we can prove the following formulas for the phase shifts

$$n_{imp} = 1 - Z(\lambda_h) \tag{3.138}$$

$$= -F(\lambda_h|B) + F(\lambda_h| - B) \tag{3.139}$$

$$= -Z(B)\left[F(B|\lambda_h) - F(-B|\lambda_h)\right]. \tag{3.140}$$

$$2d_{imp} = 1 - 2\xi(\lambda_h) \tag{3.141}$$

$$= -F(\lambda_h|B) - F(\lambda_h| - B) \tag{3.142}$$

$$= -2\xi(B)\left[F(B|\lambda_h) - F(-B|\lambda_h)\right]. \tag{3.143}$$

$$\gamma_{R,L} = \mp 2\pi Z(B) F(\pm B|\lambda_h). \tag{3.144}$$

One interesting result that follows directly from these relations is the formula for the lower edge exponent μ for $q \to 2k_F \neq \pi$ ($h \neq 0$, finite B). This corresponds to having the deep hole approaching the left Fermi point at $-k_F$ while keeping the particle at the right Fermi point k_F. From Eqs. (3.138) and (3.141), we obtain

$$n_{imp}(q = 2k_F) = 1 - \sqrt{K}, \tag{3.145}$$

$$d_{imp}(q = 2k_F) = \frac{1}{2\sqrt{K}} - \frac{1}{2}. \tag{3.146}$$

Substituting into Eq. (3.12), we find

$$\mu(2k_F) = 2\sqrt{K}(1-\sqrt{K}) < 1-K, \tag{3.147}$$

for $1/2 < K < 1$. This shows that the exponent of the singularity at the true lower threhold of the two-particle continuum for $q \to 2k_F$ is not given by the Luttinger liquid result derived by Luther and Peschel [200], which predicts $\mu = 1-K$. The Luttinger liquid result should be valid only for energies above the approximate threshold obtained within the linear dispersion approximation (see Fig. 1.4). Therefore, we expect a crossover between two power laws with different exponents as the frequency is increased above the lower threshold $\omega_L(q \approx 2k_F)$ [201].

3.6.3 Upper edge singularity as an exciton problem

Here we discuss the analogy between the upper edge singularity at zero field and the exciton problem. Before we do the actual calculation, let us give a simple argument for why the exponent of the singularity should jump from $-1/2$ (a square root divergence) to $+1/2$ (a square-root cusp) for an arbitrarily weak interaction. The argument is based on the phase shift of the relative wave function of the two high-energy particles, d_1 and d_2. As we argued briefly in section 3.3, the behavior of the upper threshold at zero field can be reduced to a two-particle problem because particle-hole symmetry implies that the operator $d_2^\dagger d_1$ which creates the symmetric particle-hole pair is invariant under the unitary transformation of Eq. (3.5). Furthermore, the transformed d fields are decoupled from the Fermi surface modes, up to irrelevant operators. Therefore, we could study this problem using the Hamiltonian in first quantization

$$H = \frac{\hat{P}_1^2}{2M} - u\hat{P}_1 + \frac{\hat{P}_2^2}{2M} + u\hat{P}_2 + V(\hat{X}_1 - \hat{X}_2), \tag{3.148}$$

where $\hat{P}_1$ and $\hat{P}_2$ are the momentum operators for the particle and hole, respectively, $M = M(q) < 0$ and $u = u(q) > 0$ are the effective mass and velocity obtained by expanding the cosine dispersion about $\pi/2 \pm q/2$, and V is a short-range interaction potential which is a function of the relative coordinate $\hat{X}_1 - \hat{X}_2$. The canonical commutation relation is $[\hat{X}_j, \hat{P}_l] = i\delta_{jl}$ for $j, l = 1, 2$. The two-body wave function for this Hamiltonian can be factored in the form

$$\Psi(X_1, X_2) = e^{iP(X_1+X_2)/2}\Phi(X_1 - X_2), \tag{3.149}$$

where P is the eigenvalue for the free center-of-mass momentum and the relative wave function $\Phi(x)$ is a solution to the Schrödinger equation

$$\left[-\frac{1}{M}\frac{\partial^2}{\partial x^2} - 2iu\partial_x + V(x)\right]\Phi(x) = E\Phi(x). \tag{3.150}$$

In general, at distances much larger than the scattering length (denoted by a) of $V(x)$, $\Phi(x)$ is written in the form

$$\Phi_k(x \gg a) \sim e^{-ikx} - e^{i2\theta(k)}e^{ikx}, \tag{3.151}$$

where $k > 0$ is the asymptotic momentum and $\theta(k)$ is the phase shift due to scattering at $x = 0$. Take, for instance, the contact interaction

$$V(x) = g\delta(x). \tag{3.152}$$

The eigenfunctions of Eq. (3.150) can be classified as even or odd under the parity transformation $x \to -x$. The odd functions vanish at the origin and do not feel the scattering potential. On the other hand, it is easy to show that the scattering phase shift for the even sector is given by

$$e^{i2\theta_e(k)} = \frac{gM + 2ik}{gM - 2ik}. \tag{3.153}$$

Therefore, in the limit of zero interaction between particle and hole, $g \to 0$, the phase shift is $\theta_e(k) \to \pi/2$. However, for any finite values of g, the phase shift assumes a different value in the limit $k \to 0$:

$$\theta_e(ka \to 0) = 0, \quad \text{for } gM > 0, \tag{3.154}$$

$$\theta_e(ka \to 0) = \pi, \quad \text{for } gM < 0, \tag{3.155}$$

where $a = -2/|gM|$ is the scattering length. The case $gM < 0$ corresponds to an effective attractive potential, for which a bound state exists.

This result shows that the phase shift for scattering in the even channel changes discontinuously in the low-energy limit when we turn on the interaction between particle and hole. We should expect that this will have a strong effect on the correlation function. In some sense, this is an extreme manifestation of the orthogonality catastrophe. In the same way that the phase shift between the deep hole and the particle at the Fermi surface determines the singularity of $S^{zz}(q, \omega)$ at the lower threshold of the two-particle continuum, the phase shift between the high-energy particle and hole controls the singularity at the upper threshold. Therefore, a discontinuity in the phase shift for low-energy scattering implies a discontinuity in the exponent.

A discontinuity in the singularity exponent due to the interaction between the particles produced in the transition ("final state interactions") is familiar in the study of excitons in semiconductors. In this context, it is known that, in 1D, the formation of a bound state below the conduction band cancels the divergence of the joint density of states and leads to a convergent absorption edge [185]. This can be easily understood in terms of Hopfield's rule of thumb [202, 203], which states that the removal of an electron from the Fermi sea to form the bound state should change the exponent of the singularity by exactly 1 (in this case, from -1/2 to +1/2). In the following, we explore this analogy more formally by treating the direct interaction between the d particles in our effective model (3.4) within the random phase approximation

(RPA), following Mahan [184].

We start from the noninteracting case, $V_{12} = 0$. The exact result for $S^{zz}(q,\omega)$ for the XY model at zero field is [167]

$$S^{zz}(q,\omega) = \frac{2\theta(\omega - \omega_L(q)\theta(\omega_U(q) - \omega))}{\sqrt{\left(2J\sin\frac{q}{2}\right)^2 - \omega^2}}, \tag{3.156}$$

where $\omega_L(q) = J\sin(q)$ and $\omega_U(q) = 2J\sin(q/2)$. This can be derived similarly to the result for small q and finite field in Eq. (2.19). Note, however, the extra factor of two, which is due to particle-hole symmetry (two particle-hole pairs with the same frequency for any given q). The square root divergence at the upper threshold can be reproduced by the X-ray edge Hamiltonian of Eq. (3.4). The relevant correlation function in this case, $\langle d_1^\dagger d_2(x,t) d_2^\dagger d_1(0,0)\rangle$, only involves the d particles defined around $k_1 = \pi/2 - q/2$ and $k_2 = \pi/2 + q/2$. As a result, the effective Hamiltonian to investigate the singularity near $\omega_U(q)$ is simply

$$H_0 = \sum_k \left[\epsilon_1(k) d_{1k}^\dagger d_{1k} + \epsilon_2(k) d_{2k}^\dagger d_{2k}\right], \tag{3.157}$$

where

$$\epsilon_{1,2}(k) = \mp\varepsilon + uk \mp \frac{k^2}{2M}, \tag{3.158}$$

with $\varepsilon = J\sin(q/2)$, $u = J\cos(q)$ and $M = -[J\sin(q/2)]^{-1}$.

Since we are going to do perturbation theory in the interaction, it is convenient to calculate $S^{zz}(q,\omega)$ by taking the imaginary part of the retarded density-density correlation function, according to Eq. (2.4). In the noninteracting case, this is just the polarization bubble

$$\chi_0^{ret}(q,\omega) = \int_{-\pi}^{+\pi} \frac{dp}{2\pi} \frac{\theta(-\epsilon_p)\,\theta(\epsilon_{p+q})}{\omega - \epsilon_{p+q} + \epsilon_p + i\eta}. \tag{3.159}$$

Calculating the integral with the exact cosine dispersion leads to the result

in Eq. (3.156). But if we are only interested in the behavior near the upper threshold, $\omega \approx \omega_U(q)$, we can take $p = k_1 + k$ and $p + q = k_2 + k$, with $k \ll q$, so that $\epsilon_p \approx \epsilon_1(k)$ and $\epsilon_{p+q} \approx \epsilon_2(k)$. It follows that

$$\chi_0^{ret}(q, \omega \approx \omega_U(q)) \approx \int_{-\Lambda}^{+\Lambda} \frac{dk}{2\pi} \frac{1}{\omega - \omega_U(q) + k^2/|M| + i\eta}. \tag{3.160}$$

where $\omega_U(q) = 2\varepsilon$ and $\Lambda \ll q$ is the subband cutoff. For $\omega < \omega_U(q)$, we obtain

$$\begin{aligned} \chi_0^{ret}(q, \omega) \approx & \frac{1}{4\pi}\sqrt{\frac{|M|}{\omega_U(q) - \omega}} \left\{ \log\left[\frac{\Lambda - \sqrt{|M|(\omega_U - \omega - i\eta)}}{-\Lambda - \sqrt{|M|(\omega_U - \omega - i\eta)}}\right] \right. \\ & \left. - \log\left[\frac{\Lambda + \sqrt{|M|(\omega_U - \omega - i\eta)}}{-\Lambda + \sqrt{|M|(\omega_U - \omega - i\eta)}}\right] \right\}. \end{aligned} \tag{3.161}$$

The real and imaginary parts for $\omega < \omega_U(q)$ are

$$\chi_0' \approx \frac{1}{2\pi}\sqrt{\frac{|M|}{\omega_U - \omega}} \ln\left|\frac{\Lambda - \sqrt{|M|(\omega_U - \omega)}}{\Lambda + \sqrt{|M|(\omega_U - \omega)}}\right| \approx -\frac{|M|}{\pi\Lambda}, \tag{3.162}$$

$$\chi_0'' \approx -\frac{1}{2}\sqrt{\frac{|M|}{\omega_U - \omega}}. \tag{3.163}$$

For $\omega > \omega_U(q)$, χ_0 is purely real

$$\chi_0^{ret}(q, \omega) = \frac{1}{\pi}\sqrt{\frac{|M|}{\omega - \omega_U}} \arctan\left(\frac{\Lambda}{\sqrt{|M|(\omega - \omega_U)}}\right) \approx \frac{1}{2}\sqrt{\frac{|M|}{\omega - \omega_U}}. \tag{3.164}$$

Note that $\chi_0(q, \omega > \omega_U(q))$ is positive because M is negative.[4] Taking the

[4]In the original exciton problem [184], the effective mass is positive for both valence and conduction bands and $\chi_0 < 0$ below the *lower* threshold of the optical transition. The sign of M is important for the formation of a bound state, see Eq. (3.155).

imaginary part of χ_0, we find that for $\Delta = 0$ ($V_{12} = 0$)

$$S^{zz}(q, \omega \approx \omega_U) = -2\chi_0''(q, \omega) \approx \theta(\omega_U - \omega)\sqrt{\frac{|M|}{\omega_U - \omega}}. \tag{3.165}$$

This gives a square-root divergence at the upper threshold $\omega_U(q)$, in agreement with Eq. (3.156).

Now consider the interacting case $V_{12} \neq 0$. The interaction between the d particles can be written as

$$H_{int} = \frac{V_{12}}{N}\sum_{kk'q} d^\dagger_{1,k+q} d_{1,k} d^\dagger_{2,k'-q} d_{2,k'}. \tag{3.166}$$

This is equivalent to a delta function scattering potential as in Eq. (3.152) with $g = -V_{12}$ (particle-hole attraction for $V_{12} > 0$). We calculate the corrections to the (Matsubara) density-density correlation function $\chi(q, i\omega)$ using perturbation theory in V_{12}. The first order diagram gives

$$\delta\chi^{(1)}(q, i\omega) = -V_{12}\left[\chi_0(q, i\omega)\right]^2. \tag{3.167}$$

Since $\chi_0'' \sim (\omega - \omega_U)^{-1/2}$ diverges at the upper threshold, the diagrams become more and more singular at each order of perturbation theory. The correct approach is to sum up the entire series of ladder diagrams in V_{12} [184]. For a momentum-independent interaction $V_{12}(q) = V_{12} = \text{const}$, the series of ladder diagrams is the same as the RPA, and reduces to a geometric series

$$\chi_{RPA} = \chi_0 - V_{12}\chi_0^2 + V_{12}^2\chi_0^3 + \ldots = \frac{\chi_0}{1 + V_{12}\chi_0}. \tag{3.168}$$

The RPA neglects diagrams with crossed interaction lines. This is known to be a dangerous mistake in the X-ray edge problem, because it leads to spurious bound states. In fact, the RPA approximation for the dynamical structure factor of spinless fermions [204] predicts a sharp peak above the

two-particle continuum, which is inconsistent with our results presented in chapter 2. However, the difference between the X-ray edge problem and the exciton problem is that in the latter there is only a single particle-hole pair, as opposed to a hole and an entire Fermi sea. Technically, the difference is in the factors of occupation numbers that appear in the calculation of the diagrams. In the exciton problem, crossed diagrams are strongly suppressed in comparison with non-crossed ones. Up to Auger processes (high-energy virtual processes in which additional particle-hole pairs are created [184]), the RPA is exact and equivalent to solving the two-body problem.

If we rewrite Eq. (3.168) as

$$\chi_{RPA} = \frac{\chi_0 \left(1 + V_{12}\chi_0' - iV_{12}\chi_0''\right)}{\left(1 + V_{12}\chi_0'\right)^2 + \left(V_{12}\chi_0''\right)^2}, \tag{3.169}$$

we obtain

$$S^{zz}\left(q,\omega\right) = S^{zz}_{reg}\left(q,\omega\right) + S^{zz}_{bs}\left(q,\omega\right) \tag{3.170}$$

where

$$S^{zz}_{reg}\left(q,\omega\right) = \frac{-2\chi_0''}{\left(1 + V_{12}\chi_0'\right)^2 + \left(V_{12}\chi_0''\right)^2}\,\theta\left(\omega_U - \omega\right) \tag{3.171}$$

is the regular part of $S^{zz}\left(q,\omega\right)$ below the upper threshold. Now, instead of a divergence we find that as $\omega \to \omega_U(q)$

$$S^{zz}_{reg}\left(q,\omega\right) \to \frac{-2}{V_{12}^2\chi_0''} \sim \sqrt{\omega_U - \omega}. \tag{3.172}$$

Therefore, $S^{zz}\left(q,\omega\right)$ vanishes at the upper threshold, which must be taken as the renormalized one, $\omega_U(q) = 2v\sin(q/2)$, calculated from the Bethe ansatz. The exponent 1/2 is independent of V_{12} (which is actually not fixed by any Bethe ansatz calculation we have done). This is consistent with the phase shift $\theta_e\left(k \to 0\right)$ in Eqs. (3.154) and (3.155) being independent of the strength of the interaction potential. The square root cusp at the upper threshold should be generic for any particle-hole symmetric model with a

short-range interaction, such that $\theta(k) \sim -ka \to 0$ as $k \to 0$. In contrast, the exact $S^{zz}(q,\omega)$ for the Haldane-Shastry model (which has a long-range interaction) exhibits a step function at the upper edge [205]. The square root cusp behavior of Eq. (3.172) appears in the frequency window

$$|V_{12}\chi_0''| \gg 1 \Leftrightarrow \omega_U - \omega \ll |M|\, V_{12}^2. \tag{3.173}$$

For $|M|\, V_{12}^2 \ll \omega_U - \omega \ll J$, the behavior of $S^{zz}(q,\omega)$ crosses over to the noninteracting result. This means that, for small V_{12} (small Δ), there is a rounded peak just below the upper threshold of the two-spinon continuum, at frequency $\omega - \omega_U \sim -|M|\, V_{12}^2$.

The bound state contribution $S_{bs}^{zz}(q,\omega)$ in Eq. (3.170) is present when $\chi_0'' \to 0$ and there is a solution to $1 + V_{12}\chi_0' = 0$. This can happen above the upper threshold if $V_{12} < 0$, in which case we find

$$\begin{aligned} S_{bs}^{zz}(q,\omega) &= \frac{2\pi}{V_{12}}\delta\left(1 - |V_{12}|\,\chi_0'\right) \\ &= \frac{8\pi}{\sqrt{|M|}V_{12}^2}\left(\omega - \omega_U\right)^{3/2}\delta\left(\omega - \omega_0\right), \end{aligned} \tag{3.174}$$

where the energy of the bound state is

$$\omega_0 = \omega_U(q) + \frac{|M|\, V_{12}^2}{2}. \tag{3.175}$$

Simplifying Eq. (3.174), we get

$$S_{bs}^{zz}(q,\omega) = 2\sqrt{2}\pi\,|MV_{12}|\;\delta\left(\omega - \omega_0\right). \tag{3.176}$$

The spectral weight of the bound state is of order $|MV_{12}| \sim |V_{12}|/\sin(q/2)$. Since $V_{12} \sim q^2$ for small q, the spectral weight of the bound state vanishes as $q \to 0$. It is interesting to note that the bound state only appears for $V_{12} < 0$ ($\Delta < 0$), which naively corresponds to particle-hole *repulsion*. However, recall that both particle and hole have a negative effective mass. For

this reason, the condition for the formation of a bound state is reversed in comparison with the original exciton problem [184].

An important question is whether the square root cusp and the bound state above the upper threshold survive when we consider higher-order decay processes. We believe that the answer is yes, but just because the XXZ model is integrable. It was argued in Ref. [187] that the high-frequency tail of $S^{zz}(q,\omega)$ for the Heisenberg chain at zero field, which is dominated by four-spinon excitations, does not remove the power-law singularity at the upper threshold of the two-spinon continuum. The line shape that results from adding all $2n$-spinon contributions to $S^{zz}(q,\omega)$ is such that, near the upper threshold, the slope of $S^{zz}(q,\omega)$ diverges as $\omega \to \omega_U(q)$ from below but not for $\omega \to \omega_U(q)$ from above. As for the fate of the bound state for $\Delta < 0$, it is reasonable to expect that it corresponds to an exact bound state (most likely a 2-string [206]) in the Bethe ansatz solution. If that is the case, the peak in $S^{zz}_{bs}(q,\omega)$ has zero width. This is only possible in an integrable model because in a generic model a coherent mode embedded in a continuum (the high-frequency tail) is expected to decay and the peak should broaden like a Lorentzian [207]. Likewise, in a generic model, shakeup processes would smooth out the power-law singularity at the upper threshold [203, 208]. The decay of the bound state for $\Delta < 0$ should have consequences for the long-time behavior of the self-correlation function, but we have not been able to decide this question by analyzing the tDMRG results. We hope to investigate this problem further in the near future.

3.6.4 High energy terms in the self-correlation function

In section 3.4, we claimed that the long time behavior of the spin-spin correlation function

$$G(x,t) = \left\langle S^z_{j+x}(t)\, S^z_j(0) \right\rangle \tag{3.177}$$

is dominated by excitations that involve states near the bottom and top of the fermionic band. Let us now make this point clear and derive the exponents of the high-energy terms in the self-correlation function $G(x=0,t) \equiv G(t)$ in Eq. (3.15). First, we note that the Luttinger liquid result for $G(x,t)$, which only includes the contributions from low-energy excitations, is, at zero field, [200]

$$G(x,t) = -\frac{K}{4\pi^2}\left[\frac{1}{(x-vt)^2} + \frac{1}{(x+vt)^2}\right] + \frac{(-1)^x A_z}{(x^2-v^2t^2)^K}. \tag{3.178}$$

The amplitude of the staggered part is cutoff dependent in the bosonization approach, but its exact value can be extracted from the Bethe ansatz [189]

$$\begin{aligned} A_z &= \frac{2}{\pi^2}\left[\frac{\Gamma\left(\frac{1}{4K-2}\right)}{2\sqrt{\pi}\Gamma\left(\frac{1}{2-1/K}\right)}\right]^{2K} e^{C_z}, \\ C_z &= \int_0^\infty \frac{ds}{s}\left[\frac{\sinh\left(\frac{s}{K-1}\right)}{\sinh\left(\frac{s}{2K}\right)\cosh\left(s-\frac{s}{2K}\right)} - 2(1-K)\,e^{-2s}\right]. \end{aligned} \tag{3.179}$$

For $0 < \Delta < 1$ ($1 > K > 1/2$), this result predicts that $G(x,t)$ decays as $G(t \gg x/v) \sim t^{-2K}$ for long times. Since the Luttinger model is Lorentz invariant, the exponent for the large t decay is the same as the one for the large x decay.

In the noninteracting case $\Delta = 0$, $G(x,t)$ reduces to the polarization bubble and can be written as the product of particle and hole propagators. For zero field, particle-hole symmetry implies that these two propagators are the same, therefore

$$G(x,t) = \left[G_F(x,t)\right]^2, \tag{3.180}$$

where

$$G_F(x,t) = \left\langle c^\dagger_{j+x}(t)c_j(0)\right\rangle = \int_{-\pi/2}^{+\pi/2}\frac{dk}{2\pi}\,e^{-ikx+\epsilon_k t} \tag{3.181}$$

is the single-hole Green's function with dispersion $\epsilon_k = -J\cos k$. The integral

in Eq. (3.181) can be evaluated numerically for arbitrary x and t. For $x = 0$, we have the analytic expression

$$G_F\left(x=0,t\right) = \frac{1}{2}\left[J_0\left(Jt\right) - iH_0\left(Jt\right)\right], \tag{3.182}$$

where J_0 and H_0 are the zeroth-order Bessel and Struve functions, respectively. The asymptotic form for long times, $Jt \gg 1$, is [209]

$$G_F\left(x=0,t\right) \sim \frac{e^{-iJt}}{\sqrt{2\pi iJt}} + \frac{1}{i\pi Jt}. \tag{3.183}$$

Therefore, the large t asymptotic behavior of the self-correlation function for $\Delta = 0$ is

$$G(x=0,t) \sim \frac{ie^{-i2Jt}}{2\pi Jt} + \frac{\sqrt{2}e^{-iJt-i\pi/4}}{\left(\pi Jt\right)^{3/2}} - \frac{1}{\left(\pi Jt\right)^2}. \tag{3.184}$$

The Luttinger liquid result of Eq. (3.178) corresponds to the last term in Eq. (3.184) ($K = 1$, $A_z = 1/2\pi^2$ for $\Delta = 0$). However, we find that the leading term for the long time behavior (the one that decays with the smallest exponent) is the first term in Eq. (3.184). This terms decays as $1/t$ and oscillates with frequency $2J$. The fact that it oscillates in time tells us that it must come from a high-energy excitation. In fact, besides the singular contribution from the Fermi points $\pm\pi/2$, the integral in Eq. (3.181) also has a saddle point contribution determined by the condition

$$\frac{d}{dk}\left[kx - \epsilon\left(k\right)t\right]\Big|_{k_s} = 0 \Rightarrow \sin k_s = \frac{x}{Jt}. \tag{3.185}$$

Assuming $x > 0$, $t > 0$, we see that the saddle point contribution at momentum k_s exists only for $x < Jt$, inside the "light cone". Therefore, *the Luttinger liquid result of Eq. (3.178) correctly describes the large distance behavior of the correlation function, but misses the saddle point contribution in the long time behavior.* In the limit $x/Jt \to 0$, or in particular for the self-correlation function, the saddle point moves to the bottom of the band,

$k = 0$, in the case of a hole, or to the top of the band, $k = \pi$, in the case of a particle.

We can reproduce the first and second terms in Eq. (3.184) by expanding $\epsilon(k)$ not only about the Fermi points, but also near the bottom of the band,

$$\epsilon(k \approx 0) \approx -J + \frac{k^2}{2m}, \tag{3.186}$$

with $m = J^{-1}$. For the hole Green's function, we get

$$\begin{aligned} G_F(x,t) &\approx e^{-i\pi x/2} \int_{-\Lambda}^{0} \frac{dk'}{2\pi}\, e^{-ik'(x-vt)} + e^{i\pi x/2} \int_{0}^{+\Lambda} \frac{dk'}{2\pi}\, e^{-ik'(x+vt)} \\ &\quad + e^{-iJt} \int_{-\Lambda}^{+\Lambda} \frac{dk'}{2\pi}\, e^{-ik'x + ik'^2 t/2m} \\ &\approx \frac{ie^{-i\pi x/2}}{2\pi\,(x-vt)} - \frac{ie^{i\pi x/2}}{2\pi\,(x+vt)} + \sqrt{\frac{m}{2\pi t}} e^{-iJt - i\pi/4 - \frac{imx^2}{2t}}. \end{aligned} \tag{3.187}$$

For fixed x and $t \gg x, mx^2$, $G_F\,(x,t)$ behaves like the self-correlation function $G_F\,(x=0,t)$ in Eq. (3.183). The result in Eq. (3.184) is obtained by taking the square of $G_F(x,t)$ in Eq. (3.187). We then have an interpretation for the high-energy terms in Eq. (3.184). The first term comes from taking the hole at $k = 0$ and the particle at $k = \pi$, which is an excitation with momentum π and energy $2J$. This term decays as $1/t$ because both hole and particle have parabolic dispersion and their individual propagators decay as $1/\sqrt{t}$. The second term in Eq. (3.184) stems from the crossed term between low-energy and high-energy terms in $G_F\,(x=0,t)$. It corresponds to either a hole at the bottom of the band and a particle at the Fermi surface, or a hole at the Fermi surface and a particle at the top of the band. In both cases, the excitation has momentum $\pi/2$ and energy J.

This procedure of expanding the dispersion about different values of momentum, including high-energy modes, is the same as that we used to study the edge singularities of $S^{zz}\,(q,\omega)$. In fact, since $S^{zz}(q,\omega)$ is by definition the Fourier transform of $G(x,t)$, we can derive the exponents of the long time

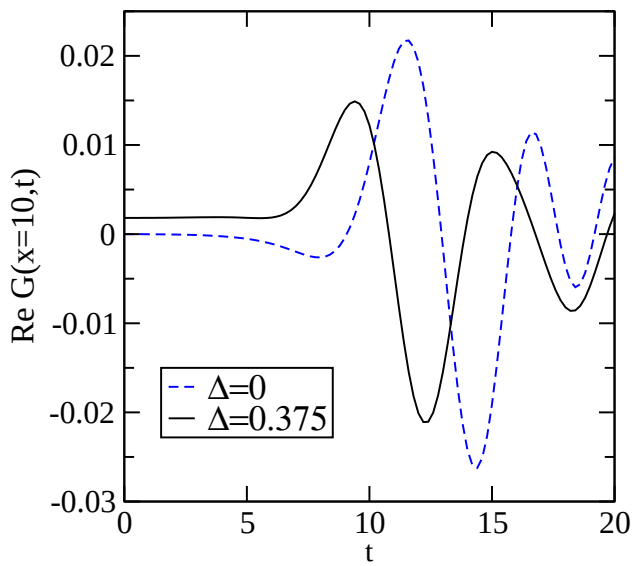

Figure 3.2: Real part of the time-dependent spin correlation function $G(x,t)$ calculated by tDMRG for fixed $x = 10$ as a function of time (t in units of J^{-1}). Inside the light cone ($vt > x$), $G(x,t)$ oscillates in time and is *not* described by the Luttinger model.

decay of $G(x,t)$ in the interacting case, $\Delta \neq 0$, by employing the X-ray edge Hamiltonian of Eq. (3.4). We just learned from the exact solution for the XY model that the dominant singular contributions come from a hole with momentum $k_1 \approx 0$ and a particle with $k_2 \approx \pi$. We assume that this is still true in the interacting case, as long as we use the renormalized parameters for the dispersion of the high-energy particles. This assumption is supported by the numerical tDMRG results, which show that, for $\Delta \neq 0$, $G(x,t)$ oscillates for long times with frequencies that match the ones calculated from the Bethe ansatz. Moreover, as Figs. 3.2 and 3.3 illustrate, there is a clear change in the behavior of the correlation function as we cross the light cone $x = vt$, where v is the renormalized velocity. The correlation function is well described by the Luttinger liquid result (a power law which oscillates in space but not in time) for $x > vt$, but not for $x < vt$.

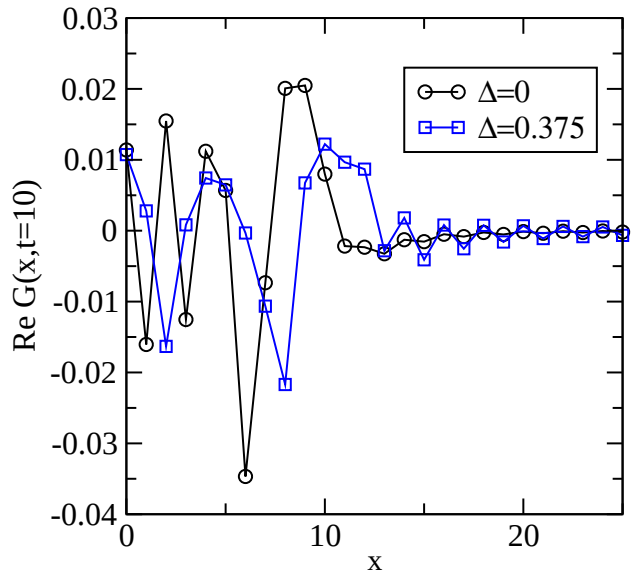

Figure 3.3: $G(x,t)$ for fixed $Jt = 10$ as a function of distance. The large distance behavior is well described by the Luttinger liquid result in Eq. (3.178).

For $h = 0$, $k_1 = 0$ and $k_2 = \pi$, the effective Hamiltonian density of Eq. (3.4) simplifies to

$$\begin{aligned}\mathcal{H} &= \frac{v}{2}\left[(\partial_x\theta)^2 + (\partial_x\phi)^2\right] - d_1^\dagger\left(W + \frac{\partial_x^2}{2m}\right)d_1 + d_2^\dagger\left(W + \frac{\partial_x^2}{2m}\right)d_2 \\ &\quad + V_{12}d_1^\dagger d_1 d_2^\dagger d_2 + \frac{\gamma v}{\sqrt{\pi K}}\partial_x\phi\left(d_1^\dagger d_1 + d_2^\dagger d_2\right), \end{aligned} \tag{3.188}$$

where $W = -\epsilon\,(k=0) = v$ is half the bandwidth of the spinon band, $m = v^{-1}$ is the absolute value of the renormalized mass at the bottom of the band, and $\gamma = \pi(1-K)$ is the coupling constant at zero field (see Eq. (3.11)). The unitary transformation that decouples the density of Luttinger bosons $\partial_x\phi$ from the "heavy" d particles is

$$d_{1,2}(x) = \bar{d}_{1,2}(x)e^{-i\gamma\bar{\theta}(x)/\sqrt{\pi K}}, \tag{3.189}$$

$$\partial_x \phi \;=\; \partial_x \bar{\phi} - \frac{\gamma}{\sqrt{\pi K}} \left(\bar{d}_1^\dagger \bar{d}_1 + \bar{d}_2^\dagger \bar{d}_2 \right). \tag{3.190}$$

After we perform the unitary transformation, the low energy modes represented by the bosonic field $\bar{\phi}$ are free. The $\bar{d}_1$ and $\bar{d}_2$ fields only interact with each other when both high energy particle and hole are present. The self-correlation function

$$G(t) \sim \left\langle \Psi^\dagger \Psi(x=0,t) \Psi^\dagger \Psi(x=0,0) \right\rangle \tag{3.191}$$

is calculated by taking all possible combinations of particle-hole excitations in the mode expansion

$$\Psi(x) \sim e^{i\pi x/2} \psi_R(x) + e^{-i\pi x/2} \psi_L(x) + d_1(x) + e^{i\pi x} d_2(x). \tag{3.192}$$

The excitation with momentum π that creates a hole at the bottom of the band and a particle at the top (equivalent to the first term in Eq. (3.184)) gives the contribution

$$G_1(t) \equiv \left\langle d_1^\dagger d_2(t) d_2^\dagger d_1(0) \right\rangle = \left\langle \bar{d}_1^\dagger \bar{d}_2(t) \bar{d}_2^\dagger \bar{d}_1(0) \right\rangle. \tag{3.193}$$

Note the cancelation of the phase factors of the unitary transformation, which is a consequence of particle-hole symmetry. For $\Delta = 0$, $G_1(t)$ factors as in Eq. (3.180)

$$G_1(t) = \left\langle \bar{d}_1^\dagger(t) \bar{d}_1(0) \right\rangle \left\langle \bar{d}_2(t) \bar{d}_2^\dagger(0) \right\rangle \sim \frac{e^{-i2Wt}}{t}. \qquad (\Delta = 0) \tag{3.194}$$

This contribution involves particle-hole excitations near the upper threshold of the two-particle continuum at $q = \pi$. We showed in section 3.6.3 that for $\Delta \neq 0$ the exponent of the upper edge singularity, $S^{zz}(q,\omega) \sim [\omega_U(q) - \omega]^\nu$, jumps from $\nu = -1/2$ to $\nu = 1/2$ due to the effect of final state interactions in the exciton problem. This same effect leads to a discontinuity in the

exponent for real time decay. The contribution $G_1(t)$ can be written as

$$\begin{aligned} G_1(x=0,t) &\sim \int dq \int d\omega\, e^{-i\omega t} S^{zz}(q \approx \pi, \omega \approx \omega_U(q)) \\ &\sim \int d\omega\, e^{-i\omega t} \int_{-\Lambda}^{+\Lambda} d\bar{q} \left(2W - \omega - \bar{q}^2/m\right)^{\nu} \\ &\sim \int d\omega\, e^{-i\omega t} \left(2W - \omega\right)^{\frac{1}{2}+\nu} \\ &\sim \frac{e^{-i2Wt}}{t^{\eta_2}}, \end{aligned} \tag{3.195}$$

where $\eta_2 = 3/2 + \nu$. For $\Delta = 0$, $\nu = -1/2$, which implies $\eta_2 = 1$, as in Eq. (3.184). However, for $\Delta \neq 0$, $\nu = 1/2$ implies $\eta_2 = 2$. Therefore, we find that the interaction between the d_1 and d_2 particles makes the exponent of the long-time decay jump from 1 to 2 *for arbitrarily small* Δ. Recall that, for $\Delta \ll 1$, the square root cusp only forms very close to the upper threshold, for $|\omega - \omega_U| \ll mV_{12}^2 \sim J\Delta^2$. This implies that the $1/t^2$ decay of the "exciton" contribution to the self-correlation function is only observed for very large times, $Jt \gg 1/\Delta^2$. For $1 \ll Jt \ll 1/\Delta^2$, $G_1(t)$ still decays as $1/t$. The exponent crosses over to the asymptotic value $\eta_2 = 2$ at $Jt \sim 1/\Delta^2$. This explains why the exponent obtained by fitting finite time tDMRG data for the smallest nonzero value of Δ in Table 3.1 does not agree very well with the prediction $\eta_2 = 2$.

It is instructive to rederive this result using the first quantization approach to the two-body problem discussed in section 3.6.3. It is easy to show that the self-correlation function can be written in the form

$$G_1(t) = \sum_{P,k} \left|\Psi_{Pk}(x=0)\right|^2 e^{-iE(P,k)t}, \tag{3.196}$$

where $\Psi_{Pk}(x)$ is the eigenfunction of the Hamiltonian (3.148) with center-of-mass momentum P and relative momentum k, taken at $x = 0$ (when the two

particles occupy the same position), and $E(P,k)$ is the corresponding energy

$$E(P,k) = 2W - \frac{P^2}{4m} - \frac{k^2}{m}. \tag{3.197}$$

The center-of-mass part of the wave function is just a plane wave. The relative coordinate part is given by $\Phi(x)$, which according to Eq. (3.151) can be written as

$$\Phi_e(x) \sim \sin\left[k|x| + \theta_e(k)\right] \tag{3.198}$$

for the even sector.[5] Then we have

$$\begin{aligned} G_1(t) &\sim e^{-i2Wt} \int_{-\infty}^{+\infty} dP\, e^{iP^2t/4m} \int_0^\infty dk\, \sin^2[\theta_e(k)]\, e^{ik^2t/m}, \\ &\sim \frac{e^{-i2Wt}}{\sqrt{t}} \int_0^\infty dk\, \sin^2[\theta_e(k)]\, e^{ik^2t/m}. \end{aligned} \tag{3.199}$$

In the noninteracting case, $\theta_e(k) = \pi/2$, and we obtain

$$G_1(t) \sim \frac{e^{-i2Wt}}{\sqrt{t}} \int_0^\infty dk\, e^{ik^2t/m} \sim \frac{e^{-i2Wt}}{t}. \qquad (\Delta = 0) \tag{3.200}$$

In the interacting case, the long time behavior is dominated by the value of the phase shift for $k \to 0$. For $\Delta > 0$, $\theta_e(k) \sim -ka$ for $k \ll |a|^{-1}$. For $\Delta < 0$, $\theta_e(k) \sim \pi - ka$. Either way, we find

$$G_1(t) \sim \frac{e^{-i2Wt}}{t}\left[1 - e^{-ima^2/t}\right] \sim \frac{e^{-i2Wt}}{t^2}, \tag{3.201}$$

for $t \gg ma^2 \sim 1/(v\Delta^2)$.

For $\Delta < 0$, we expect an additional contribution to $G_1(t)$ coming from the bound state above the upper threshold of the two-particle continuum. In

[5] The wave functions in the odd sector vanish in the limit $kx \to 0$, regardless of the interaction V_{12}.

the first quantization approach, this is given by

$$G_1(t) = e^{-i(2W+\omega_0)t} \sum_P e^{iP^2 t/4m} \left|\Phi_{bs}(x=0)\right|^2 \sim \frac{e^{-i(2W+\omega_0)t}}{\sqrt{t}}, \tag{3.202}$$

where we assumed that the peak has zero width. This should be the dominant term in the long-time decay for $-1 < \Delta < 0$.

Finally, let us consider what happens to the second high-energy term in Eq. (3.184) when we turn on the interaction Δ. This term corresponds to a deep hole at $k = 0$ and a particle at $k = k_F = \pi/2$. In terms of the fields in the effective Hamiltonian (3.188), this "X-ray edge" contribution comes from

$$\begin{aligned} G_2(t) &\sim \left\langle d_1^\dagger \psi_R(t) \psi_R^\dagger d_1(0) \right\rangle \\ &\sim \left\langle \bar{d}_1^\dagger(t) \bar{d}_1(0) \right\rangle \left\langle e^{-i\sqrt{2\pi K}\bar{\varphi}_R(t)} e^{i\sqrt{2\pi K}\bar{\varphi}_R(0)} \right\rangle \\ &\sim \frac{e^{-iWt}}{\sqrt{t}} \frac{1}{t^K}, \end{aligned}$$

where we used $\gamma = \pi(1-K)$ to simplify the correlation function for the exponentials of bosonic fields. This result shows that the exponent $3/2$ for $\Delta = 0$ in Eq. (3.184) becomes $\eta = K + 1/2$ for $\Delta \neq 0$. Unlike the exponent η_2 in the exciton contribution, the X-ray edge exponent η varies continuously with the interaction strength Δ. Since η_2 jumps from $\eta_2 = 1$ to $\eta_2 = 2$ for $\Delta > 0$, $G_2(t) \sim e^{-iWt}/t^\eta$ becomes the dominant term in the long-time behavior of the self-correlation function for $0 < \Delta \leq 1$.

3.6.5 Double peak structure at finite field

In section 1.6, we mentioned that neutron scattering experiments revealed a double peak structure for the line shape of $S^{zz}(q,\omega)$ for Heisenberg chains at finite field. Müller *et al.* suggested in [210] that a generalization of the Müller ansatz for finite field should contain two divergent power-law singularities.

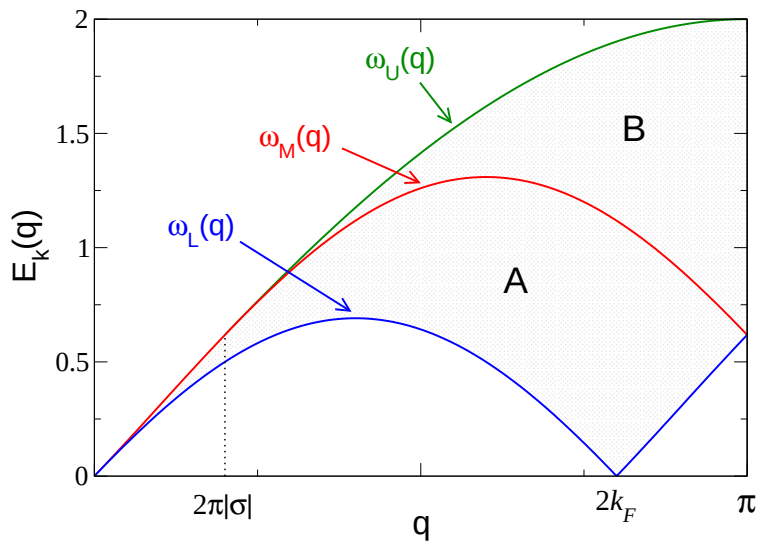

Figure 3.4: Particle-hole continuum for the XY model at finite magnetic field. The magnetization is $\sigma = k_F/\pi - 1/2 = -0.1$. For $q > 2\pi|\sigma|$, besides a lower and upper threshold, there is a "middle threshold" $\omega_M(q)$ defined by a high-energy particle excitation. The density of states doubles when crossing from region A to region B.

Here we wish to discuss how the X-ray edge approach to the DSF supports this picture by predicting an extra edge singularity between the lower and upper thresholds of the two-particle continuum.

Consider the XY model ($\Delta = 0$) at finite magnetic field. This model is equivalent to free fermions on a lattice with Fermi momentum

$$k_F = \frac{\pi}{2} + \pi\sigma, \tag{3.203}$$

where $\sigma = \langle S_j^z \rangle$ is the magnetization per site. In the following we will assume $\sigma < 0$ ($k_F < \pi/2$). The particle-hole continuum for $\sigma = -0.1$ is illustrated in Fig. 3.4.

The range of momentum $0 < q < 2\pi\,|\sigma|$ corresponds to the small q case that we already discussed in chapter 2. In this case, the two-particle

continuum has a lower threshold defined by a deep hole excitation and an upper threshold defined by a high-energy particle excitation. Now we want to focus on the more complicated line shape that develops when $q > 2\pi|\sigma|$. This is the interesting case if we want to understand the crossover to the zero field line shape for fixed q and $\sigma \to 0$. For $2\pi|\sigma| < q < 2k_F$, the lower threshold $\omega_L(q)$ is still given by the energy of the deep hole excitation. However, for $q > 2\pi|\sigma|$ it becomes possible to create the symmetric excitation (the "exciton") with a hole at $\pi/2 - q/2$ and a particle at $\pi/2 + q/2$. This has the maximum energy and defines the upper threshold $\omega_U(q)$ of the continuum. The energy of the high-energy particle excitation is between the energies of the deep hole and the energy of the exciton. Nonetheless, the high-energy particle excitation still plays an important role in the line shape of $S^{zz}(q,\omega)$: It defines a threshold for the doubling of the density of states. For $\omega_M(q) < \omega < \omega_U(q)$, there are two choices of hole momentum k, with $|k| < k_F$ and $|k+q| > k_F$, which yield the same energy. These are given by the two solutions of

$$\epsilon_{k+q} - \epsilon_k = 2\sin(k + q/2)\sin(q/2) = \omega. \tag{3.204}$$

For $\omega_L(q) < \omega < \omega_M(q)$, there is only one choice of k for each ω. Following Müller *et al.* [167], we call this the "middle threshold".[6] The excitations that define the thresholds are represented in Fig. 3.5.

The exact result for $S^{zz}(q,\omega)$ for the XY model in the momentum range $2\pi|\sigma| < q < \pi$ is [167]

$$S^{zz}(q,\omega) = \frac{\theta(\omega_U(q) - \omega)\left[\theta(\omega - \omega_L(q)) + \theta(\omega - \omega_M(q))\right]}{\sqrt{\omega_U^2(q) - \omega^2}}. \tag{3.205}$$

The threshold energies are

$$\omega_L(q) = 2J\sin\frac{q}{2}\cos\left(\frac{q}{2} - \pi\sigma\right), \tag{3.206}$$

[6] Please forgive the oxymoron.

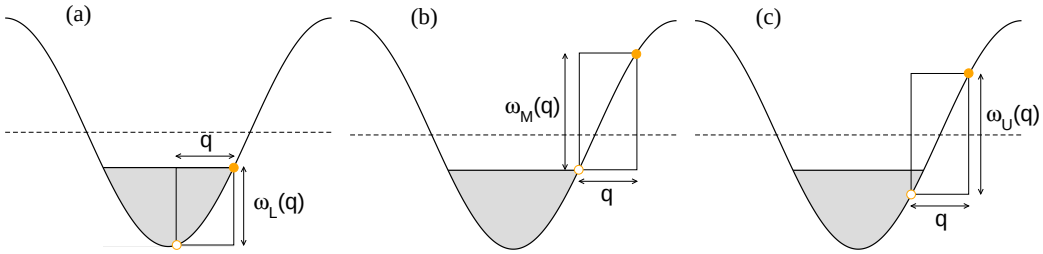

Figure 3.5: Particle-hole excitations that define the energies of the thresholds of $S^{zz}(q,\omega)$ for $2\pi|\sigma| < q < 2k_F$: a) deep hole; b) high-energy particle; c) exciton.

$$\omega_M(q) = 2J\sin\frac{q}{2}\cos\left(\frac{q}{2}+\pi\sigma\right), \tag{3.207}$$

$$\omega_U(q) = 2J\sin\frac{q}{2}. \tag{3.208}$$

For $\Delta = 0$, $S^{zz}(q,\omega)$ vanishes outside the two-particle continuum. Fig. 3.6 shows the exact line shape for $\Delta = 0$, $q = \pi/2$ and three values of magnetization σ. In the limit $\sigma \to 0$, the lower threshold $\omega_L(q)$ merges with the middle threshold $\omega_M(q)$ and we recover the zero field line shape. For fixed q and increasing $|\sigma|$, the middle threshold $\omega_M(q)$ approaches the upper threshold $\omega_U(q)$ as $|\sigma| \to q/2\pi$. For $|\sigma| > q/2\pi$, the exciton disappears and $\omega_M(q)$ becomes the upper threshold with a finite value for $S^{zz}(q,\omega=\omega_U(q))$ as depicted in Fig. 2.1.

We are interested in what happens near the thresholds in the interacting case $\Delta > 0$. Even the case $\Delta \ll 1$ will already give us some insight into the line shape at the Heisenberg point $\Delta = 1$. We already know that for $\Delta > 0$ the lower threshold turns into a divergent power-law singularity

$$S^{zz}(q,\omega\to\omega_L(q)) \sim [\omega-\omega_L(q)]^{-\mu}. \tag{3.209}$$

At finite field, μ is q dependent and must be calculated by solving the integral

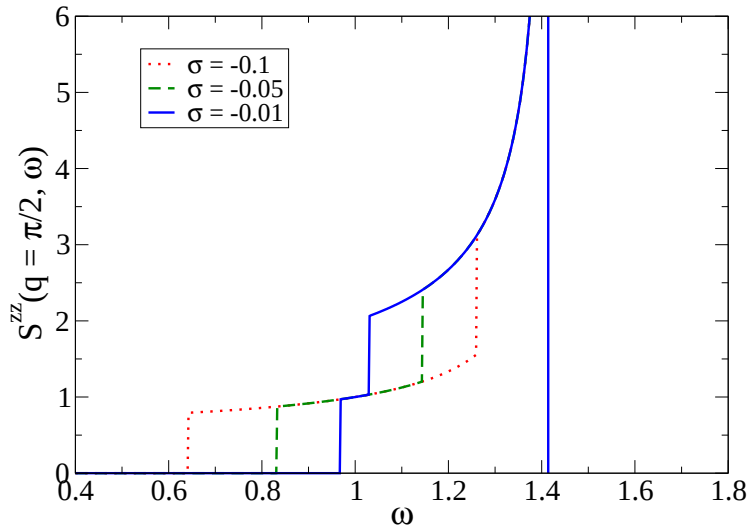

Figure 3.6: Exact line shape of $S^{zz}(q,\omega)$ for $\Delta = 0$, $q = \pi/2$ and three values of σ: $\sigma = -0.1$ ($k_F = 2\pi/5$), $\sigma = -0.05$ ($k_F = 9\pi/20$) and $\sigma = -0.01$ ($k_F = 49\pi/100$).

equation Eq. (3.9) numerically. To first order in Δ, we have from Eq. (3.14)

$$\mu(q) \approx \frac{2\Delta(1-\cos q)}{\pi(v_F - u_1)} = \frac{2\Delta(1-\cos q)}{\pi[\sin k_F - \sin(k_F - q)]}, \tag{3.210}$$

where u_1 is the velocity of the deep hole with momentum q below the Fermi surface. We also know that the singularity at the upper threshold changes discontinuously for arbitrarily small Δ. The square root divergence must turn into a convergent power-law singularity. However, for $h \neq 0$, the upper edge singularity is not simply a square root cusp. The reason is that, in the absence of particle-hole symmetry, the operator $d_2^\dagger d_1$ is not invariant under the unitary transformation that decouples the d particles (see Eq. (3.33)). The correlation function that determines the singularity also involves exponentials of bosonic fields; as a result, the singularity exponent depends on the coupling constants $\gamma_{R,L}^{(1,2)}$ in the effective Hamiltonian of Eq. (3.4). We

expect that in this case the slope of $S^{zz}(q,\omega)$ will diverge as ω approaches $\omega_U(q)$ from both sides, but with different singularity exponents for $\omega \to \omega_U(q)^-$ and $\omega \to \omega_U(q)^+$. In any case, here we want to discuss the singularity that develops at the middle threshold $\omega_M(q)$. To study the behavior of $S^{zz}(q,\omega)$ near $\omega_M(q)$, we use the effective Hamiltonian which includes a high-energy particle at $k_2 = k_F + q$

$$\begin{aligned}\mathcal{H} &= \frac{v}{2}\left[(\partial_x\varphi_L)^2 + (\partial_x\varphi_R)^2\right] + d_2^\dagger\left(\varepsilon_2 - iu_2\partial_x\right)d_2 \\ &\quad + \frac{1}{\sqrt{2\pi K}}\left(\kappa_L^{(2)}\partial_x\varphi_L - \kappa_R^{(2)}\partial_x\varphi_R\right)d_2^\dagger d_2, \end{aligned} \tag{3.211}$$

where ε_2 and u_2 are, respectively, the energy and velocity of the d_2 particle, v is the renormalized velocity, and $\kappa_{R,L}^{(2)}$ are the coupling constants as introduced in Eq. (3.4). Similarly to Eq. (3.50), we calculate the singularity for $\omega \approx \omega_M(q)$ as follows

$$\begin{aligned} S^{zz}(q,\omega\approx\omega_M) &\sim \int dx \int dt\, e^{i\omega t}\left\langle \psi_R^\dagger d_2(x,t)\, d_2^\dagger \psi_R(0,0)\right\rangle \\ &\sim \int dx \int dt\, e^{i(\omega-\omega_M)t}\delta(x-u_2t) \\ &\quad \times \left(\frac{1}{x-vt+i\eta}\right)^{\nu_+^{(2)}}\left(\frac{1}{x+vt-i\eta}\right)^{\nu_-^{(2)}} \\ &\sim \int dt\, \frac{e^{i(\omega-\omega_M)t}}{\left[(u_2-v)t+i\eta\right]^{\nu_+^{(2)}}\left[(u_2+v)t-i\eta\right]^{\nu_+^{(2)}}}, \end{aligned} \tag{3.212}$$

where

$$\nu_\pm^{(2)} = \frac{1}{4}\left[\sqrt{K} \pm \frac{1}{\sqrt{K}}\left(1 - \frac{\gamma_{R,L}^{(2)}}{\pi}\right)\right]^2. \tag{3.213}$$

The difference from the calculation for the upper threshold for small q in Eq. (3.50) is that, for $q > 2\pi|\sigma| = |2k_F - \pi|$, the velocity of the high-energy

particle is smaller than the renormalized Fermi velocity

$$u_2 < v \qquad \text{for } q > 2\pi\left|\sigma\right|. \tag{3.214}$$

As a result, the integral in Eq. (3.212) becomes

$$S^{zz}(q,\omega \approx \omega_M) \sim \int_{-\infty}^{+\infty} dt \frac{e^{i(\omega-\omega_M)t}}{(t-i\eta')^{\nu_+^{(2)}+\nu_-^{(2)}}}. \tag{3.215}$$

This integral is similar to the one we encountered for the lower threshold in Eq. (3.43). The integrand has a single branch point above the real axis, which means that this singular contribution vanishes for $\omega < \omega_M$. This is reasonable because the middle threshold is, in a sense, a lower threshold for the appearance of the double excitations. Another way to see the difference from the convergent upper threshold for small q is that, in the case of the middle threshold, the energy of the high-energy particle excitation *increases* if we move the hole away from the Fermi surface. It follows from Eq. (3.215) that $S^{zz}(q,\omega)$ has a power-law *divergence* at $\omega_M(q)$

$$S^{zz}(q,\omega) \sim \theta\left(\omega-\omega_M\right)\left(\omega-\omega_M\right)^{-\mu_M}, \tag{3.216}$$

with exponent

$$\mu_M = 1 - \nu_+^{(2)} - \nu_-^{(2)} > 0. \tag{3.217}$$

For $\Delta \ll 1$, μ_M is given by

$$\mu_M \approx \frac{2\Delta\left(1-\cos q\right)}{\pi\left(v_F-u_2\right)} = \frac{2\Delta\left(1-\cos q\right)}{\pi\left[\sin k_F - \sin\left(k_F+q\right)\right]}. \tag{3.218}$$

For $k_F < \pi/2$ and $q < \pi - 2k_F$, we have $u_1 < u_2 < v$. Comparing Eq. (3.218) with Eq. (3.210), we conclude that, for $\Delta \ll 1$, μ_M is *larger* than the exponent μ at the lower threshold. In the limit $h \to 0$, particle hole symmetry implies that both exponents approach the q-independent value

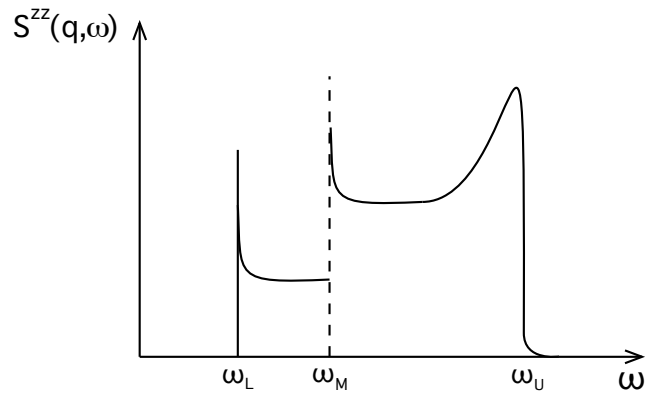

Figure 3.7: Line shape of $S^{zz}(q,\omega)$ for $q > 2\pi|\sigma|$ and small $\Delta > 0$.

$\mu = 1 - K$. We therefore expect that for $h \to 0$ the lower and middle singularities collapse and give rise to the two-spinon line shape shown in Fig. 3.1. The line shape for finite field and $q > 2\pi|\sigma|$ suggested by this weak coupling picture is represented in Fig. 3.7.

The extrapolation of this result to strong coupling (finite Δ) is consistent with the existence of two divergent edges conjectured by Müller *et al.* for the Heisenberg chain in a field. As we increase Δ from $\Delta = 0$ towards $\Delta = 1$, we expect that the peak near the upper threshold of $S^{zz}(q,\omega)$ will disappear as it did for zero field. (In Fig. 3.1, the slope of $S^{zz}(q,\omega)$ near the center of the two-particle continuum changes sign for $\Delta \approx 0.25$). Therefore, the remaining sharp features in the line shape for $\Delta = 1$ should be the divergences at the lower and middle thresholds. At finite temperature, these would presumably correspond to the two rounded peaks observed in experiments. However, we have not yet been able to determine the exact exponent μ_M from the Bethe ansatz. The reason is that we cannot identify the excitation in the Bethe ansatz solution that corresponds to the high-energy particle state represented in Fig. 3.5. As discussed in section 2.3.2, for the simplest class of excited states (single particle-hole pair with real rapidities), there is a restriction on

the choice of quantum numbers which implies a maximum value of q,

$$q < \mathrm{Min}\{\pi\,(1-2\sigma)\,, 2\sigma(\pi - \arccos\Delta)\}. \tag{3.219}$$

This means that it is not possible to add a single particle with momentum $k > \pi/2$. The solution to this puzzle is to consider classes of states with complex rapidities, namely states with two holes and a single negative parity one-string (see discussion at the end of section 2.4.3). The need to identify two classes of Bethe ansatz eigenstates at nonzero field had already been realized in [210] and was discussed more recently in [211]. How to calculate the finite size spectrum for this other class of states in order to fix the parameters of our effective field theory is an open question.

3.7 Summary

In summary, we presented a method to calculate the singularities of $S^{zz}(q,\omega)$ for the XXZ model. The exponents for general anisotropy, magnetic field and momentum can be obtained by solving the Bethe ansatz equations which determine the exact phase shifts. For the particle-hole symmetric zero field case, we showed that the lower edge exponent is q-independent and the ("exciton-like") upper edge has a universal square root singularity. The combination of analytic methods with the tDMRG overcomes the finite t limitation on the resolution of the tDMRG and can be used to study dynamics of other one-dimensional systems (integrable or not).

Bibliography

[160] T. Giamarchi, *Quantum Physics in One Dimension* (Clarendon Press, Oxford, 2004).

[161] B. C. Watson, V. N. Kotov, M. W. Meisel, D. W. Hall, G. E. Granroth, W. T. Montfrooij, S. E. Nagler, D. A. Jensen, R. Backov, M. A. Petruska, et al., Phys. Rev. Lett. **86**, 5168 (2001).

[162] K. Totsuka, Phys. Rev. B **57**, 3454 (1998).

[163] L.-M. Duan, E. Demler, and M. D. Lukin, Phys. Rev. Lett. **91**, 090402 (2003).

[164] V. E. Korepin, N. M. Bogoliubov, and A. G. Izergin, *Quantum inverse scattering method and correlation functions* (Cambridge University Press, 1993).

[165] M. B. Stone, D. H. Reich, C. Broholm, K. Lefmann, C. Rischel, C. P. Landee, and M. M. Turnbull, Phys. Rev. Lett. **91**, 037205 (2003).

[166] M. Karbach, G. Müller, A. H. Bougourzi, A. Fledderjohann, and K.-H. Mütter, Phys. Rev. B **55**, 12510 (1997).

[167] G. Müller, H. Thomas, H. Beck, and J. C. Bonner, Phys. Rev. B **24**, 1429 (1981).

[168] S. R. White, Phys. Rev. Lett. **69**, 2863 (1992).

[169] S. R. White, Phys. Rev. B **48**, 10345 (1993).

[170] U. Schollwöck, Rev. Mod. Phys. **77**, 259 (2005).

[171] A. J. Daley, C. Kollath, U. Schollwöck, and G. Vidal, J. Stat. Mech.: Theory Exp. p. P04005 (2004).

[172] S. White and A. Feiguin, Phys. Rev. Lett. **93**, 076401 (2004).

[173] A. Feiguin and S. White, Phys. Rev. B **72**, 020404(R) (2004).

[174] N. Kitanine, J. M. Maillet, and V. Terras, Nucl. Phys. B **554**, 647 (1999).

[175] J.-S. Caux and J. M. Maillet, Phys. Rev. Lett. **95**, 077201 (2005).

[176] M. Pustilnik, M. Khodas, A. Kamenev, and L. I. Glazman, Phys. Rev. Lett. **96**, 196405 (2006).

[177] R. G. Pereira, J. Sirker, J.-S. Caux, R. Hagemans, J. M. Maillet, S. R. White, and I. Affleck, Phys. Rev. Lett **96**, 257202 (2006).

[178] A. H. Castro Neto and M. P. A. Fisher, Phys. Rev. B **53**, 9713 (1996).

[179] L. Balents, Phys. Rev. B **61**, 4429 (2000).

[180] Y. Tsukamoto, T. Fujii, and N. Kawakami, Phys. Rev. B **58**, 3633 (1998).

[181] V. V. Cheianov and M. Pustilnik, Phys. Rev. Lett. **100**, 126403 (2008).

[182] G. Müller, H. Thomas, M. Puggat, and H. Beck, J. Phys. C: Solid State Phys. **14**, 3399 (1981).

[183] M. Pustilnik, Phys. Rev. Lett. **97**, 036404 (2006).

[184] G. D. Mahan, *Many-Particle Physics* (Kluwer/Plenum, New York, 2000), 3rd ed.

[185] T. Ogawa, J. Phys. Cond. Matter **16**, S3567 (2004).

[186] V. S. Viswanath, S. Zhang, G. Müller, and J. Stolze, Phys. Rev. B **51**, 368 (1995).

[187] J.-S. Caux and R. Hagemans, J. Stat. Mech.: Theory Exp. p. P12013 (2006).

[188] J. Sirker, Phys. Rev. B **73**, 224424 (2006).

[189] S. Lukyanov and V. Terras, Nucl. Phys. B **654**, 323 (2003).

[190] M. Khodas, M. Pustilnik, A. Kamenev, and L. I. Glazman, Phys. Rev. B **76**, 155402 (2007).

[191] R. G. Pereira, S. R. White, and I. Affleck, Phys. Rev. Lett **100**, 027206 (2008).

[192] P. W. Anderson, Phys. Rev. Lett. **18**, 1049 (1967).

[193] G. D. Mahan, Phys. Rev. **163**, 612 (1967).

[194] P. Nozieres and T. DeDominicis, Phys. Rev. **178**, 1097 (1969).

[195] K. D. Schotte and U. Schotte, Phys. Rev. **182**, 479 (1969).

[196] H. J. Schulz, Phys. Rev. B **34**, 6372 (1986).

[197] S. Eggert and I. Affleck, Phys. Rev. B **46**, 10866 (1992).

[198] F. Woynarovich, J. Phys. A: Math. Gen. **22**, 4243 (1989).

[199] P. Di Francesco, P. Mathieu, and D. Sénéchal, *Conformal Field Theory* (Springer-Verlag, New York, 1997).

[200] A. Luther and I. Peschel, Phys. Rev. B **12**, 3908 (1975).

[201] A. Imambekov and L. I. Glazman, arXiv:0711.2697 (unpublished) (2008).

[202] J. J. Hopfield, Comments Solid State Phys. **2**, 40 (1969).

[203] K. Ohtaka and Y. Tanabe, Rev. Mod. Phys. **62**, 4 (1990).

[204] P. Pirooznia and P. Kopietz, Eur. Phys. J. B **58**, 291 (2007).

[205] F. D. M. Haldane and M. R. Zirnbauer, Phys. Rev. Lett. **71**, 4055 (1993).

[206] B. Sutherland, *Beautiful Models* (World Scientific, 2004).

[207] S. Teber, Eur. Phys. J. B **52**, 233 (2006).

[208] A. E. Ruckenstein and S. Schmitt-Rink, Phys. Rev. B **35**, 7551 (1987).

[209] I. S. Gradshteyn and I. M. Ryzhik, *Tables of Integrals, Series and Products* (Academic Press, San Diego, 1994).

[210] G. Müller, H. Beck, and J. C. Bonner, Phys. Rev. Lett. **43**, 75 (1979).

[211] M. Karbach, D. Biegel, and G. Müller, Phys. Rev. B **66**, 054405 (2002).

Chapter 4

Conclusion

The main lesson from this work is that the study of dynamical correlation functions can teach us new things about the excitations of spin chains. The quantity we chose to investigate, the longitudinal dynamical structure factor, probes the spectrum as well as transition rates to excited states in more detail than static thermodynamic quantities do. The standard theoretical approach based on the Luttinger model fails to describe the interesting features of the dynamical structure factor. Fortunately, this difficulty can be overcome by a combination of various analytical and numerical methods, and the picture that emerges reveals some novel physics.

In order to understand the nontrivial line shape of the dynamical structure factor, it is important to go beyond the Luttinger model and treat interactions between the collective bosonic excitations in the effective field theory. Usually, one is not concerned about these residual interactions because they are irrelevant in the sense of the renormalization group. However, it turns out that dynamical properties are extremely sensitive to interactions between quasi-particles. In Chapter 2, we showed that the decay processes of Luttinger bosons give rise to very singular contributions to the expansion of the spin-spin correlation function. This breakdown of perturbation theory was a consequence of the linear dispersion approximation. To go around this problem, we made a conjecture about the summation of diagrams which is inspired by a refermionization of the bosons. This led to an approximate line shape for the dynamical structure factor at finite magnetic field in the limit of small momentum q. We checked that our formula for the width of the on-shell peak was correct by comparing it with the width of the particle-hole

continuum computed directly from the Bethe ansatz.

Both the field theory and the Bethe ansatz approaches rely on approximations. On the one hand, the field theory approach only treats the leading irrelevant operators that perturb the Luttinger liquid fixed point. On the other hand, the Bethe ansatz approach has to focus on a particular class of eigenstates. Nonetheless, the agreement between these two different methods support our conclusions. That we have found a good approximation can be confirmed by checking sum rules which are either known analytically or can be computed by independent numerical methods such as the DMRG.

Another example of agreement between field theory and Bethe ansatz discussed in Chapter 2 was the result for the high-frequency tail, which describes the small spectral weight of the dynamical structure factor outside the two-particle continuum. The tail for small q is interpreted in terms of the decay of a single boson into two bosons that propagate in opposite directions. Both in the calculation of the width of the on-shell peak and in the calculation of the tail, the basic idea of our approach is to use the Bethe ansatz solution to compute standard thermodynamic quantities that fix the parameters of the effective field theory, which can then be used to calculate dynamical properties. The perfect agreement with the numerical results from the Algebraic Bethe Ansatz gives us confidence that we have a reliable parameter-free effective model. It would be interesting to see if more detailed features of the line shape, such as the exponents of the edge singularities for small q, can also be extracted from the coupling constants of higher dimension operators.

In Chapter 3, we worked out an effective field theory which incorporates high-energy modes in analogy with the X-ray edge problem. We applied this model to study the edge singularities of the dynamical structure factor for the XXZ model, which were interpreted as Fermi edge singularities of the Jordan-Wigner fermions. Again we had to resort to the Bethe ansatz to fix the coupling constants which we related to renormalized phase shifts. This approach is able to explain the singularities of the exact two-spinon result

for the Heisenberg chain at zero field, and makes new predictions about the exact singularities for anisotropic chains in the critical regime.

Another effect we were able to elucidate was the long-time behavior of the spin correlation function. We discussed the counterintuitive result according to which the long time asymptotic behavior is dominated by a high-energy excitation. This effect is unique to one dimension and stems from the fact that a saddle point contribution to the self-correlation function coming from a hole at the bottom of the band or a particle at the top of the band decays more slowly than the contribution from a Fermi surface excitation. Using the X-ray edge approach, we derived the exponent for the power-law decay at large times, which is not predicted by Luttinger liquid theory. For zero magnetic field, we found that the exponent of the leading high-energy term can be expressed in terms of the Luttinger parameter, which is a property of the low-energy sector. We also showed that interactions are important, because the exponent of the leading term in the long-time behavior changes discontinuously when we switch on the interaction. When we further combined these analytic results, which capture the long-time behavior, with the tDMRG, which provides time-dependent correlation functions for short to intermediate times, we were able to produce line shapes for the dynamical structure factor with unprecedented resolution.

A promising direction to proceed with this combination of field theory, Bethe ansatz and tDMRG is a more detailed study of the line shape for the Heisenberg chain at finite field, where very little is known. We believe that these theoretical results could inspire more experimental effort to obtain better neutron scattering data, which would allow one to resolve some features predicted by the theory, such as the magnetic field dependence of the width for small q and the double peak structure for large q. To analyze experimental data one always has to take the convolution of the theoretical dynamical structure factor with the experimental resolution function. The typical energy and wave vector resolution of currently used neutron spectrometers

($\delta\omega \approx 0.1$ meV, $\delta q \approx 0.3$ Å[212]) is not enough to resolve power-law singularities at the thresholds, for instance. It is necessary to improve resolution and counting statistics in the experiments before we can make a meaningful comparison with our theoretical results.

We learned by calculating the high-frequency tail for zero magnetic field in chapter 2 that an effective field theory intended to be accurate at the level of irrelevant operators must reflect the integrability of the original lattice model. We proposed that integrability must be regarded as an extra symmetry, in the sense that nontrivial conservation laws impose constraints on the coupling constants of the effective field theory and even rule out some of the decay processes. The issue appeared again in Chapter 3, where it was argued that the power-law singularity at the upper threshold of the two-particle continuum was protected by the integrability of the XXZ model. In a generic model the singularity should be smoothed out and the upper threshold is not even well defined. This type of approach based on an effective field theory that is sensitive to integrability can be very useful to study other general dynamical properties of one-dimensional systems, particularly in the debate about finite temperature transport of spin or charge in integrable versus nonintegrable models. A field theory approach to these problems is highly desirable. Although the knowledge of exact eigenstates of a many-body system is certainly an invaluable tool, Bethe ansatz solvable models have special symmetries which are not shared by generic models and are inevitably broken in real systems. The difference between integrable and nonintegrable models was not so important for thermodynamic quantities because all 1D gapless models fall into the same universality class (they are all Luttinger liquids), regardless of integrability. But, as we have argued, integrability does matter if we are interested in dynamics.

The results of the work presented here suggest that the study of dynamics of strongly correlated systems, particularly one-dimensional ones, is an interesting road to explore. Many surprising effects are likely to be discovered as

we begin to unravel the realm of time-dependent phenomena in condensed matter physics. In a broader perspective, we can dream of the day we will be able to map out and even control the spectrum and excited states of a many-body system by the thorough knowledge of its dynamical correlation functions. Quantum computation is the application that first comes to mind, but what will actually come out of this exciting possibility is yet to be seen.

Bibliography

[212] C. Broholm, G. Aeppli, Y. Chen, D. C. Dender, M. Enderle, P. R. Hammar, Z. Honda, K. Katsumata, C. P. Landee, M. Oshikawa, et al., *High Magnetic Fields – Applications in Condensed Matter Physics and Spectroscopy* (Springer Verlag, 2002), p. 211, edited by C. Berthier, L. P. Lévy, and G. Martinez.

Appendix A

High-frequency tail for the zero field case

In this appendix we derive the results in Eqs. (2.222) and (2.223).

A.1 Tail from ζ_+ interaction

Since the ζ_+ vertex in (2.206) has two R and two L legs, the correction to $\chi(q, i\omega)$ is separable into $\delta\chi = \delta\chi_{RR} + \delta\chi_{LL}$, where

$$\delta\chi_{RR}(q, i\omega) = \frac{K}{2\pi}\left[D_R^{(0)}(q, i\omega)\right]^2 \Pi_{RLL}(q, i\omega). \tag{A.1}$$

Π_{RLL} is the bubble with one right- and two left-moving bosons (first diagram of figure A.1) given by

$$\Pi_{RLL}(q, i\omega) = -2\pi^2\zeta_+^2 \int_0^L dx\, e^{-iqx} \int_0^\beta d\tau e^{i\omega\tau} D_R^{(0)}(x, \tau)\left[D_L^{(0)}(q, \tau)\right]^2. \tag{A.2}$$

The expression for $\delta\chi_{LL}$ is obtained from (A.1) and (A.2) by exchanging $R \leftrightarrow L$. After doing the Fourier transform and integrating over the internal frequencies, we find

$$\Pi_{RLL}(q, i\omega) = \frac{2\pi^2\zeta_+^2}{L^2} \sum_{k_1,k_2>0} \frac{k_1 k_2 (q + k_1 + k_2)}{i\omega - vq - 2v(k_1 + k_2)}, \tag{A.3}$$

where $k_{1,2} = 2\pi n_{1,2}/L$, with $n_{1,2}$ integers. Taking the imaginary part of the retarded self-energy, we have

$$\begin{aligned} -\,\mathrm{Im}\;\Pi^{ret}_{RLL}(q,\omega) &= \frac{2\pi^3\zeta_+^2}{vL^2}\left(\frac{2\pi}{L}\right)^2 \sum_{n_1,n_2>0} n_1 n_2 (n+n_1+n_2) \\ &\quad \times\delta(\ell - n - 2n_1 - 2n_2), \end{aligned} \tag{A.4}$$

where we have used $q = q_n = 2\pi n/L$ and $\omega = \omega_\ell = 2\pi v\ell/L$. Notice that this implies that the energy levels in the tail are discrete and separated by $4\pi v/L$. We evaluate the sum on the righthand side of (A.4) as follows

$$\begin{aligned} &\sum_{n_1,n_2>0} n_1 n_2 (n+n_1+n_2)\,\delta(\ell - n - 2n_1 - 2n_2) \\ &= \sum_{m=1}^{\infty}(n+m)\,\delta(\ell-n-2m)\sum_{n_1=0}^{m} n_1(m-n_1) \\ &= \sum_{m=1}^{\infty}\frac{m^3(n+m)}{6}\left(1-\frac{1}{m^2}\right)\delta(\ell-n-2m) \\ &= \frac{1}{6}\sum_{\ell}\left(\frac{\ell-n}{2}\right)^3\left(\frac{\ell+n}{2}\right)\left[1-\left(\frac{2}{\ell-n}\right)^2\right]\frac{2\pi v}{L}\delta(\omega-\omega_\ell), \end{aligned} \tag{A.5}$$

with $\omega_\ell = 2\pi v\ell/L$, $\ell = n+2, n+4, \ldots$. Substituting (A.5) in (A.4) and using (A.1), we find

$$\begin{aligned} -\,2\mathrm{Im}\chi^{ret}_{RR}(q,\omega) &= \frac{K\zeta_+^2}{192v^2}\left(\frac{2\pi}{L}\right)^5 n^2 \\ &\quad \times\sum_{\ell}\left(\ell^2-n^2\right)\left[1-\left(\frac{2}{\ell-n}\right)^2\right]\delta(\omega-\omega_\ell). \end{aligned} \tag{A.6}$$

Likewise, we have

$$-\,2\mathrm{Im}\chi^{ret}_{LL}(q,\omega) = \frac{K\zeta_+^2}{192v^2}\left(\frac{2\pi}{L}\right)^5 n^2$$

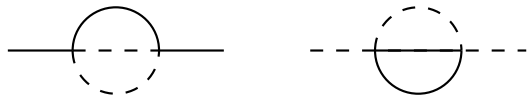

Figure A.1: Diagrams at $O(\zeta_+^2)$ for the calculation of the tail.

$$\times \sum_{\ell} \left(\ell^2 - n^2\right) \left[1 - \left(\frac{2}{\ell + n}\right)^2\right] \delta(\omega - \omega_\ell). \quad \text{(A.7)}$$

Finally, the contribution of the ζ_+ interaction to the high-frequency tail is

$$\delta S^{zz}_{\zeta_+}(q,\omega) = \frac{2\pi}{L} \sum_{\ell} F^2_{\zeta_+}(q_n, \omega_\ell) \delta(\omega - \omega_\ell), \quad \text{(A.8)}$$

with

$$F^2_{\zeta_+}(q_n, \omega_\ell) = \frac{K\zeta_+^2}{96v^2} \left(\frac{2\pi}{L}\right)^4 n^2 \left(\ell^2 - n^2\right) \left[1 - \frac{2}{(\ell - n)^2} - \frac{2}{(\ell + n)^2}\right]. \quad \text{(A.9)}$$

In the thermodynamic limit $L \to \infty$ (and $\ell \pm n \gg 1$), we obtain

$$\delta S^{zz}_{\zeta_+}(q,\omega) = \frac{K(\zeta_+/v)^2}{192v} q^2 \left(\frac{\omega^2 - v^2 q^2}{v^2}\right) \theta(\omega - vq). \quad \text{(A.10)}$$

A.2 Tail from λ_1 interaction

The perturbation theory in the Umklapp interaction for a finite system requires that we treat the zero mode operators. So consider the expressions for spin operators

$$S^z_j \sim \sqrt{\frac{K}{\pi}} \partial_x \phi + (-1)^j \text{const} \times \cos\left(\sqrt{4\pi K}\phi\right), \quad \text{(A.11)}$$

$$S^-_j \sim \text{const} \times e^{-i\sqrt{\pi/K}\theta} \left[(-1)^j + \cos\left(\sqrt{4\pi K}\phi\right)\right]. \quad \text{(A.12)}$$

Periodic boundary conditions for the spin operators imply that we can regard ϕ and θ as compactified fields with radius $R = (1/4\pi K)^{1/2}$ and $\tilde{R} = (K/\pi)^{1/2}$, respectively. In general, we can have

$$\phi(x+L) = \phi(x) + \mathcal{S}^z \sqrt{\frac{\pi}{K}} \tag{A.13}$$

$$\theta(x+L) = \theta(x) + m\sqrt{4\pi K}, \tag{A.14}$$

where $\mathcal{S}^z$ and m are integers. In a finite system with periodic boundary conditions we use the mode expansion for the bosonic fields

$$\begin{aligned}\phi(x,t) &= \phi_0 + \Pi_0 \frac{vt}{L} + Q_0 \frac{x}{L} \\ &\quad + \sum_{n>0} \frac{1}{\sqrt{2q_n L}} \left[-a_n^R e^{-iq_n(vt-x)} + a_n^L e^{-iq_n(vt+x)} + h.c. \right]\end{aligned} \tag{A.15}$$

where $q_n = 2\pi n/L$. The operators ϕ_0 and Π_0 are associated with the zero mode and satisfy $[\phi_0, \Pi_0] = i$. The compactification of ϕ quantizes the eigenvalues of Q_0 to be $\mathcal{S}^z\sqrt{\pi/K}$. It follows from Eqs. (A.11) and (A.15) that $\mathcal{S}^z$ corresponds to the total spin in the chain. We shall be restricted to the subspace $\mathcal{S}^z = 0$, to which the ground state for even L belongs. From $\partial_t \phi = v \partial_x \theta$, we get

$$\begin{aligned}\theta(x,t) &= \theta_0 + \Pi_0 \frac{x}{L} + Q_0 \frac{vt}{L} \\ &\quad + \sum_{n>0} \frac{1}{\sqrt{2q_n L}} \left[a_n^R e^{-iq_n(vt-x)} + a_n^L e^{-iq_n(vt+x)} + h.c. \right],\end{aligned} \tag{A.16}$$

with $[\theta_0, Q_0] = i$. The eigenvalues of Π_0 are then $m\sqrt{4\pi K}$, m integer. Therefore, for the Hamiltonian

$$H = \frac{v}{2} \int dx \left[(\partial_x \theta)^2 + (\partial_x \phi)^2 \right] \tag{A.17}$$

$$= \frac{v}{2L}\left(\Pi_0^2 + Q_0^2\right) + \frac{2\pi v}{L}\sum_{n>0} n\left[a_n^{R\dagger}a_n^R + a_n^{L\dagger}a_n^L\right], \tag{A.18}$$

we obtain the spectrum ($\mathcal{S}^z = 0$)

$$E = \frac{2\pi v}{L}\left[m^2 K + \sum_{n>0} n\left(m_n^R + m_n^L\right)\right], \tag{A.19}$$

where $m_n^{R,L} = 0, 1, 2, \ldots$. The corresponding wave function is

$$|\Psi\rangle = \exp\left[im\sqrt{4\pi K}\phi_0\right]\prod_{n>0}\left(a_n^{R\dagger}\right)^{m_n^R}\left(a_n^{L\dagger}\right)^{m_n^L}|0\rangle. \tag{A.20}$$

Since translation by one site takes $\phi \to \phi + \pi R$ and $|\Psi\rangle \to (-1)^m |\Psi\rangle$ [213], this symmetry implies that only intermediate states with even m couple to the ground state via S_q^z.

For the Umklapp interaction defined in (2.206), the $O(\lambda_1^2)$ correction to $\chi(q, i\omega)$ is

$$\begin{aligned}\delta\chi\left(q, i\omega\right) &= -\frac{K}{8\pi}\left(\frac{\lambda_1}{2\pi}\right)^2\int_0^L dx\, e^{-iqx}\int_0^\beta d\tau\, e^{i\omega\tau}\int d^2x_1\int d^2x_2 \\ &\quad\times\left\langle\partial_x\phi(x)e^{i4\sqrt{\pi K}\phi(1)}e^{-i4\sqrt{\pi K}\phi(2)}\partial_x\phi(0)\right\rangle + (1\leftrightarrow 2)\end{aligned} \tag{A.21}$$

Following [214] we can show that

$$\begin{aligned}&\left\langle\phi\left(x\right)\phi\left(0\right)e^{i4\sqrt{\pi K}\phi(1)}e^{-i4\sqrt{\pi K}\phi(2)}\right\rangle_{\text{con}} \\ =\ & 16\pi K\left[\langle\phi(x)\phi(1)\rangle\langle\phi(0)\phi(1)\rangle - \langle\phi(x)\phi(1)\rangle\langle\phi(0)\phi(2)\rangle + (1\leftrightarrow 2)\right] \\ &\quad\times\left\langle e^{i4\sqrt{\pi K}\phi(1)}e^{-i4\sqrt{\pi K}\phi(2)}\right\rangle.\end{aligned} \tag{A.22}$$

As a result, $\delta\chi$ can be cast in the form

$$\delta\chi\left(q, i\omega\right) = 2\left(\frac{\lambda_1 K}{2\pi}\right)^2\left[\frac{D^{(0)}(q, i\omega)}{q}\right]^2\left[\Pi(q, i\omega) - \Pi(0, 0)\right], \tag{A.23}$$

where

$$\Pi(q, i\omega) = -\int_0^L dx\, e^{-iqx} \int_0^\beta d\tau\, e^{i\omega\tau} \left\langle e^{i4\sqrt{\pi K}\phi(x,\tau)} e^{-i4\sqrt{\pi K}\phi(0,0)} \right\rangle . \tag{A.24}$$

The correlation function $\Pi(x,\tau) = \left\langle e^{i4\sqrt{\pi K}\phi(x,\tau)} e^{-i4\sqrt{\pi K}\phi(0,0)} \right\rangle$ for a finite system has to be calculated using the mode expansion (A.15) including the zero mode. Note that the operators in (A.21) couple the ground state to states with $m = \pm 2$, since we are calculating matrix elements of the form

$$\left\langle \alpha \left| \partial_x \phi\, e^{i2\sqrt{4\pi K}\phi_0 + \cdots} \right| 0 \right\rangle . \tag{A.25}$$

Since $e^{i4\sqrt{\pi K}\phi(z,\bar{z})}$ is a primary field of holomorphic weight $(2K, 2K)$, the correlation function in the infinite complex plane is given by

$$\Pi(z, \bar{z}) = \left(\frac{1}{z}\right)^{4K} \left(\frac{1}{\bar{z}}\right)^{4K} . \tag{A.26}$$

We use the "CFT normalization condition" of [215]. The correlation function for a finite system is obtained using the conformal mapping $z = e^{2\pi\xi/L}$, $\bar{z} = e^{2\pi\bar{\xi}/L}$, where $\xi = v\tau + ix$ and $\bar{\xi} = v\tau - ix$, with $0 < x < L$. The result is

$$\Pi(x,\tau) = \Pi(\xi, \bar{\xi}) = \left[\frac{\pi/L}{\sin \pi(x - iv\tau)/L}\right]^{4K} \left[\frac{\pi/L}{\sin \pi(x + iv\tau)/L}\right]^{4K} . \tag{A.27}$$

In order to calculate $\mathrm{Im}\, \Pi^{ret}$ at zero temperature, we switch back to real time with the prescription $iv\tau \to vt - i\alpha$, $\alpha \to 0^+$. We then calculate

$$\begin{aligned} \Pi(q,\omega) \;\equiv\; & -i \int_0^L dx\, e^{-iqx} \int_{-\infty}^{+\infty} dt\, e^{i\omega t} \left[\frac{\pi/L}{\sin \pi(x - vt + i\alpha)/L}\right]^{4K} \\ & \times \left[\frac{\pi/L}{\sin \pi(x + vt - i\alpha)/L}\right]^{4K} , \end{aligned} \tag{A.28}$$

which has the property $\Pi(q,\omega) = 2i\mathrm{Im}\Pi^{ret}(q,\omega)$. We also use the fact that

for a periodic function with discrete modes $q_n = 2\pi n/L$

$$f(x) = \sum_n \frac{f_n}{L} e^{i2\pi nx/L}. \tag{A.29}$$

We have

$$\begin{aligned}
\int_{-\infty}^{+\infty} dx\, e^{-iqx} f(x) &= \sum_n f_n \frac{1}{L} \int_{-\infty}^{+\infty} dx\, e^{-i(q-2\pi n/L)x} \\
&= \sum_n f_n \delta\left(\frac{qL}{2\pi} - n\right) \\
&= f(q) \sum_n \delta\left(\frac{qL}{2\pi} - n\right).
\end{aligned} \tag{A.30}$$

So we will consider the integral on the entire plane and eventually cancel a sum over delta functions for the discrete momenta. Performing a change of variables

$$\begin{aligned}
\tilde{\Pi}(q,\omega) &= \Pi(q,\omega) \sum_n \delta\left(\frac{qL}{2\pi} - n\right) \\
&= -\frac{i}{2v}\left(\frac{\pi}{L}\right)^{8K} \int_{-\infty}^{+\infty} dx_+ e^{i(\omega - vq)x_+/2v} \left[\sin\frac{\pi(x_+ - i\alpha)}{L}\right]^{-4K} \\
&\quad \times \int_{-\infty}^{+\infty} dx_- e^{-i(vq+\omega)x_-/2v} \left[\sin\frac{\pi(x_- + i\alpha)}{L}\right]^{-4K},
\end{aligned} \tag{A.31}$$

where $x_\pm \equiv x \pm vt$, we are left with integrals of the form

$$\begin{aligned}
I_1 &= \int_{-\infty}^{+\infty} du\, e^{iru} \left[\sin\frac{\pi(u - i\alpha)}{L}\right]^{-4K} \\
&= -\theta(r) \sum_{n=-\infty}^{+\infty} \int_{BC_n} dz\, e^{irz} \mathrm{Disc} \left[\sin\frac{\pi(z - i\alpha)}{L}\right]^{-4K},
\end{aligned} \tag{A.32}$$

where BC_n is the branch cut $z = nL + i\alpha + iy$, $0 < y < \infty$ and $\mathrm{Disc}\, f(z) \equiv f(z - 0^-) - f(z + 0^+)$ is the discontinuity of the function across the branch

cut. By shifting to $z' = z - nL$, we get

$$I_1 = -\theta(r) \sum_n e^{irnL} e^{-in4\pi K} \int_{BC_0} dz\, e^{irz} \mathrm{Disc}\left[\sin \frac{\pi(z - i\alpha)}{L}\right]^{-4K}. \quad \text{(A.33)}$$

We have

$$\mathrm{Disc}\left[\sinh \frac{\pi(z - i\alpha)}{L}\right]^{-4K} = \left|\sinh \frac{\pi y}{L}\right|^{-4K} 2i \sin 4\pi K. \quad \text{(A.34)}$$

Then

$$\begin{aligned} I_1 &= -\theta(r)\, 2i \sin 4\pi K\, e^{i4\pi K} \left[\sum_n e^{in(rL-4\pi K)}\right] ie^{-r\alpha} \\ &\quad \times \int_0^\infty dy\, e^{-ry} \left|\sinh \frac{\pi y}{L}\right|^{-4K}. \end{aligned} \quad \text{(A.35)}$$

We use

$$\sum_n e^{in(rL-4\pi K)} = \sum_m \delta\left(\frac{rL - 4\pi K}{2\pi} - m\right). \quad \text{(A.36)}$$

and (from [216])

$$\int_0^\infty ds\, [\sinh(\pi T s)]^{-4K} e^{isz} = \frac{2^{4K-1}}{\pi T} B\left(2K - i\frac{z}{2\pi T}, 1 - 4K\right), \quad \text{(A.37)}$$

where $B(x, y) = \Gamma(x)\Gamma(y)/\Gamma(x + y)$ is the Euler Beta function, and finally get

$$\begin{aligned} I_1 &= \frac{2^{4K} L}{\pi} \sin(4\pi K)\, \theta(r)\, B\left(2K + \frac{rL}{2\pi}, 1 - 4K\right) \\ &\quad \times \sum_m \delta\left(\frac{rL - 4\pi K}{2\pi} - m\right). \end{aligned} \quad \text{(A.38)}$$

Likewise, the integral

$$I_2 = \int_{-\infty}^{+\infty} du\, e^{-i\tilde{r}u} \left[\sin \frac{\pi\,(u+i\alpha)}{L}\right]^{-4K} \tag{A.39}$$

is given by

$$\begin{aligned} I_2 &= \frac{2^{4K} L}{\pi} \sin(4\pi K)\, \theta\,(\tilde{r})\, B\left(2K + \frac{\tilde{r}L}{2\pi}, 1-4K\right) \\ &\quad \times \sum_{m'} \delta\left(\frac{\tilde{r}L - 4\pi K}{2\pi} - m'\right). \end{aligned} \tag{A.40}$$

In our case, $r = (\omega - vq)\,/2v$ and $\tilde{r} = (\omega + vq)\,/2v$. The two delta functions can be recombined to replace the second condition by $q = q_n = 2\pi n/L$.

$$\begin{aligned} &\sum_m \delta\left(\frac{rL - 4\pi K}{2\pi} - m\right) \sum_{m'} \delta\left(\frac{\tilde{r}L - 4\pi K}{2\pi} - m'\right) \\ &= \sum_m \delta\left(\frac{(\omega - vq)\,L}{4\pi v} - m - 2K\right) \sum_n \delta\left(\frac{qL}{2\pi} - n\right). \end{aligned} \tag{A.41}$$

We can then cancel the second delta function and write

$$\begin{aligned} \Pi\,(q,\omega) &= -4i \left(\frac{2\pi}{L}\right)^{8K-2} \sin^2(4\pi K) B\left(2K + \frac{(\omega - vq)\,L}{4\pi v}, 1-4K\right) \\ &\quad \times B\left(2K + \frac{(\omega + vq)\,L}{4\pi v}, 1-4K\right) \frac{2\pi}{L} \sum_\ell \delta\,(\omega - \omega_\ell)\,, \end{aligned} \tag{A.42}$$

where $\omega_\ell = 2\pi v(\ell + 4K)/L$, $\ell = n, n+2, \ldots$. Finally, the contribution from the Umklapp operator to the high-frequency tail is

$$\delta S^{zz}_{\lambda_1}(q,\omega) = \frac{2\pi}{L} \sum_\ell F^2_{\lambda_1}(q_n, \omega_\ell) \delta(\omega - \omega_\ell), \tag{A.43}$$

with

$$\begin{aligned} F^2_{\lambda_1}(q_n,\omega_\ell) &= 2\left(\frac{2\lambda_1 K}{\pi v}\right)^2\left(\frac{2\pi}{L}\right)^{8K-4}\sin^2(4\pi K)\frac{n^2}{\left(\ell^2-n^2\right)^2} \\ &\quad\times B\left(4K+\frac{\ell-n}{2},1-4K\right) \\ &\quad\times B\left(4K+\frac{\ell+n}{2},1-4K\right). \end{aligned} \tag{A.44}$$

In the limit $L\to\infty$, we can use $B(x,y)\sim\Gamma(y)x^{-y}$ for $x\to\infty$ and we find

$$\delta S^{zz}_{\lambda_1}(q,\omega)=\frac{2\lambda_1^2K^2}{\Gamma^2(4K)}(2v)^{3-8K}q^2\left(\omega^2-v^2q^2\right)^{4K-3}\theta(\omega-vq). \tag{A.45}$$

A.3 Infrared-divergent tail for $\zeta_3\neq 0$

The tail of order ζ_+^2 vanishes at $\omega\to vq$ because the ω dependence of Π_{RLL} (equation A.5) cancels the factor of $(\omega-vq)^{-2}$ from the external legs of the corresponding diagram in $\delta\chi_{RR}$. It is easy to see that if the internal bubble had a different combination of R and L bosons (*e.g.*, if we replaced Π_{RLL} by Π_{RRL}) this cancellation would not happen, leading to a divergence at $\omega\to vq$. The dangerous combinations of external legs and three-boson bubbles are excluded for the XXZ model, but are allowed for non-integrable models with $\zeta_3\neq 0$. The extra diagrams that contribute to the tail ($\delta\omega_q\ll\omega-vq\ll J$) to second order in the coupling constants are illustrated in figure A.2. The calculation is similar to the $O(\zeta_+^2)$ diagram. The result in the thermodynamic limit is

$$\delta S^{zz}_3(q,\omega)=\frac{3K}{128v}q^2\left[\frac{\zeta_3^2}{v^2}\frac{\omega^4+6v^2q^2\omega^2+v^4q^4}{v^2\left(\omega^2-v^2q^2\right)}+\frac{2\zeta_3\zeta_+}{v^2}\frac{\omega^2+v^2q^2}{v^2}\right]. \tag{A.46}$$

Note the divergence as $\omega\to vq$ in the $O(\zeta_3^2)$ term. As in the finite field case, this divergence stems from the breakdown of perturbation theory in the band curvature terms at $\omega\sim vq$. We expect that this ζ_3 contribution, which again

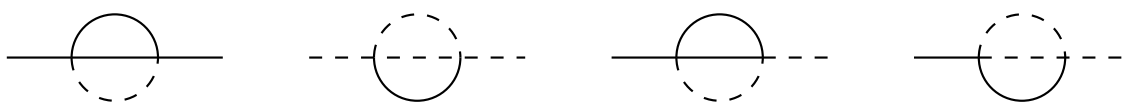

Figure A.2: Diagrams for the high-frequency tail involving the ζ_3 interaction.

is only finite for nonintegrable models, smoothes out the behavior of $S^{zz}(q,\omega)$ near the upper threshold $\omega_U(q)$, where the high-frequency tail joins the on-shell peak.

Bibliography

[213] S. Eggert and I. Affleck, Phys. Rev. B **46**, 10866 (1992).

[214] M. Oshikawa and I. Affleck, Phys. Rev. B **65**, 134410 (2002).

[215] S. Lukyanov, Nucl. Phys. B **522**, 533 (1998).

[216] H. J. Schulz, Phys. Rev. B **34**, 6372 (1986).